A Kinetic and Electrochemical Study of the Dissolution of Gold in Aerated Cyanide Solutions: The Role of Solid and Solution Phase Purity

By

Matthew Ian Jeffrey

B.E. (Chem)

This thesis is presented for the
Degree of Doctor of Philosophy
of the Curtin University of Technology
Western Australia
1997

I declare that this thesis is my own account of my research and contains as it main content work which has not been submitted for a degree at any tertiary education institution

Matthew Ian Jeffrey

September, 1997

ABSTRACT

Over the last 100 years, the cyanidation process has been the most popular method for recovering gold from its ores. Despite this, there are still efforts to improve the efficiency of the process, particularly as ores become more difficult to treat. Many investigators have studied the cyanidation process, although a large proportion of these studies have obtained contradictory results. This thesis presents a kinetic and electrochemical study of the leaching of gold in cyanide solutions, and emphasis is placed on rationalising the conflicting results which have been published in the past.

The leaching rate of gold was measured using a rotating electrochemical quartz crystal microbalance, an instrument which allows the simultaneous measurement of electrochemical data and mass changes at the solid-solution interface in real time. A proportion of this project was devoted to the on-going design of this instrument, and a number of modifications are discussed in detail. Initially, the leaching of gold in cyanide solutions was investigated under conditions of high purity. Under these conditions, it was found that the gold surface is blocked by a passive film, presumably AuCN. The presence of such a film results in the reaction being chemically controlled, and under typical cyanidation conditions (4 mM cyanide, pH 10.0), the rate of dissolution is very low. These kinetic results were supported by complimentary electrochemical studies, which showed that gold is passive in the potential region where cyanidation occurs.

The second part of this thesis presents a study of the effect of system purity on the leaching of gold in cyanide solutions. Solution phase purity was investigated by adding controlled amounts of lead or silver to the leach solutions. It was found that in the presence of low concentrations of lead, the dissolution of gold in 20 mM cyanide solutions was oxygen diffusion controlled (as compared to chemical control for gold in the absence of lead). However, high concentrations of lead were found to be detrimental to the leaching process. It is believed that the role of lead is to modify the surface by cementation, hence reducing the effect of the passive film. Silver was

also found to be effective at reducing passivation, and the role of silver is believed to be similar to that of lead. It was found that unlike lead, high concentrations of silver are not detrimental to the dissolution of gold in cyanide solutions.

Solid phase purity was also found to be important in the leaching of gold, and it was found that the leaching of a gold sample which contains 1 % silver is diffusion controlled. This finding is important from an industrial viewpoint, as most native gold contains some silver. Consequently, attempts were made to rationalise the leaching of gold/silver with current plant practice. Discussion on the effect of cyanide and oxygen concentrations, temperature and lead addition is presented.

TABLE OF CONTENTS

Abstract i
Acknowledgements ix
Publications And Conferences x
List of Figures xi
List of Tables xv

CHAPTER 1 – INTRODUCTION 1

1.1. Importance of Gold 1
1.1.1. History and Uses of Gold 1
1.1.2. Production of Gold 2
1.2. Chemistry of Gold 3
1.3. Processing of Gold by Cyanidation 5
1.3.1. Leaching 5
1.3.2. Recovery 7
1.3.2.1. Cementation 8
1.3.2.2. Carbon Adsorption 8
1.4. Areas of Uncertainty in Leaching 9

CHAPTER 2 – REVIEW 11

2.1. Chemistry of Cyanidation 11
2.1.1. The Gold Cyanide Complex 11
2.1.2. Oxidation of Au to $Au(CN)_2^-$ 12
2.1.3. Leaching of Gold in Aerated Cyanide Solutions 14
2.2. Kinetics of Cyanidation 16
2.2.1. Methods of Studying Kinetics 16
2.2.1.1. Agitation and Sample Geometry 16

2.2.1.2. Analysis 19
2.2.2. Mechanistic Considerations 22
2.2.2.1. Mechanisms of Cyanidation 23
2.2.2.2. Factors Leading to Chemical Control 26
2.2.2.3. Criteria for Diffusion and Chemical Control 31
2.2.3. Published Kinetic Results 32
2.2.3.1. Dissolution of Gold 32
2.2.3.2. Dissolution in the Presence of Additives 44
2.3. Electrochemistry of Cyanidation 47
2.3.1. Mixed Potential Theory 47
2.3.2. The Gold Oxidation Half Reaction 50
2.3.2.1. Peak at -400 mV 56
2.3.2.2. Peak at 300 mV 63
2.3.2.3. Peak at 600 mV 64
2.3.3. Oxygen Reduction Half Reaction 64
2.3.3.1. Reduction at the Solid-Solution Interface 64
2.3.3.2. Reduction of Oxygen on Gold 67
2.3.3.3. Reduction on Silver 69

CHAPTER 3 – STUDIES OF OXYGEN REDUCTION 71

3.1. Introduction 71
3.2. Experimental 71
3.2.1. Solutions and Electrodes 71
3.2.2. Electrochemical Measurements 73
3.3. Results and Discussion 73
3.3.1. Surface Effects 74
3.3.1.1. Effect of Electrode Substrate 74
3.3.1.2. Electrode Pre-treatment 80
3.3.1.3. Surface Modification 83
3.3.2. Other Experimental Variables 85
3.3.2.1. Effect of Oxygen Concentration 85

3.3.2.2. Effect of Temperature 87
3.3.2.3. Effect of pH 87
3.4. Summary 90

CHAPTER 4 - DISSOLUTION OF GOLD IN CYANIDE SOLUTIONS 91

4.1. Introduction 91
4.2. Experimental 91
4.2.1. Solutions and Electrodes 91
4.2.2. Kinetic Measurements 94
4.2.2.1. Principles of EQCM 94
4.2.2.2. The REQCM 95
4.2.3. Surface Studies 100
4.3. Results and Discussion 101
4.3.1. Dissolution of Gold in Aerated Cyanide 101
4.3.1.1. Kinetics 101
4.3.1.2. Surface Studies 105
4.3.1.3. Electrochemistry – Oxidation 107
4.3.1.4. Evans' Diagrams 109
4.3.2. Effect of Cyanide Concentration 113
4.3.2.1. Kinetics 113
4.3.2.2. Electrochemistry – Oxidation 118
4.3.3. Effect of Rotation Rate 120
4.3.3.1. Kinetics 120
4.3.3.2. Electrochemistry – Oxidation 121
4.3.4. Effect of Temperature 125
4.3.4.1. Kinetics 126
4.3.4.2. Electrochemistry – Oxidation 129
4.3.4.3. Electrochemistry – Evans' diagrams 131
4.3.5. Effect of Oxygen Concentration 135
4.3.5.1. Kinetics 135
4.3.6. Effect of pH 136

4.3.6.1. Kinetics 136
4.3.6.2. Electrochemistry – Oxidation 136
4.3.7. Effect of Solution Purity 140
4.4. Summary 142

CHAPTER 5 – THE EFFECT OF SOLUTION PHASE ADDITIVES 143

5.1. Introduction 143
5.2. Experimental 143
5.3. Results and Discussion 144
5.3.1. The Action of Lead 144
5.3.1.1. Kinetics Studies 144
5.3.1.2. Surface Studies 150
5.3.1.3. Electrochemistry – Oxidation of Gold 153
5.3.1.4. Electrochemistry – Evans' Diagrams 160
5.3.2. Effect of Cyanide Concentration 165
5.3.2.1. Kinetic Studies 165
5.3.2.2. Electrochemistry – Oxidation 167
5.3.2.3. Electrochemistry – Evans' Diagrams 169
5.3.3. Effect of Rotation Rate 172
5.3.3.1. Kinetic Studies 172
5.3.3.2. Electrochemistry – Oxidation 174
5.3.3.3. Electrochemistry – Evans' Diagrams 176
5.3.4. Effect of Temperature 176
5.3.4.1. Kinetic Studies 176
5.3.4.2. Electrochemistry – Oxidation 181
5.3.4.3. Electrochemistry – Evans' Diagrams 184
5.3.5. Effect of Oxygen Concentration 184
5.3.5.1. Kinetic Studies 184
5.3.5.2. Electrochemistry – Evans' Diagrams 187
5.3.6. Effect of pH 187
5.3.6.1. Kinetics 187

5.3.6.2. Electrochemistry – Oxidation 190
5.3.6.3. Electrochemistry – Evans' Diagrams 193
5.3.7. Effect of Lead Concentration 195
5.3.7.1. Kinetics 195
5.3.7.2. Electrochemistry – Oxidation. 196
5.3.7.3. Electrochemistry – Evans' Diagrams 199
5.3.8. Effect of Other Solution Additives 199
5.3.8.1. Kinetics 199
5.3.8.2. Electrochemistry – Oxidation 204
5.3.8.3. Electrochemistry – Evans' diagrams 206
5.4. Summary 208

CHAPTER 6 – THE EFFECT OF SOLID PHASE ADDITIVES 209

6.1. Introduction 209
6.2. Experimental 209
6.3. Results and Discussion 210
6.3.1. Effect of Solid Phase Impurities 210
6.3.1.1. Kinetic Studies 210
6.3.1.2. Electrochemistry – Oxidation. 213
6.3.1.3. Electrochemistry – Evans' Diagrams 218
6.3.2. Effect of Cyanide Concentration 221
6.3.2.1. Kinetics 221
6.3.2.2. Electrochemistry – Oxidation. 225
6.3.2.3. Electrochemistry – Evans' Diagrams. 228
6.3.3. Effect of Rotation Rate 231
6.3.3.1. Kinetics 231
6.3.3.2. Electrochemistry – Oxidation 233
6.3.3.3. Electrochemistry – Evans' Diagrams. 234
6.3.4. Effect of Temperature 237
6.3.4.1. Kinetics 237
6.3.4.2. Electrochemistry – Oxidation. 241

6.3.4.3. Electrochemistry – Evans' Diagrams. 241
6.3.5. Effect of Oxygen Concentration 244
6.3.5.1. Kinetics 244
6.3.5.2. Electrochemistry – Evans' Diagrams 245
6.3.6. Effect of pH 247
6.3.6.1. Kinetics 247
6.3.6.2. Electrochemistry – Oxidation 247
6.3.6.3. Electrochemistry – Evans' Diagrams 248
6.3.7. Effect of Lead 248
6.3.7.1. Kinetics 248
6.3.7.2. Electrochemistry – Oxidation 252
6.3.7.3. Electrochemistry – Evans' Diagrams 252
6.4. Summary 255

CHAPTER 7 – CONCLUSIONS AND RECOMMENDATIONS 256

REFERENCES 260

ACKNOWLEDGEMENTS

I would like to express my appreciation for the tireless guidance and support which my supervisors, Professor Ian Ritchie, and Dr Steve La Brooy have given throughout the course of this research.

I am also thankful to my colleagues, Dr Sherryl Robertson, Dr Kitty Drok, Dr Honguang Zhang, and Ms Elizabeth Ho for their assistance and suggestions, and for proof-reading some parts of this thesis. I would also like to thank the staff of the AJ Parker CRC for Hydrometallurgy, including Ms Margaret Davidson, Dr Jim Avraamides and Ms Betty Bright for their advice.

I would like to especially thank Mr Laurence Guilfoyle, Mr Fritz Wagner, and Mr Kleber Klaus for the time and effort which was spent on the design and construction of the rotating electrochemical quartz crystal microbalance. I am also grateful to the work that Mr Doug Clarke performed in preparing the ultrapure cyanide solutions.

Financial assistance for this project was provided by the AJ Parker CRC for Hydrometallurgy, and the Minerals and Energy Research Institute of WA, and for this support, I am very grateful. This project was also carried out in collaboration with the AMIRA gold project P420, and I would like to extend my thanks to AMIRA and the sponsors of this project. I would also like to also thank the project personnel, in particular, Ms Ann Bax, for their assistance during the course of these studies.

Last, but not least, I would like to thank my wife and three children for their support during the long hours associated with a PhD study. Without their assistance, I would never have completed this project. This thesis is devoted to my grandfather, who passed away during the final stages my studies.

PUBLICATIONS AND CONFERENCES

Jeffrey, M.I., Drok, K.J., La Brooy, S.R., Ritchie, I.M. In Press, "Oxygen reduction during the dissolution of gold and copper in alkaline cyanide solutions", *Submitted to Hydrometallurgy*, March 1997.

Jeffrey, M.I., Ritchie, I.M., La Brooy, S.R. 1997, "The leaching of gold in cyanide solutions as a function of impurities", *Presented at World Gold*, Singapore.

Jeffrey, M.I., Guilfoyle, L., Drok, K.J., Ritchie, I.M., La Brooy, S.R. 1997, "The rotating electrochemical quartz crystal microbalance: design and applications to hydrometallurgy", *Presented at Electrochemistry 97*, London.

Jeffrey, M.I., Ritchie, I.M., La Brooy, S.R. 1997, "Gold dissolution in cyanide solutions as a function of impurities in both the solid and solution phases", *Presented at 10th Australian Electrochemistry Conference*, Gold Coast.

Drok, K.J., Jeffrey, M.I., Ritchie, I.M., La Brooy, S.R. 1997, "Oxygen reduction during the dissolution of gold and copper in alkaline cyanide solutions", *Presented at 10th Australian Electrochemistry Conference*, Gold Coast.

Jeffrey, M.I., La Brooy, S.R., Ritchie, I.M. 1996, "The effect of lead on the electrochemistry of gold: Myth or magic", in *Electrochemistry in Minerals and Metals Processing IV*, Eds. Woods, R., Doyle, F. and Richardson. P., The Electrochemical Society, Pennington, New Jersey.

La Brooy, S.R., Jeffrey, M.I. 1996, "Gold cyanidation - recent developments", *AJ Parker CRC Workshop Course: Advances in Hydrometallurgy*, Perth.

LIST OF FIGURES

Figure 1.1 – Typical flowsheet for a cyanidation plant. 6

Figure 2.1 – The gold cyanide complex. 11
Figure 2.2 – Pourbaix diagram for the gold-cyanide-water system. 13
Figure 2.3 – Limiting rates as a function of cyanide concentration. 25
Figure 2.4 - Evans' diagrams representing the effect of a resistive film. Oxygen in excess of cyanide. 28
Figure 2.5- Evans' diagrams representing the effect of a resistive film. Cyanide in excess of oxygen. 30
Figure 2.6 – Published kinetic data for cyanidation. 34
Figure 2.7 – Change in the activation energy with temperature. 39
Figure 2.8 – Reported values of the critical cyanide concentration. 40
Figure 2.9 – Published kinetic data showing the effect of oxygen. 43
Figure 2.10 – Schematic polarisation curves representing the oxidation of gold and the reduction of oxygen. 49
Figure 2.11 – Gold oxidation polarisation curve published by Bek, Rogozhnikov and Kosolapov (1997). 51
Figure 2.12 – Comparison of the published gold oxidation polarisation curves measured using the rotating disc system. 54
Figure 2.13 – Comparison of gold oxidation polarisation curves published prior to 1980. 55
Figure 2.14 – Effect of lead on the oxidation of gold in cyanide solutions. 60
Figure 2.15 – Effect of electrode pretreatment on the oxidation of gold. 62

Figure 3.1 – Oxygen reduction on gold and silver. 75
Figure 3.2 – Detection of peroxide using a ring-disc electrode. 78
Figure 3.3 – Cyclic voltammogram for fast cycling of gold. 81
Figure 3.4 – Effect of fast cycling on oxygen reduction. 82
Figure 3.5 – Effect of lead on oxygen reduction. 84
Figure 3.6 – Effect of oxygen concentration on oxygen reduction. 86

Figure 3.7 – Effect of temperature on oxygen reduction..... 88
Figure 3.8 – Effect of pH on oxygen reduction. 89

Figure 4.1 – Illustration showing how the quartz crystals are mounted in the cylindrical PVC adapter. 93
Figure 4.2 – Illustration showing the new design of the REQCM..... 97
Figure 4.3 – Circuit diagram for the REQCM..... 98
Figure 4.4 – Mass versus time response for the leaching of gold..... 102
Figure 4.5 – SEM image at 200x of gold after 24 hours of leaching. 106
Figure 4.6 – SEM image at 1000x of gold after 24 hours of leaching..... 106
Figure 4.7 – Oxidation of polycrystalline gold. 108
Figure 4.8 – Evans' diagrams representing the leaching of gold..... 111
Figure 4.9 – Rate of dissolution versus cyanide concentration. 114
Figure 4.10 – Published and measured critical cyanide concentrations 117
Figure 4.11 – Effect of cyanide concentration on the oxidation of gold. 119
Figure 4.12 – Rate of dissolution of gold versus $\omega^{1/2}$..... 122
Figure 4.13 – Effect of rotation rate on the oxidation of gold. 123
Figure 4.14 – Oxidation current density versus $\omega^{1/2}$. 124
Figure 4.15 – Arrhenius plot of the corrected rate of dissolution. 128
Figure 4.16 – Effect of temperature on the oxidation of gold..... 130
Figure 4.17 – Arrhenius plot of gold oxidation current density..... 132
Figure 4.18 – Evans' diagram representing the leaching of gold at 60 °C.. 133
Figure 4.19 – Effect of pH on the oxidation of gold..... 137
Figure 4.20 – Passivation potential as a function of pH..... 139
Figure 4.21 – Gold oxidation in ultrapure and AR grade cyanide. 141

Figure 5.1 – Effect of lead on the leaching of gold. 145
Figure 5.2 – Mass versus time for the cementation of lead on gold. 148
Figure 5.3 – Effect of lead pretreatment on the dissolution of gold..... 149
Figure 5.4 – SEM image at 200x of gold after leaching with lead..... 151
Figure 5.5 – SEM image at 200x of gold after leaching without lead..... 151
Figure 5.6 – Optical image of gold after leaching with lead. 152
Figure 5.7 – SEM image of gold at 500x showing grain boundaries..... 152

Figure 5.8 – SEM image of gold at 500x showing pits..... 154
Figure 5.9 – Effect of lead on the oxidation of gold 155
Figure 5.10 – Recorded and calculated current densities. 157
Figure 5.11 – Oxidation of lead and gold in cyanide solutions with lead. ... 159
Figure 5.12 – Pourbaix diagram for the lead-water system. 161
Figure 5.13 – Evans' diagrams representing gold leaching with lead..... 162
Figure 5.14 – Rate of dissolution versus cyanide concentration. 166
Figure 5.15 – Effect of cyanide concentration on the peak current density 168
Figure 5.16 – Evans' diagram representing the dissolution of gold in 2 mM air saturated cyanide solutions..... 170
Figure 5.17 – Rate of dissolution of gold versus $\omega^{1/2}$..... 173
Figure 5.18 – Oxidation current density versus $\omega^{1/2}$ 175
Figure 5.19 – Evans' diagram representing the dissolution of gold in air saturated 20 mM cyanide solutions at 75 rpm..... 177
Figure 5.20 – Effect of temperature on the dissolution of gold. 178
Figure 5.21 – Arrhenius plot of the corrected rate of dissolution. 180
Figure 5.22 – Gold oxidation as a function of temperature..... 182
Figure 5.23 – Arrhenius plot of the oxidation current density 183
Figure 5.24 – Evans' diagram representing the leaching of gold at 60 °C in air saturated 20 mM cyanide solutions..... 185
Figure 5.25 – Evans' diagram representing the leaching of gold in oxygen saturated 20 mM cyanide solutions..... 188
Figure 5.26 – Effect of pH on the dissolution of gold..... 189
Figure 5.27 – Effect of pH on the gold oxidation peak P2.. 191
Figure 5.28 – Passivation potential of peak P2 as a function of pH..... 192
Figure 5.29 – Evans' diagram representing the leaching of gold in air saturated 20 mM cyanide solutions at pH 11.5. 194
Figure 5.30 – Mixed potential versus time for the cementation of lead..... 197
Figure 5.31 – Effect of lead concentration on the oxidation of gold..... 198
Figure 5.32 – Evans' diagram representing the dissolution of gold in air saturated 20 mM cyanide solutions containing 1 and 10 ppm lead..... 200
Figure 5.33 – Leaching of gold in the presence of 1 ppm silver. 202
Figure 5.34 – Effect of silver on the oxidation of gold..... 205

Figure 5.35 –Evans' diagrams representing the dissolution of gold in air and oxygen saturated 20 mM cyanide solutions containing 1 ppm silver... 207

Figure 6.1 – Leaching of gold/lead and gold/silver.. 211
Figure 6.2 – Oxidation of gold/lead and gold/silver..... 214
Figure 6.3 – Effect of potential scan rate on the oxidation of gold/silver..... 216
Figure 6.4 – Evans' diagrams representing the leaching of gold and gold/silver in air saturated 20 mM cyanide solutions. 219
Figure 6.5 – Leaching of gold/silver in 2 and 20 mM cyanide solutions..... 222
Figure 6.6 – Rate of dissolution versus cyanide concentration 223
Figure 6.7 – Published and measured critical cyanide concentrations..... 226
Figure 6.8 – Effect of cyanide concentration on the oxidation of gold/silver.227
Figure 6.9 – Evans' diagrams representing the leaching of gold/silver in air saturated 2 and 20 mM cyanide solutions. 229
Figure 6.10 – Rate of dissolution of gold/silver versus $\omega^{1/2}$. 232
Figure 6.11 – Effect of rotation rate on gold/silver oxidation..... 235
Figure 6.12 – Evans' diagrams representing the leaching of gold/silver at 75 and 300 rpm in air saturated solutions containing 20 mM cyanide..... 236
Figure 6.13 – Effect of temperature on the dissolution of gold/silver. 238
Figure 6.14 – Arrhenius plot of the corrected rate of dissolution 240
Figure 6.15 – Arrhenius plot of the gold/silver limiting current density..... 242
Figure 6.16 – Evans' diagrams representing the leaching of gold/silver at 25 and 60 °C in air saturated 20 mM cyanide solutions. 243
Figure 6.17 – Evans' diagrams representing the leaching of gold/silver in air and oxygen saturated 20 mM cyanide solutions. 246
Figure 6.18 – Evans' diagrams representing the leaching of gold/silver in air saturated 20 mM cyanide solutions at pH 10.0 and 12.5. 249
Figure 6.19 – Rate of dissolution versus cyanide concentration with lead . 251
Figure 6.20 – Effect of lead on the oxidation of gold/silver..... 253
Figure 6.21 – Evans' diagrams representing the effect of lead on the leaching of gold/silver in air saturated 20 mM cyanide solutions..... 254

LIST OF TABLES

Table 1.1 – Stability constants and standard reduction potentials of a variety of gold complexes of metallurgical importance..... 4

Table 2.1 – Published values of the activation energy. 37
Table 2.2 – Variation in the measured critical cyanide concentration with different surface film characteristics. 41
Table 2.3 – The effect of lead on the dissolution of gold 45

Table 4.1 – Calculated flux of oxygen and cyanide to a rotating disc..... 104
Table 4.2 – Comparison of measured and calculated rates. 105
Table 4.3 – Calculated and measured mixed potentials and rates of dissolution of plated and solid gold 112
Table 4.4 – Rate of dissolution of gold as a function of temperature..... 127
Table 4.5 – Measured and calculated mixed potential and rate of dissolution of gold at 60 °C. 134
Table 4.6 – Effect of oxygen concentration on the dissolution of gold..... 136

Table 5.1 – Calculated and measured mixed potentials and rates of dissolution of gold in the presence and absence of lead. 164
Table 5.2 – Comparison of the dissolution rates in 7.5 and 20 mM cyanide solutions in the presence and absence of lead. 167
Table 5.3 – Calculated mixed potential and corrosion rate at the three intersection points between the anodic and cathodic curves 169
Table 5.4 – Effect of temperature on the dissolution of gold with lead 179
Table 5.5 – Effect of oxygen on the dissolution of gold with lead 186
Table 5.6 – Effect of some additives on the dissolution of gold..... 201
Table 5.7 – The effect of lead and silver on the rate of dissolution..... 203
Table 5.8 – Effect of oxygen on the dissolution of gold with silver..... 204

Chapter 1 – Introduction

1.1. Importance of Gold

Gold was the first metal known to humans (Eagleson, 1994), and in recorded times, it has also been the most sought after. Throughout history, gold has been regarded as a symbol of wealth, with the accumulation of gold being reported as early as 4000 BC (Eagleson, 1994). Our enchantment with gold originates from the unique properties of the metal: its ductility, lustre, colour, durability and availability in a relatively pure form. The value of gold is also accentuated by its rarity, comprising only 5×10^{-7} % of the earth's crust (Eagleson, 1994).

1.1.1. History and Uses of Gold

The human fascination with gold has continued into modern society, where golden jewellery and artefacts are still regarded as precious possessions. The use of gold in the fabrication of jewellery is continuing to increase, and over the last 10 years, the demand for this purpose has exceeded the annual mine production (Maxey *et al.*, 1997).

Gold has also been very important to the international monetary system over a number of decades. The use of gold as money has been recorded since 2000 BC (Eagleson, 1994), and from the 1870's until World War I, the gold standard was the major system of currency (Morgan, 1993). Today, gold is still accepted by all nations as a medium of international payment, and it is regarded as a reserve asset, with over 15 times the worlds annual production being held by the central banks and other financial institutions as backing for their currency (Morgan, 1993).

The use of gold in the electronics industry is becoming more widespread, and over the last ten years the demand for gold for this purpose has increased by 35 %. In 1995, 185 t of gold was sold for electronic purposes, representing 9.8 % of the

total mine production (Maxey *et al.*, 1997). Gold is especially useful in electronic applications where corrosion resistance is an issue, although its use in a range of different devices has been recorded. Such applications include thermoelements, contacts in semiconductors and switches, and solders. In many of these instances, gold is alloyed with other metals, such as copper, nickel, silver and palladium to improve its mechanical properties (Eagleson, 1994).

1.1.2. Production of Gold

The production of gold is an integral part of the history and economics of many nations around the world, and the impact of 'gold rushes' on countries such as Colombia, South Africa, the U.S.A and Australia is well documented. For example, during the gold rushes of the 1850's, Australia's non-aboriginal population increased from 400,000 to 1.15 million (Morgan, 1993). In the late 20th century, gold still has a large impact on the economies of many countries, and its production is dominated by four nations: South Africa, Russia, U.S.A, and Australia. South Africa alone accounts for 23 % of the worlds total production, while Australia's production accounts for 11% (Gold Fields Mineral Services, 1996).

In the past 15 years, the world has seen another gold boom, with western mine production increasing from 962 t in 1980 (Morgan, 1993) to 1890 t in 1995 (Maxey *et al.*, 1997). This modern 'gold rush' is due to two main factors: 1) the collapse of the Bretton Woods agreement in 1971, after which the price of gold increased by a factor of 10; and 2) the introduction of the efficient carbon in pulp extraction process. In Australia, gold has become the nation's second highest export earner, with sales in 1996 totaling A$5.5 billion (Department of Minerals and Energy, 1997). However, the gold industry is facing new challenges which threaten its value to the Australian economy. As the free milling ores are exhausted, the cost of processing is increasing, although the economic return has remained constant. Consequently, improving the efficiency of the traditional cyanidation process has become a major focus of gold research in the 1990's.

1.2. Chemistry of Gold

Gold is the most noble metal (Nicol, Fleming & Paul, 1987) and occurs naturally in the metallic form. Gold is not reactive in air, and is not corroded by strong acids or bases. The chemistry of gold in aqueous solution is related to its very low electrodeposivity, which is related to its standard reduction potential. The two most common oxidation states of gold are +1 (aurous) and +3 (auric), for which the standard reduction potentials are 1690 and 1500 mV respectively (Nicol, Fleming & Paul, 1987). These values are more positive than the standard reduction potential for water, 1230 mV (Bard, 1973), indicating that Au^+ and Au^{3+} are thermodynamically unstable in aqueous solution.

The aurous and auric cations can be stabilised by a number of ligands, including chloride and cyanide (Marsden & House, 1992). The reaction between the aurous ion (as an example), and a ligand, L^n with charge n (either positive or negative charge), can be represented by Equation 1.1, and the stability constant, β, for this reaction is given by Equation 1.2.

$$Au^+ + xL^n \rightarrow AuL_x^{1+nx} \qquad \textbf{Equation 1.1}$$

$$\beta = \frac{[AuL_x^{1+nx}]}{[Au^+][L^n]^x} \qquad \textbf{Equation 1.2}$$

The standard reduction potential of the gold complex, $E^O_{Complex}$, can be related to the standard reduction potential of the aurous ion, $E^O_{Au^+/Au}$ and the stability constant for the complex, β, by Equation 1.3,

$$E^O_{Complex} = E^O_{Au^+/Au} - \frac{RT}{F}\ln(\beta) \qquad \textbf{Equation 1.3}$$

where R is the universal gas constant (J K^{-1} mol^{-1}), T is the absolute temperature (K). and F is the Faraday constant (C mol^{-1}). It is clear that for large values of β (strong complexes), the gold complex will be thermodynamically stable in aqueous solution (E^O more negative than 1230 mV). Therefore, the aqueous chemistry of gold is dominated by the formation of a limited number of stable aurous and auric complexes.

There are a number of ligands which are known to form stable complexes with either the aurous or auric cations. Those which are of metallurgical importance are listed inTable 1.1, together with the stability constant and the standard reduction potential of their gold complexes. The complexes are listed in order of stability, of which the gold cyanide complex, $Au(CN)_2^-$, is the most stable (has the most negative E^O).

Complex	β	Reaction	E^O/mV
$Au(CN)_2^-$	2×10^{38}	$Au(CN)_2^- + e^- = Au + 2CN$	-570
AuS^-	2×10^{36}	$AuS^- + e^- = Au + S$	-460
$Au(HS)_2^-$	1.3×10^{30}	$Au(HS)_2^- + e^- = Au + 2HS$	-90
$Au(S_2O_3)_2^{3-}$	5×10^{28}	$Au(S_2O_3)_2^{3-} + e^- = Au + S_2O_3^{2-}$	150
$Au(thiourea)_2^+$	2×10^{23}	$AuTu_2^+ + e^- = Au + 2Tu^+$	352
$Au(CN)_4^{3-}$	$\sim10^{56}$	$Au(CN)_4^{3-} + e^- = Au + 4CN$	400
AuI_4^-	5×10^{47}	$AuI_4^- + 3e^- = Au + 4I^-$	560
$Au(SCN)_4^{3-}$	10^{42}	$Au(SCN)_4^{3-} + 3e^- = Au + 4SCN$	623
$AuBr_4^-$	10^{32}	$AuBr_4^- + 3e^- = Au + 4Br^-$	870
$AuCl_4^-$	10^{26}	$AuCl_4^- + 3e^- = Au + 4Cl^-$	1002

Table 1.1 – Stability constants and standard reduction potentials of a variety of gold complexes of metallurgical importance (after Zhang, 1997).

Due to its high stability, the gold cyanide complex, $Au(CN)_2^-$, is the most important of the gold complexes to hydrometallurgy. While other ligands, such as chloride and thiourea, have been investigated as alternative lixiviants in recent years, they have only ever been utilised in niche applications (La Brooy, Linge & Walker, 1994). Consequently, the remainder of this thesis will focus on cyanidation, and in the following section, a brief review of the cyanidation process is presented.

1.3. Processing of Gold by Cyanidation

The cyanidation process for gold was patented by MacArthur, Forrest and Forrest in 1888, and since then, has been the most important process in the extraction of gold from its ores. Shown in Figure 1.1 is a typical flowsheet for a modern cyanidation plant. Cyanidation, like all hydrometallurgical operations, involves two main processes: leaching and recovery. These two processes are labelled in Figure 1.1, and it can be seen that the recovery method used in this case is carbon in pulp (CIP) adsorption. CIP adsorption is the most commonly used recovery process in cyanidation, although many older plants, particularly those in South Africa, utilise filtration followed by zinc cementation. A discussion of the leaching and recovery processes of a cyanidation plant is presented in the following sections.

1.3.1. Leaching

The first step in any hydrometallurgical process is the leaching of a high value component, in this case gold, from the low value gangue material. In cyanidation, cyanide is employed as a lixiviant, and oxygen is utilised as an oxidant. The leaching of gold in cyanide solutions can be represented by the Elsner equation, in which the gold is dissolved to form the gold cyanide complex, $Au(CN)_2^-$.

$$4Au + 8CN^- + O_2 + 2H_2O \rightarrow 4Au(CN)_2^- + 4OH^- \qquad \textbf{Equation 1.4}$$

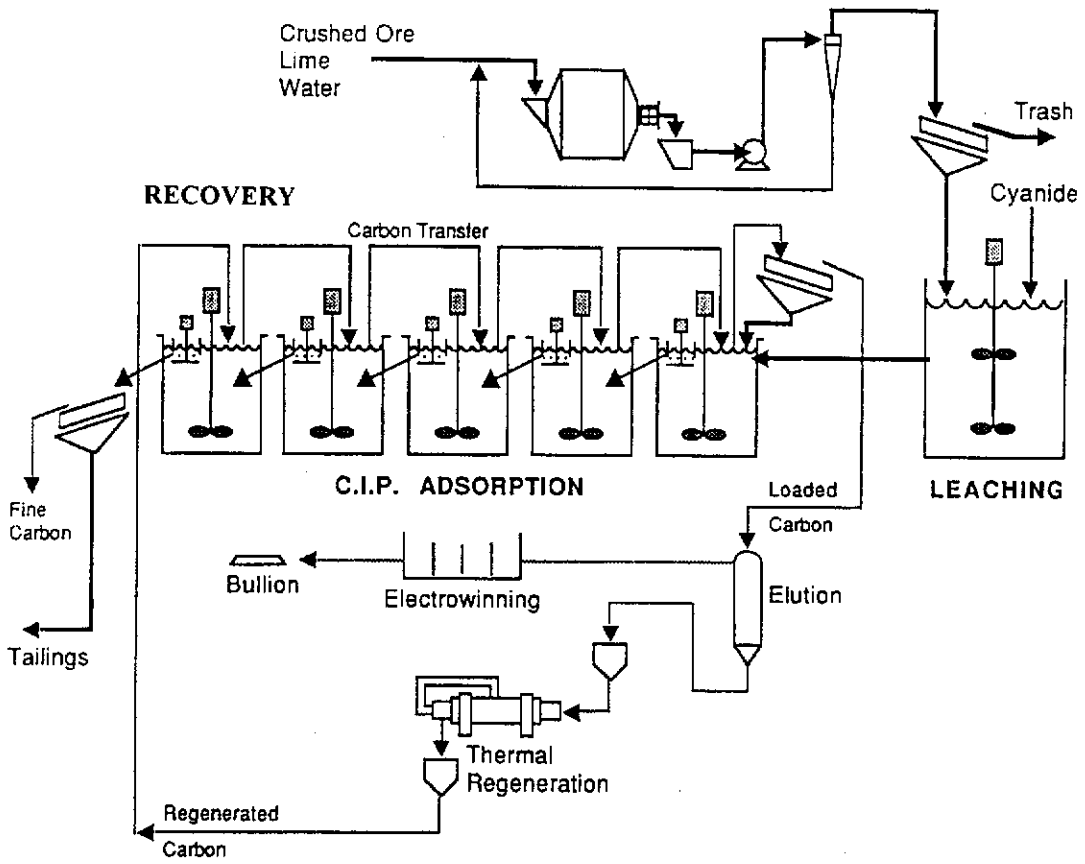

Figure 1.1 – Typical flowsheet for a cyanidation plant incorporating cyanide leaching and carbon in pulp adsorption as the recovery process.

In practice, the first step in leaching is the crushing and grinding of the ore in order to liberate the gold particles from their host mineral. After grinding and classification, a slurry of approximately 50 % solids is introduced into an agitated tank for the leaching process. The leaching is accomplished by bubbling oxygen through the slurry, to which cyanide and lime has been added. The most important aspects of cyanide leaching of gold are:

1) **Control of cyanide and oxygen concentrations:** If cyanide or oxygen are consumed by reactive minerals, then their respective concentrations can fall to low levels. Under these conditions, the leaching rate of gold will be low, and consequently the extraction of gold may decrease. In most modern gold plants, monitoring or control of cyanide and oxygen concentrations is accomplished by computerised control systems.

2) **Control of pH:** In cyanidation, the addition of lime is essential to prevent the volatilisation of toxic HCN, which has a pKa of 9.3 (Fleming, 1992). Most modern gold plants automatically control the pH via a control system. This prevents excess consumption of cyanide, and ensures that the gold plant is a safe working environment.

3) **Agitation:** During leaching, agitation is required to ensure that the slurry remains in suspension. It is also important as increasing the agitation rate increase the mass transfer rate of cyanide and oxygen to the gold particles. Increased leaching kinetics are often achieved by simply increasing the agitation of the slurry.

1.3.2. Recovery

Once the gold has been leached to form the gold cyanide complex, $Au(CN)_2^-$, the next step in cyanidation is the recovery of the gold. There are two main processes that have been used industrially for recovery of gold: cementation and carbon adsorption.

1.3.2.1. Cementation

For most of this century, zinc cementation in the form of the Merill-Crowe process, has been the most widely used process to recover gold from solution. The process involves a metal displacement reaction, where the zinc displaces the gold from solution, as shown in Equation 1.5.

$$2Au(CN)_2^- + Zn \rightarrow Zn(CN)_4^{2-} + 2Au \qquad \textbf{Equation 1.5}$$

Gold recovery by this route usually consists of two main steps, separation and cementation. In the first stage, the leach solution is separated from the pulp by counter current decantation or vacuum filtration. The solution is then clarified and degassed to remove the remaining solids and oxygen respectively. Zinc powder is then added to the solution, and the metallic gold produced is recovered by filtration.

The biggest drawback with the Merrill-Crowe process is the separation stage prior to cementation. Such a process is costly, and usually results in a loss of approximately 1% of the gold in solution (Fleming, 1992). These problems have led to the widespread development of the CIP process over the last 20 years, as discussed below.

1.3.2.2. Carbon Adsorption

Although the use of carbon adsorption to recover gold from solution was patented in 1894 (Johnson, 1894), the process was not significantly used on an industrial scale until the late 1970's. With the development of the carbon in pulp process, the use of carbon adsorption spread rapidly throughout South Africa in the late 1970's, and then throughout the world in the early 1980's (Fleming, 1992). The main advantage of the CIP process is that the leach solution does not need to be separated from the pulp in order for the recovery of the gold to be effected. Today, due to its relatively low capital and operating costs, the CIP process is the preferred method of recovering gold from leach solutions.

While the practical aspects of the CIP process are relatively simple, the mechanisms by which gold adsorbs onto carbon are unclear. Most of the evidence suggests that gold cyanide is co-adsorbed with cations, particularly calcium. However, it has been suggested that ion exchange with the functional carbon groups is also important. In any event, it has been shown that gold adsorbed onto the carbon without undergoing any chemical change (Zhang, 1997).

The CIP process is usually carried out in two steps, adsorption and elution, which are shown in detail in Figure 1.1. In the adsorption stage, granular activated carbon is agitated with the leaching slurry to ensure adequate mixing of the solution and carbon phases. The carbon is transferred counter current with the pulp through a number of tanks, during which the gold cyanide complex is adsorbed onto the carbon. The carbon is withdrawn from the first CIP tank, separated from the pulp by screening, and usually washed with hot hydrochloric acid. The gold is then eluted from carbon at high temperature by a solution containing sodium cyanide and sodium hydroxide. These conditions are known to favour the de-sorption of gold from the activated carbon (Fleming, 1992). Metallic gold is recovered from the eluate by electrowinning, and the carbon is thermally regenerated and rejoins the CIP circuit at the last tank.

1.4. Areas of Uncertainty in Leaching

Due to the widespread use of the cyanidation process, the leaching of gold in cyanide solutions has been studied on numerous occasions at both industrial and laboratory scale. Despite this, there is still some uncertainty over the rate at which the process proceeds. In some of the early studies, it was established that the leaching of gold in cyanide solutions was diffusion controlled (Kudryk, 1954). More recently though, it has been suggested that the reaction is chemically controlled, and as a result, the use of leach accelerators, such as lead (Weichselbaum, Tumilty & Schmidt, 1989) and some organic molecules (Trindade & Monhemius, 1993) has been advocated.

The leaching of gold in cyanide solutions is reviewed in detail in Chapter 2 of this thesis, and the areas discussed include the chemistry of the gold cyanide complex, and the kinetics and electrochemistry of gold in solutions containing cyanide. A brief review of the oxygen reduction half reaction is also presented in this chapter. In Chapter 3, the results obtained from an electrochemical investigation of oxygen reduction are presented, primarily to demonstrate how the reduction reaction varies with experimental conditions appropriate to cyanidation. In Chapter 4, the results from a kinetic and electrochemical study of the leaching of pure gold in cyanide solutions are presented and discussed, and in Chapters 5 and 6, the effect of solution and solid phase purity is discussed. Conclusions and recommendations are given in Chapter 7.

Chapter 2 – Review

2.1. Chemistry of Cyanidation

2.1.1. The Gold Cyanide Complex

The gold cyanide complex is the most stable of the gold complexes, and thus is of great importance to gold hydrometallurgy (Nicol, 1980a). The cyanide ion contains a triple bond between the nitrogen and carbon atoms, which consists of one σ bond and two π bonds (Wang & Forssberg, 1990). The stability of the gold cyanide complex is due to the strong π bonding between the d-orbital electrons of the gold ion and the π electrons of cyanide (Wang & Forssberg, 1990). The oxidation state of gold in the gold cyanide complex is gold(I), and the preferred co-ordination number is two (Nicol, Fleming & Paul, 1987). Therefore, $Au(CN)_2^-$ is a linear complex, with the carbon acting as a donor atom, and its chemical structure is shown in Figure 2.1.

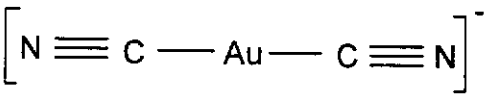

Figure 2.1

The very high stability constant of gold cyanide, 2×10^{38} M (Nicol, 1980a), ensures that the gold cyanide complex will not dissociate, even if the cyanide concentration is effectively zero. This aspect is important in hydrometallurgical operations, as the ligand concentration can be reduced without causing problems with dissociation of the gold complex.

2.1.2. Oxidation of Au to $Au(CN)_2^-$

The dissolution of gold to form the gold cyanide complex is an electrochemical process, which involves the oxidation of gold to gold(I). The oxidation of gold is shown in Equation 2.1, and the standard reduction potential for this reaction, E^0, is -570 mV (Nicol, Fleming & Paul, 1987).

$$Au + 2CN^- \rightarrow Au(CN)_2^- + e^- \qquad \textbf{Equation 2.1}$$

The thermodynamics of both chemical and electrochemical processes can be effectively examined with potential-pH diagrams, which are also referred to as Pourbaix diagrams (Pourbaix, 1963). Pourbaix diagrams are constructed from thermodynamic data, and thus represent the thermodynamic behaviour of the system considered. The application of Pourbaix diagrams to hydrometallurgical processes is well documented by Osseo-Assare, Xue and Ciminelli (1984). Figure 2.2 shows a Pourbaix diagram published by these authors for the gold-cyanide-water system at 25 °C. The dashed lines represent the reaction equilibria of water, with line (a) representing the reduction of water to hydrogen, and line (b) representing the oxidation of water to oxygen. The solid lines represent the thermodynamic boundaries of the specified species in solutions containing 10^{-4} M Au and 10^{-3} M CN^-. The area labelled (1) represents the conditions under which gold cyanide is stable in aqueous solutions. It is clear that under most conditions of potential and pH, the gold cyanide complex is the dominant species in aqueous solution. The area labelled (2) in the Pourbaix diagram represents the conditions under which gold metal is stable in contact with aqueous solution. It can be seen that at any pH, the stability regions for water and gold overlap. Therefore, water is not a sufficiently strong oxidant to oxidise gold to gold cyanide. Thus, an oxidant is required for the leaching of gold in cyanide solutions, and examples of oxidants which could be used to dissolve gold in cyanide solutions include oxygen, hydrogen peroxide, iron (III),

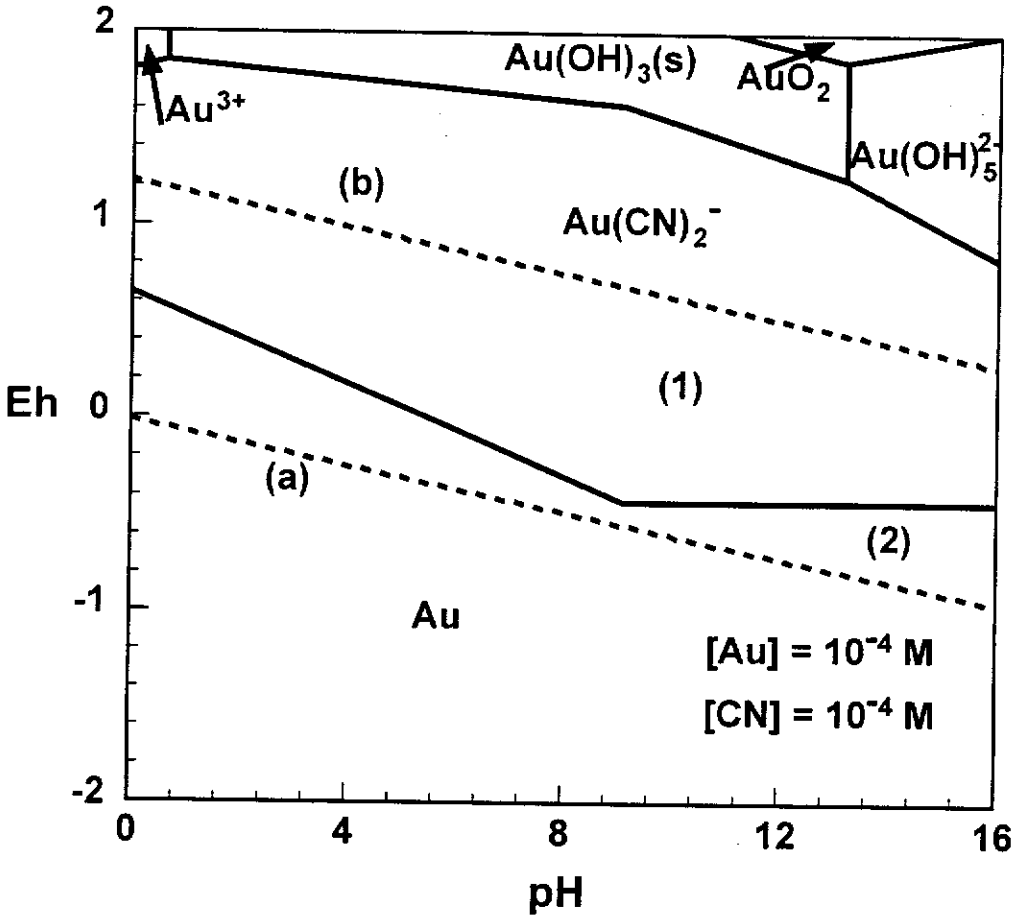

Figure 2.2 – Pourbaix diagram for the gold-cyanide-water system at 25 °C (after Osseo-Asare, Xue & Ciminelli, 1984).

permanganate, and hypochlorite. In the cyanidation process, the oxidant that is almost exclusively used is air/oxygen, although in a few cases, this is supplemented by hydrogen peroxide (Marsden & House, 1992).

2.1.3. Leaching of Gold in Aerated Cyanide Solutions

The oxidation of gold by oxygen in the presence of cyanide can be considered to be made up from two redox couples, as shown in Equation 2.2. The standard reduction potential for the reduction of oxygen to hydroxide at pH 14 is 401 mV (Bard, 1973), which is significantly more positive than the standard reduction potential of gold cyanide, -570 mV (Nicol, Fleming & Paul, 1987). Therefore, under standard conditions, gold should spontaneously react with oxygen and cyanide to form the gold cyanide complex.

$$4Au + 8CN^- \rightarrow 4Au(CN)_2^- + 4e^-$$
$$O_2 + 2H_2O + 4e^- \rightarrow 4OH^-$$

Equation 2.2

Under typical cyanidation conditions, the reduction potentials can be calculated using the Nernst equation. For the reaction O + ne^- —> R, the Nernst relationship is shown in Equation 2.3,

$$E = E^0 + \frac{RT}{nF} \ln\left[\frac{a_O}{a_R}\right]$$

Equation 2.3

where E^0 is the standard reduction potential (V), R is the universal gas constant (J mol^{-1} K^{-1}), T is the temperature (K), n is the number of electrons, F is the Faraday constant (C mol^{-1}), a_o is the activity of species O, and a_R is the activity of species R. In dilute aqueous solutions, the activities are often approximated by the solution concentrations. The activity of solid phase species is taken to be unity.

A typical cyanidation plant operates at 100 ppm CN^-, 1 ppm $Au(CN)_2^-$, 8 ppm oxygen and at a pH of 10.0 (AMIRA Project P420, 1995). Under these conditions, using the Nernst equation, the reduction potentials of gold cyanide and oxygen can be calculated to be -600 mV, and 580 mV respectively. The driving force of the overall reaction is thus 1180 mV. This potential is related to the Gibbs free energy, ΔG, by Equation 2.4 (Bard & Faulkner, 1980). Thus for gold cyanidation, the Gibbs free energy is approximately -114 kJ per mole of gold, and there is a very large thermodynamic driving force.

$$\Delta G = -nFE \qquad \textbf{Equation 2.4}$$

The leaching of gold in aerated cyanide solutions can occur by two possible mechanisms. Elsner (1846) proposed that the leaching reaction is the sum of the two half reactions shown in Equation 2.2. The leaching of gold in aerated solutions containing cyanide can thus be represented by Equation 2.5.

$$4Au + 8CN^- + O_2 + 2H_2O \rightarrow 4Au(CN)_2^- + 4OH^- \qquad \textbf{Equation 2.5}$$

Bodländer (1896) proposed that peroxide is formed as a product during the leaching of gold, and this reaction is shown in Equation 2.6. It is believed that some of the peroxide which is formed is then able to further react with gold, as shown in Equation 2.7, and the extent to which this reaction occurs depends on the leaching conditions. If all of the peroxide is reduced to hydroxide, then the reaction stoichiometry is identical to the Elsner equation, as shown in Equation 2.5.

$$2Au + 4CN^- + 2H_2O + O_2 \rightarrow 2Au(CN)_2^- + H_2O_2 + 2OH^- \qquad \textbf{Equation 2.6}$$

$$2Au + 4CN^- + H_2O_2 \rightarrow 2Au(CN)_2^- + 2OH^- \qquad \textbf{Equation 2.7}$$

2.2. Kinetics of Cyanidation

It was shown in the previous section that from the thermodynamics of the system, it can be predicted that when gold is immersed in an aerated solution containing cyanide, it should dissolve to yield the gold cyanide complex. In general, however, it is not possible to estimate reaction rates from thermodynamic information. Such information can only be obtained by measurement.

2.2.1. Methods of Studying Kinetics

Many authors have investigated the kinetics of cyanidation over the last 100 years, and thus, many different techniques have been used for the kinetic studies. It is therefore necessary to review these techniques in order to make a quantitative comparison of the published kinetic results. In this section, some of the methods for measuring leaching kinetics will be described. In any kinetic experiment, there are two main choices to be made: the sample geometry and agitation; and the analytical method by which the rate of consumption of reactants or the rate of appearance of products was determined.

2.2.1.1. Agitation and Sample Geometry

The majority of leaching reactions are mass transport controlled (Marsden & House, 1992), and therefore, the method that is used to stir the system is extremely important. In deciding upon the agitation method and sample geometry for the kinetic measurements, there are two factors which are critical, reproducible mass transfer and calculable mass transfer, i.e. mass transfer which can be represented by a mathematical expression. When conducting kinetic experiments, it is essential that the mass transfer conditions are reproducible from one experiment to the next. Only then is it possible to measure the effect of differing experimental conditions on the leaching rate. It is also advantageous if the mass transfer conditions are reproducible from one laboratory to the next. If this is the case, then the measured reaction rates

can be compared to the work of other authors. The ideal situation is when the mass transfer flux can be calculated, and compared with the reaction rates. If the reaction rate is equivalent to the mass transfer flux of reactants, then it can be concluded that the reaction is diffusion controlled under that particular set of experimental conditions.

The following sections illustrate some of the common techniques that have been used to measure leaching rates, and the techniques are evaluated in terms of reproducible and calculable mass transport.

(a) Rotating Disc

The rotating disc (RD), is a sample of the material with a flat disc surface, which is rotated about its central axis. It is constructed from a cylinder of the material of interest (in this case gold), which is encased in an inert material, such as an epoxy resin. The fluid flow to the disc surface is laminar over a wide range of conditions, and is very reproducible. Therefore, the kinetic results that are obtained from a RD can be compared to the work of other authors who have also used this technique. The RD has the added advantage that the flux of reactants to the disc surface can be calculated from a theoretical expression. Levich (1962) showed that the flux is a function of $\omega^{1/2}$, where ω is the angular rotation rate (s^{-1}), as shown in Equation 2.8. This is known as the Levich equation,

$$J_o = 0.62 D_o^{2/3} \nu^{-1/6} \omega^{1/2} [O] \qquad \textbf{Equation 2.8}$$

where J_o is the flux of species O (mol m^{-2} s^{-1}), D_O is the diffusion coefficient of species O in solution (m^2 s^{-1}), ν is the kinematic viscosity of the solution (m^2 s^{-1}) and [O] is the bulk solution concentration of species O (mol m^{-3}). Gregory and Riddiford (1956) have experimentally verified that the Levich equation has a high degree of accuracy.

(b) Rotating Cylinder

The rotating cylinder is of a similar construction to the RD, but the curved cylinder surface is exposed to solution instead of the flat disc surface. One advantage of the rotating cylinder is that all points on the surface of the cylinder have an equal linear velocity. Like the RD, the rotating cylinder also offers good reproducibility, and thus can be compared with other published work using this technique. The major disadvantage of the rotating cylinder is that there is no mathematical solution to the mass transfer flux to the cylinder surface. There is however, an empirical relationship that describes the mass transfer flux (Eisenberg, Tobias & Wilke, 1954). This relationship is only valid under certain conditions, and provided the fluid flow is turbulent, the flux can be represented by Equation 2.9.

$$J = 0.079u^{0.7}D_O^{0.644}\nu^{0.344}d^{-0.3}[O] \qquad \textbf{Equation 2.9}$$

where u is the peripheral velocity of the cylinder, d is the cylinder diameter, and the other variables are the same as defined for the Levich equation, Equation 2.8. Another disadvantage of the rotating cylinder is that during leaching, the surface is not equiaccessible. It has been shown that the mass transfer is enhanced at the ends of the cylinder, although this problem can be minimised by adding a length of inert material to the ends of the cylinder (Pang & Ritchie, 1981).

(c) Stirred Solution

The stirred solution is probably the cheapest and easiest method of promoting mass transfer to the solid surface, but unfortunately, is also the least reproducible. There are a number of forms of stirred solution agitation that have been used to measure leaching rates, including rolling bottles, impellor agitation and gas sparging. Each of these methods can give reasonably reproducible mass transfer for a particular experimental design, but the results cannot be compared to the work of other authors using different designs (Power & Ritchie, 1975). The kinetic data that is obtained from stirred solutions is consequently of less value. Using stirred

solutions, it is often difficult to determine whether a reaction is diffusion or chemically controlled. The interpretation of results from stirred solutions can present some problems, particularly when investigating the effect of agitation rate. With many agitation techniques, such as stirrers, the mass transfer flux reaches an upper limit at a certain critical stirring rate (Power & Ritchie, 1975). Thus, measuring kinetic data at stirring rates higher than the critical value can be misleading. The published results of Nadkarni *et al.* (1967), investigating cementation reactions, effectively demonstrate the problem in interpreting results from stirred solutions.

From the above discussion, it is clear that the RD is the best method of measuring leaching kinetics. Despite this, due to its simplicity the stirred solution is still commonly used in the measurement of cyanidation rates. Published kinetic data using each of these methods will be discussed later in this review, in which the advantages of the RD will become more apparent.

2.2.1.2. Analysis

The analysis of kinetic experiments can be split into two broad areas: loss of reactants and appearance of products. Each of these techniques have been used by authors in measuring cyanidation kinetics, and are discussed in detail below.

(a) Loss of Reactants

For gold cyanidation, there are three reactants: oxygen, cyanide and gold. The rate at which the reaction occurs can be estimated by analysis of the loss of one or more of these species with time. The measurement of the rate of consumption of oxygen or cyanide is not generally used to estimate the kinetics of cyanidation, as the analysis techniques are not accurate enough. However, these methods have been utilised in the measurement of the reaction stoichiometry of gold, oxygen and cyanide (e.g. Beyers, 1936, Kameda, 1949a), for which the appearance of gold cyanide is also measured. On the other hand, the measurement of the rate of loss of

gold has been used to estimate the gold leaching rate in many investigations in the past (e.g. Fink, 1950), and this technique is discussed in detail below.

It is clear that the most direct method of estimating the gold dissolution rate is to measure the rate of gold mass loss with time. The mass loss can be measured using two techniques: measuring the time required to dissolve a known mass of gold, and measuring the mass of gold as a function of time (using the quartz crystal microbalance). The traditional method of measuring the rate of mass loss is to measure the time required to dissolve a known mass of gold, usually gold foil. The main disadvantages with this technique is that it only allows for a single point measurement and a very large period is required to dissolve gold samples. Chronopotentiometry is a variation of the simple mass loss experiment, in which the time required to dissolve an electroplated film is measured. This method is well described by Zheng *et al.* (1996), and its advantages are that thin films can be used so that the experiments are very rapid, and information can be obtained about the leaching rate during the first few minutes of dissolution. To date, there have not been any reports of using this method to measure the leaching of gold in aerated cyanide solutions. This is probably because the electroplating efficiency of gold (in this work) has been found to vary, thus resulting in a variable quantity of deposited gold.

In the past, estimating the rate of dissolution of gold in cyanide solutions by mass loss has not been the favoured analytical technique. However, with the emergence of the quartz crystal microbalance (QCM) in recent years, the principle of measuring mass loss has become more attractive. Although the QCM has been used extensively to measure mass changes during processes such as adsorption and deposition, little work has been done on measuring leaching rates. This is because commercial quartz crystal microbalances, such as the Elchema Nanobalance, can only be purchased as a stationary system, and so stirred solutions must be used. However, recent work has been published on the measurement of leaching rates with a commercial QCM that had been converted into a rotating QCM (Zheng *et al.*, 1995). The advantage with this technique is that it is an *in situ* method which can measure very small mass changes (of the order of 1 ng). Therefore the leaching rates

can be measured with a great deal of accuracy and precision over a very short period, with sample intervals as low as one second. Consequently, the rotating QCM is the best method that is currently available for measuring leaching kinetics. The leaching of copper in cyanide solutions is an example which effectively demonstrates the advantages of the rotating QCM. It has been shown that the leaching is hindered in its initial stages, due the presence of an oxide film (Jeffrey *et al.*, in press). With any other technique, the sample period would be too long to observe such a characteristic. The rotating QCM is the method that is used throughout this thesis, and an overview of the technique is presented in Chapter 3.

(b) Appearance of Products

In the cyanidation process, the main reaction product is the gold cyanide complex, and measuring the rate of appearance of $Au(CN)_2^-$ has been the most used of the analysis techniques for estimating the dissolution rate of gold in cyanide solutions. This is because the analysis of gold is relatively easy, and modern techniques can detect minute changes in solution concentration (Hosking, 1982). The major disadvantage of measuring the appearance of $Au(CN)_2^-$ is that if leaching rates are low, experiments need to be run for a long period to produce detectable changes in solution concentration. This results in the measurement of the average rate of dissolution over the sampling period, and thus gives little information on how the rate changes with time. Such a problem can be reduced by using samples of large surface area, although for the investigation of gold cyanidation, this can become expensive. Nevertheless, in numerous investigations, the leaching rate has been estimated by measuring the appearance of gold cyanide in solution.

It is also possible to estimate the leaching rate by measuring the rate of appearance of the products of oxygen reduction, which are hydroxide if dissolution proceeds by the Elsner equation, and hydroxide and peroxide if dissolution proceeds by the Bodländer equation. To date, the analysis of either peroxide or hydroxide formation has not been used to estimate the leaching kinetics of gold in cyanide solutions. However, the measurement of peroxide has been used to determine

whether dissolution occurs by the Elsner or Bodländer equations (Bodländer, 1896, Kameda, 1949a).

2.2.2. Mechanistic Considerations

Once the kinetics of gold cyanidation have been determined, the mechanism by which the leaching occurs is usually considered. For leaching reactions, there are generally five steps involved in dissolution (Marsden & House, 1992):

(1) Mass transport of gaseous reactants into the solution phase;
(2) Mass transport of reacting species to the solid-solution interface;
(3) Mass transport of reacting species through the Nernst boundary layer;
(4) Electrochemical/chemical reaction at the solid surface;
(5) Mass transport of reaction products away from the surface.

The rate at which leaching occurs is equivalent to the slowest of the above steps, and in most cases, the maximum rate of dissolution that can be achieved is equivalent to the rate of mass transfer of reactants through the boundary layer (Marsden & House, 1992). Thus, to improve the kinetics of the reaction, it is beneficial to determine the nature of the limiting step for the process. For example, if step 4 controls the overall reaction rate, then the process is said to be chemically controlled, and marked improvements in kinetics can be achieved by increasing the system temperature. If any of the other steps controls the reaction rate, the process is said to be diffusion controlled, and increases in reaction rate can be simply achieved by increasing agitation of the solution (Marsden & House, 1992).

2.2.2.1. Mechanisms of Cyanidation

The dissolution of gold in cyanide solutions involves two solution phase reactants, oxygen and cyanide. Therefore, in assessing the possible mechanisms by which the dissolution rate can be limited, the mass transport of both oxygen and cyanide must be considered. The maximum rate of cyanidation can be limited by either the flux of cyanide or oxygen, depending on which is lower. For a rotating disc, it can be seen from the Levich equation that the cyanide and oxygen diffusion rates are proportional to the cyanide and oxygen concentrations respectively. Therefore, at a given cyanide and oxygen concentration, the maximum rate of dissolution can be readily calculated.

In practice, the solubility of oxygen in water is low, and so, cyanidation is usually carried out under conditions of air saturation. In this instance, the oxygen concentration is fixed, and the objective of the kinetic studies is to establish the optimum cyanide concentration. The following discussion details the effect of cyanide concentration on the dissolution rate. It will be shown that there is a critical cyanide concentration at which the rate becomes independent of cyanide concentration. A similar analysis can be performed for the effect of oxygen concentration at a fixed cyanide concentration, although this is not presented in this review, and the reader is referred to the paper by Zheng *et al.* (1995).

According to the Levich equation, a plot of cyanide flux versus cyanide concentration will be linear with a zero intercept and a slope that can be calculated from Equation 2.10. Hence, the flux of cyanide, J_{CN}, as a function of concentration can be readily calculated

$$\text{Slope} = \frac{J_{CN}}{[CN]} = 0.62 D_{CN}^{2/3} \omega^{1/2} \nu^{-1/6} \qquad \textbf{Equation 2.10}$$

where [CN] is the cyanide concentration (mol m^{-3}), D_{CN} is the cyanide diffusion coefficient (m^2 s^{-1}), ω is the rotation rate (s^{-1}), and ν is the kinematic viscosity of

solution (m^2 s^{-1}). Using a published value of 2.18×10^{-9} m^2 s^{-1} for D_{CN} (Guan & Han, 1994) the cyanide flux can be calculated for a given rotation rate. The kinematic viscosity enters the expression to the power of -1/6, and hence the flux is insensitive to changes in ν. Therefore, a value of 0.8904×10^{-6} m^2 s^{-1} for water at 25 °C was chosen for ν (Lide, 1995). To compare the cyanide diffusion rate with the maximum gold dissolution rate, the reaction stoichiometry must be considered. From Equation 2.5, it can be seen that the molar ratio of gold to cyanide is 0.5. Therefore, if all of the cyanide that reaches the surface is consumed, the gold dissolution rate, which will be termed the cyanide limiting rate, is equal to half of the cyanide flux. The cyanide limiting rate is plotted as a function of cyanide concentration, and is shown as line (a) in Figure 2.3. By similar analysis, the oxygen limiting rate can also be calculated. It should be recalled from section 2.1.3 that gold dissolution can follow either the Elsner or Bodländer equations, in which the stoichiometric ratio of gold to oxygen is 4 or 2 respectively. For air saturated solutions at 25 °C, the dissolved oxygen concentration is 0.25 mol m^{-3} (Kudryk, 1954) and given that the diffusion coefficient of oxygen is 1.94×10^{-9} m^2 s^{-1} (Guan & Han, 1994) the oxygen limiting rate can be estimated. The oxygen limiting rate is shown in Figure 2.3, where lines (b) and (c) represent the diffusion of oxygen when dissolution proceeds according to the Elsner and Bodländer equations respectively. It is clear that at low cyanide concentrations, the cyanide limiting rate is lower than the oxygen limiting rate, and thus the maximum rate of gold dissolution is equal to the cyanide limiting rate. At high cyanide concentrations, the converse is true. The cyanide concentration at which the oxygen limiting rate is equal to the cyanide limiting rate is defined as the theoretical critical cyanide concentration. This is the optimum cyanide concentration for a plant to operate at, as further increases in cyanide concentration do not result in an increase in leaching kinetics. So if gold leaching is mass transfer controlled, the dissolution rate will be cyanide diffusion limiting for $[CN^-] < [CN^-]_{crit}$, and oxygen diffusion limiting for $[CN^-] > [CN^-]_{crit}$. It is worth noting that the critical cyanide concentration for the Bodländer equation is exactly half the critical cyanide concentration for the Elsner equation. In the following discussion, the theoretical critical cyanide concentration will be calculated for each of these equations.

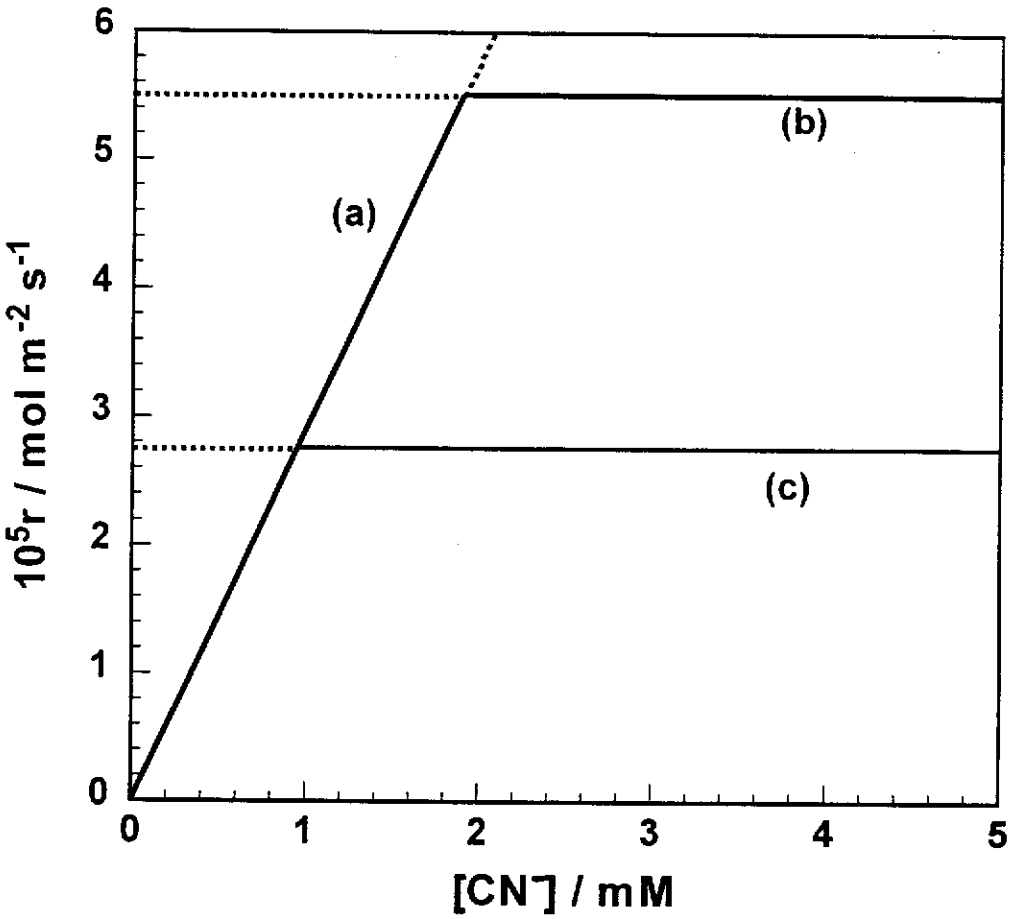

Figure 2.3 – The oxygen and cyanide limiting rates as a function of cyanide concentration. Line (a) represents the cyanide limiting rate, while lines (b) and (c) represent the oxygen limiting rate for the Elsner and Bodländer equations respectively. The solid lines represent the maximum gold dissolution rate.

The theoretical critical cyanide concentration can be calculated by combining the Levich equations for oxygen and cyanide diffusion, as these are equal at the critical cyanide concentration. The resulting equation (Equation 2.11) shows that the theoretical critical cyanide concentration for a RD is only dependent on the oxygen concentration of the system, the ratio of the diffusion coefficients, and the molar ratios of gold to oxygen, x_O, and gold to cyanide, x_{CN}. The molar ratio of gold to oxygen is 4 for the Elsner equation, and 2 for the Bodländer equation, while the molar ratio of gold to cyanide is 0.5. Using the values already specified in this chapter for the diffusion coefficients, the theoretical critical cyanide concentration is calculated to be 1.9 and 0.95 mM for the Elsner and Bodländer equations respectively (Zheng *et al.*, 1995).

$$[CN]_{crit} = \frac{x_O D_O^{2/3} [O_2]}{x_{CN} D_{CN}^{2/3}}$$

Equation 2.11

It should be noted that, as shown in Equation 2.11, the critical cyanide concentration is independent of the rotation rate, and therefore should be insensitive to the agitation method and sample geometry. Consequently, published critical cyanide concentrations which have been measured using a range of different techniques can be compared.

2.2.2.2. Factors Leading to Chemical Control

It is well known that electrochemical reactions can be complicated by the formation of stable surface films, and a classic example of such a situation is the dissolution of iron in nitric acid. In dilute solutions of HNO_3, iron is readily oxidised, and corrosion occurs at a high rate. In concentrated solutions of HNO_3, although the nitrate ion is a powerful oxidant, the reaction occurs at a low rate. The reason for this is that the higher oxidation potential results in the formation of a resistive film of iron oxide which blocks the surface of the iron (Power & Ritchie, 1983). It is believed that the surface of gold during cyanidation is blocked by a film of AuCN (Zheng *et al.*, 1995), and therefore, before discussing the published kinetic

data, it is essential to understand the effects that such a film will have on the dissolution rate. In the following discussion, Evans' diagrams are used to demonstrate the impact of a surface film on the gold dissolution mechanism for two experimental conditions: oxygen in excess of cyanide; and cyanide in excess of oxygen.

(a) Oxygen in Excess of Cyanide

It will be recalled from section 2.2.2.1, that for gold dissolution in cyanide solutions, there exists a critical cyanide concentration. At cyanide concentrations below the critical cyanide concentration, the rate of dissolution is dependent upon cyanide concentration, and at the gold-solution interface the concentration of oxygen exceeds the concentration of cyanide. The dissolution of gold under these conditions can be effectively represented by Evans' diagrams. For more detailed information on this aspect, a review of the application of electrochemistry in studying cyanidation is presented in section 2.3. Figure 2.4 shows an Evans' diagram for the dissolution of gold in the absence of a surface film, where the lines G1 and O represent the oxidation of gold and the reduction of oxygen respectively. The gold oxidation polarisation curve consists of two defined regions: 1) the Tafel region, where log|i| varies proportionally with E; and 2) the diffusion limited region, where log|i| is independent of E, and the oxidation rate is limited by the transport of cyanide from the bulk solution to the electrode surface. For the oxygen reduction polarisation curve, the diffusion limited region is not evident, as it occurs at a higher current density than that for gold oxidation (due to oxygen being in excess of cyanide). It is clear from Figure 2.4 that in the absence of a resistive film, the two polarisation curves intersect in the gold oxidation diffusion limited region, indicating that gold dissolution at low cyanide concentrations is cyanide diffusion controlled.

In the presence of a resistive surface film, the oxidation reaction is complicated by the iR drop between the anodic and cathodic sites. In addition, the diffusion of cyanide of also complicated by the film; the cyanide must diffusion through the film in order for the reaction to occur. In this instance, the gold oxidation

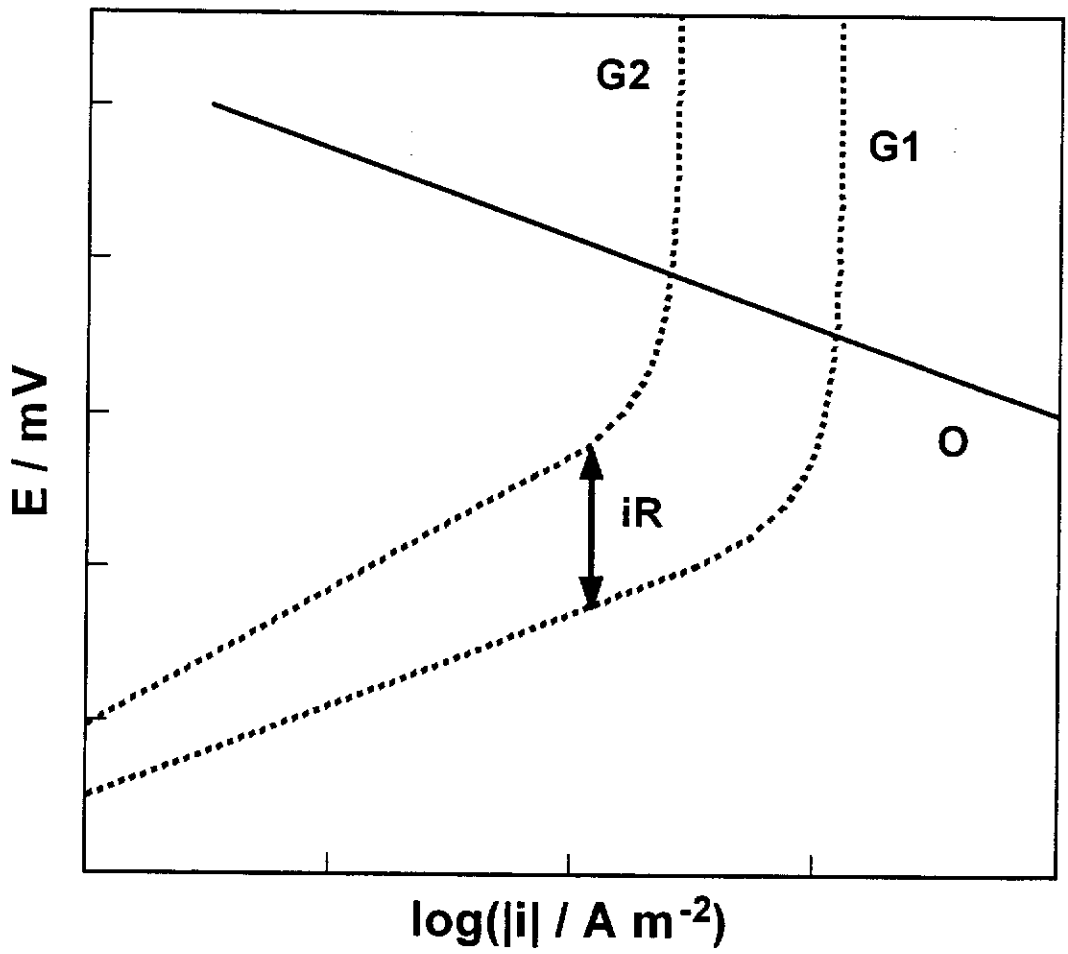

Figure 2.4 – Evans' diagrams representing the effect of a resistive film on the dissolution of gold in aerated cyanide solutions. Lines G1 and G2 represent the oxidation of gold in the absence and presence of the film respectively. Line O represents the reduction of oxygen. Experimental conditions: oxygen concentration in excess of cyanide.

polarisation curve in Figure 2.4 is represented by G2. The shape of the oxidation polarisation curve is similar to that in the absence of a resistive film, with the exception that the diffusion limiting current density is significantly lower. For simplicity, it is assumed that the oxygen reduction polarisation curve in the presence of the surface film is identical to that in the absence of the film. It is clear from Figure 2.4 that in the presence of a surface film, the two polarisation curves, G2 and O, intersect at a lower current density, and thus gold dissolution will occur at a lower rate. It is also interesting to note that the limiting step in this instance the diffusion of cyanide through the surface film, which will be referred to as *quasi* cyanide diffusion control. Therefore, in the presence of a surface film, the Evans' diagrams predict that the dissolution rate at low cyanide concentrations will be dependent on cyanide concentration.

(b) Cyanide in Excess of Oxygen

At cyanide concentrations above the critical cyanide concentration, the rate of dissolution is independent of cyanide concentration, and at the gold-solution interface the concentration of cyanide exceeds the concentration of oxygen. In a similar manner to the previous section, the dissolution of gold under these conditions can be represented by Evans' diagrams, as shown in Figure 2.5. In the absence of a resistive film, the oxygen reduction polarisation curve is represented by line O, and the gold oxidation polarisation curve is represented by line G1. As the concentration of cyanide is in excess of oxygen, the diffusion limited region for line O is evident, while that for line G1 is not. It is clear from Figure 2.5 that in the absence of a resistive film, the two polarisation curves, G1 and O, intersect in the oxygen reduction diffusion limited region. Therefore, at high cyanide concentrations, the Evans' diagram indicates that gold dissolution is oxygen diffusion controlled.

In the presence of a resistive film, the gold oxidation polarisation curve is represented by line G2. Under these conditions, it can be seen from Figure 2.5 that the gold oxidation and oxygen reduction polarisation curves intersect at a lower current density, indicating that the presence of a resistive film will result in a

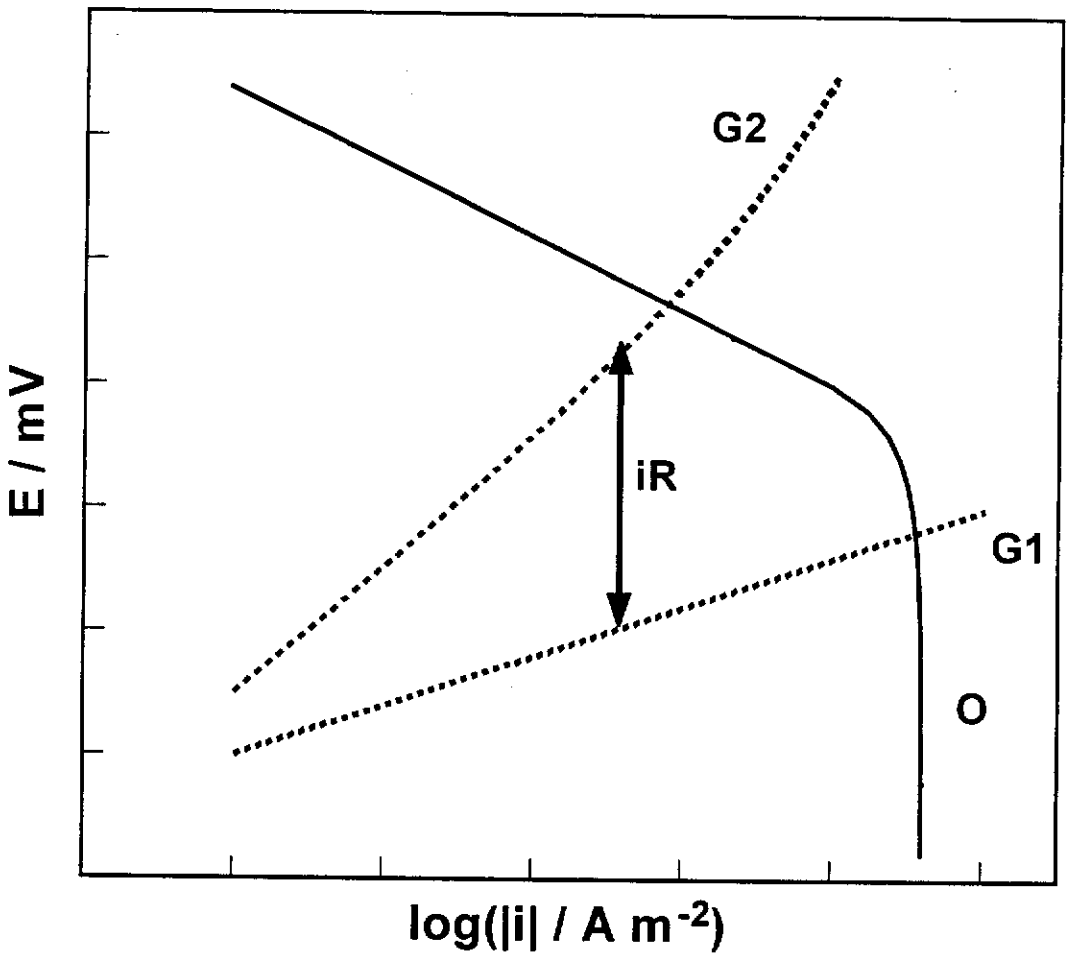

Figure 2.5- Evans' diagrams representing the effect of a resistive film on the dissolution of gold in aerated cyanide solutions. Lines G1 and G2 represent the oxidation of gold in the absence and presence of the film respectively. Line O represents the reduction of oxygen. Experimental conditions: cyanide concentration in excess of oxygen.

decrease in the observed dissolution rate of gold. It is also clear that in the presence of a surface film, the two polarisation curves intersect in the corresponding Tafel regions, and so oxygen diffusion is no longer the limiting step for dissolution. This is known as chemical control, and occurs when the reaction rate is limited by a slow surface step. Under these conditions, the gold dissolution rate will be independent of cyanide concentration and agitation.

2.2.2.3. Criteria for Diffusion and Chemical Control

In the previous two sections, the limiting step for gold dissolution was discussed, and it was shown that the reaction can be either diffusion or chemically controlled. The objective of this section is to detail the criteria for diffusion and chemically controlled reactions, and this involves investigating the kinetics of a reaction as a function of agitation rate, and measuring the activation energy for the process.

(a) Effect of Agitation

By definition, reactions which are mass transfer controlled across the Nersnt diffusion layer are dependent on agitation rate, while processes which are chemically controlled are not. Therefore, investigating the dissolution rate of gold as a function of agitation will demonstrate whether the process is diffusion or chemically controlled. If the kinetic studies are performed using a rotating disc electrode, then according to the Levich equation, the flux of reactants to the gold surface vary with the square root of rotation rate. Thus, for a diffusion controlled process investigated using a RD, a plot of dissolution rate versus $\omega^{1/2}$ will yield a straight line with a zero intercept. With the development of the RD, this has become one of the most straight forward criteria for distinguishing between diffusion and chemical control.

(b) Effect of Temperature

While a plot of the dissolution rate versus $\omega^{1/2}$ is a useful technique for differentiating between chemical and diffusion control, this method is only applicable to the RD. A more general method of differentiation is by calculating the activation energy for the process. According to the Arrhenius equation,

$$k = Ae^{-Ea/RT}$$ **Equation 2.12**

where k is the rate constant ($mol\,m^{-2}s^{-1}$), A is the frequency factor ($mol\,m^{-2}s^{-1}$), E_a is the activation energy ($J\,mol^{-1}$), R is the universal gas constant ($8.314\ JK^{-1}mol^{-1}$), and T is the absolute temperature (K) (Power & Ritchie, 1975). Clearly, a plot of ln(k) versus 1/T will yield a straight line with a slope of $-E_a/R$. According to Power and Ritchie (1975), the activation energy is a good guide to determining whether a process is diffusion or chemically controlled. These authors state that diffusion controlled processes usually have an activation energy of less than 25 $kJmol^{-1}$, while chemically controlled processes have an activation energy in excess of 25 $kJmol^{-1}$.

2.2.3. Published Kinetic Results

A review of the published kinetic data for gold cyanidation is presented below, and the discussion is split into two main sections. The first section focuses on the dissolution of gold in cyanide solutions, while the second section discusses the effect of different additives, including lead, on the dissolution of gold.

2.2.3.1. Dissolution of Gold

(a) Dissolution Rates

It can be recalled from section 2.2.1.1, that when kinetic data are obtained using a RD, the results of different authors can easily be compared, and the flux of

reactants can be calculated. For gold leaching in aerated solutions containing cyanide, the flux of cyanide and oxygen can be calculated from the respective Levich equations, which are shown in Equations 2.13 and 2.14. It is clear that the flux to a RD increases with concentration and rotation rate. Therefore to compare kinetic results, the experiments for each publication should have been performed at the same rotation rate, and cyanide and oxygen concentrations. This condition obviously does not often occur, and can be overcome in a number of ways, as outlined below.

$$J_O = 0.62 D_O^{2/3} \omega^{1/2} \nu^{-1/6} [O_2] \qquad \textbf{Equation 2.13}$$

$$J_{CN} = 0.62 D_{CN}^{2/3} \omega^{1/2} \nu^{-1/6} [CN^-] \qquad \textbf{Equation 2.14}$$

The first condition which must be considered when comparing published kinetic results is the effect of cyanide concentration. It is fortunate that for all the publications reviewed, with the exception of Lorenzen and van Deventer (1992), Pesic and Sergent (1991) and Chen, Lung and Wan (1980), the kinetics have been reported as a function of cyanide concentration. In every case, the rate of gold dissolution reaches a limiting value at high cyanide concentrations. Thus, differences in cyanide concentration between experiments are not important if the kinetic results are reported as the limiting dissolution rate at high cyanide concentrations. When comparing the published kinetic data, the effect of oxygen concentration must also be considered. Fortunately, all of the authors have measured the dissolution rate of gold in air saturated solutions at a similar temperature, and hence the oxygen concentration remains effectively constant. The third consideration with comparing published results is the effect of rotation rate. This problem can be overcome by plotting the gold leaching rates against $\omega^{1/2}$, and this graph is shown in Figure 2.6. As it is uncertain whether the kinetic results of Lorenzen and van Deventer (1992), Pesic and Sergent (1991) and Chen, Lung and Wan (1980) are actually limiting rates, these results are represented by different symbol (star). It is worth noting that in each of these investigations, the cyanide concentration is higher than the theoretical critical cyanide concentrations (1.9 and 0.95 for the Elsner and Bodländer equations respectively).

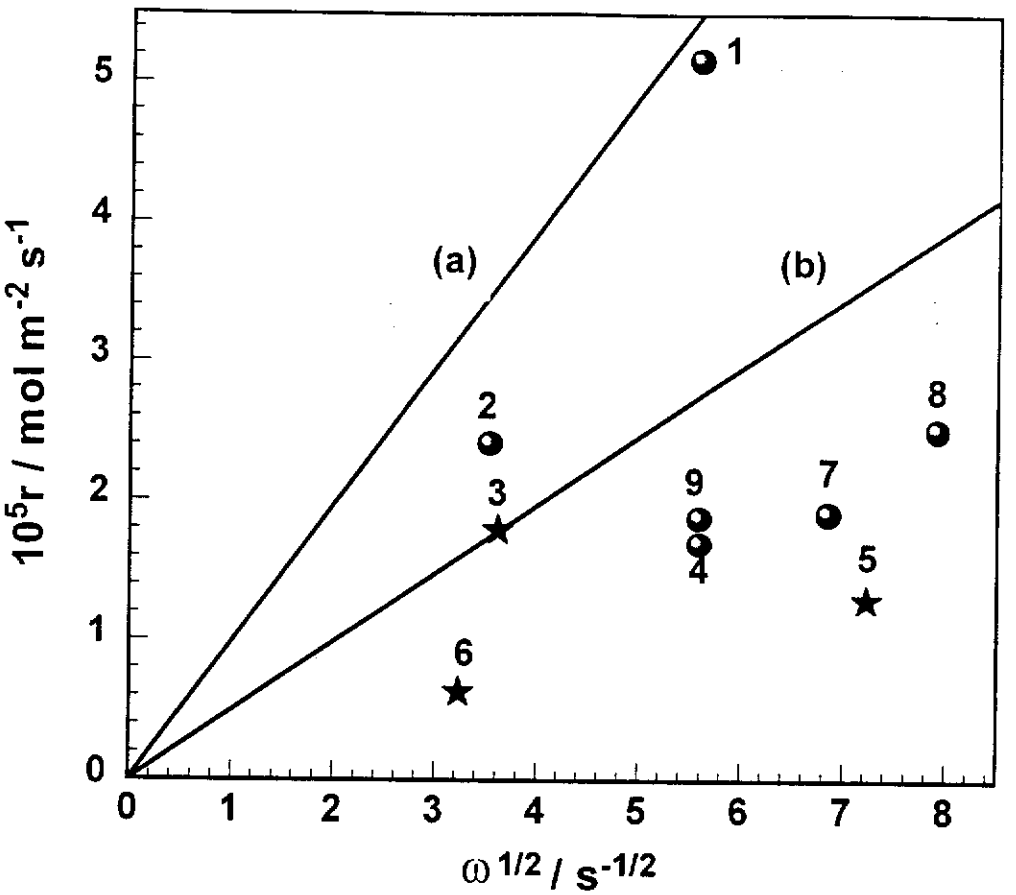

	Author		Author
1	Kudryk and Kellogg (1954)	6	Lorenzen and van Deventer (1992)
2	Kakovskii and Kholmanskikh (1960)	7	Guan and Han (1993)
3	Chen, Lung and Wan (1980)	8	Trindade and Monhemius (1993)
4	La Brooy, Komosa and Muir (1991)	9	Zheng *et al.* (1995)
5	Pesic and Sergent (1991)		

Figure 2.6 – Comparison of the published results of authors who have used rotating disc electrodes to study the kinetics of gold dissolution in air saturated cyanide solutions. The kinetic data are presented as the limiting dissolution rate (with the exception of the data with the star symbols), and are thus independent of cyanide concentration. The oxygen limiting rate is also shown as lines (a) and (b) for the Elsner and Bodländer equations respectively.

From Figure 2.6, it is clear that there is a significant variation in the measured rates from different authors, with the observed dissolution rates for the older work of Kudryk and Kellogg (1954) and Kakovskii and Kholmanskikh (1960), being significantly faster than the rates reported in the more recent publications. It has been suggested (Zheng *et al.*, 1995) that the differences in the published data are due to variations in the purity of either the gold or the solutions used in the kinetic studies. This aspect will be examined in detail in the experimental chapters to follow, where the dissolution rate will be measured under different conditions of solid and solution phase purity.

The published kinetic data in Figure 2.6 have been obtained from RD experiments, and thus, the measured kinetics can be compared with the mass transfer rates of reactants. The kinetic data which appear in Figure 2.6 are limiting dissolution rates, and hence are independent of cyanide concentration. Therefore, it is only necessary to compare the flux of oxygen with the published kinetic data. The flux is calculated from the Levich equation, Equation 2.13, using the values of D_O and $[O_2]$ already specified in this chapter. To compare the flux of oxygen with the dissolution rate of gold, the reaction stoichiometry must be known. It can be recalled from section 2.1.3 that leaching can occur by either the Elsner or Bodländer equations, for which the molar ratio of gold to oxygen is 4 or 2 respectively. The diffusion of oxygen is shown in Figure 2.6, with lines (a) and (b) representing leaching by the Elsner and Bodländer equations respectively.

It can be seen from Figure 2.6 that the work of Kudryk and Kellogg (1954) is close to line (a), suggesting that the dissolution of gold is diffusion controlled with the majority of oxygen being reduced to hydroxide under the specified set of conditions. The remainder of the results can be analysed by considering the processes that could lead to deviation from line (a). Take for instance, the work of Zheng *et al.* (1995). The measured rate of dissolution is below line (b), so a change in the reaction mechanism from the Elsner to Bodländer equations can not alone account for the observed lower dissolution rate. There are, however, three possibilities which can account for these results:

1) The surface is fully covered by a resistive film, and the rate of dissolution is reduced as a result of the iR drop across the film (as discussed in section 2.2.2.2). The dissolution rate published by Zheng *et al.* (1995) is reported at high cyanide concentrations, and so the presence of a film will lead to chemical control (see Figure 2.5). In this instance, the reaction rate will be independent of rotation.

2) The surface is partially blocked by a film, and only a proportion of the surface is reacting, for example pitting corrosion. In this instance, the reduced rate is due to a lower surface area, and the reaction rate will be dependent on agitation.

3) The surface is not covered by a film, and the dissolution rate is limited by a slow chemical or electrochemical step. In this case, the reaction rate will be independent of agitation.

To determine what causes the deviation from line (a) for all of the data shown in Figure 2.6, with the exception of the work of Kudryk and Kellogg (1954), it is necessary to further review the published data. In the following sections, the effect of agitation, temperature and cyanide and oxygen concentrations are discussed, and it will be shown that the published experimental results are consistent with passivation by a resistive film, as discussed above in 1.

(b) Effect of Agitation

There have been a number of kinetic studies of gold dissolution in cyanide solutions at rotating disc electrodes, and of those, some have published data on the effect of agitation. Zheng *et al.* (1995) have shown that for ω in the range of 300 to 900 rpm, the dissolution rate of gold is almost independent of rotation rate, and they concluded that the dissolution of gold in cyanide solutions is chemically controlled. This is supported by the work of Sheveleva and Kakovskii (1979), who have shown that the dissolution rate of gold is diffusion controlled at rotation rates below 100 rpm, while above 100 rpm, the process is chemically controlled. These results suggest that the low dissolution rates, as discussed in the previous section, are not a result of partial blocking of the gold surface (mechanism 2)

Guan and Han (1993) have investigated the effect of agitation on the dissolution of gold at 25 and 45 °C. At 25 °C, they found that the dissolution rate was independent of agitation, while at 45 °C, they found that a plot of rate versus $\omega^{1/2}$ was almost linear. Thus, they concluded that at 25 °C, gold dissolution in cyanide solutions is chemically controlled, while at 45 °C, the process is diffusion controlled.

(c) Effect of Temperature

A number of authors have measured the dissolution rate as a function of temperature, and consequently, the activation energy for gold dissolution in aerated cyanide solutions has been calculated on a number of occasions; these results are shown in Table 2.1. It is clear that most of the published values of E_a suggest that gold dissolution is diffusion controlled, which is in direct contradiction to the results of the previous section. This is a very interesting result, as most of the RDE studies have been performed recently, while the majority of the activation energies were measured a number of years ago. It is thus believed that the inconsistencies observed with these results is due to differences in the experimental conditions, in particular, variations in the purities of the solutions or gold used in the kinetic studies.

Author	Temperature Range	E_a / kJ mol^{-1}
Kudryk and Kellogg (1954)	27 - 66 °C	16
Cathro (1963)	30 - 60 °C	26
Kameda (1949a)	15 - 40 °C	22
Guan and Han (1993)	15 - 35 °C	60
Guan and Han (1993)	35 - 65 °C	22

Table 2.1 – Published values of the activation energy for the dissolution of gold in aerated cyanide solutions.

The results by Guan and Han (1993) are very interesting, as they predict that the dissolution of gold is chemically controlled at low temperatures, and diffusion

controlled at high temperatures. This is not uncommon for heterogeneous systems, and can be easily explained with the aid of Figure 2.7. Line (a) represents a diffusion controlled process, while line (b) represents a sequential chemically controlled process. It is clear that, as the slope of line (b) is more negative than line (a), the two lines will intersect at a certain temperature. Therefore, at low temperatures, process (b) is slower than process (a), and hence, the overall reaction is chemically controlled. At high temperatures, the converse is true.

(d) Effect of Cyanide Concentration

It can be recalled from section 2.2.2.1 that the critical cyanide concentration is believed to be relatively insensitive to sample geometry and agitation method. Thus, the measured critical cyanide concentrations reported in a wide range of publications can be readily compared, and this comparison is shown in Figure 2.8. Also shown are the lines (a) and (b), which are the theoretical critical cyanide concentrations for the Elsner and Bodländer equations respectively. It is clear that there is a large variation in the published values of the critical cyanide concentration. The critical cyanide concentrations reported by Kudryk and Kellogg (1954), Kakovskii and Kholmanskikh (1960) and Guan and Han (1993) are close to the theoretical value for the Elsner equation, while the other published values are higher than expected and show a large scatter. It should be recalled from section 2.2.3.1, that Kudryk and Kellogg (1954), and Kakovskii and Kholmanskikh (1960) found that gold dissolution was diffusion controlled, and therefore, it is not surprising that the measured values of $[CN^-]_{crit}$ are close to the calculated ones.

For the remainder of the published results, interpreting the unexpectedly high critical cyanide concentrations can provide information on the dissolution mechanism. If the gold surface is blocked by some form of film, the critical cyanide concentration will reflect the way in which this film impedes the reaction of cyanide and oxygen with the surface. Shown in Table 2.2 are the different possible properties of a surface film on gold in aerated cyanide solutions, and how these properties can affect the critical cyanide concentration.

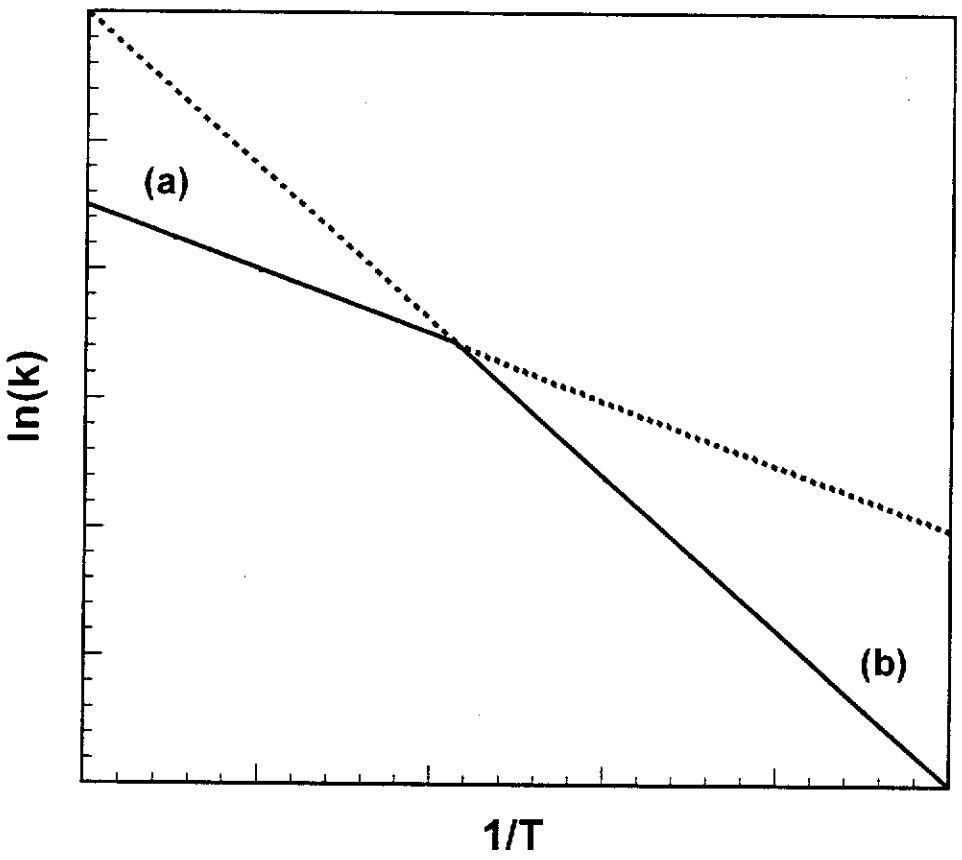

Figure 2.7 – Schematic diagram showing the change in the activation energy with an increase in temperature. Lines (a) and (b) represent a diffusion and chemically controlled process respectively. The solid line represents the expected rate – temperature response of the system.

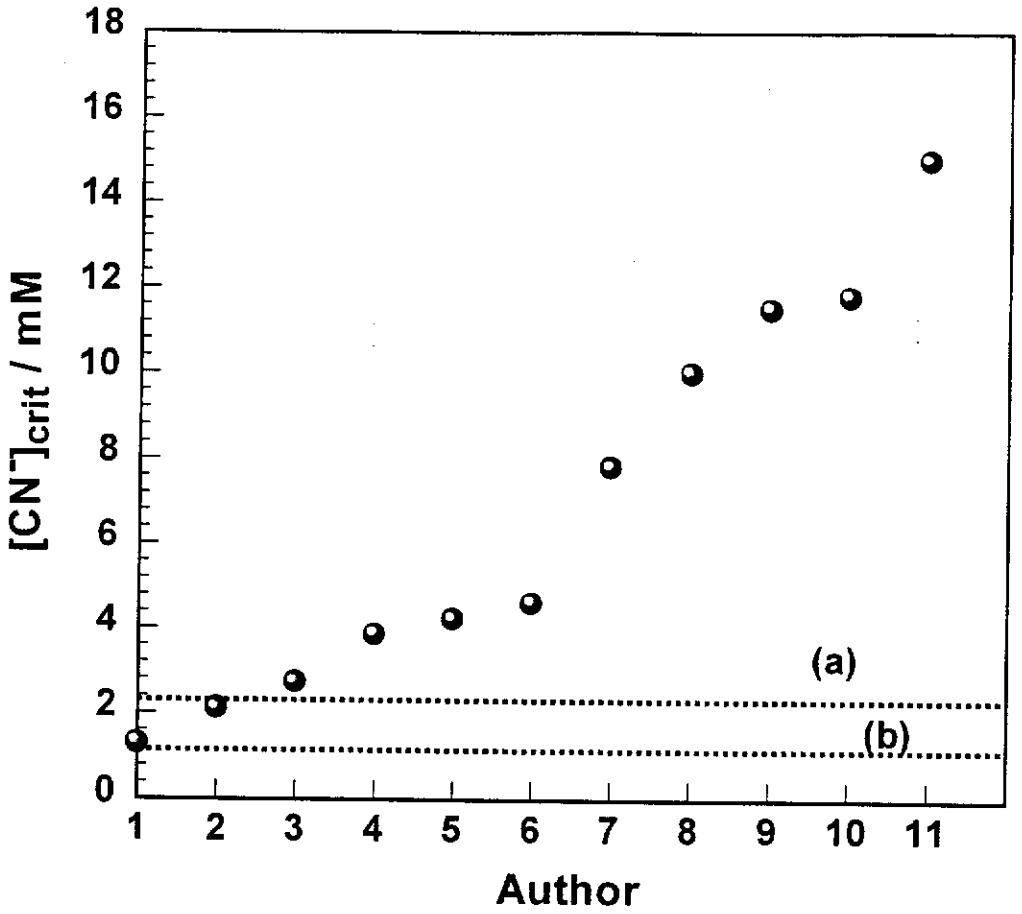

	Author		Author
1	Kakovskii and Kholmanskikh (1960)	7	Churchill and Laxen (1966)
2	Guan and Han (1993)	8	Trindade and Monhemius (1993)
3	Kudryk and Kellogg (1954)	9	Beyer (1936)
4	Barksy, Swainson, and Hedley (1934)	10	La Brooy, Komosa and Muir (1991)
5	White (1919)	11	Zheng *et al.*, (1995)
6	Kameda (1949a)		

Figure 2.8 – Comparison of the reported values of the critical cyanide concentration for the dissolution of gold in air saturated cyanide solutions. Lines (a) and (b) represents the theoretical critical cyanide concentration for the Elsner and Bodländer equations respectively.

System	$[CN^-]_{crit}$
Blocking action of film is independent of $[CN^-]$.	=Theoret. $[CN^-]_{crit}$
Blocking action of film decreases with increasing $[CN^-]$.	> Theoret. $[CN^-]_{crit}$
Blocking action of film increases with increasing $[CN^-]$.	< Theoret. $[CN^-]_{crit}$

Table 2.2 – Variation in the measured critical cyanide concentration with different surface film characteristics.

It is clear that the critical cyanide concentration will be higher than the theoretical value only if the film is more passive at low cyanide concentrations. Further information about such a film will be discussed in section 2.3.2.1, where oxidation of gold will be presented. It has been proposed that the anodic reaction is blocked by the formation of AuCN (Nicol, 1980a), and thus for the dissolution reaction to proceed, the AuCN must react with a further CN^- molecule, as shown in Equation 2.15.

$$Au + CN^- \rightarrow AuCN \xrightarrow{+CN^-} Au(CN)_2^- \qquad \textbf{Equation 2.15}$$

At low cyanide concentrations, there is little cyanide to dissolve the film as $Au(CN)_2^-$. In this instance, the film of AuCN will be relatively thick. Coversely, at high cyanide concentrations, the film will be considerably thinner. It is thus clear that the blocking action of AuCN is dependent on cyanide concentration. Consequently, the majority of published values of the critical cyanide concentrations are consistent with the surface being blocked by a film of AuCN.

(e) Effect of Oxygen Concentration

It will be recalled from Equation 2.11 that the critical cyanide concentration increases linearly with oxygen concentration. For example, in oxygen saturated solutions, where the oxygen concentration is 1.28 mM (Fogg & Gerrard, 1991), the theoretical critical cyanide concentration when gold dissolution follows the Elsner

equation, is 9.7 mM, as compared to 1.9 mM for air saturated solutions. Thus care must be taken when comparing published results on the effect of oxygen concentration, as at high oxygen concentrations, the process may be cyanide diffusion limited rather than oxygen diffusion limited. To ensure that the dissolution remains oxygen diffusion limiting when the oxygen concentration is increased from $[O_2]_1$ to $[O_2]_2$, it is a simple matter to show from Equation 2.11 that

$$[CN^-] \geq [CN^-]_{crit} \times \frac{[O_2]_1}{[O_2]_2} \qquad \textbf{Equation 2.16}$$

where $[CN^-]_{crit}$ is the critical cyanide concentration measured at an oxygen concentration of $[O_2]_1$.

The best method of assessing the published kinetic data on the effect of oxygen concentration on the dissolution of gold is to compare the proportional increase in rate relative to that in air saturated solutions, with the corresponding proportional increase in oxygen concentration. In this way, the effect of sample geometry and agitation method are minimised. Figure 2.9 shows a plot of the ratio of dissolution rates, r/r_{air}, versus the ratio of oxygen concentrations, $[O_2]/[O_2]_{air}$, for a change in oxygen concentration from air saturated to a concentration designated $[O_2]$. Line (a), which extends from the origin at 45°, signifies a linear increase in the rate of dissolution with oxygen concentration, although it should be noted, that data correlating to line (a) does not necessarily imply that the reaction is oxygen diffusion controlled under these conditions.

It is clear from Figure 2.9 that the effect of oxygen concentration on the dissolution rate of gold in cyanide solutions shows considerable variability. The majority of the published results show that increasing the oxygen concentration increases the rate of dissolution, although the work of Guan and Han (1993) has shown that increasing the oxygen concentration actually decreases the rate. For each of the data points, the condition set out in Equation 2.16 is satisfied, and thus, any variations in Figure 2.9 are not due to a change in dissolution mechanism from

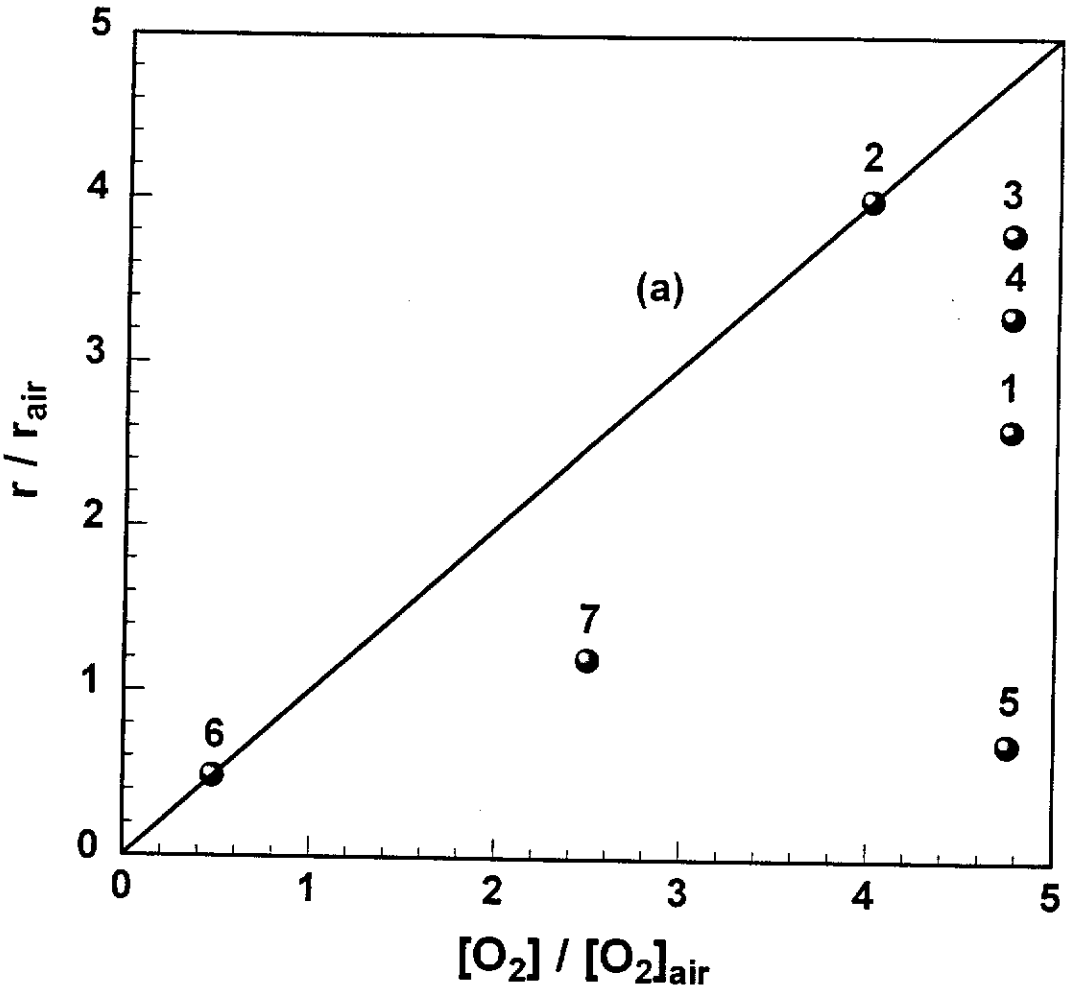

Label	Author	Label	Author
1	Kameda, (1949a)	5	Guan and Han (1993)
2	Kudryk and Kellogg (1954)	6	Zheng *et al.* (1995) low oxygen
3	Cathro and Koch (1963)	7	Zheng *et al.* (1995) high oxygen
4	Sheveleva and Kakovskii (1979)		

Figure 2.9 – Comparison of the published kinetic data on the effect of oxygen on the dissolution rate of gold. Line (a) represents a linear increase in dissolution rate with an increase in oxygen concentration.

oxygen to cyanide diffusion control. It is therefore believed that the large variation in the results, as in the previous sections, is due to differences in either solid or solution phase purity.

2.2.3.2. Dissolution in the Presence of Additives

It has been shown throughout this chapter that gold dissolution in cyanide solutions is not well understood, and many of the published kinetic results are contradictory. It will be shown in the experimental chapters of this thesis that the variation in these results is almost certainly due to purity variations within the system. It was therefore decided to review the effect of additives on the kinetics of gold dissolution in cyanide solutions. Fink and Putnam (1950) have shown that lead, thallium, bismuth and mercury can enhance the dissolution rate of gold, while sulfide ions can retard the dissolution process. The action of these ions has also been reported on a number of other occasions (e.g. Beyers, 1936, Lorenzen, 1992, Weichselbaum, Tumilty & Schmidt, 1989). Of these additives, this thesis is most concerned with the effect of lead. Therefore, the remainder of the review on gold leaching kinetics will focus on the effect of lead on the dissolution of gold in cyanide solutions, a topic which is investigated in detail in Chapter 4.

A number of authors have published data on the effect of lead on the dissolution of gold in cyanide solutions, and these are summarised in Table 2.3. The data is presented as the ratio r_{Pb}/r, where r_{Pb} and r represent the dissolution rate in the presence and absence of lead respectively.

Author	[Pb] /ppm	[CN^-] /mM	r_{Pb}/r
Beyers (1936)	2.5	15	1.2
Lorenzen and van Deventer (1992)	6.4	3.1	1.2
Sheveleva and Kakovskii (1979)	0.4	10	1.3
Kameda (1949b)	0.3	5	1.3
Liu and Yen (1995)	Galena[1]	3.8	3.9
Fink and Putnam (1950)	6.3	20	4

[1] Ground galena added as a source of lead

Table 2.3 – Published data on the effect of lead on the dissolution of gold in aerated cyanide solutions.

Some of the published data in Table 2.3 show that lead increases the dissolution rate by 20 to 30 %, while other published data, for example Fink and Putnam (1950), show that lead increases the dissolution rate by a factor of 400 %. In the reviewed literature, there are no suggestions as to the cause of this variation, although, as outlined in the following discussion, significant evidence has been published on the mechanism by which lead affects gold cyanidation.

Kameda (1949b) has extensively investigated the leaching of gold in a solution containing cyanide and lead, and has shown that during dissolution, lead is present on the surface of gold. It was also demonstrated that the enhancing effects of lead on gold dissolution were observed when the gold sample was removed from the leach solution and placed in a fresh lead-free leach solution. It was thus concluded that the action of lead was to modify the surface of the gold. Fink and Putnam (1950) also investigated the action of lead, and they calculated that lead was more noble than gold under typical cyanidation conditions. Therefore, they concluded that the role of lead was to modify the gold surface by cementation. A number of other authors investigating the effect of lead on cyanidation have also reached this conclusion (e.g. Nicol, 1980a, Weichselbaum, Tumilty & Schmidt, 1989, Sheveleva, 1979).

It is generally believed that the effectiveness of lead is dependent on leaching conditions, such as pH, and cyanide and oxygen concentration. The effect of lead on the dissolution of gold in cyanide solutions under different experimental conditions is summarised below.

(a) Effect of Cyanide and Lead Concentrations

It has been established that both the cyanide and lead concentrations are important to the effectiveness of lead, and it is generally agreed that gold dissolution in cyanide solutions can either be enhanced or retarded, depending on the relative concentrations of lead and cyanide (Habashi, 1967). Beyers (1936) found that the dissolution rate was enhanced providing that the cyanide concentration was above 10 mM, and Fink and Putnam (1950) have shown that lead is ineffective at low cyanide concentrations. Sheveleva and Kakovskii (1979) also noted this, and they attributed the retarding action to the formation of high valency lead compounds, which block the gold surface. A number of authors, including Beyers (1936), Sheveleva and Kakovskii (1979) and Lorenzen and van Deventer (1992), have observed a similar retarding effect at high lead concentrations. Thus, it has been concluded that the ratio of cyanide to lead is important to the dissolution mechanism, and there is a critical ratio where the dissolution behaviour changes from retarded to enhanced compared to the lead free system (Habashi, 1967, Lorenzen, 1992, Weichselbaum, Tumilty & Schmidt, 1989).

(b) Effect of pH and Oxygen Concentration

The effect of pH and oxygen concentration on the dissolution of gold in solutions containing cyanide and lead has been studied on a number of occasions (e.g. Fink, 1950, Habashi, 1967, Beyers, 1936). It has been found that in solutions with either high concentrations of oxygen or with a pH above 11.5, lead does not increase the dissolution rate of gold (Sheveleva, 1979, Fink, 1950). Therefore, it is believed that lead only enhances gold dissolution under a narrow range of pH, and cyanide, lead and oxygen concentrations.

2.3. Electrochemistry of Cyanidation

It has been known since 1947 that gold cyanidation is a corrosion process (Thompson, 1947), and thus the process can be readily studied using electrochemical techniques. Like all electrochemical processes, cyanidation occurs as a result of two redox half reactions, the oxidation of gold and the reduction of oxygen. The oxidation of gold is shown in Equation 2.17, and it is believed that the reduction of oxygen can occur by two mechanisms, as shown in Equations 2.18 and 2.19 (Evans, 1963). It is worth noting that on combining the gold oxidation half reaction, Equation 2.17, with the oxygen half reactions, Equations 2.18 and 2.19, the overall reaction will be described by the Elsner and Bodländer equations respectively.

$$Au + 2CN^- \rightarrow Au(CN)_2^- + e^- \qquad \textbf{Equation 2.17}$$

$$O_2 + 2H_2O + 4e^- \rightarrow 4OH^- \qquad \textbf{Equation 2.18}$$

$$O_2 + 2H_2O + 2e^- \rightarrow 2OH^- + H_2O_2 \qquad \textbf{Equation 2.19}$$

To investigate a process electrochemically, each constituent half reaction can be studied independently. For cyanidation, studies of gold oxidation and oxygen reduction are performed separately, and therefore each of these reactions is reviewed. This section of the review is split into three main sections. The first section details how cyanidation can be studied electrochemically. The second section reviews published results on the gold oxidation half reaction, while the final section briefly reviews the oxygen reduction half reaction.

2.3.1. Mixed Potential Theory

Any corrosion reaction, such as gold cyanidation, can be represented by two redox half reactions. One of these half reactions must involve oxidation, which for cyanidation is the oxidation of gold to gold cyanide, and the other half reaction must involve reduction, which for cyanidation is oxygen reduction to peroxide or

hydroxide. Mixed potential theory involves studying each of the constituent half reactions independently; for example, gold oxidation must be studied in the absence of oxygen. The electrochemical characteristics of each half reaction is studied by measuring the current density as a function of electrode potential, most often using linear sweep voltammetry, and the resultant plot is often called a polarisation curve (Power & Ritchie, 1983). Figure 2.10 shows a schematic diagram of gold oxidation and oxygen reduction polarisation curves. These curves comply with the IUPAC convention where anodic current densities are considered to be positive, and cathodic currents densities negative (Power & Ritchie, 1983).

It is shown in Figure 2.10 that the polarisation curves can be considered to consist of three defined areas, E_R, T and i_L as marked for the anodic polarisation curve. The potential marked E_R is the rest potential, and is simply the potential at which no net reaction occurs, i.e. no current flows. As the potential is increased in the positive direction, the current density increases exponentially with potential. This is often referred to as the tafel region, and is denoted T. In this region, the rate of gold oxidation is usually controlled by a chemical or electrochemical reaction. At high overpotentials, the current density reaches a limit, i_L, where the rate of gold oxidation is controlled by the diffusion of cyanide to the surface of the electrode. Therefore, further increases in potential do not result in an increase in current density (Power & Ritchie, 1983).

Once the anodic and cathodic polarisation curves have been measured, they can be superimposed, as shown in Figure 2.10. For a corrosion reaction, the anodic and cathodic currents must always be equal. The potential at which this condition is satisfied is called the mixed potential, E_m, or the corrosion potential, E_{corr}. The anodic and cathodic current densities are equal at this potential, $i_A = i_C$, assuming the anodic and cathodic areas are equal, and are often called the corrosion current. This is equivalent to the corrosion rate. Therefore, from mixed potential theory, the rate of reaction and the mixed potential can be easily estimated. Mixed potential theory can also be used to determine the rate determining step for the process (Power & Ritchie, 1983). It is clear from Figure 2.10 that, in this case, the rate of reaction is controlled by the diffusion of the oxidant to the electrode surface.

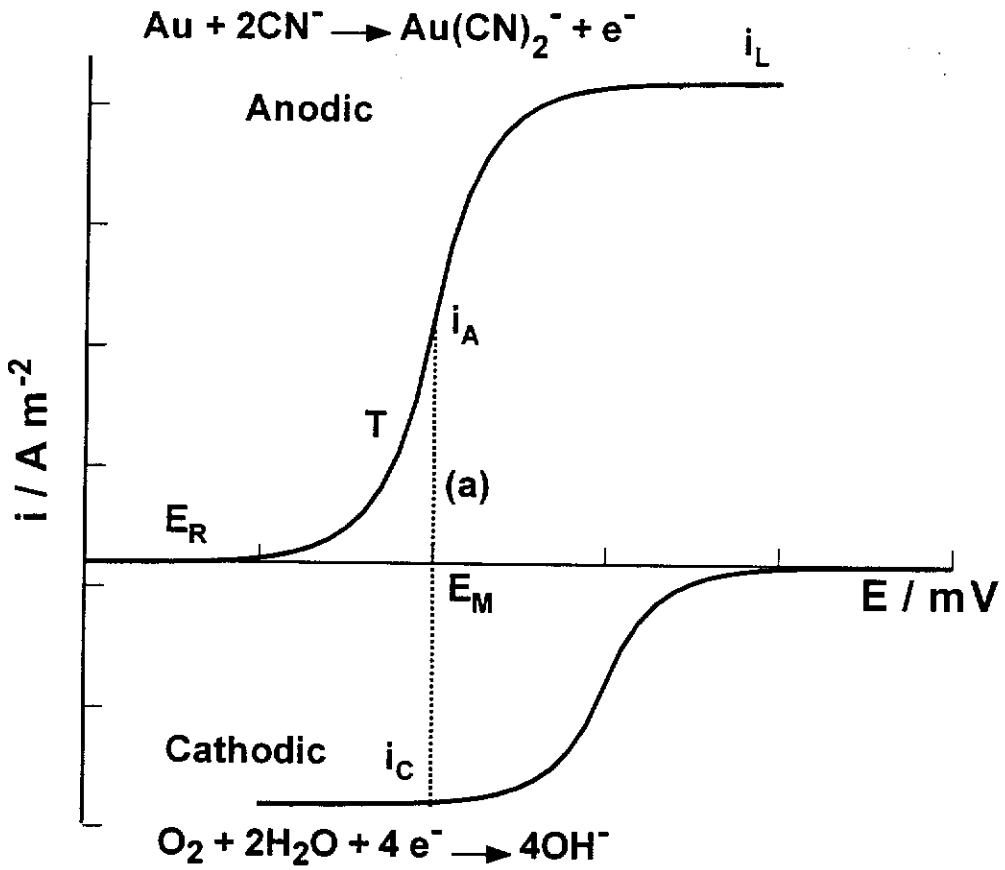

Figure 2.10 – Schematic diagram showing the polarisation curves for the oxidation of gold and the reduction of oxygen. The rest potential is designated E_R, the Tafel region T, the diffusion limiting current density i_L. When combining the anodic and cathodic curves, the mixed potential, E_M, and corrosion current density, $i_A = i_C$ can be estimated.

Kudryk and Kellogg (1954) were the first investigators to apply mixed potential theory to the leaching of gold in cyanide solutions. They found that the measured kinetic data and mixed potentials matched very well with the mixed potential and rate of dissolution for cyanidation of gold which was estimated from mixed potential theory. They also showed that the dissolution rate was controlled by the diffusion of oxygen to the gold surface.

2.3.2. The Gold Oxidation Half Reaction

The gold / gold cyanide half reaction has been investigated on a number of occasions, due to its importance in the leaching and electroplating of gold. The bulk of the publications report the use of linear sweep voltammetry (Nicol, 1980a) to study the oxidation of gold, although other techniques, such as impedance spectroscopy (Rogozhnikov & Bek, 1987), and scanning tunneling microscopy (STM) (Sawaguchi *et al.*, 1995) have also been utilised. STM, which allows *in situ* imaging of surfaces, is complementary to electrochemical techniques, and has provided valuable information regarding changes to the state of the surface during the oxidation process, as discussed later in this review.

Since the pioneering work of Kudryk and Kellogg (1954), many authors have published polarisation curves for gold oxidation in cyanide solutions. Before detailing the great variation in the reported curves, it is of value to examine the characteristics of one of the more recently published polarisation curves. Figure 2.11 shows the polarisation curve published by Bek, Rogozhnikov and Kosolapov (1997) for the oxidation of gold. It will be apparent that, unlike the schematic diagram shown in Figure 2.11, gold oxidation does not exhibit a limiting current density due to cyanide diffusion. Instead, the gold oxidation current density is low at potentials more negative than -50 mV, and given that the standard reduction potential of $Au(CN)_2^-$ is -570 mV (Nicol, Fleming & Paul, 1987), this represents a large overpotential, $\approx$ -520 mV. The inactive nature of gold in cyanide solutions at low

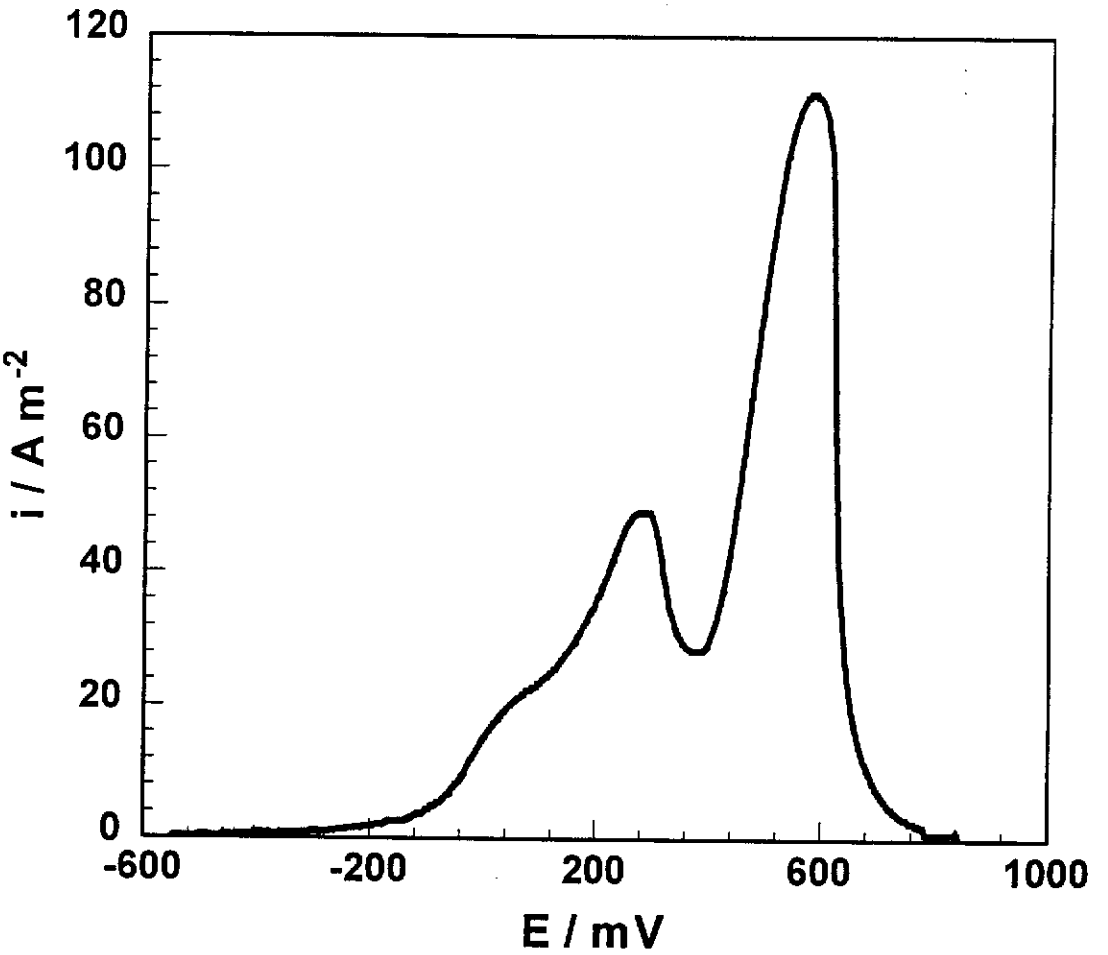

Figure 2.11 – The gold oxidation polarisation curve published by Bek, Rogozhnikov and Kosolapov (1997). Experimental conditions: 0.1 M KCN, 0.1 M KOH, 0.002 M $Au(CN)_2^-$, 7.5 rpm, Scan rate = 2 mVs^{-1}.

overpotentials is surprising, as the oxidation of other metals, such as silver and copper, in cyanide solutions is diffusion controlled (Hiskey & Sanchez, 1990, Guan & Han, 1994). Bek, Rogozhnikov and Kosolapov (1997) believed that an adsorbed cyanide species blocks the gold surface, and prevents oxidation from occurring at low overpotentials. At potentials more positive than -50 mV, the current density increases with potential, suggesting that the blocking film which is present at low overpotentials has been removed, allowing oxidation to occur. When the potential reaches approximately 250 mV though, the current density begins to decrease. As the electrode is rotating, the decrease in current density indicates that the dissolution of gold has been partially blocked, which is known as partial passivation (Kiss, 1987). At 400 mV, the blocking film is removed from the electrode surface, and in the potential range 400 to 600 mV, the current density increases with potential. At potentials more positive than 600 mV, the gold is fully passivated, and the current density drops to zero. A detailed discussion on each of the oxidation peaks appears later in this section, where the polarisation curves published by other authors are compared.

It will be recalled from section 2.2.1.1, that kinetic experiments which are performed using the rotating disc system can be compared to the calculated mass transfer of reactants, and also the published results from other authors. In a similar manner, the published polarisation curves measured at rotating discs by different authors can be readily compared, and the diffusion limiting current density can be calculated. For the gold / gold cyanide half reaction, cyanide is the only solution phase reactant, and the cyanide diffusion limiting current density can be calculated from the electrochemical form of the Levich equation, as shown in Equation 2.20 (Bard & Faulkner, 1980).

$$i_L = 0.5 \times 0.62 n F D_{CN}^{2/3} \nu^{-1/6} \omega^{1/2} [CN] \qquad \textbf{Equation 2.20}$$

where i_L is the diffusion limiting current density (A m^{-2}), n is the number of electrons involved in the oxidation of one atom of gold, F is the Faraday constant (C mol^{-1}), and the other symbols are the same as defined previously. In this instance,

the factor of 0.5 is used to correct for the stoichiometric ratio of cyanide to gold. A quantitative comparison of the gold oxidation polarisation curves measured using the rotating disc system can then be performed by plotting the dimensionless current, i/i_L versus E, and the resultant graphs are shown in Figure 2.12. It is clear that there is a large variation in the measured potential-current response of gold in cyanide solutions. The polarisation curve of Dorin and Woods (1991) is the only published data that exhibits a diffusion limiting current, for which the magnitude of i/i_L is close to one, indicating that the current is limited by cyanide diffusion. The remainder of the published polarisation curves comprise two or three oxidation peaks, labelled (a), (b) and (c), for which i/i_L is less than one. From these results, two conclusions can be obtained: 1) as the electrode is rotating, the presence of oxidation peaks, rather than plateaus, at −400, 300 and 600 mV corresponds to passivation of the gold surface; and 2) The oxidation of gold under these conditions is chemically controlled. The activation energy for each of the oxidation peaks has been measured by Thurgood *et al.* (1981), and the values for each of the peaks were found to be 93, 51 and 17 kJ mol^{-1} respectively. These results suggest that the oxidation of gold in the region of the first two peaks is chemically controlled, a result which agrees with the published polarisation curves shown in Figure 2.12. Conversely though, the activation energy for the third peak suggests that the oxidation is diffusion controlled, while the polarisation curves in Figure 2.12 suggest that it is chemically controlled. Given the observed variation in i/i_L, 0.55 to 0.84, for peak (c), it is not surprising that the studies of Thurgood *et al.* (1981) do not agree with the literature data presented in Figure 2.12.

While comparing gold oxidation polarisation curves measured using a rotating disc system is extremely useful, some qualitative information can also be obtained by comparing polarisation curves measured using a range of different agitation techniques. Nicol (1980a) has made such a comparison for a range of publication prior to 1980, and this graph is shown in Figure 2.13. In this instance, it is difficult to quantitatively compare the data by different authors, although, like in Figure 2.12, it can be seen that there is considerable variation in the published results. For the polarisation curves shown in Figure 2.13, with the exception of the

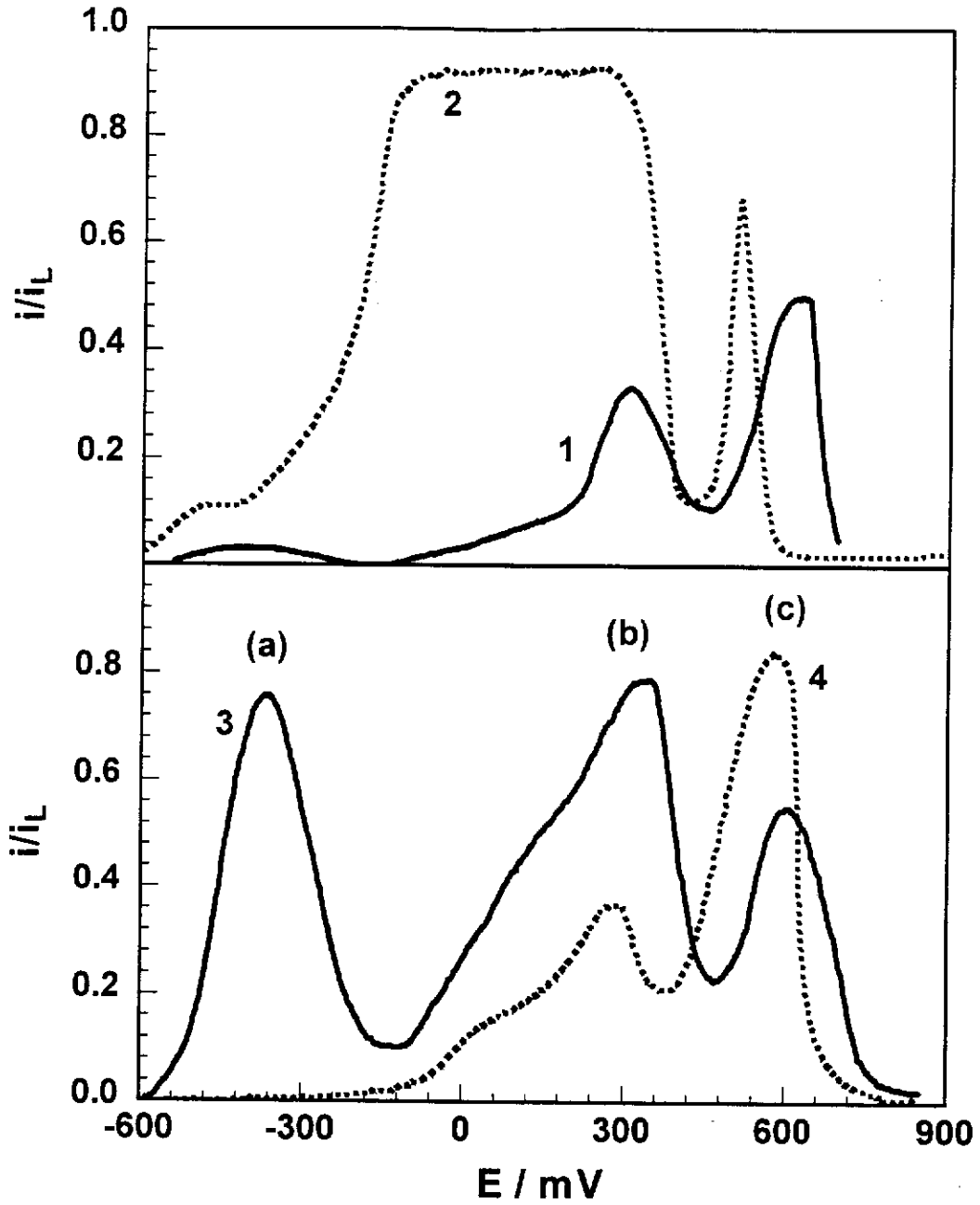

	Author		Author
1	Nicol (1980b)	3	Guan and Han (1994)
2	Dorin and Woods (1991)	4	Bek, Rogozhnikov and Kosolapov (1997)

Figure 2.12 – Comparison of the published gold oxidation polarisation curves measured using the rotating disc system.

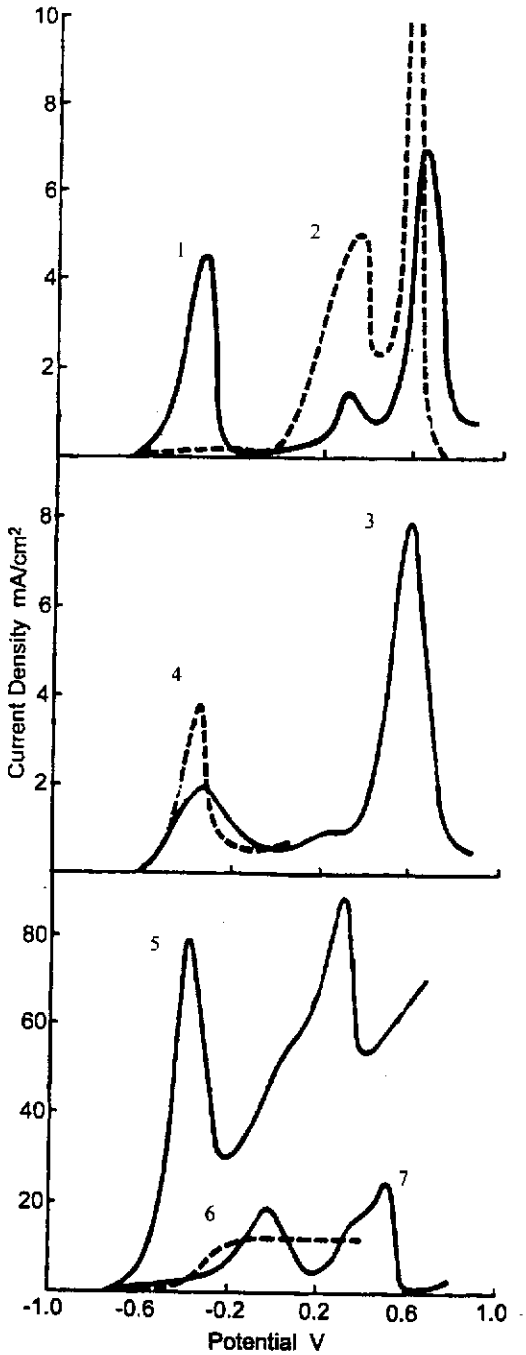

1	Cathro and Koch (1964)	5	Eisenmann (1978)
2	Kirk, Foulkes and Graydon (1978)	6	Kudryk and Kellogg (1954)
3	Pan and Wan (1979)	7	Mac Arthur (1972)
4	Cathro (1963)		

Figure 2.13 – Comparison of the gold oxidation polarisation curves published prior to 1980 for a number of authors (after Nicol, 1980a).

results of Kudryk and Kellogg (1954), the three passivation peaks at -400, 300 and 600 mV are evident. These three gold oxidation peaks will be discussed individually in the following sections, and reasons suggested for the observed variations in the published results will be evaluated. The main emphasis will be placed on peak (a), as gold cyanidation only occurs at potentials lower than 0 mV.

2.3.2.1. Peak at -400 mV

The discussion of the oxidation peak at -400 mV, which follows below, is split into three main sections. In the first section, peak identification is discussed, and then the reasons for the variation in the peak current density are evaluated. The conditions under which gold is passive or active are discussed in the second and third sections respectively.

(a) Peak Identification

One problem with electrochemical measurements is that although the reaction rate can be easily measured, it is not always possible to determine which species is being oxidised or reduced. For example, with gold in cyanide solutions, the oxidation of cyanide, which has a standard reduction potential of -970 mV (Bard, 1973), needs to be considered. By simultaneously measuring the rate, r, of appearance of $Au(CN)_2^-$ in solution, and the oxidation current density, i, Kirk *et al.* (1979) have shown the peak at -400 mV is a gold oxidation peak. The authors also estimated that 0.85 moles of electrons were transferred for every mole of $Au(CN)_2^-$ produced, which was lower than the expected value of 1 mole of electrons per mole of $Au(CN)_2^-$. They concluded that another process was occurring simultaneously with gold oxidation, such as hydrogen evolution, as shown in Equation 2.21. It is also possible that trace levels of oxygen in solution affected their results.

$$2Au + 2HCN + 2CN^- \rightarrow 2Au(CN)_2^- + H_2 \qquad \textbf{Equation 2.21}$$

Once it has been established that the peak at -400 mV is due to gold oxidation, it is possible to examine the properties of the peak in detail. It can be seen from Figure 2.13, that the gold oxidation peak at -400 mV shows the largest variation in current density from one publication to the next. In fact, in some of the more recent publications, such as the work shown in Figure 2.11 (Bek, Rogozhnikov & Kosolapov, 1997), this peak does not exist, and the gold remains completely passive. The large variation in the height of the peak at -400 mV is discussed in detail below. It is worth noting that as cyanidation occurs at low overpotentials, the observed variation in the peak current density can explain why the published kinetic data, discussed in section 2.2.3.1, also show large variations.

Nicol (1980a) showed that the oxidation peak at -400 mV was not present if the potential scan was initiated immediately after the gold was placed in solution. On the other hand, if the electrode was allowed to stand at open circuit for 30 minutes under enhanced mass transport conditions, i.e. fast rotation, the oxidation peak was observed. Bek, Rogozhnikov and Kosolapov (1997) have published similar results, and concluded that: 1) gold is passive in pure solutions at low overpotentials and; 2) the presence of trace elements in the leach solution can accumulate at the gold surface and remove the passivation, thus allowing the gold to oxidise. These features of the gold oxidation peak at low overpotentials are discussed in detail in the following sections. Given that the oxidation peak at -400 mV is only observed in the presence of trace levels of impurities, it is not surprising that there is a large variation in the published polarisation curves at low overpotentials.

(b) Passivation of Gold at Low Overpotentials

The passivation of gold at -400 mV is believed to result from the formation of a surface film, and it is generally agreed that this surface film is a form of gold cyanide (Nicol, 1980a, Bek, Rogozhnikov & Kosolapov, 1997). Kirk (1979) proposed that oxidation in this potential region occurred in three steps, as shown in Equation 2.22, and it is believed that the rate of oxidation is controlled by the second step. Other authors, including Cathro and Koch (1964), Pan and Wan (1979), and MacArthur (1972), have agreed that the oxidation of gold proceeds by the

mechanism shown in Equation 2.22, and that the second step is rate determining. Surface studies have also been used to confirm the mechanism shown in Equation 2.22, and these results are discussed in detail below.

$$Au + CN^- \xrightarrow{\text{adsorption}} AuCN^-_{ads} \qquad \text{Step 1}$$
$$AuCN^-_{ads} \xrightarrow{\text{oxidation}} AuCN_{ads} + e^- \qquad \text{Step 2}$$
$$AuCN_{ads} + CN^- \xrightarrow{\text{desorption}} Au(CN)^-_2 \qquad \text{Step 3}$$

Equation 2.22

The first step in the dissolution of gold, the adsorption of cyanide, has been studied in detail on a number of occasions. Poškus and Agafonovas (1995) have measured the surface coverage of cyanide on gold as a function of potential by tracing ^{14}C radioactively labelled CN^- ions. They showed that approximately a monolayer of cyanide was adsorbed onto gold at low overpotentials. Similar results have also been obtained using other techniques, including fourier transform infrared reflection-adsorption spectroscopy (FT-IRRAS) (Kunimatsu *et al.*, 1988), grazing incidence infrared spectroscopy (McCarley & Bard, 1992), surface enhanced Raman spectroscopy (SERS) (Mahoney & Cooney, 1985, Baltruschat & Heitbaum, 1983), and electrochemical impedance spectroscopy (EIS) (Rogozhnikov & Bek, 1996).

The second step in the dissolution mechanism presented in Equation 2.22, the formation of $AuCN_{ads}$, has been studied in detail by Sawaguchi *et al* (1995). By using a combination of scanning tunnelling microscopy (STM), low energy electron diffraction (LEEDS) and Auger emission spectroscopy (AES), they showed that a layer of $AuCN_{ads}$ was formed on the surface of the gold at low overpotentials. They concluded that during the oxidation process, the gold surface would be likely to be blocked by a layer of $AuCN_{ads}$. Nicol (1980a) has suggested that the surface is actually blocked by a film of AuCN (rather than an adsorbed layer), which could be of a polymeric nature with the cyanide ion acting as a bidendate ligand. Such a compound, which can be denoted $[AuCN]_X$ is known to exist, and is often formed upon the reaction of $Au(CN)^-_2$ with strong acids (Nicol, Fleming & Paul, 1987). It has been suggested that during the dissolution process, such a compound could form in two dimensions to block the surface of the gold (Nicol, 1980a).

(c) Activation of Gold at Low Overpotentials

It will be recalled from Figures 2.12 and 2.13. that some of the published polarisation curves show that gold is active at low overpotentials. It is therefore essential to review the conditions under which the gold is not completely passivated by a film of AuCN. A number of authors, including Bek, Rogozhnikov and Kosolapov (1997), and Nicol (1980a) have shown that trace levels of impurities, such as lead, prevent the passivation of gold at low overpotentials. This is demonstrated in Figure 2.14, which is a polarisation curve published by Nicol (1980a) for the oxidation of gold in 0.1 M cyanide solutions containing 1×10^{-6} M (0.2 ppm) Pb^{2+}. It is clear that at low overpotentials, lead activates the gold surface, resulting in an additional oxidation peak at -400 mV. Nicol (1980a) has shown that during the oxidation process, the gold surface is modified by a layer of underpotentially deposited lead. It is thus believed that the lead, which is present on the gold surface, in some way disrupts the formation of the passive AuCN film, thus enabling the cyanide ions to access the gold surface. These findings demonstrate why the presence of low concentrations of lead causes an increase in the dissolution rate of gold in aerated cyanide solutions, which was touched on in section 2.2.3.2.

Another interesting aspect of the oxidation of gold at low overpotentials can be demonstrated by comparing the polarisation curves shown in Figure 2.13 with the polarisation curve in the presence of lead, Figure 2.14. The peak at -400 mV reported by a number of authors, including Cathro and Koch (1964), Pan and Wan (1979), and Eisenmann (1978), is only observed in the presence of lead by Nicol (1980a) and Bek, Rogozhnikov and Kosolapov (1997). It is therefore likely that the variation in the peak current density at low overpotentials for the polarisation curves shown in Figure 2.13, is due to the presence of trace levels of lead in solution. To further analyse the variation in peak current density, it is important to understand under what conditions accumulation of lead at the gold surface is likely to occur. This has been discussed in detail by Nicol (1980a), who measured the oxidation of gold as a function of electrode pretreatment. The pretreatment process used was the immersion of the gold electrode in the experimental solution under varied conditions

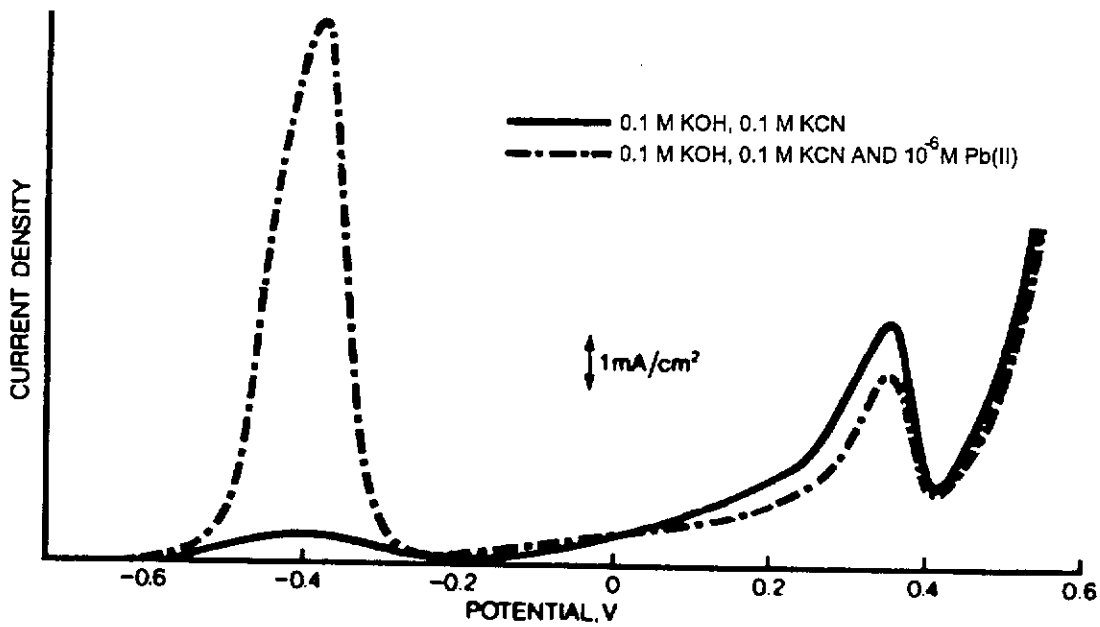

Figure 2.14 – Effect of lead on the oxidation of gold in cyanide solutions (after Nicol, 1980a).

of mass transport, and the published polarisation curves are shown in Figure 2.15. It is clear that the gold oxidation peak at -400 mV is only present when the electrode is subjected to a long pretreatment period under conditions of enhanced mass transfer. It is believed that such conditions result in the accumulation of lead at the gold surface by cementation, thus preventing the formation of a passive film of AuCN (Nicol, 1980a). A similar analysis of the experimental methods adopted by other authors can be used to explain the variation in the observed peak current density at -400 mV, which is discussed below.

A number of authors investigating the oxidation of gold in cyanide solutions have used pretreatment methods which could result in the accumulation of impurities, such as lead, on the gold surface prior to measuring the polarisation curves. These methods include: soaking the electrode in concentrated cyanide solutions for a long period (Dorin & Woods, 1991); holding the electrode at large negative potentials prior to initiating the potential scan (Guan & Han, 1994); and using steady state measurements to construct the polarisation curve (Cathro, 1964). Consequently, it is believed that at low overpotentials, the large variations in the published polarisation curves that are shown in Figures 2.12 and 2.13 is due to activation of the gold surface by trace levels of lead or other impurities.

A discussion of the activation of the gold surface at low overpotentials in the presence of lead would not be complete without examining why an oxidation peak is observed rather than a limiting current density due to the diffusion of cyanide. The presence of an oxidation peak suggests that the activation of gold is followed by subsequent passivation. A number of authors, including Lorenzen and van Deventer (1992) and Mughogho and Crundwell (1996), have shown that the gold oxidation peak potential shifts with pH, and such a shift is not explained by the formation of a film of AuCN. It has been suggested that passivation could be due to the formation of a basic gold cyanide species (Cathro, 1964), although these species are not known to exist in alkaline solutions (Nicol, 1980a). Mussati, Mager and Martins (1997) suggested that the formation of lead oxide, PbO, could account for the decrease in current density at -400 mV. This reaction has a standard reduction potential of

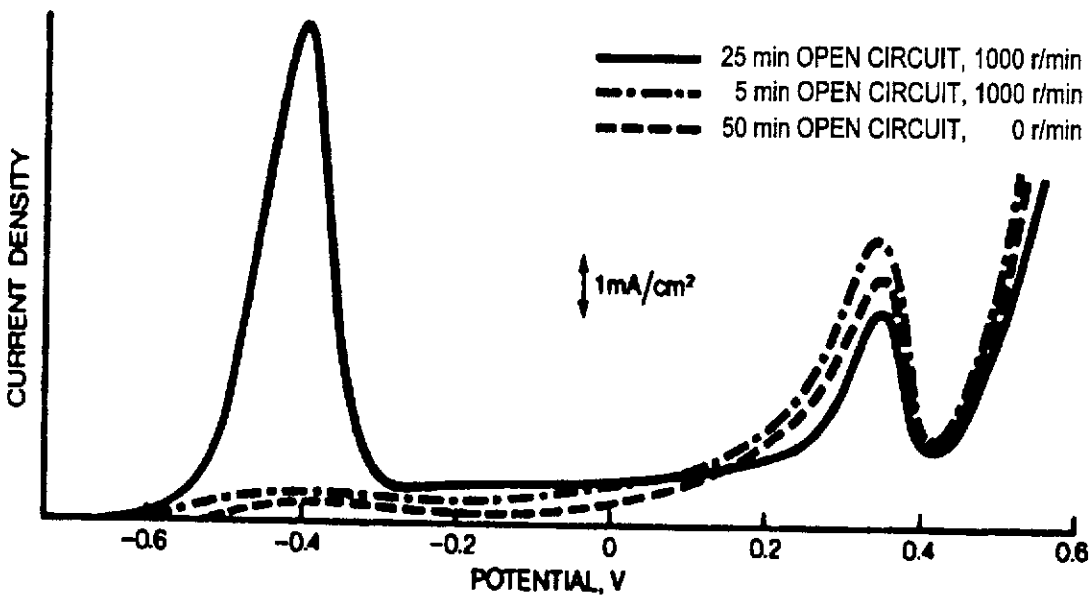

Figure 2.15 – Effect of electrode pretreatment on the oxidation of gold (after Nicol, 1980a).

-580 mV (Bard, 1973), and given the proximity to the passivation peak at -400 mV, it is more likely that passivation is a result of the oxidation of the lead on the gold surface to lead oxide.

2.3.2.2. Peak at 300 mV

It can be seen from Figure 2.13 that as the potential exceeds approximately 100 mV, the current density increases, indicating that the rate of gold oxidation is increasing. Therefore, the passive film described in the previous section has dissolved, allowing access of cyanide to the gold surface. At approximately 300 mV, the gold passivates again. It is uncertain what causes this passivation, although processes such as oxygen adsorption (Dorin & Woods, 1991), gold oxide formation (Guan & Han, 1994) and the formation of gold (I) and gold (III) cyanide species have been suggested (Kirk, Foulkes & Graydon, 1979, Cathro, 1964). It has been shown that the oxidation occurs by a single electron process in this potential region (Kirk, Foulkes & Graydon, 1979), and therefore, the formation of a gold(III) cyanide or oxide is unlikely. It is also known that the peak potential is independent of pH (Mughogho & Crundwell, 1996), but decreases with increasing cyanide concentration (Cathro, 1964), which suggests that passivation is caused by the formation of a cyanide film. Poškus and Agafonovas (1995) have measured the adsorption of cyanide by using ^{14}C labelled cyanide, and showed that surface coverage increases abruptly at 400 mV. This is further evidence to suggest that adsorption of cyanide initiates the passivation of the second gold oxidation peak. Kirk (1980) has suggested that passivation is due to formation of AuCN, although it is uncertain why such a film would reform after being dissolved at lower potentials. It is more likely that the surface film is a different form of gold cyanide, although no data has been published to confirm this.

2.3.2.3. Peak at 600 mV

In the reported gold oxidation polarisation curves, a third oxidation peak is shown to occur at approximately 600 mV. At the passivation potential, it is estimated that oxidation proceeds via a three electron transfer (Kirk, Foulkes & Graydon, 1979), suggesting that passivation is caused by the formation of a gold (III) species. Given that the peak potential shifts with pH, it was concluded that passivation was caused by the formation of gold (III) oxide (Kirk, Foulkes & Graydon, 1979). This has been confirmed by Nicol (1980a), who showed that an oxide was formed in the absence of cyanide at 600 mV.

2.3.3. Oxygen Reduction Half Reaction

Due to its importance in corrosion reactions and the development of fuel cells and rocket engines, oxygen reduction is one of the most widely studied electrochemical half reactions. Consequently, detailed studies have been published with regards to the kinetics and mechanisms of oxygen reduction, and a number of reviews are available (e.g. Hoare, 1968, Conway *et al.*, 1993). This review of the oxygen reduction half reaction is not intended to be comprehensive, and only those aspects relevant to cyanidation will be discussed. Initially, the reduction of oxygen at the solid-solution interface is briefly examined below, followed by a detailed discussion on the reduction of oxygen in alkaline solutions at gold and silver substrates respectively.

2.3.3.1. Reduction at the Solid-Solution Interface

During cyanidation, oxyen reduction occurs at the solid-solution interface. Therefore, it is important to understand what factors influence such a reaction. In electrochemical investigations, oxygen reduction is usually studied at noble substrates, such as platinum and gold (Conway *et al.*, 1993), although results have been published for active metals, such as copper and silver (Vazquez *et al.*, 1994,

Fischer & Heitbaum, 1980). It is well documented that oxygen reduction at the solid-solution interface exhibits a significant overpotential which is substrate dependent (Hoare, 1968). In alkaline solutions, the substrate dependence of the overpotential can be represented as follows: silver < platinum < gold < carbon (Bard, 1973). Hence, when discussing oxygen reduction at the solid-solution interface, the interaction between oxygen and the substrate material must be considered.

Oxygen reduction at a solid-solution interface is believed to occur by a series of reactions, as shown in Equation 2.23 (Hiskey & Sanchez, 1990). The initial step in the process is the transfer of oxygen from the bulk solution to the interface, labelled (a), and then the subsequent adsorption of oxygen onto the electrode surface, (b). Oxygen reduction can then occur by either two sequential reduction steps, (c) and (d), producing peroxide as an intermediate, or by a single four electron reduction to hydroxide, (e). The process is also complicated by the possible decomposition of peroxide, which is labelled k_d.

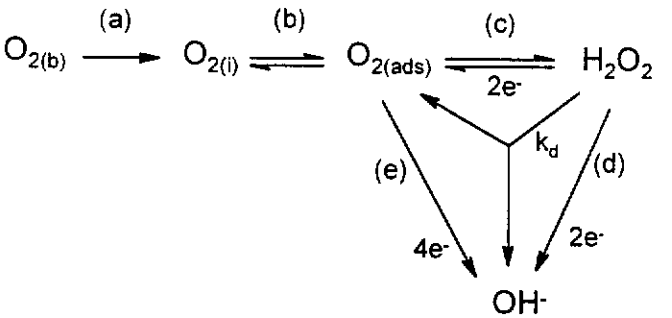

Equation 2.23

It is generally agreed that the steps involving the transfer of electrons, steps (c), (d) and (e) in Equation 2.23, can occur by three possible mechanisms, the Griffith, Pauling and Bridge models, which are shown in Equation 2.24 (Fischer & Heitbaum, 1980). It is clear that the way in which the oxygen bonds to the surface determines which mechanism is applicable during reduction. In the Griffith model, both of the oxygen atoms in the oxygen molecule bond to a central metal atom, while the Pauling model involves the bonding of only one oxygen atom in an 'end-on' manner. The Bridge model involves the bonding of each of the oxygen atoms to a different metal atom, in a similar manner to bridged complexes.

In the Griffith and Bridge models, the first step in the reduction process is the breaking of the O—O bond of oxygen, which will only occur if the M—O bond is stronger than the O—O bond. In both of these models, the reduction of oxygen proceeds by a four electron step, with hydroxide as the product. Alternately, if oxygen reduction procceds by the Pauling model, the two electron production of peroxide is favorable, and this mechanism will occur if the M—O bond is weaker than the O—O bond.

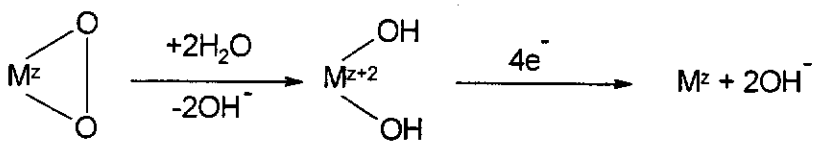

Griffith Model

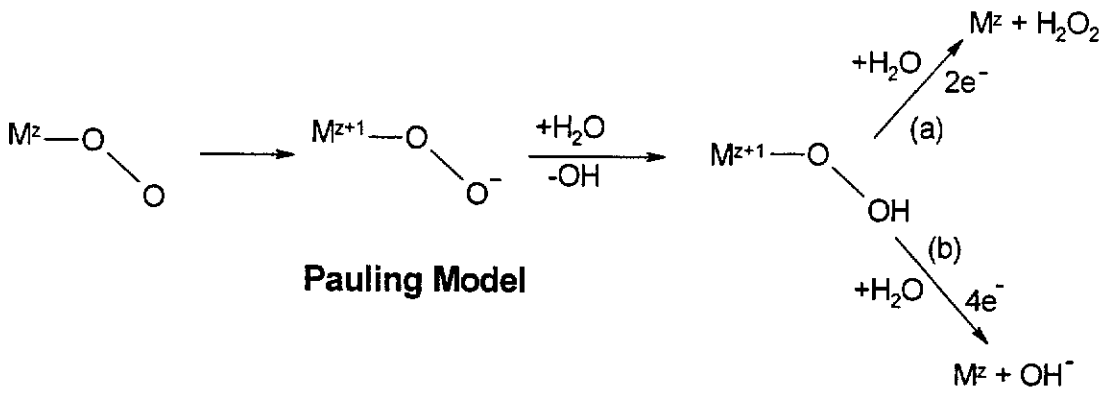

Pauling Model

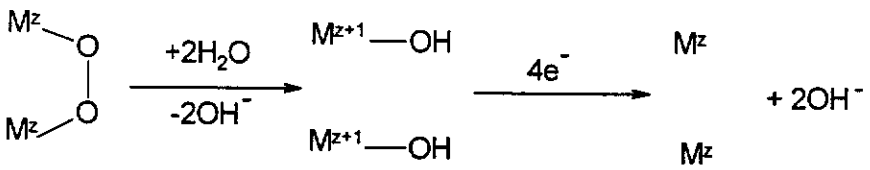

Bridge Model

Equation 2.24

In the following sections, the reduction of oxygen on gold and silver substrates is examined in terms of the above models, and consequently, the conditions under which peroxide is formed as a stable intermediate are discussed.

2.3.3.2. Reduction of Oxygen on Gold

The reduction of oxygen on gold in alkaline solutions has been studied on a number of occasions, and it is generally agreed that reduction proceeds by two steps (Hoare, 1968). The first step is believed to be the reduction of oxygen to peroxide, and the second step is the reduction of peroxide to hydroxide. These steps are shown in Equations 2.25 and 2.26.

$$O_2 + 2H_2O + 2e^- \xrightarrow{(I)} 2OH^- + H_2O_2$$ **Equation 2.25**

$$H_2O_2 + 2e^- \xrightarrow{(II)} 2OH^-$$ **Equation 2.26**

It has also been established that oxygen reduction on gold exhibits a large overpotential (Bard, 1973), which suggests that the reduction of oxygen on gold is surface sensitive. The surface variability of oxygen reduction on gold has been demonstrated by Markovic Adzic and Vesovic (1984), who showed that the reduction is different on the various gold crystal faces. They found that the half wave potential for the reduction of oxygen on the gold (100) face was 180 mV more positive than that for the gold (111) face. This implies that for a polycrystalline electrode, oxygen may preferentially occur at certain sites, depending on the crystal orientation.

A number of workers have measured the formation of peroxide during the electrochemical reduction of oxygen with a rotating ring disc electrode (RRDE). In every case, peroxide was detected as a stable intermediate during the reduction process, although there is some variation in the quantity of peroxide produced (Conway *et al.*, 1993). Fischer and Heitbaum (1980), and Anastasijevic, Strbac, and Adzic (1988) have reported that, after correcting for the collection efficiency, the quantity of peroxide produced is significantly less than the observed disc current. Given that the decomposition of peroxide on gold is slow (Bianci, Mazza & Mussini, 1962), these results suggest that peroxide and hydroxide are produced simultaneously. Zurilla, Sen and Yeager (1978) have addressed this problem by

developing a RRDE model which accounts for both the reduction of oxygen to peroxide and the subsequent reduction of peroxide. Using such a model, they showed that the calculated current density was close to that measured, and thus concluded that only a small amount of the peroxide decomposes before reaching the ring.

A number of radioactive tracer experiments have been conducted in conjunction with oxygen reduction. By using ^{18}O, Davies *et al.* (1959) has shown that when peroxide is formed, the O—O bond of the oxygen molecule is not broken, and thus the peroxide ion is formed by the joining of the oxygen molecule with a hydrogen atom. These results confirm that the when peroxide is formed, as it is in the case of oxygen reduction on gold, the reduction reaction proceeds by the Pauling model.

Effect of Lead on Oxygen Reduction

In section 2.2.3.2 it was shown that lead is present on the gold surface during cyanidation in solutions containing trace amounts of lead. Therefore, it is important to understand the effect that lead has on the oxygen reduction reaction. Adzic, Tripkovic and Markovic (1980) have shown that oxygen reduction in alkaline solutions is altered by adsorbed atoms, such as lead, on the gold surface. They found that gold containing adsorbed lead exhibited a lower oxygen reduction overpotential, and that the reduction reaction proceeded by a direct four electron mechanism in place of the normal sequential two electron process. They also measured the quantity of peroxide that was formed during reduction on a lead modified gold surface with a RRDE, and showed that the ring current was only a fraction of that in the absence of lead. This indicates that peroxide is not formed as a major reaction product of oxygen reduction in the presence of adsorbed lead. Jüttner (1984) obtained similar results, and consequently, suggested that in the presence of adsorbed lead, the reduction mechanism changed from the Pauling model to the Bridge model. He believed that the lead – oxygen bond was strong enough so that the O—O bond would be broken. These results suggest that one of the roles of lead in cyanidation is

to catalytically enhance oxygen reduction. Therefore, bimetallic corrosion of gold in aerated solutions containing cyanide and lead is likely to occur.

2.3.3.3. Reduction on Silver

The reduction of oxygen on silver has been studied on a number of occasions, and it has been shown that the reaction is complicated by the active nature of silver in both acid and alkaline solutions (Hoare, 1968). In alkaline solutions, it is known that the reduction overpotential on silver is considerably lower than on gold (Conway *et al.*, 1993), and according to Delahay (1950), oxygen reduction occurs by a four electron reduction process. Fischer and Heitbaum (1980) have studied the reduction process with a RRDE, and have confirmed that in pure solutions, there is very little peroxide detected. Consequently, they proposed that oxygen reduction on silver proceeded by the Bridge model. Similar results have also been published by Jüttner (1984).

The published results of Adanuvor and White (1988), who studied oxygen reduction in concentrated sodium hydroxide solutions, are contradictory to those discussed above. They found that the Bridge model did not fit the experimental results, and proposed that reduction proceeded by a two electron step, followed immediately by the decomposition of peroxide. Jüttner (1984) has demonstrated that a shift in reduction mechanism from the Bridge model to the Pauling model occurs when silver is modified by underpotentially deposited lead. It is therefore possible that trace levels of impurities, such as lead, have affected the results of Adanuvor and White (1988).

It is generally agreed that at low overpotentials, oxygen reduction on silver is significantly faster than the reduction on gold (Hoare, 1968, Conway *et al.*, 1993). This has been demonstrated by Sun *et al.* (1996), who studied oxygen reduction on gold/silver alloys. They showed that as the proportion of silver in the alloy was increased, the reduction of oxygen occurred at a faster rate. This suggests that in the leaching of gold/silver alloys, the reduction of oxygen is more likely to occur at

silver sites. Therefore, it is probable that bimetallic corrosion of the gold from the alloy will occur.

Chapter 3 – Studies of Oxygen Reduction

3.1. Introduction

For a complete understanding of the cyanidation process, a prior knowledge of oxygen reduction is important. For example, when discussing the effect of lead on the dissolution of gold, as will be presented in Chapter 5, an understanding of how lead affects the reduction of oxygen is essential. Hence, in this chapter, a brief investigation of the oxygen reduction half reaction will be presented, with the objective of discussing the reaction under conditions which are relevant to cyanidation.

The oxygen reduction process is one of the most extensively studied electrochemical process, and thus a great deal of information on the mechanism of the reduction reaction exists in the literature (Conway *et al.*, 1993, Hoare, 1968). The main focus of this chapter is on the effect of the substrate on the reaction, and the conditions under which bimetallic corrosion is likely to occur are also discussed.

3.2. Experimental

3.2.1. Solutions and Electrodes

All solutions were prepared using analytical grade reagents and Millipore Milli-Q water. The solutions of pH lower than 12 were buffered with 0.01 M sodium bicarbonate and the pH was adjusted to the desired value with either sodium hydroxide or perchloric acid. Sodium perchlorate (0.2 M) was used as a background electrolyte as it was found to be electrochemically inactive over the potential window of interest. The solutions were oxygenated with pure oxygen for 30 minutes prior to and during the experiments. Fast cycling, at 500 mV s^{-1}, of the gold electrode was carried out in a 1 M Aristar grade sulfuric acid solution, which had been sparged with high purity argon for 30 minutes prior to each experiment. The temperature,

unless specified, was maintained at 25 ± 1 °C. The rotation rate, unless specified, was maintained at 300 rpm.

The solid gold electrodes were constructed from metals of 99.99 % purity which had been purchased from Precious Metals Engineering. The electrodes were of the same design as these used by Power and Ritchie (1981), and were constructed at Murdoch University. They were successively polished on 1200, 2400 and 4000 grade silicon carbide paper prior to each experiment, and then thoroughly rinsed with Millipore water.

While the majority of the experiments were performed using solid electrodes, some of the results refer to plated electrode surfaces. These deposits were prepared by electroplating at 25 $A\,m^{-2}$ from a solution containing 0.02 M potassium dicyanoaurate, 0.23 M potassium cyanide and 0.086 M potassium carbonate. The lead modified deposits were plating using the same plating solution, with the exception that 0.1 mM lead nitrate was added. The plating solutions were purged with argon for 30 minutes prior to and during the plating process.

During the oxygen reduction experiments, the quantity of peroxide produced was measured with a rotating ring-disc electrode (RRDE). The disc was constructed from a 3 mm diameter gold rod, while the ring consisted of platinum with an inner diameter of 3.4 mm, and outer diameter of 4.4 mm. The collection efficiency, 0.39, was measured using the ferro-ferricyanide couple, using the method described by Albery, Hitchman and Ulstrup (1968). During the oxygen reduction experiments, the disc potential was varied in the same manner as a conventional RDE, and the ring potential was set at 1200 mV. In this potential region, the oxidation of peroxide is diffusion controlled, and hence all of the peroxide that reaches the ring is oxidised.

3.2.2. Electrochemical Measurements

The rotating disc apparatus and cell used for the electrochemical measurements were the same as described previously (Power, Ritchie & Sjepcevich, 1981). Linear sweep voltammetry was performed using an EG&G PAR 273A potentiostat, which was interfaced to a PC by a multi-channel data acquisition card. The RRDE experiments were performed using a Pine bipotentiostat. Data acquisition and analysis were performed with software that was written in Q-Basic. All potentials were measured with respect to a saturated calomel electrode (SCE), but are reported here relative to the standard hydrogen electrode (SHE). The SCE has a potential of 0.2412 V vs SHE at 25 °C (Bard & Faulkner, 1980). Linear sweep voltammetry was carried out at a scan rate of 1 mVs^{-1}, unless otherwise specified.

3.3. Results and Discussion

Oxygen reduction at a solid-solution interface is believed to occur by a series of reactions (Hiskey & Sanchez, 1990), as shown in Equation 3.1. The initial step of the process is the transfer of oxygen from the bulk solution to the interface, labelled (a), and then the subsequent adsorption of oxygen onto the electrode surface, (b). Oxygen reduction can then occur by either two sequential reduction steps, (c) and (d), producing peroxide as an intermediate, or by a single four electron reduction to hydroxide, (e). The process is also complicated by the possible decomposition of peroxide to oxygen and hydroxide, which is labelled k_d.

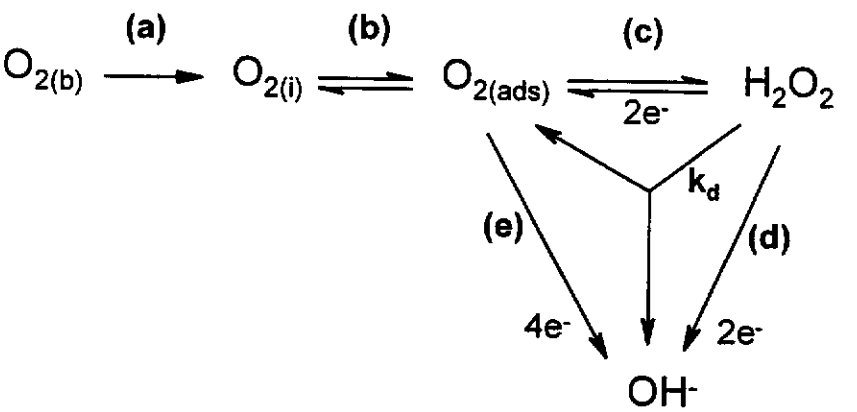

Equation 3.1

During the adsorption of oxygen onto the electrode surface, a bond will form between the oxygen and the substrate atoms. Therefore, an important aspect of oxygen reduction is the interaction of oxygen with the electrode substrate, and the first set of experimental results below will show how oxygen reduction varies with the surface properties of the substrate. The second set of results will show how oxygen reduction varies with other experimental variables, such as oxygen concentration and temperature.

3.3.1. Surface Effects

3.3.1.1. Effect of Electrode Substrate

Oxygen reduction was investigated on two different conducting electrodes: gold and silver, and the resultant polarisation curves are shown in Figure 3.1. In this chapter, the polarisation curves comply with the IUPAC convention of representing reduction reactions by negative currents densities. It is immediately obvious that the shape of each of the polarisation curves is different, and thus the oxygen reduction half reaction is dependent on the electrode substrate. The reduction behaviour of oxygen on gold is the most relevant to this work, and hence will be discussed first, followed by silver.

a) Reduction on Gold

It can be seen from Figure 3.1 that oxygen reduction on gold occurs in two waves, with the first wave occuring in the potential range −100 to −450 mV, and the second wave in the potential range −450 to −800 mV. It is believed that the first wave is a result of the reduction of oxygen to peroxide, while the second wave is a result of the reduction of oxygen to hydroxide (Hoare, 1968). These two reactions are shown in Equations 3.2 and 3.3, for which the reduction proceeds by two and four electron processes respectively.

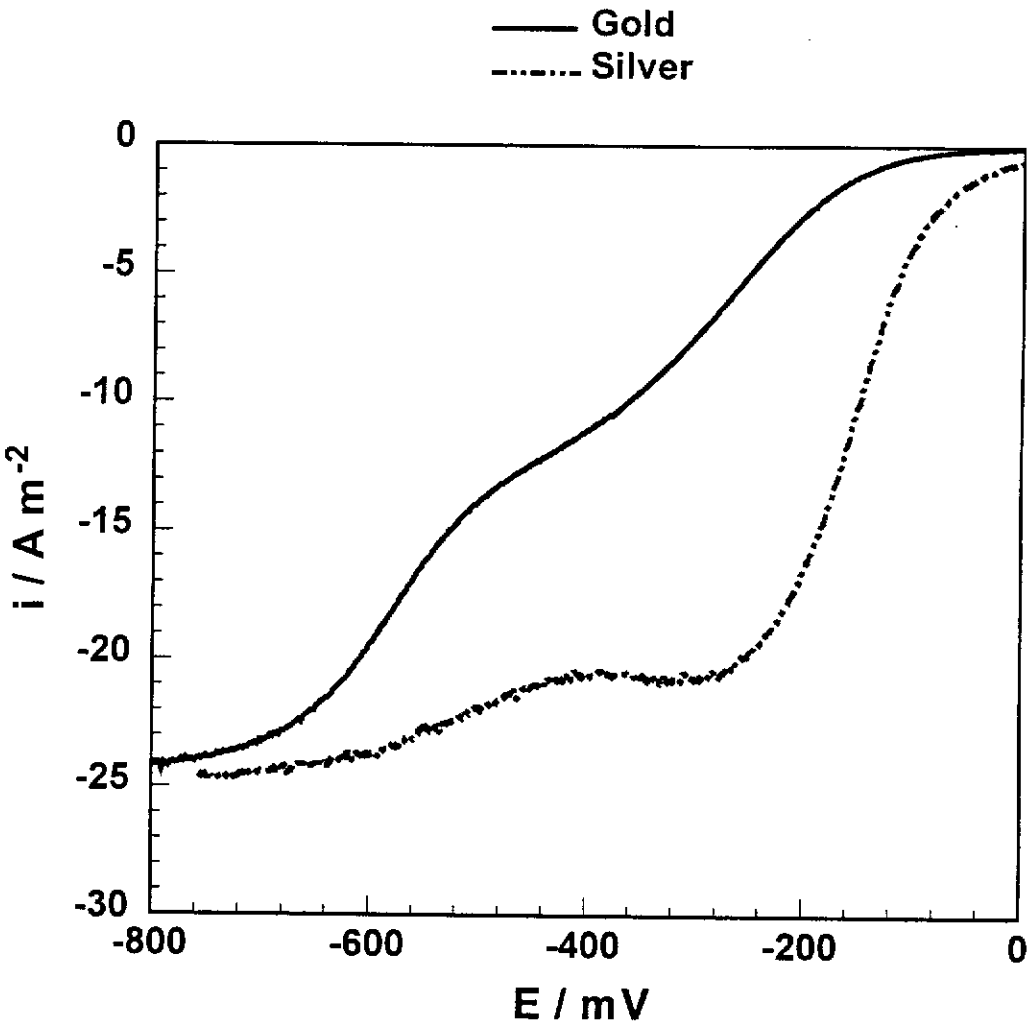

Figure 3.1 – Oxygen reduction on gold and silver. Experimental conditions: oxygen saturated solutions, pH 10.0, 1 mV s^{-1}, 25 °C, 300 rpm.

$$O_2 + 2H_2O + 2e^- \rightarrow H_2O_2 + 2OH^-$$ **Equation 3.2**

$$O_2 + 2H_2O + 4e^- \rightarrow 4OH^-$$ **Equation 3.3**

It can be seen from Figure 3.1 that for each of the reduction waves on gold, a limiting plateau is obtained at −400 and −800 mV respectively. At these potentials, the reduction reaction is limited by oxygen diffusion to the gold surface, and the current density is proportional to n, the number of electrons involved in the reduction of an oxygen molecule. By rearranging the Levich equation, as shown in Equation 3.4, n can be estimated for each of the diffusion limiting plateaus,

$$n = \frac{i_L}{0.62FD_O^{2/3}\omega^{1/2}\nu^{-1/6}[O_2]}$$ **Equation 3.4**

where i_L is the diffusion limiting current density (A m^{-2}), F is the Faraday constant (96484 C mol^{-1}), D is the diffusion coefficent of oxygen in the electrolyte (m^2 s^{-1}), ω is the angular rotation rate (s^{-1}), ν is the kinematic viscosity (m^2 s^{-1}), and $[O_2]$ is the concentration of oxygen in solution (mol m^{-3}). Given that the oxygen concentration of an oxygen saturated solution at atmospheric pressure is 1.28 mM (Fogg & Gerrard, 1991), and diffusion coefficient of oxygen is 1.94×10^{-9} m^2 s^{-1} (Guan & Han, 1994), n can be readily calculated. At −400 mV, the limiting current density is 12.2 A m^{-2}, and thus the number of electrons, n, is calculated to be 1.9. This confirms that the first reduction wave is due to the two electron reduction of oxygen, where peroxide is produced as a stable intermediate, as shown in Equation 3.2. At −800 mV, n is calculated to be 3.7, which is consistent with the reduction of oxygen, in the potential region of the second wave, occuring by a four electron process, as shown in Equation 3.3. Therefore, it can be inferred from the polarisation curve that at large overpotentials, peroxide is not produced during the reduction of oxygen.

The mechanism of oxygen reduction on gold can be validated using a rotating ring-disc electrode (RRDE), which detects the quantity of peroxide that leaves the gold disc and reaches the platinum ring. This is accomplished by setting the

potential of the ring to a value where all of the peroxide that reaches the ring is oxidised, i.e. the potential where the oxidation of peroxide is diffusion controlled. The oxidation current at the ring is then related to the formation of peroxide at the disc by the collection efficiency, N, which is dependent only on the geometry of the electrode. For further information about the RRDE technique, the reader is referred to the book published by Albery and Hitchman (1971).

Shown in Figure 3.2 are the voltammograms for the disc and ring, which correspond to oxygen reduction and peroxide oxidation respectively. For both of the polarisation curves, the x-axis represents the potential of the gold disc. It is clear that at disc potentials lower than -100 mV, the ring current increases, which shows that as oxygen reduction begins, so does the production of peroxide. The ring current, and hence peroxide production reaches a maximum at -400 mV, and at potentials more negative than -400 mV, the ring current decreases. This indicates that the oxygen is reduced to hydroxide at potentials more negative than -400 mV, an observation that is consistent with the shape of the disc voltammogram.

Also shown in Figure 3.2 is the calculated current due to the formation of peroxide, I_c, which is calculated using the collection efficiency of the electrode, as shown in Equation 3.5 (Albery & Hitchman, 1971),

$$I_c = \frac{-(I_r - I_{r,b})}{N} \qquad \textbf{Equation 3.5}$$

where I_r is the ring current (μA), $I_{r,b}$ is the background ring current (μA), which is shown in Figure 3.2 to be 57.3 μA, and N is the collection efficiency, 0.39. It is clear that at any disc potential, the calculated current due to peroxide formation is less than the measured disc current. Similar results have been reported in other publications (Fischer & Heitbaum, 1980, Zurilla, Sen & Yeager, 1978), and it has been suggested that the first reduction wave produces some hydroxide as well as peroxide (Zurilla, Sen & Yeager, 1978). The presence of two equal reduction waves in the disc voltammograms indicates that the undetected peroxide is more likely to be a result of

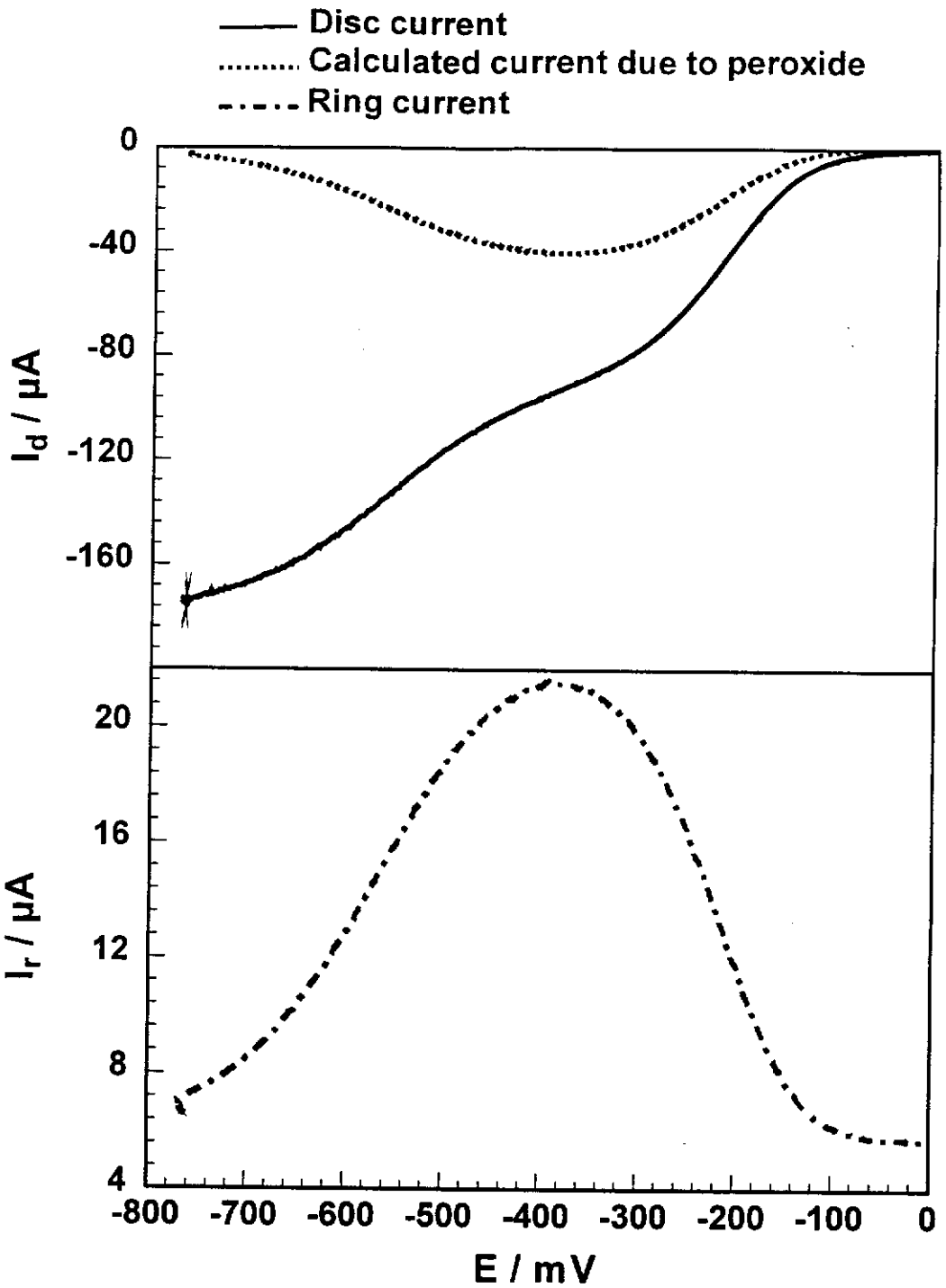

Figure 3.2 – Reduction of oxygen at a gold disc and the corresponding oxidation of peroxide at the platinum ring. Experimental conditions: oxygen saturated solutions, pH 10.0, 1 mV s^{-1}, 25 °C, 300 rpm, E_R = 1200 mV, N = 0.39.

decomposition before reaching the platinum ring, although there is no simple technique to confirm this.

b) Reduction on Silver

The reduction of oxygen on silver is also of considerable interest to gold leaching as it can reveal information about the reaction mechanism during the dissolution of a gold-silver alloy. It can be seen from Figure 3.1 that for oxygen reduction on silver the overpotential is lower and rate of increase in current density with potential is higher than for the reduction on gold. Therefore, silver enhances the reduction of oxygen.

From Figure 3.1, it can be seen that the reduction of oxygen on silver occurs in two waves, with diffusion limiting plateaus at -300 and -650 mV respectively. In a similar manner to the previous section, n can be calculated for each of these plateaus, and the values obtained are 3.2 and 3.8 respectively. These values indicate that: 1) during the first wave, oxygen reduction on silver is considerably different to that on gold; and 2) during the second wave, oxygen is directly reduced to hydroxide by a four electron process. Adanuvor and White (1988) have published similar polarisation curves for the reduction of oxygen in concentrated caustic solutions. They suggested that during the first wave, oxygen reduction on silver occurs by a two electron process coupled with simultaneous peroxide decomposition, as shown in Equation 3.6. A model based on this assumption was developed and was found to fit the experimental data very well. Given the similarity in the oxygen reduction polarisation curves shown in Figure 3.1 with those published by Adanuvor and White (1988), it is believed that the mechanism shown in Equation 3.6 can also account for the results obtained in this work.

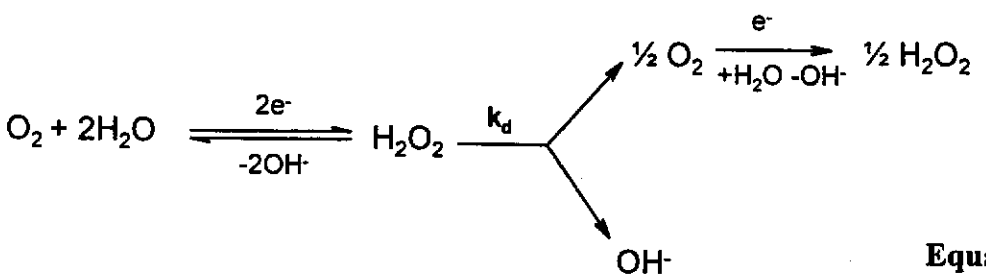

Equation 3.6

The increased activity of silver towards oxygen reduction suggests that for gold-silver alloys, oxygen reduction will preferentially occur at silver sites. Also, in cyanide solutions, silver has a higher oxidation potential than gold, and thus is more noble (Bard, 1973). Therefore, for the dissolution of gold-silver alloys, the cathodic reaction is likely to be the reduction of oxygen on silver sites, and the anodic reaction is likely to be the oxidation of gold to gold cyanide. This is known as bi-metallic corrosion.

3.3.1.2. Electrode Pre-treatment

In the previous section, it was shown that oxygen reduction is very senstive to the electrode substrate. Consequently, many authors have used a variety of surface preparation techniques to ensure that surface state is reproducible. Fast cycling is one such technique, where the electrode is rapidly cycled in sulfuric acid between the areas of oxygen and hydrogen evolution. This is believed to remove adsorbed impurities and cause partial faceting of the electrode surface (Perdriel, Arvia & Ipohorski, 1986). Fast cycling of the electrode is carried out for around 15 minutes at 500 mV s^{-1} until a uniform voltammogram is obtained, which is shown in Figure 3.3. It can be seen that there are two distinct peaks, one an oxidation peak, and one a reduction peak. On the forward cycle, the gold is oxidised to form a layer of gold oxide at 1400 mV. At 1750 mV, oxygen evolution occurs. On the reverse cycle, at around 1200 mV, the gold oxide is reduced back to metallic gold. At around -200 mV, there is a sharp increase in current density as hydrogen evolution occurs.

The reduction of oxygen on freshly polished and fast cycled gold is shown in Figure 3.4, and it can be seen that the polarisation curves are almost identical. This suggests that polishing of the electrode gives a similar surface to the electrochemically cycled surface. Consistent with these results, the major reproducibility problems encountered in this work were found to be associated with the preparation of the electrolyte solutions. It is speculated that this is due to trace levels of impurities in different batches of stock solutions. Fischer and Heitbaum

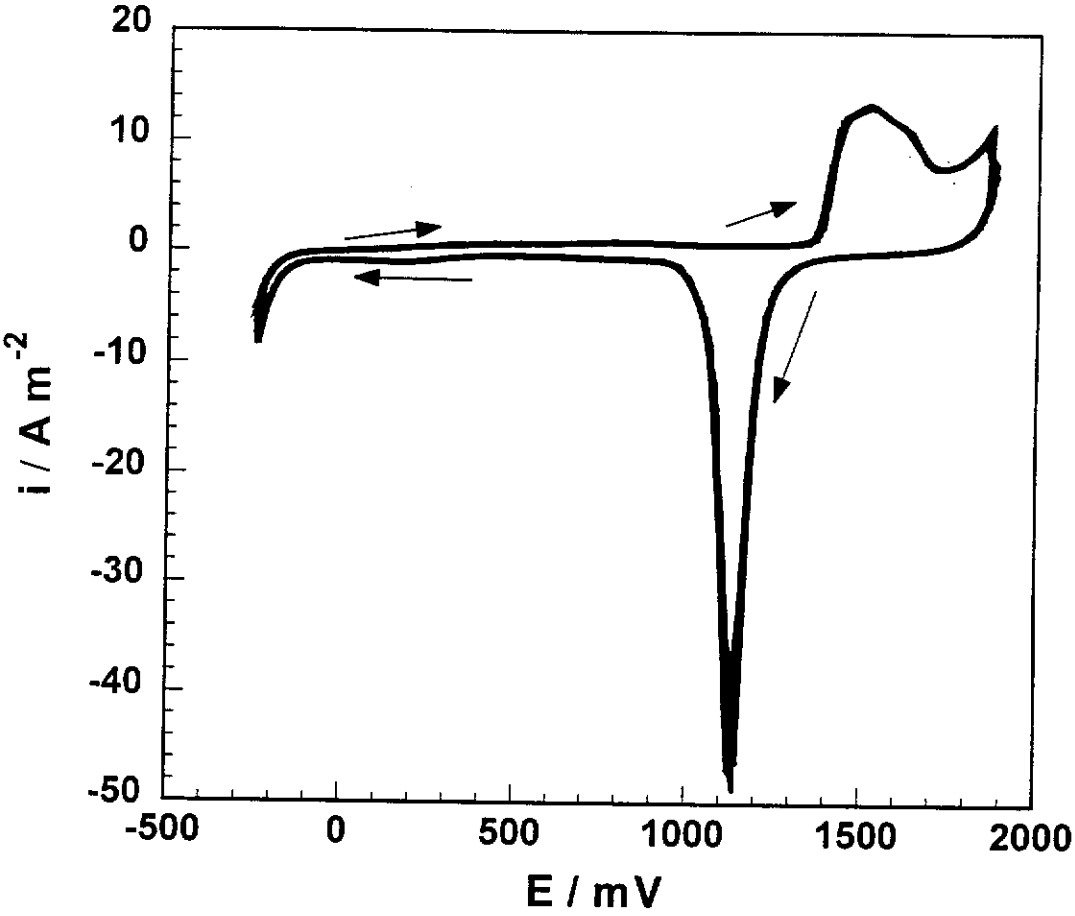

Figure 3.3 – Cyclic voltammogram for fast cycling of gold at 500 mV s^{-1} in 1 M H_2SO_4. Experimental conditions: 25 °C, 300 rpm.

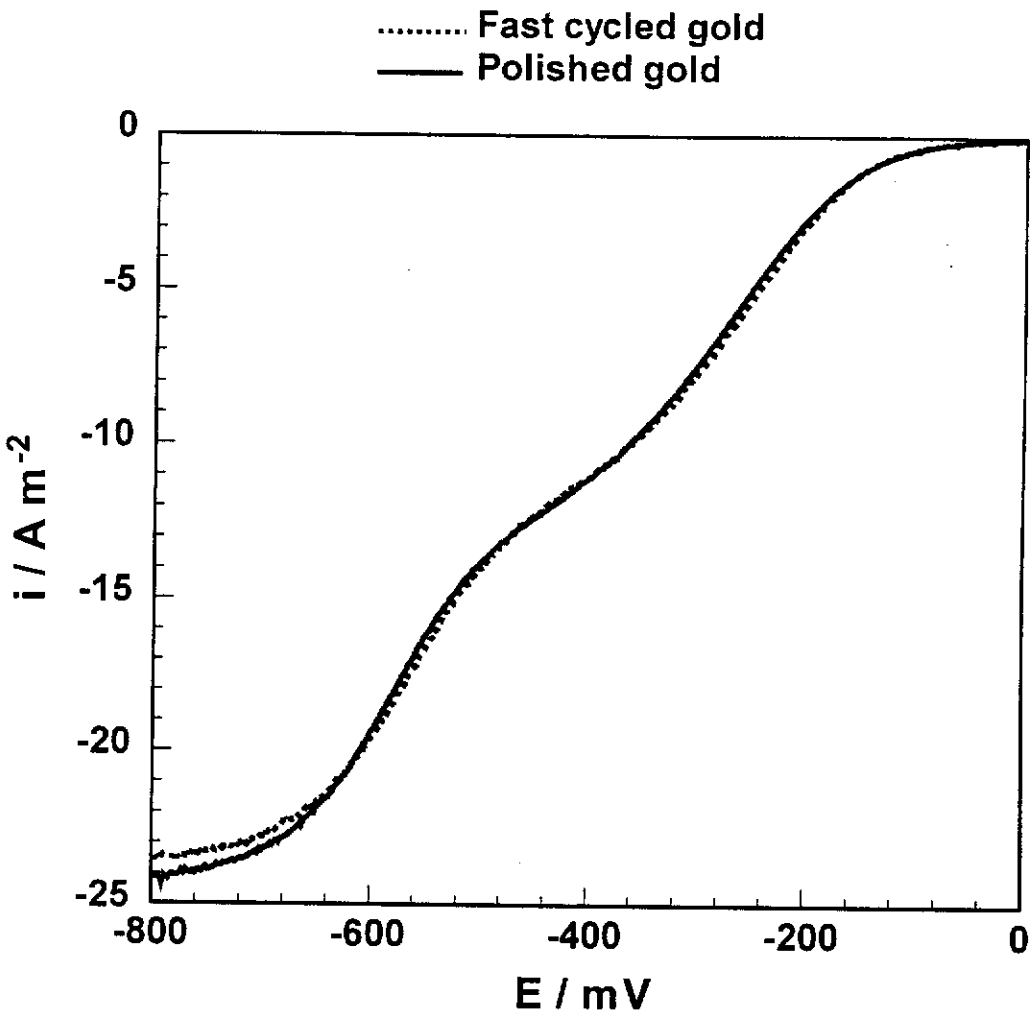

Figure 3.4 – Oxygen reduction of a freshly polished gold surface and a surface which had been pretreated by fast cycling. Experimental conditions: oxygen saturated solutions, pH 10.0, 1 mV s^{-1}, 25 °C, 300 rpm.

(1980) have shown that trace levels of impurities, such as lead, can have a marked effect on the reduction reaction.

3.3.1.3. Surface Modification

It is well known that oxygen reduction is catalytically enhanced by lead (Adzic, Tripkovic & Markovic, 1980). Unfortunately, it is difficult to study the reduction of oxygen on a massive lead surface, as the reaction is complicated by the redox couple Pb|PbO, which has a standard reduction potential of -0.70 V in alkaline solutions. Consequently, the reduction of oxygen was studied on a lead modified gold surface, where the concentration of lead is low enough so that the current from the Pb|PbO couple is insignificant. The lead modified surfaces were prepared by electroplating gold from a plating solution which had been altered by the addition of 0.1 mM lead nitrate. This plating process will be described in detail in Chapter 6, and it produces a gold deposit that contains approximately 1 % lead. Shown in Figure 3.5 is the polarisation curve for oxygen reduction on the gold/lead co-deposit, and also the polarisation curve on gold which is overlaid for comparison. It can be seen that both of the polarisation curves exhibit two reduction waves, and the limiting current density for the second wave is the same in each instance. These are the only similarities between the polarisation curves, and the major differences include: 1) the reduction overpotential is lower on gold/lead than it is on gold; 2) the current density increases more rapidly with potential on gold/lead than it does on gold; and 3) the limiting current density of the first wave is higher for gold/lead than it is for gold. These observations indicate that oxygen reduction is enhanced by the presence of lead on the surface of the gold.

The enhancing effect of lead on oxygen reduction was also noted by Jüttner (1986), who proposed that in the presence of lead, oxygen is able to form a bridged complex, $Au\diagup^{O}\!-\!{}^{O}\diagdown Pb$. This causes the oxygen reduction mechanism to change from the sequential Pauling model, to the direct, 4 electron Bridge model, as discussed in the review. The results in Figure 3.5 suggest that the reduction on

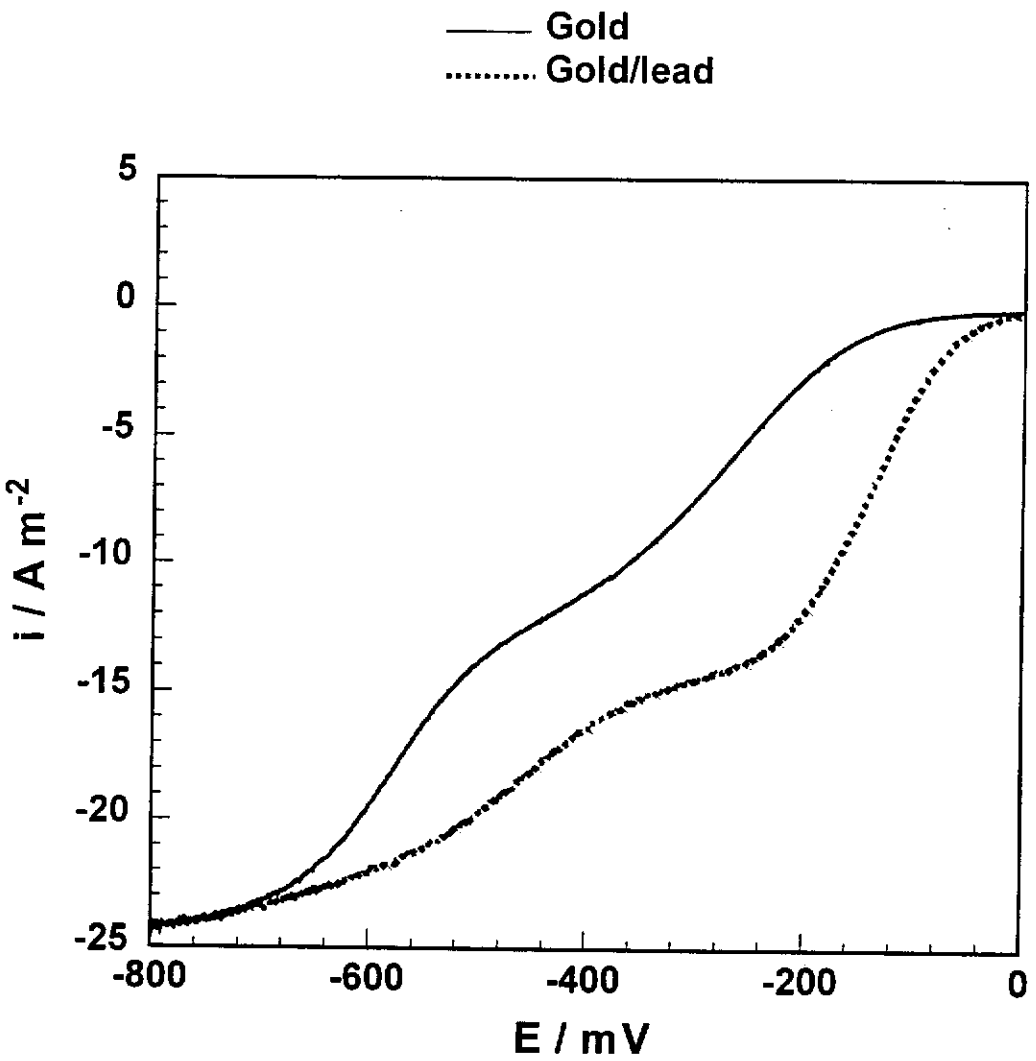

Figure 3.5 – Oxygen reduction on gold surfaces which contain trace levels of lead. Experimental conditions: oxygen saturated solutions, pH 10.0, 1 mV s^{-1}, 25 °C, 300 rpm.

gold/lead is a combination of the direct and sequential mechanisms. Thus, some of the oxygen is likely to be reduced at gold sites, and some reduced at lead sites. This is not surprising, as is believed that only a small proportion of the gold surface contains lead.

It will be shown in Chapter 5 that when gold is leached in a solution containing lead, the lead deposits on the gold surface. Therefore, during the dissolution of gold in solutions containing lead, oxygen reduction will be more likely to occur at the lead sites on the gold surface. The rate of dissolution will thus be enhanced by lead on the surface, and bi-metallic corrosion will occur, similarly to the situation encountered for gold-silver alloys.

3.3.2. Other Experimental Variables

In this section, oxygen reduction on gold will be investigated further. The main objective is to demonstrate how oxygen reduction changes with conditions that are appropriate to cyanidation. Therefore, only experimental variables that are important to gold cyanidation will be discussed, including oxygen concentration, temperature and pH.

3.3.2.1. Effect of Oxygen Concentration

The polarisation curves for oxygen reduction in air and oxygen saturated solutions are shown in Figure 3.6. It is clear that for oxygen saturated solutions, the reduction current density is significantly higher than for air saturated solutions, as expected. The two polarisation curves are almost identical in shape, although this is not obvious because of the different magnitude of current densities. Increasing the oxygen concentration in leach solution has become a widely used method of enhancing the gold cyanidation rate, as it is believed that under typical plant conditions, the rate of gold dissolution is limited by oxygen reduction (Marsden & House, 1992).

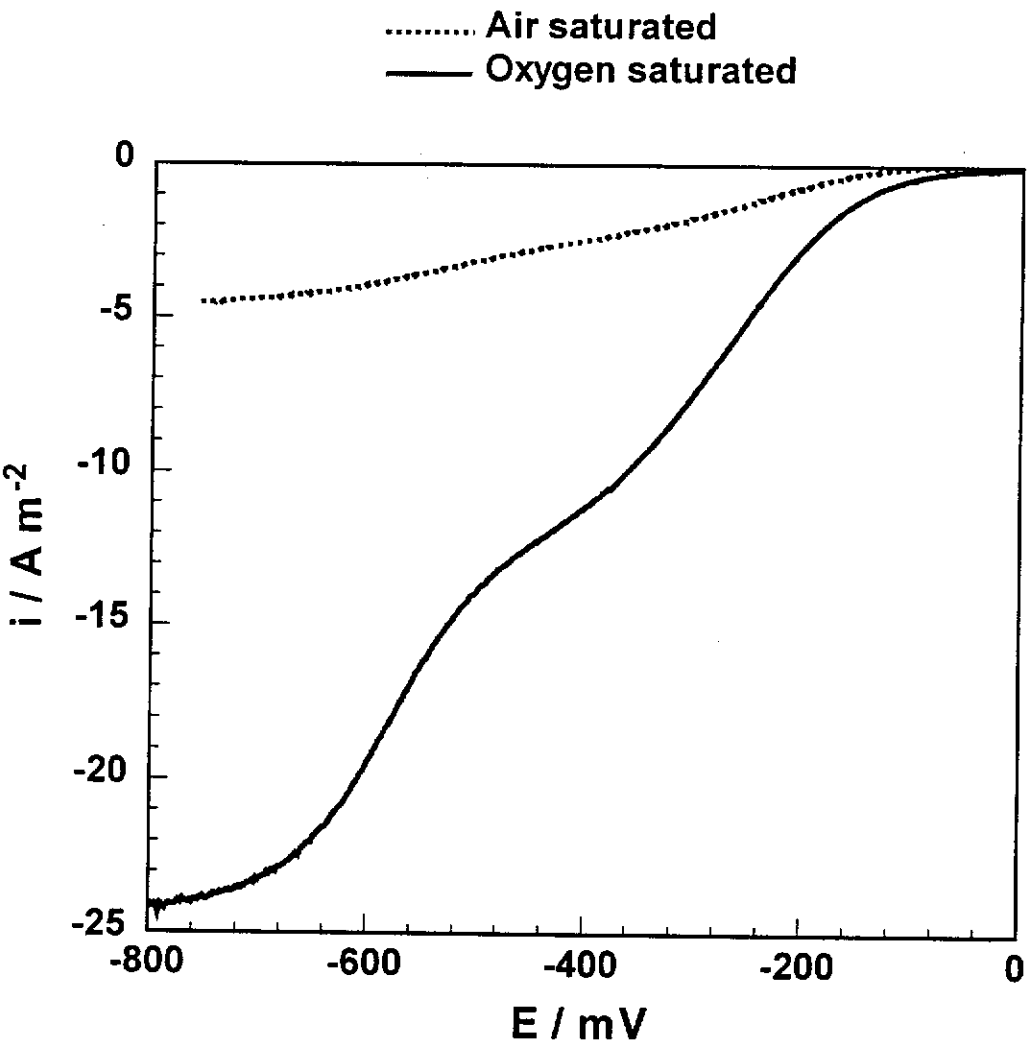

Figure 3.6 – Oxygen reduction as a function of oxygen concentration. Experimental conditions: pH 10.0, 1 mV s^{-1}, 25 °C, 300 rpm.

3.3.2.2. Effect of Temperature

The reduction of oxygen on gold was measured as a function of temperature, and the resultant polarisation curves are shown in Figure 3.7. It can be seen that: 1) increased temperature has little effect on the polarisation curves, an observation which is explained by the increase in the diffusion rate being offset by a decrease in the solubility of oxygen with temperature; and 2) the first oxygen reduction wave is enhanced to some extent at higher temperatures, suggesting that the process which results in the first wave has a higher activation energy than the process which occurs during the second wave. These results suggest that under cyanidation conditions where the rate is limited by oxygen reduction, temperature will not have a significant effect on the dissolution of gold.

3.3.2.3. Effect of pH

The polarisation curves for the reduction of oxygen as a function of pH are shown in Figure 3.8. It can be seen that at each pH, there exists two oxygen reduction waves, although the position of each wave is affected differently by increases in pH. According to the Nernst equation, the reduction potential should shift by -59.2 mV pH^{-1}. In the first reduction wave, polarisation curve shifts by approximately 20 mV pH^{-1}. For the second wave, there is a considerable shift in the polarisation curve with pH, and this shift is more pronounced at higher pH. Thus, the change in oxygen reduction with pH was not just a Nernstian effect. One possibility is that the manner in which oxygen bonds to the gold surface is dependent on pH, although this was not investigated further. These results show that increasing the pH of gold leach solutions will decrease the rate at which oxygen reduction occurs, a fact that has been recognised by a number of authors, including Guan and Han (1994), who showed that the rate of dissolution of gold decreases with pH.

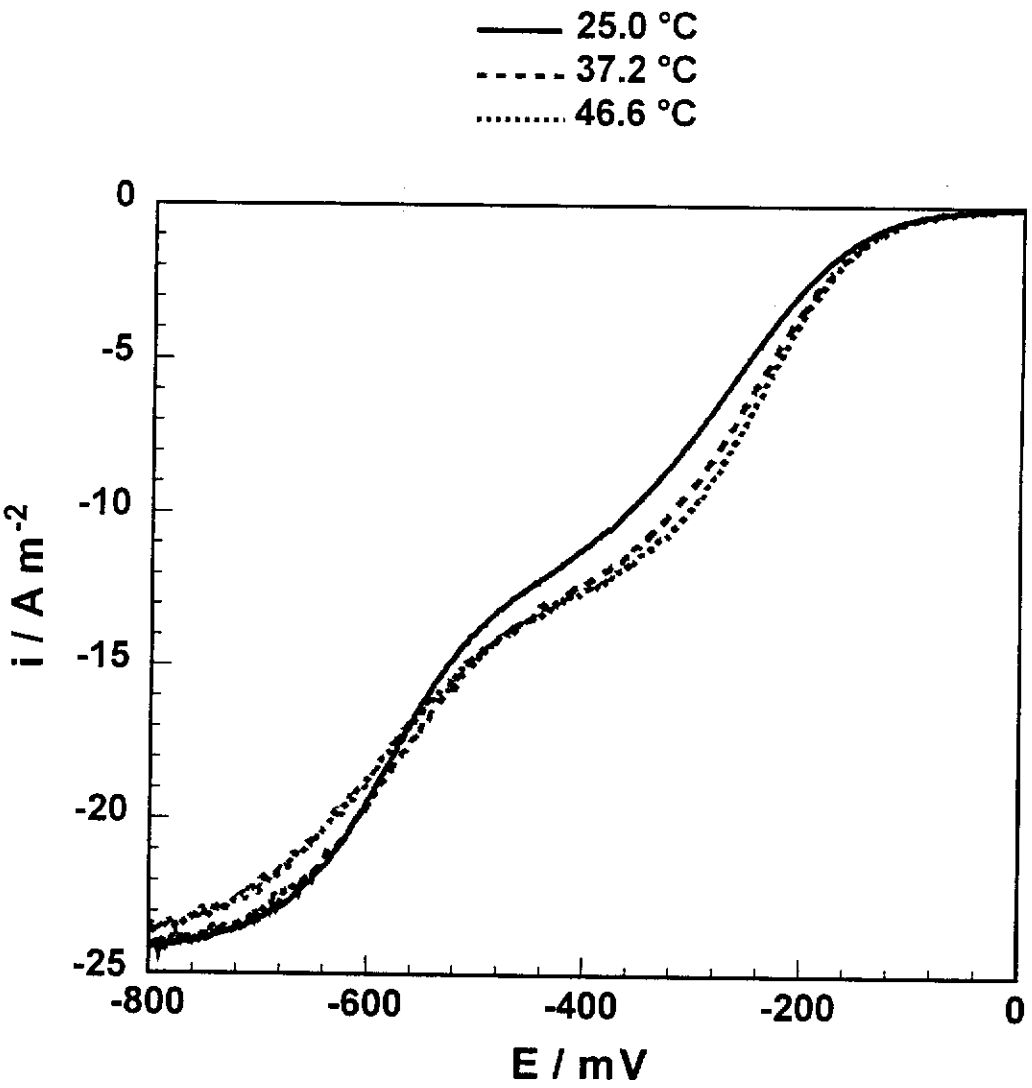

Figure 3.7 – Oxygen reduction as a function of temperature. Experimental conditions: oxygen saturated solutions, pH 10.0, 1 mV s^{-1}, 300 rpm.

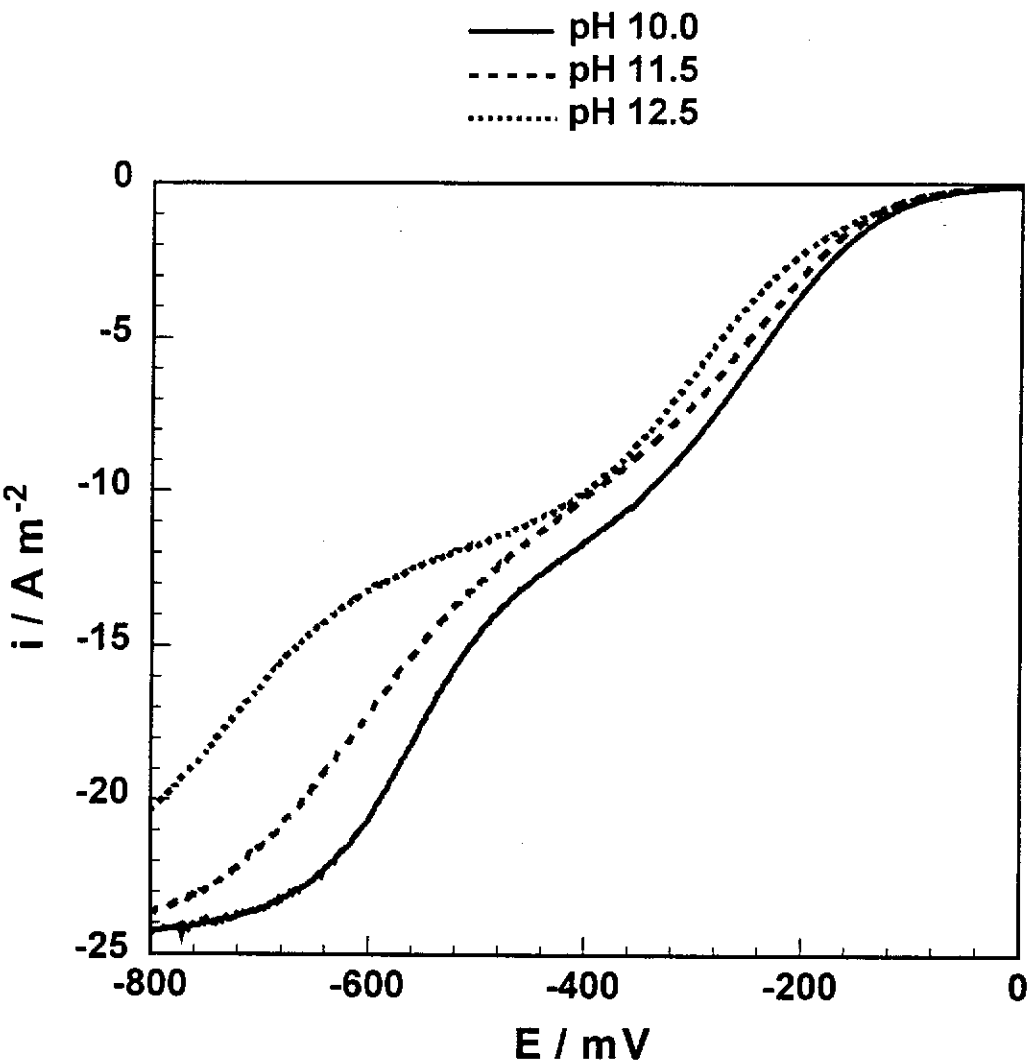

Figure 3.8 – Oxygen reduction as a function of pH. Experimental conditions: oxygen saturated solutions, 1 mV s^{-1}, 25 °C, 300 rpm.

3.4. Summary

1) Oxygen reduction is dependent on the electrode substrate, with the overpotential on silver being lower than that on gold. It is also shown that co-deposited lead enhances the reduction of oxygen. It is thus believed that during gold dissolution in the presence of either silver or lead on the surface, bimetallic corrosion will occur.

2) Oxygen reduction on gold occurs by two sequential reactions, with the formation of peroxide as an intermediate. The peroxide was detected using a ring disc electrode, although the quantity produced is lower than the amount expected. This discrepancy is believed to be a result of peroxide decomposing before reaching the ring.

3) Oxygen reduction on silver is more complex than gold, with occurrence of two non-equal reduction waves. It is believed that peroxide decomposition occurs simultaneously with reduction, therefore producing oxygen. This oxygen is then able to reduce further, resulting in a higher limiting current density for the first wave.

4) It is shown that oxygen reduction is enhanced under conditions of high oxygen concentration and low pH, and that temperature has little effect on the reaction. This information is important is assessing the effect of experimental variables, such as oxygen concentration and pH on the dissolution of gold in the remaining chapters.

Chapter 4 – Dissolution of Gold in Cyanide Solutions

4.1. Introduction

In the review, it was shown that the kinetic and electrochemical results for the dissolution of gold in cyanide solutions from many publications were conflicting. These variations are believed to result from variations in either solid or solution phase purity in the reported experiments. In this chapter, the dissolution of gold in cyanide solutions is investigated under conditions of high purity, and the results are compared with those published previously. The main emphasis of this chapter is on the measurement of the leaching rate with the rotating quartz crystal microbalance, although complementary electrochemical studies are also presented.

4.2. Experimental

4.2.1. Solutions and Electrodes

The majority of solutions used in this chapter were prepared from AR grade sodium cyanide, and contained 0.01 M sodium bicarbonate and 0.2 M sodium perchlorate as buffer and background electrolyte respectively. For the kinetic studies, reproducibility was only obtained if the buffer and background electrolyte were omitted from solution. The solutions for the kinetic and oxygen reduction studies were oxygenated with compressed air or pure oxygen for 30 minutes prior to and during the experiments. All other solutions were degassed with high purity argon in the same manner.

In order to obtain high purity sodium cyanide, it was necessary to prepare the solutions using hydrogen cyanide. Initially, sodium peroxide was dissolved in Milli-Q water and then heated. This promotes the decomposition of the peroxide ion to hydroxide, and this was found to be the most pure source of sodium hydroxide available (Clarke, 1996). The solution was then boiled with silver metal to destroy

the remaining peroxide and remove trace quantities of chloride ions, after which the silver was removed from solution. Sodium cyanide was then mixed with dilute sulfuric acid, and the resultant hydrogen cyanide was bubbled into the prepared caustic solution. The sodium cyanide solution was analysed using ion chromatography, and the solution was found to contain much less chloride contamination than standard AR grade solutions (< 0.0005 % and 0.01 % w/w Cl^- as solid respectively). The ultrapure cyanide solution, which contained 0.29 M OH^- and 0.1 M CN^-, was also found to contain a much lower level of heavy metal contamination.

Kinetic measurements were performed using a 10 MHz AT cut quartz crystal. The quartz crystal was mounted onto a PVC cylinder to form a rotating disc, as shown in Figure 4.1. The wires were connected to each side of the quartz crystal electrode with silver loaded epoxy resin, and the gap between the edge of the crystal and the PVC cylinder was filled with silicon sealant. The quartz crystal, which has a thin layer of either chromium or titanium on either side, was then cleaned by ultrasonication for 10 minutes, firstly in 10 % Decon cleaning solution, then Milli-Q water and finally propan-2-ol. The quartz crystal electrodes were prepared by sputtering a layer of either platinum or gold onto the electrode. Prior to sputtering, the electrode was rinsed with Milli-Q water and dried with compressed argon. The platinum or gold was sputtered over the layer of chromium or titanium with a Balzers Union sputter coating unit (model 020). The flag of the crystal was covered with insulating varnish to leave a disc of platinum or gold. The platinum electrodes were coated with gold by electroplating at 25 A m^{-2} from a solution containing 0.02 M potassium dicyanoaurate, 0.23 M potassium cyanide and 0.086 M potassium carbonate. The plating solutions were purged with argon for 30 minutes prior to and during the plating process. The gold was plated for 2 to 4 minutes, which resulted in a deposit of 100 to 200 μg of gold.

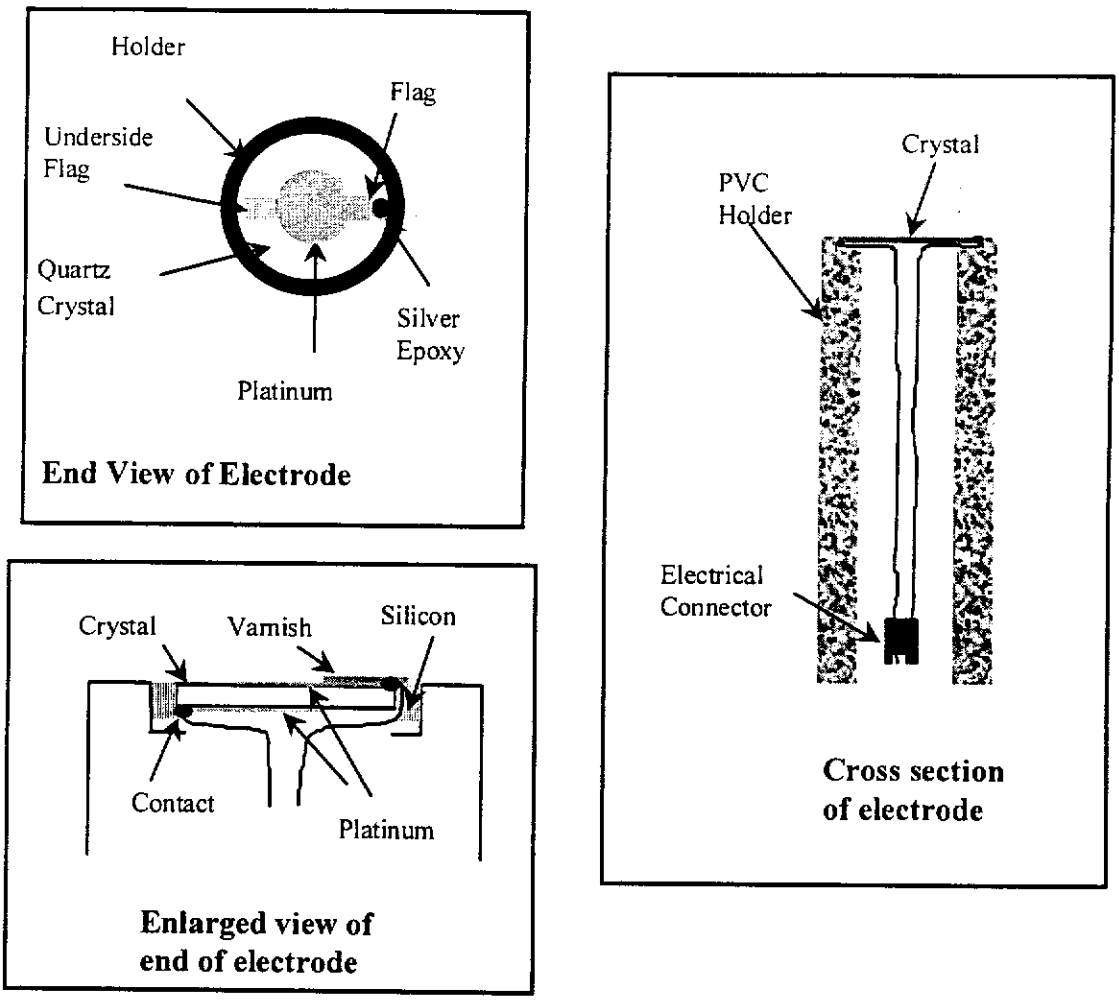

Figure 4.1 – Illustration showing how the quartz crystals are mounted in the cylindrical PVC adapter.

4.2.2. Kinetic Measurements

The kinetic measurements were performed using a rotating quartz crystal microbalance (RQCM), which was interfaced with a potentiostat to enable the simultaneous measurement of mixed potentials. This apparatus was also used for a number of electrochemical experiments, for which the apparatus is termed a rotating electrochemical quartz crystal microbalance (REQCM). For simplicity, the apparatus will be referred to as the REQCM, regardless of whether electrochemical measurements are being performed.

The REQCM is a unique instrument, as it can be used *in situ* to directly measure the leaching rate of metals over a short period. A brief review of the EQCM, the stationary version of the REQCM, and its application to hydrometallurgy is presented below. The EQCM has also been used to study many other processes, such as deposition and adsorption, and for further information, Ward (1995) presents a good summary.

4.2.2.1. Principles of EQCM

When a stress is applied to a quartz crystal, an electric potential is created across the crystal, and its magnitude is proportional to the applied stress (Ward, 1995). This is known as the piezoelectric effect. The basis of the EQCM is the converse piezoelectric effect, in which the application of a potential across a quartz crystal results in a mechanical strain. When the polarity of the applied potential is reversed, the induced strain will be equal, but in the opposite direction. Thus, when an alternating potential is applied to the quartz crystal, mechanical oscillation occurs with its amplitude parallel to the surface of the crystal (Ward, 1995).

In practice, the quartz crystal has thin metal coatings on either side of the electrode, forming a pair of electrodes. This enables an AC potential to be applied to the electrodes on the crystal, and the resultant frequency of oscillation can be represented by Equation 4.1

$$f_o = \frac{v_{tr}}{2t_Q}$$ **Equation 4.1**

where f_o is the fundamental frequency of oscillation, v_{tr} is the transverse velocity of sound in quartz (3.34×10^4 m s^{-1}), and t_Q is the thickness of the quartz (Ward, 1995). This equation assumes that the velocity of sound in the electrode material is the same as that in quartz, which is valid if the thickness of the electrodes is small compared to that of quartz. If it is further assumed that the density of the electrode material is the same as quartz, then the frequency change, Δf, during deposition or leaching can be equated to the mass change by the Sauerbrey equation. This is shown in Equation 4.2

$$\Delta f = \frac{-2f_o^2 \Delta m}{A\sqrt{\mu_q \rho_q}}$$ **Equation 4.2**

where Δm is the mass change, A is the area of the piezoelectically active area, ρ_q is the density of quartz and μ_q is the shear modulus of AT cut quartz (2.947×10^{11} dyn cm^{-2}) (Ward, 1995). This equation is valid if the electrode thickness is less than 2 % of the quartz thickness, which is usually the case for EQCM applications. To measure mass changes during chemical or electrochemical processes, all that is required is a circuit to apply an AC potential to the quartz crystal, and a frequency counter to measure the resultant frequency of oscillation. Therefore, the EQCM is a very powerful, inexpensive technique for measuring reactions occurring at the solution-solid interface.

4.2.2.2. The REQCM

In principle, the electrochemical quartz crystal microbalance is an extremely useful instrument for measuring leaching kinetics, although commercially available instruments have a stationary electrode. Thus, it is not possible to obtain reproducible and defined hydrodynamic conditions with these instruments, and

consequently a rotating EQCM has been developed to address this problem. The first application of a REQCM was described by Ritchie *et al.* (1994), who measured the deposition of copper from copper cyanide solutions. In another publication, they used the REQCM to measure leaching rates of gold in cyanide solutions in the presence of copper and ammonia (Zheng *et al.*, 1995). These authors simply used a commercial EQCM, and mounted the crystal to a rotating PVC cylinder. Although this instrument proved to be very useful, some stability problems were observed. This instability was probably due to the long length of wires between the crystal and the oscillation circuitry, which is discussed in detail below. Therefore, a new design for the REQCM was developed, in which the entire oscillator circuitry was contained within the rotating shaft.

The critical feature in constructing the REQCM was the circuitry and its interaction with the crystal. To ensure maximum stability, the distance from the circuit to the crystal must be minimised as long leads tend to act as antennae for picking up noise. This was accomplished by inserting the electronic circuit inside the shaft of the rotating head, as shown in Figure 4.2. The shaft was constructed of stainless steel, and a mild steel liner was inserted inside the shaft to shield the circuit. The entire shaft and shielding was connected to ground to minimise interference. The circuit is connected to the power supply, frequency counter and potentiostat by silver impregnated carbon brushes and copper slip rings. Each of the slip rings are insulated by teflon. The insulation around the frequency out slip ring is thickest, to minimise noise pickup from the other slip rings. The shaft can be dismantled by unscrewing the lock rings, which hold it in place. This enables easy access to the circuit for troubleshooting.

The circuit for the REQCM is shown in Figure 4.3, and was of essentially the same design as described by Bruckenstein *et al.* (1994). The circuit requires a very stable 5 V power supply, and this is provided by a voltage regulator and associated capacitors. The voltage regulator labled 7805 outputs a stable 5V power supply to the circuit. The small 0.047 μF capacitors on the input and output of the volatge regulator stop the regulator from oscillating, which is an inherent problem with this

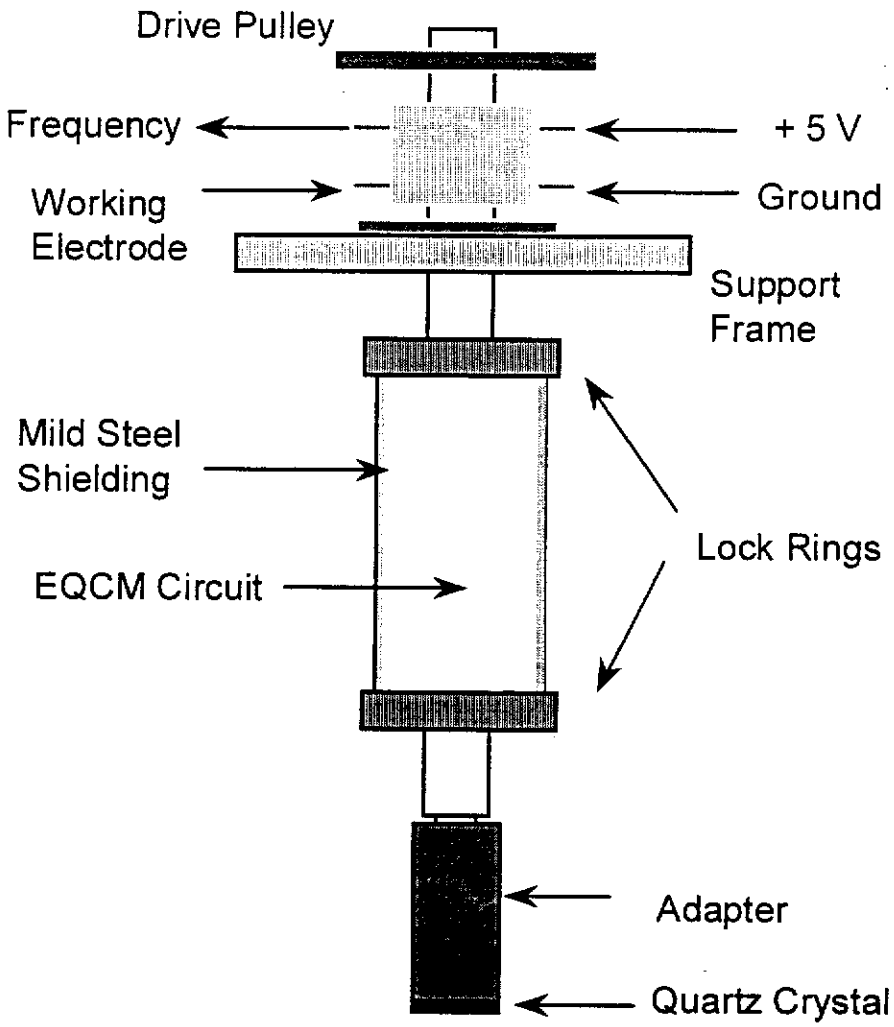

Figure 4.2 – Illustration showing the new design of the rotating electrochemical quartz crystal microbalance.

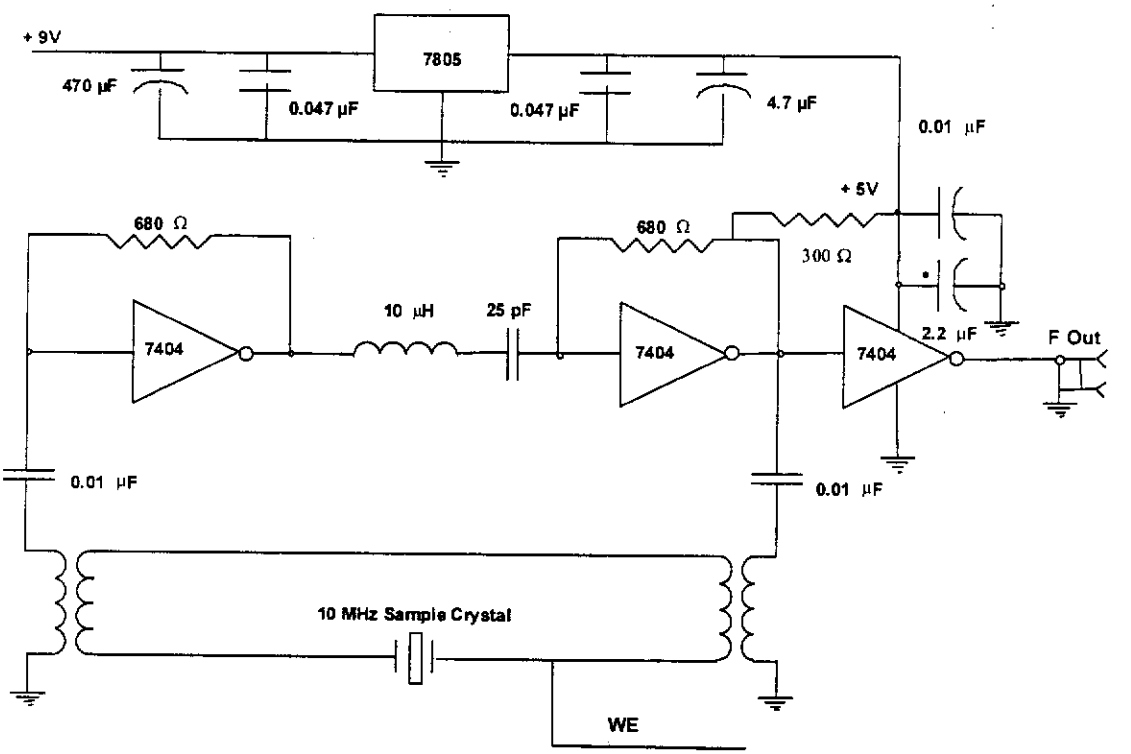

Figure 4.3 – Circuit diagram for the rotating electrochemical quartz crystal microbalance.

type of circuit. The 470 and 4.7 μF capacitors on the input and output side respectively, act as filters, protecting the circuit from sudden surges or drops in voltage. The circuit can be powered either from batteries or a DC power supply, provided the voltage is at least 8.5 V (5V required for the circuit and the additional required to run the regulator). In this case the power was supplied from a fully isolated laboratory power supply.

The heart of the circuit is the quartz crystal, and as outlined in the previous section, when an AC signal is applied across both sides of the crystal, oscillation will occur. The AC excitation for the quartz crystal is generated by the digital oscillation circuit, which must be able to oscillate at the same frequency as the quartz crystal. The main component of the digital oscillation circuit are the TTL inverters, labelled 7404. These inverters simply invert the signal from 5 V (called high) to 0 V (called low). That is, if 5 V is applied to the input of the invertor, 0 V is produced at the output and vice versa. The two 680 Ω resistors provide positive feedback to the inverters, which produces the oscillation. This oscillation is in the form of two out of phase 5 V square waves to either side of the crystal. When one side of the crystal is at 5 V, the other side is at 0 V and vice versa. This causes the crystal to oscillate at its resonant frequency.

The 10 μH inductor and 25 pF capacitor are essential to the operation of the crystal in solution. They form an oscillating tank circuit, where the frequency of oscillation, f_0, is that shown in Equation 4.3

$$f_0 = \frac{1}{2\pi\sqrt{LC}} = 10.065\,\text{MHz}$$

Equation 4.3

where L is the inductance and C is the capacitance (Floyd, 1996, p. 889). This tank network provides tuning to the circuit, and hence prevents the crystal from oscillating at any frequency (such as the harmonics) apart from the fundamental frequency. The third inverter acts as an output buffer to the frequency counter, which counts the frequency of the circuit. The circuit incorporates transformer isolation to stop DC

current flowing from the potentiostat into the circuit, a critical feature when using a potentiostat with the working electrode at virtual ground (as in most commercial potentiostats) (Ward, 1995).

The frequency of the crystal oscillation was measured with an Optoelectronics model 3000A hand held frequency counter, which was interfaced with an IBM compatible PC through the serial port. Data acquisition and analysis was completed with software that was written in Q-Basic. A commercial software package, Microsoft Excel, was used to calculate the gradients from the graphed data, and the errors in the slope are expressed as the 95 % confidence interval.

4.2.3. Surface Studies

Surface analysis was performed on some of the electrodes following deposition or leaching. After the experiment was completed, the electrode was rinsed thoroughly and dried under vacuum overnight prior to analysis. Optical imaging was performed with a Nikon microscope. The microscope was equipped with a Nikon camera, allowing colour photographs to be taken. Scanning electron microscopy was used to obtain images at higher magnification. This work was carried out on a Phillips model XL SEM, which was equipped with an ISIS Energy Dispersive Spectrometer. This allowed elemental analysis of the gold surfaces to be performed.

4.3. Results and Discussion

4.3.1. Dissolution of Gold in Aerated Cyanide

4.3.1.1. Kinetics

When gold is immersed in an aerated solution containing cyanide, it should dissolve to form the stable gold cyanide complex. As discussed in the review in section 2.1.3, the dissolution of gold can occur by two possible mechanisms. Elsner (1846) proposed that gold dissolved according to Equation 4.4, producing both hydroxide and the gold cyanide complex as products. Bodländer (1896) suggested that oxygen reduction proceeds by a two electron process, producing hydrogen peroxide rather than hydroxide, as shown in Equation 4.5. Throughout this thesis, the stoichiometry of the dissolution of gold will be expressed as the percentage of oxygen which is reduced to hydroxide. Thus, if dissolution proceeds by Equation 4.4, then 100 % of oxygen is fully reduced to hydroxide, while for Equation 4.5, 0 % of the oxygen is fully reduced to hydroxide.

$$4Au + 8CN^- + O_2 + 2H_2O \rightarrow 4Au(CN)_2^- + 4OH^- \qquad \textbf{Equation 4.4}$$

$$2Au + 4CN^- + O_2 + 2H_2O \rightarrow 2Au(CN)_2^- + 2OH^- + H_2O_2 \qquad \textbf{Equation 4.5}$$

The rate of dissolution of electroplated gold was measured using the rotating electrochemical quartz crystal microbalance. Shown in Figure 4.4 is the mass versus time response for the leaching of gold in air saturated 20 mM sodium cyanide at pH 10.0 and at a rotation rate of 300 rpm. The mass of the electrode decreases as the gold is leached, and dissolution rate is calculated from the differential of mass with respect to time, dM/dT. It is clear from Figure 4.4 that the dissolution rate varies slightly for the first 1000 seconds of dissolution, after which, it became constant at

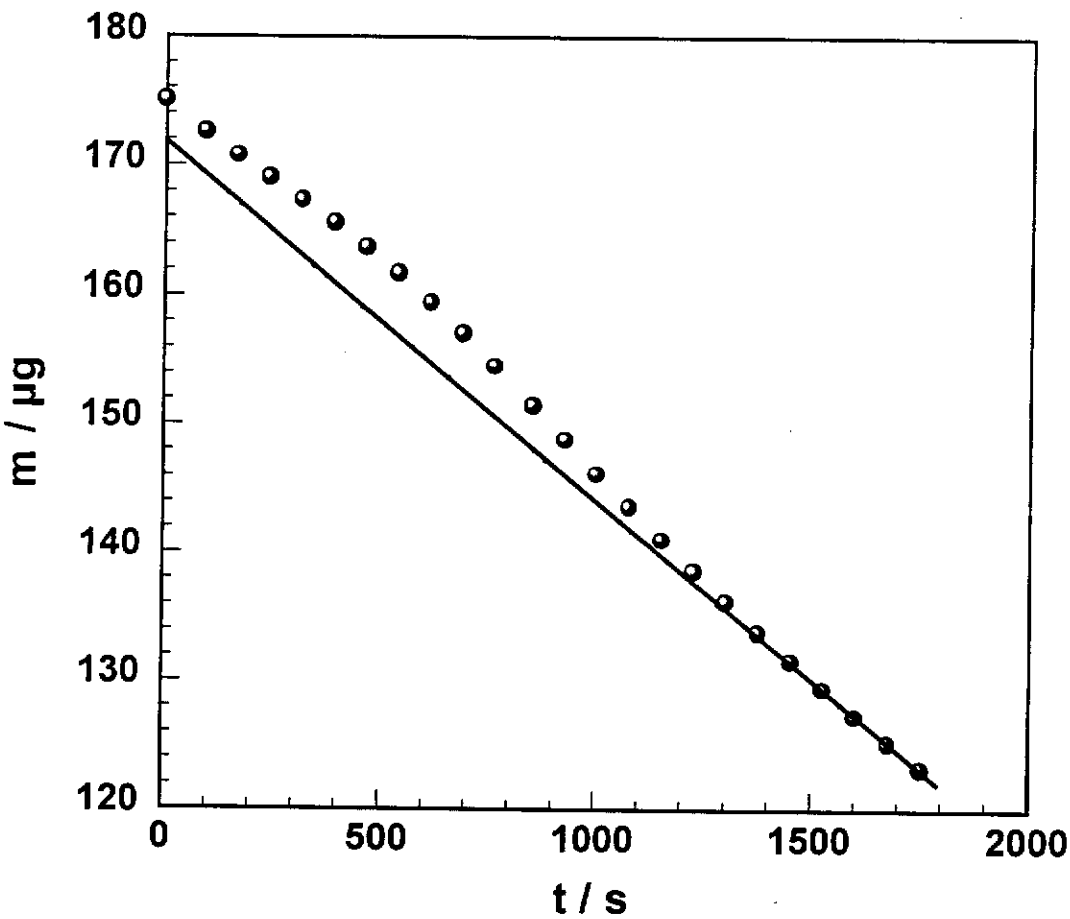

Figure 4.4 – Mass versus time response for the leaching of gold. Experimental conditions: air saturated 20 mM cyanide, pH 10.0, 25 °C, 300 rpm.

0.69×10^{-5} mol m^{-2} s^{-1}. This is taken as the rate of dissolution of gold in aerated 20 mM cyanide solutions. Due to the accuracy and sensitivity of the REQCM, there is minimal error associated with the measurement of the rate of dissolution for a single kinetic experiment. However, the reproducibility of a number of identical experiments was within 5 %, and this is taken as the error in the measurement of leaching rates.

It is worth noting that the dissolution rate of gold in cyanide solutions was dependent on the age of the plating solution. For example, a number of experiments were conducted with gold which had been electroplated from a one month old plating solution. The rate of dissolution in this instance was found to be 2.5 times higher than gold plated from a fresh solution. It is believed that the difference in the rates is a result of the incorporation of impurities into the plating solution with time, resulting in a slightly less pure plated gold sample. Thus, to ensure that the system was of the highest possible purity, fresh gold cyanide electroplating solutions were prepared prior to each set of experiments.

The main advantage of performing experiments at a rotating gold disc is that the measured rate of dissolution can be easily compared to the rate of mass transfer of the reactants. If the rate of dissolution is equal to the flux of one of the reactants, then the reaction is diffusion controlled under that set of conditions. It will be recalled from the review that the flux of reactants can be calculated from the Levich equation, which is shown again in Equation 4.6

$$J = 0.62D^{2/3}\omega^{1/2}\nu^{-1/6}[O] \qquad \textbf{Equation 4.6}$$

where J is the flux of reactant (mol m^{-2} s^{-1}), D is the diffusion coefficient of reactant in solution (m^2 s^{-1}), ω is the disc rotation rate (s^{-1}), ν is the kinematic viscosity of solution (m^2 s^{-1}) and [O] is the bulk concentration of reactant O (mol m^{-3}). For gold dissolution in cyanide solutions, there are two solution phase reactants, cyanide and oxygen. Therefore, the flux of both cyanide and oxygen need to be considered. To calculate the flux, values of the diffusion coefficients, concentrations of cyanide and

oxygen, and the kinematic viscosity of solution are required. According to Guan and Han (1994), the values of D_{CN} and D_O are 2.18×10^{-9} $m^2 s^{-1}$ and 1.94×10^{-9} $m^2 s^{-1}$ respectively. The concentration of oxygen in air saturated solutions is 0.25 mM (Kudryk, 1954), and a value of 0.8904×10^{-6} $m^2 s^{-1}$ for water at 25 °C was chosen for ν (Lide, 1995). An exact quantity of ν is not required as it only enters the expression for the flux as the minus one sixth power. The calculation of the oxygen and cyanide flux is shown in Table 4.1, and is based on a rotation rate of 300 rpm and a cyanide concentration of 20 mM. It is clear that, under these conditions, the flux of cyanide is significantly higher than the flux of oxygen.

Reactant (X)	D_X / $m^2 s^{-1}$	[X] / mM	J_X / mol $m^{-2} s^{-1}$
Oxygen	1.94×10^{-9}	0.25	1.35×10^{-5}
Cyanide	2.18×10^{-9}	20	117×10^{-5}

Table 4.1 – Calculated flux for oxygen and cyanide to a rotating disc at 300 rpm in an air saturated solution containing 20 mM cyanide.

The flux of reactants can be equated to the dissolution rate of gold, r, by the reaction stoichiometry. On inspection of Equations 4.4 and 4.5, it is clear that if the dissolution rate is limited by the diffusion of cyanide, then $r = J_{CN} / 2$, while if the dissolution rate is limited by oxygen diffusion, there are two possible equations: $r = 2 \times Jo$ if the dissolution of gold produces peroxide; and $r = 4 \times Jo$ if dissolution produces hydroxide. The comparison between the measured rates and the calculated diffusion rates are thus shown in Table 4.2. It is clear that the dissolution of gold in aerated 20 mM cyanide solutions is not diffusion controlled. Therefore, the dissolution process is controlled by a slow surface step, and a proportion of the oxygen and cyanide that reaches the disc surface will be swept away unreacted.

System	10^5 r /mol m^{-2} s^{-1}
Measured rate	0.69
Rate based on cyanide diffusion	58.50
Rate based on oxygen diffusion (2 electron)	2.75
Rate based on oxygen diffusion (4 electron)	5.50

Table 4.2 – Comparison of measured rate of dissolution of gold with calculated dissolution rates based on the diffusion of cyanide and oxygen to the electrode surface. Experimental conditions: air saturated 20 mM cyanide solutions, pH 10.0, 25 °C, 300 rpm.

It is well known that the presence of surface films can cause a heterogeneous reaction to become chemically controlled, as discussed in the review. It has been proposed that during the dissolution of gold, a film of AuCN is formed on the surface (Nicol, 1980a). Such a film could result in a resistance between the surface and the solution interface, causing a decrease in the observed rate of dissolution. In the ensuing sections, the evidence for such a film is discussed, and it is shown that the experimental results are consistent with passivation of the gold surface by AuCN.

4.3.1.2. Surface Studies

The leaching of gold in aerated 20 mM cyanide solutions can also be characterised using scanning electron microscopy. In this instance, a polycrystalline gold electrode was leached for 24 hours, and the images of the surface after leaching are shown in Figures 4.5 and 4.6. The only difference between the two images is the magnification, which is 200x for the first image, Figure 4.5, and 1000x for the second, Figure 4.6. From both of these images, it can be seen that a proportion of the original surface of the electrode, which is characterised by the polishing marks, is still intact. Although the cyanide has attacked a number of sites on the gold surface, the quantity of gold which has been leached is minimal. This is particularly evident when these images are compared to those in Chapter 5, which show the leaching of

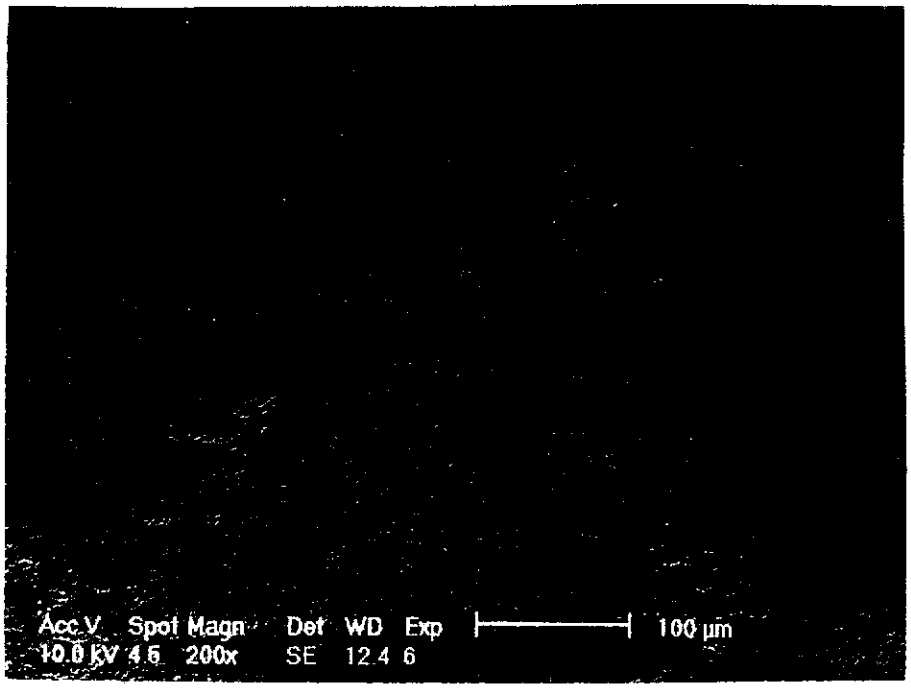

Figure 4.5 – SEM image of polycrystalline gold after 24 hours of leaching. Experimental conditions: 200x, air saturated 20 mM cyanide, pH 10.0, 25 °C, 300 rpm.

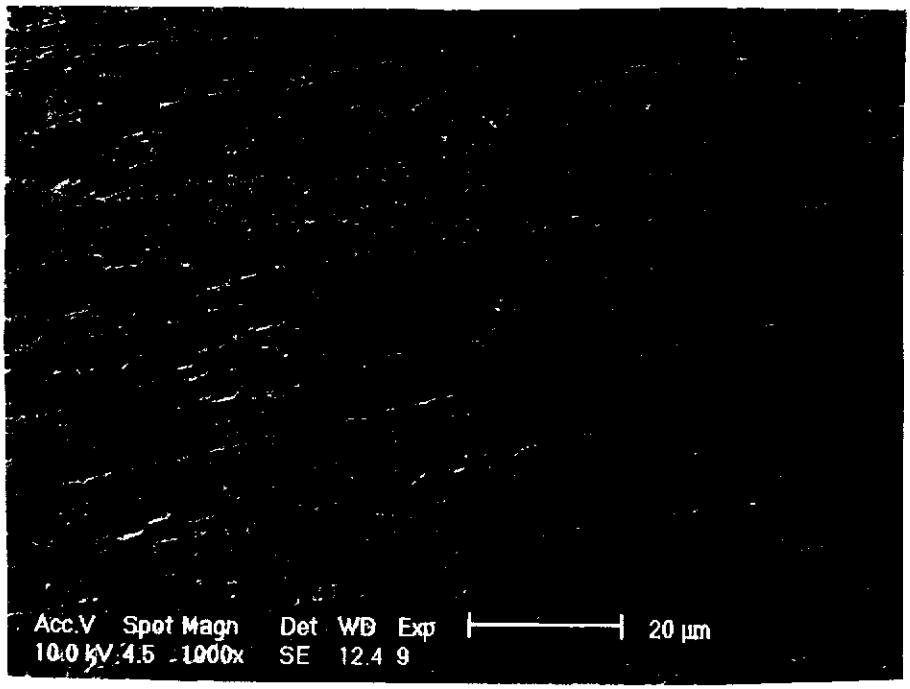

Figure 4.6 – SEM image of polycrystalline gold after 24 hours of leaching. Experimental conditions: 1000x, air saturated 20 mM cyanide, pH 10.0, 25 °C, 300 rpm.

gold in solutions containing 1 ppm lead (where the rate of dissolution is diffusion controlled). Therefore, the images of the gold surface are consistent with the kinetic studies in showing that the dissolution of gold in cyanide solutions is very slow.

4.3.1.3. Electrochemistry – Oxidation

Useful information about the leaching of gold in cyanide solutions can be obtained by using electrochemical techniques to investigate the gold oxidation half reaction (as discussed in Chapter 2). The oxidation of gold in 20 mM cyanide solutions was investigated using linear sweep voltammetry, and the gold oxidation polarisation curve was measured by scanning the electrode potential in the positive direction at 1 mV s^{-1}. In this section, gold oxidation was studied using polycrystalline gold, so that the polarisation curves are directly comparable with the work of other authors. The gold oxidation polarisation curve is shown in Figure 4.7, and it can be seen that there is a large gold oxidation peak, labelled P1, for which, gold readily oxidises to form the gold cyanide complex. The rest potential of gold in cyanide was found to be around -550 mV, which is close to the standard reduction potential of gold cyanide of -570 mV (Nicol, 1980a). Unfortunately, the reduction potential under the experimental conditions cannot be calculated using the Nersnt equation, as the effective concentration of $Au(CN)_2^-$ at the surface is not known. Gold oxidation begins when the potential is scanned in the positive direction. It can be seen that in the potential range of -550 to 300 mV, the current density, and hence rate of oxidation, is low. In the potential range 300 mV to 750 mV, the current density increases exponentially with potential. At 750 mV, which is labelled as potential (a) in Figure 4.7, the current density reaches a maximum and begins to decrease. When the potential reaches 850 mV, which is labelled (b), the current density decreases rapidly to zero, indicating that passivation has occurred. Throughout this chapter, the properties of the gold oxidation peak at high potentials are investigated. It will be shown that the passivation at (a) is due to the formation of a protective cyanide film, while the passivation at (b) is due to the formation of gold oxide.

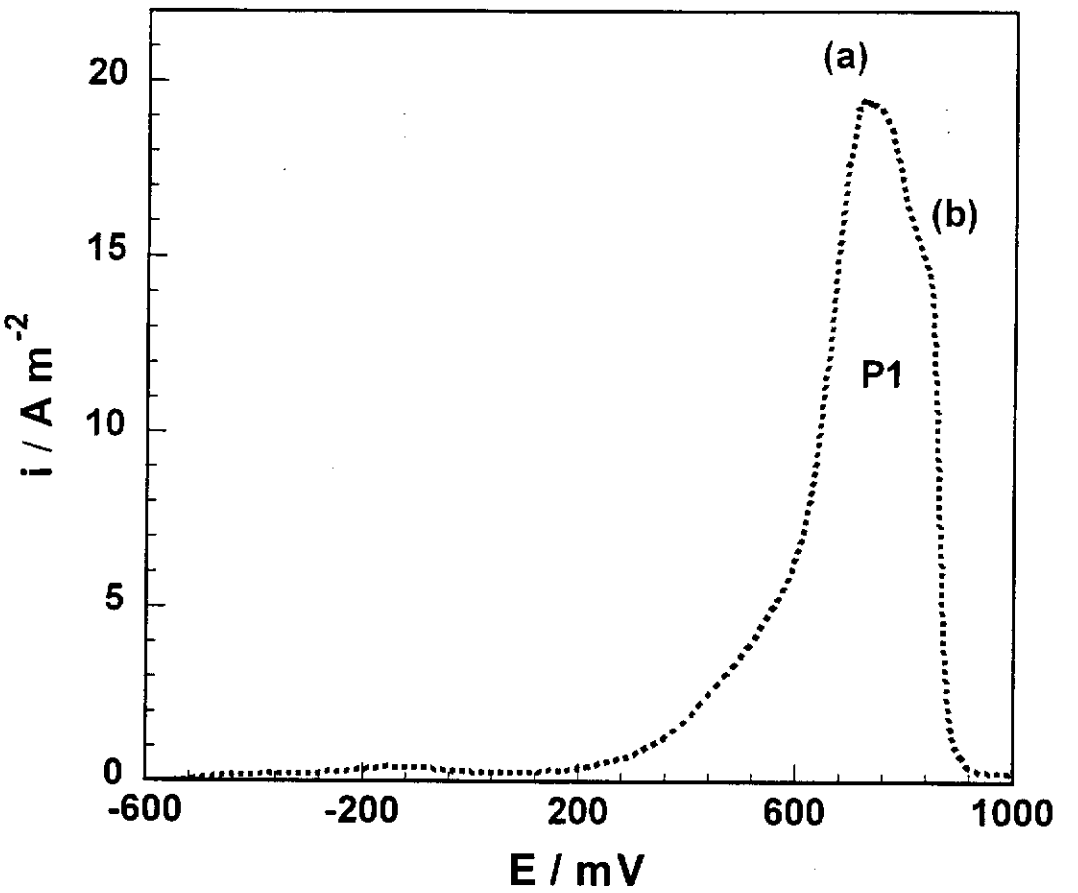

Figure 4.7 – Oxidation of polycrystalline gold. Experimental conditions: 20 mM sodium cyanide, pH 10.0, 1 mV s^{-1}, 25 °C, 300 rpm.

The area of the polarisation curve that is of most interest with respect to cyanidation is the region below 0 mV, and the observed low current density explains why the measured dissolution rates of gold in aerated 20 mM cyanide solutions are low. It has been suggested in numerous investigations, (e.g. Nicol, 1980a), that at low overpotentials, the gold is passivated by a surface film. This surface film is believed to be gold cyanide, AuCN, and the formation of such a species can occur by the reaction shown in Equation 4.7. The discussion of the blocking of the gold surface in the low overpotential region is continued throughout this chapter, and it will be shown that the proposed mechanism for passivation accounts for many of the results in the following sections.

$$Au + CN^- \rightarrow AuCN + e^- \qquad \textbf{Equation 4.7}$$

For gold dissolution to occur, the proposed AuCN blocking film must react with another cyanide ion, as shown in Equation 4.8. Therefore, simultaneous film formation and dissolution will occur, and the relative rates at which these processes occur will determine whether the film increases or decreases in thickness with time. At equilibrium, the rate of film growth will be equal to the rate of film dissolution, and the film thickness will remain constant.

$$AuCN + CN^- \rightarrow Au(CN)_2^- \qquad \textbf{Equation 4.8}$$

4.3.1.4. Evans' Diagrams

Information such as the mixed potential and rate of reaction of an electrochemical system can predicted from Evans' diagrams. For an Evans' diagram, each of the constituent half reactions are measured independently. The gold oxidation polarisation curve is measured in the same manner as discussed in the previous section, that is, in the absence of oxygen. The oxygen reduction polarisation curve can be measured by two methods. The first method is to measure the reduction polarisation curve on gold in the absence of cyanide, and the second

method is to measure the polarisation curve on an inert electrode in the presence of cyanide. It will be recalled from Chapter 3 that oxygen reduction is sensitive to the electrode substrate. Therefore, to obtain the best representation of reduction during gold dissolution, the oxygen reduction polarisation curve is measured on gold in the absence of cyanide.

In a traditional Evans' diagram, the polarisation curves are plotted as E vs. log |i|. However, to maintain uniformity with the oxidation polarisation curves, the data is plotted as |i| vs. E throughout this Thesis. These figures will be referred to as Evans' diagrams as they convey similar information. Shown in Figure 4.8 is the Evans' diagram for the leaching of gold in 20 mM cyanide solutions. The cathodic polarisation curve shows the reduction of oxygen on gold, and the anodic polarisation curve represents the oxidation of plated gold in 20 mM cyanide. Plated gold was used so that the Evans' diagrams closely matched the conditions that were used in the kinetic studies. The oxidation of solid gold has also been added as a comparison. At any potential, the oxidation current density for solid gold is considerably lower than that for plated gold. This suggests that the blocking of solid gold is more severe than for the plated gold, a result which is hardly surprising, as you would expect the plated gold surface to be considerably rougher, and to have a greater number of surface defects. It is also likely that the plated gold would be of lower purity, as the reagents used in the plating solution contain trace levels of impurities, which may co-deposit with the gold during the plating process. It is thus expected that solid gold would leach more slowly than the plated gold that is used in the kinetic studies.

For an Evans' diagram, the rate of reaction can be estimated from the current density at the intersection point of the anodic and cathodic polarisation curves. According to Faraday's law, the oxidation current density can be related to the rate of dissolution, as shown in Equation 4.9

$$r = \frac{i}{nF}$$ **Equation 4.9**

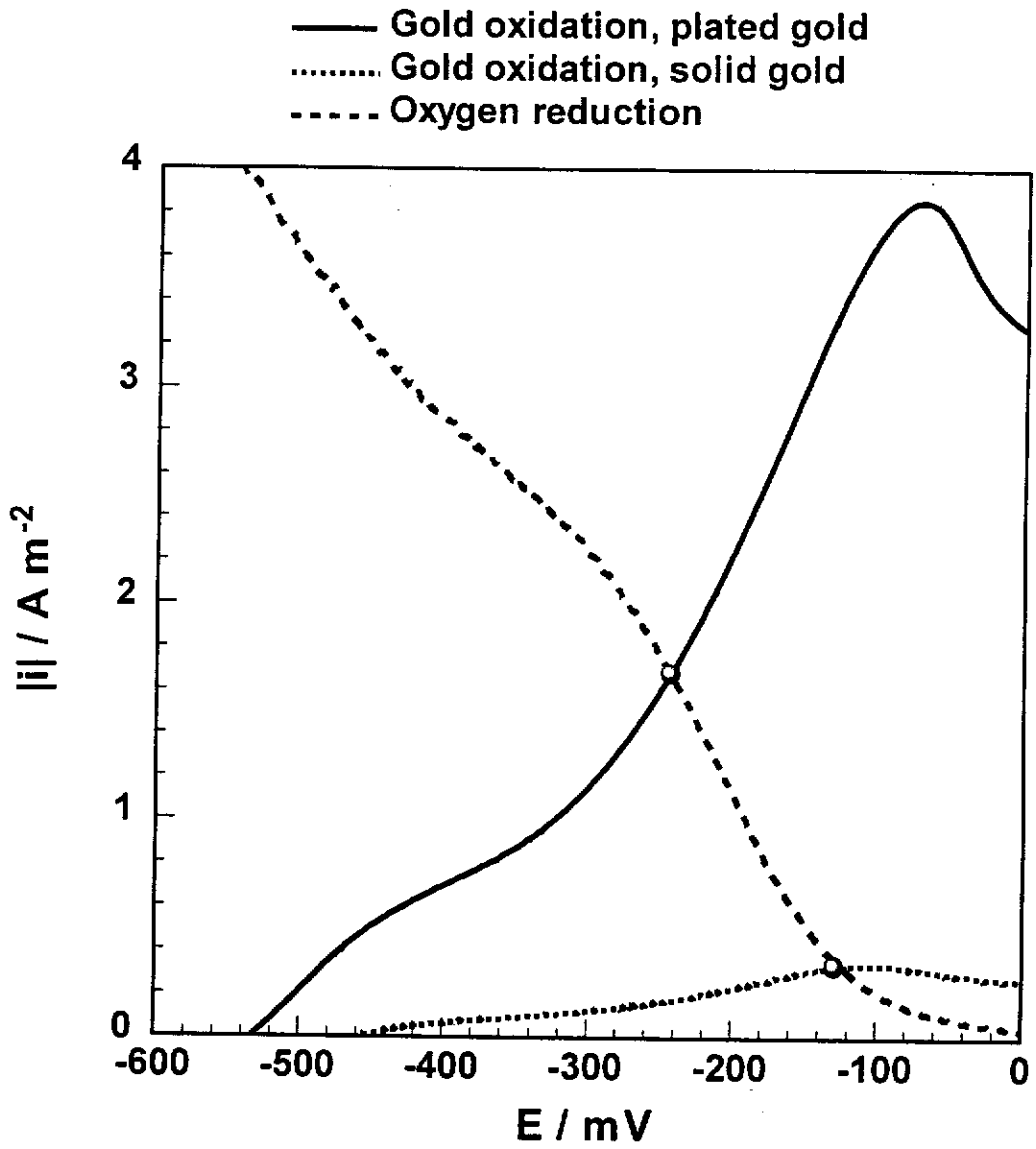

Figure 4.8 – Evans' diagrams representing the leaching of plated and solid gold in air saturated 20 mM sodium cyanide. Experimental conditions: pH 10.0, 25 °C, 300 rpm.

where r is the rate of dissolution (mol m^{-2} s^{-1}), i is the current density (A m^{-2}), n is the number of electrons involved in the oxidation of a single gold atom, and F is the Faraday constant (96484 C mol^{-1}). The calculated mixed potentials and rates of dissolution for solid and plated gold have thus been estimated, and are shown in Table 4.3. The results from the kinetic studies have also been added for comparison.

System		10^5r /mol m^{-2} s^{-1}	E_m /mV
Solid Gold	Measured	N.A.[1]	-148
	Calculated	0.34	-127
Plated Gold	Measured	0.69	-220
	Calculated	1.74	-243

[1] Rate of dissolution of solid gold cannot be measured using the REQCM

Table 4.3 – Calculated and measured mixed potentials and rates of dissolution of plated and solid gold in aerated 20 mM cyanide solutions. Experimental conditions: pH 10.0, 25 °C, 300 rpm.

It is clear that the calculated rate of dissolution of plated gold does not match well with the measured rate. This result is not surprising as an Evans' diagram always suffers from the inherent problem that it is only an approximation to the real system. Perhaps the biggest problem with this Evans' diagram is that the reduction of oxygen is studied on a clean gold surface in the absence of cyanide. Such a surface is likely to be very different to the surface of dissolving gold, which is believed to be covered by a film of AuCN. It will be recalled from Chapter 3 that oxygen reduction is substrate dependent, and thus it is likely that oxygen reduction on AuCN will occur at a different rate to the reduction on a clean surface. It was therefore decided that in this chapter, with the exception of section 4.3.4.3 (in which the gold is shown to be active at 60 °C), Evans' diagrams would not be used to predict the dissolution process. Instead, the main emphasis is placed on the kinetic studies, in which the actual rate of dissolution is determined. In Chapters 4 and 5, it will be shown that the influence of the passive film is minimal in the presence of certain impurities, and that Evans' diagrams are invaluable under these conditions.

In summary, both the kinetic and electrochemical studies show that the dissolution of gold in cyanide solutions is not diffusion controlled. To obtain further information about the rate determining step, the dissolution reaction is investigated as a function of cyanide concentration, rotation rate and temperature, and these results are presented in the following sections. For each of the experimental variables, both kinetic and electrochemical data is presented in a similar manner to the previous sections.

4.3.2. Effect of Cyanide Concentration

4.3.2.1. Kinetics

The dissolution of gold was investigated as a function of cyanide concentration, and the results are shown in Figure 4.9. In a similar manner to section 4.3.1.1, the measured dissolution rates can also be compared to the theoretical rates based on diffusion. There are three situations that need to be considered: 1) diffusion of cyanide; 2) diffusion of oxygen when dissolution occurs by the Elsner equation; and 3) diffusion of oxygen when dissolution occurs by the Bodländer equation. The diffusion of cyanide is shown in Figure 4.9 as line (a), and it can be seen that the flux increases linearly with cyanide concentration. The diffusion of oxygen is independent of cyanide concentration, and thus will be represented on a rate vs. cyanide graph by horizontal lines at 5.5 and 2.75×10^{-5} mol m^{-2} s^{-1} for cases 2 and 3 respectively. The diffusion of oxygen when dissolution occurs by the Bodländer equation, case 3, is shown in Figure 4.9 as line (b), and case 2 has been omitted for simplicity.

It is clear from Figure 4.9 that there are two mechanisms by which the dissolution of gold occurs, one at low cyanide concentrations, and one at high cyanide concentrations. By analysing the dissolution behaviour in each of these

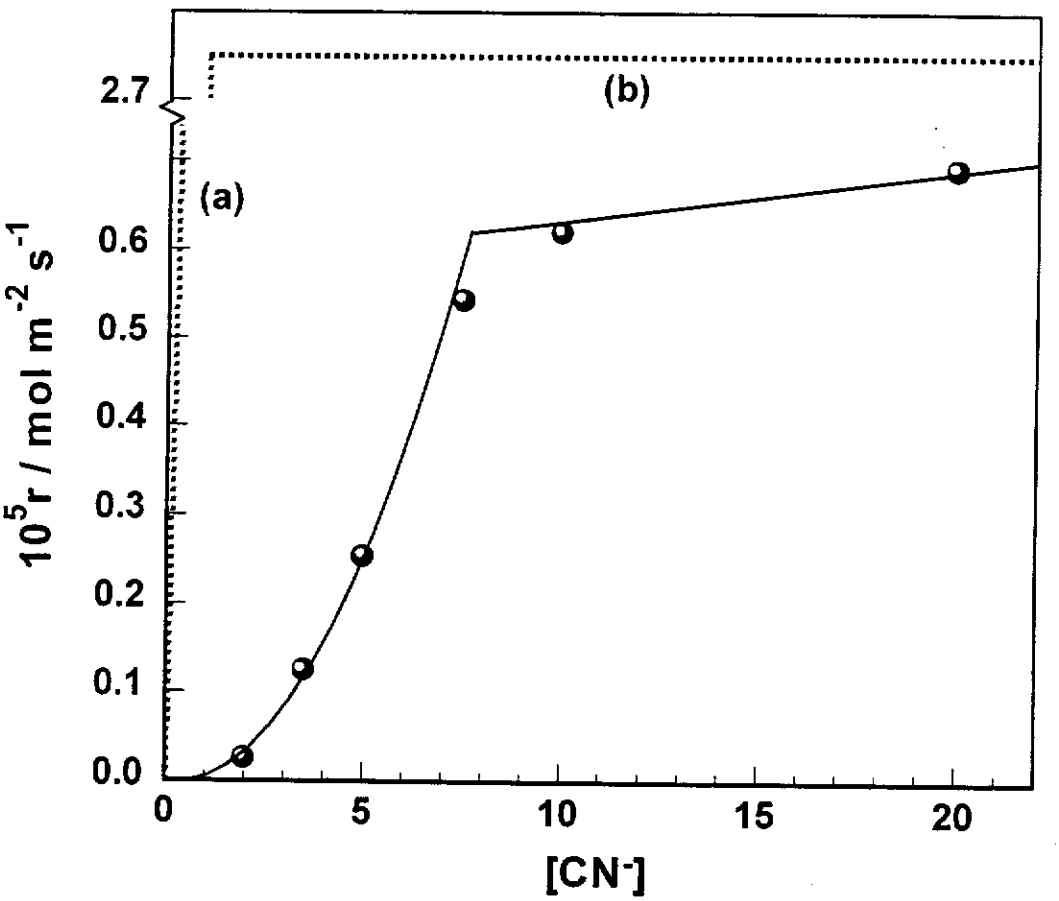

Figure 4.9 – Rate of dissolution of gold as a function of cyanide concentration. Line (a) represents the cyanide diffusion limiting rate, and line (b) represents the oxygen diffusion limiting rate when dissolution occurs by the Bodländer equation. Experimental conditions: air saturated, pH 10.0, 25 °C, 300 rpm.

concentration ranges, information about the mechanism of cyanidation can be obtained. This analysis is discussed in terms of evidence for a surface film, and evidence for a film of AuCN, as presented below.

(a) Evidence for a Surface Film

From Figure 4.9 it can be seen that:

1) At any cyanide concentration, the measured dissolution rate is lower than the calculated rates based on the diffusion of cyanide and oxygen. Hence, the dissolution of gold over the range of cyanide concentrations investigated is not diffusion controlled. In the review, it was shown that low dissolution rates can be caused by blocking of the surface by a resistive film, resulting in an iR drop between the gold and the solution interface.

2) At low cyanide concentrations, the rate of dissolution increases with cyanide, suggesting that the rate determining step at low concentrations is dependent on cyanide. In the review, it was shown that when a surface film is present and oxygen is in excess of cyanide, the iR drop across the film reduces the reaction rate, and the limiting reaction step is the diffusion of cyanide through the surface film (see Figure 2.4). This is referred to as *quasi* cyanide diffusion control, and explains why the dissolution rate increases with cyanide concentration.

3) At high cyanide concentrations, the rate of dissolution is almost independent of cyanide concentration. Therefore, the rate determining step at high cyanide concentrations is different to that at low cyanide concentrations. In the review, it was shown that when a surface film is present and cyanide is in excess of oxygen, the iR drop across the film results in the reaction being chemically controlled and independent of cyanide concentration (see Figure 2.5).

Therefore, the results shown in Figure 4.9 at both low and high cyanide concentrations are consistent with the surface being blocked by a resistive film.

(b) Evidence for a Film of AuCN

The experimental results shown in Figure 4.9 can be analysed to determine whether the passivation is due to a film of AuCN, as has been suggested in the past (Nicol, 1980a). From Figure 4.9, it can be seen that:

1) At low cyanide concentrations, the increase in the rate of dissolution of gold with cyanide concentration is parabolic, rather than linear, as is expected for *quasi* cyanide diffusion control. If the surface is covered by a film of AuCN, then a further cyanide ion is required for the dissolution reaction to proceed, as shown in Equation 4.7 and discussed in section 4.3.1.3. At low cyanide concentrations, a greater proportion of the cyanide ions are consumed in the formation of AuCN, leaving less cyanide to react with AuCN and form $Au(CN)_2^-$. Thus, at low cyanide concentrations, the surface film is more stable, and increasing the cyanide concentration has two effects: 1) increases the flux of cyanide diffusion; and 2) decreases the stability of the film of AuCN (and so increases the rate of dissolution). In this way, the non-linear increase in dissolution rate with cyanide concentration is consistent with passivation of gold by AuCN.

2) The critical cyanide concentration, defined as the concentration at which the rate of dissolution becomes independent of cyanide, is estimated to be 8 mM. This is considerably higher than the theoretical critical cyanide concentrations of 0.95 and 1.9 mM for the Bodländer and Elsner equations respectively. It will be recalled from the review that a critical cyanide concentration in excess of the theoretical value is consistent with passivation of the surface by a film of AuCN.

3) The measured critical cyanide concentration, 8 mM, can be compared to the work of other authors, as shown in Figure 4.10. It is clear that most of the published critical cyanide concentrations are above the theoretical values. Hence, the majority of the data on the dissolution of gold as a function of cyanide solution is also consistent with passivation by a film of AuCN.

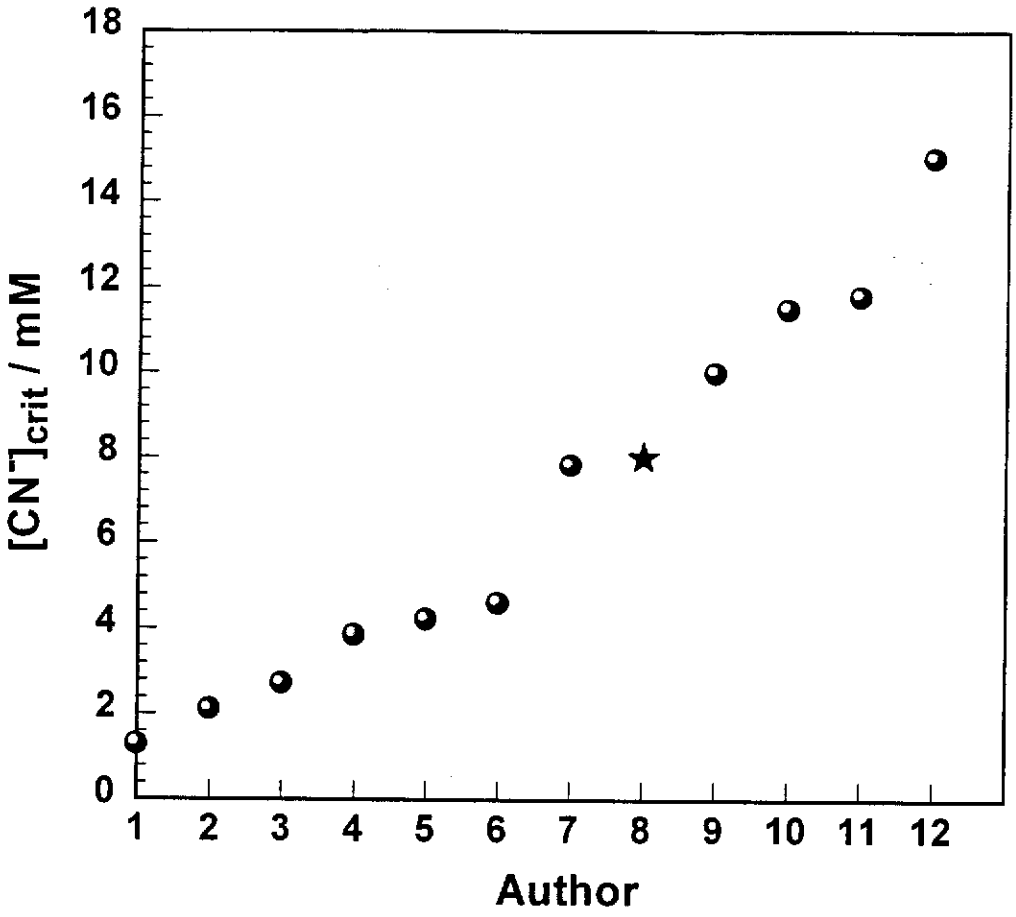

	Author		Author
1	Kakovskii and Kholmanskikh (1960)	7	Churchill and Laxen (1966)
2	Guan and Han (1993)	**8**	**This Work**
3	Kudryk and Kellogg (1954)	9	Trindade and Monhemius (1993)
4	Barksy, Swainson, and Hedley (1934)	10	Beyer (1936)
5	White (1919)	11	La Brooy, Komosa and Muir (1991)
6	Kameda (1949a)	12	Zheng *et al.*, (1995)

Figure 4.10 – Critical cyanide concentration for gold from this work compared with the published critical cyanide concentrations of previous authors.

In summary, it is clear that the dissolution behaviour of gold over a wide range of cyanide concentrations is consistent with passivation of the surface by AuCN. In the remaining kinetic and electrochemical sections in this chapter, the dissolution of gold over a wide range of experimental conditions is investigated, and it is shown that these results are also consistent with the mechanism discussed above.

4.3.2.2. Electrochemistry – Oxidation

The effect of cyanide concentration on the oxidation of gold at both low and high overpotentials was investigated, and the resultant polarisation curves are shown in Figure 4.11. The oxidation polarisation curves at low overpotentials, which are shown as an inset, were measured using plated gold. In this way, these polarisation curves can be directly compared with the kinetic data, which were discussed in the previous section. It can be seen that for plated gold at low overpotentials, the current density increases with increasing cyanide concentration, as expected. These polarisation curves are consistent with the kinetic data, which showed that the dissolution rate increases when the cyanide concentration is increased from 2 to 20 mM.

At high overpotentials, it can be seen from Figure 4.11 that, with increasing cyanide concentration, the shape of the polarisation curves change, and the peak oxidation current density increases. The potential at which the gold peak initially passivates, labelled (a), decreases with increasing cyanide concentration, suggesting that that passivation at potential (a) is caused by some type of cyanide film. The ratio of the magnitude of the oxidation current density to cyanide concentration was also found to decrease with increasing cyanide concentration. This indicates that at high overpotentials the oxidation of gold is not cyanide diffusion controlled.

It is interesting that there appears to be 4 different peaks associated with passivation of gold in 50 mM cyanide:

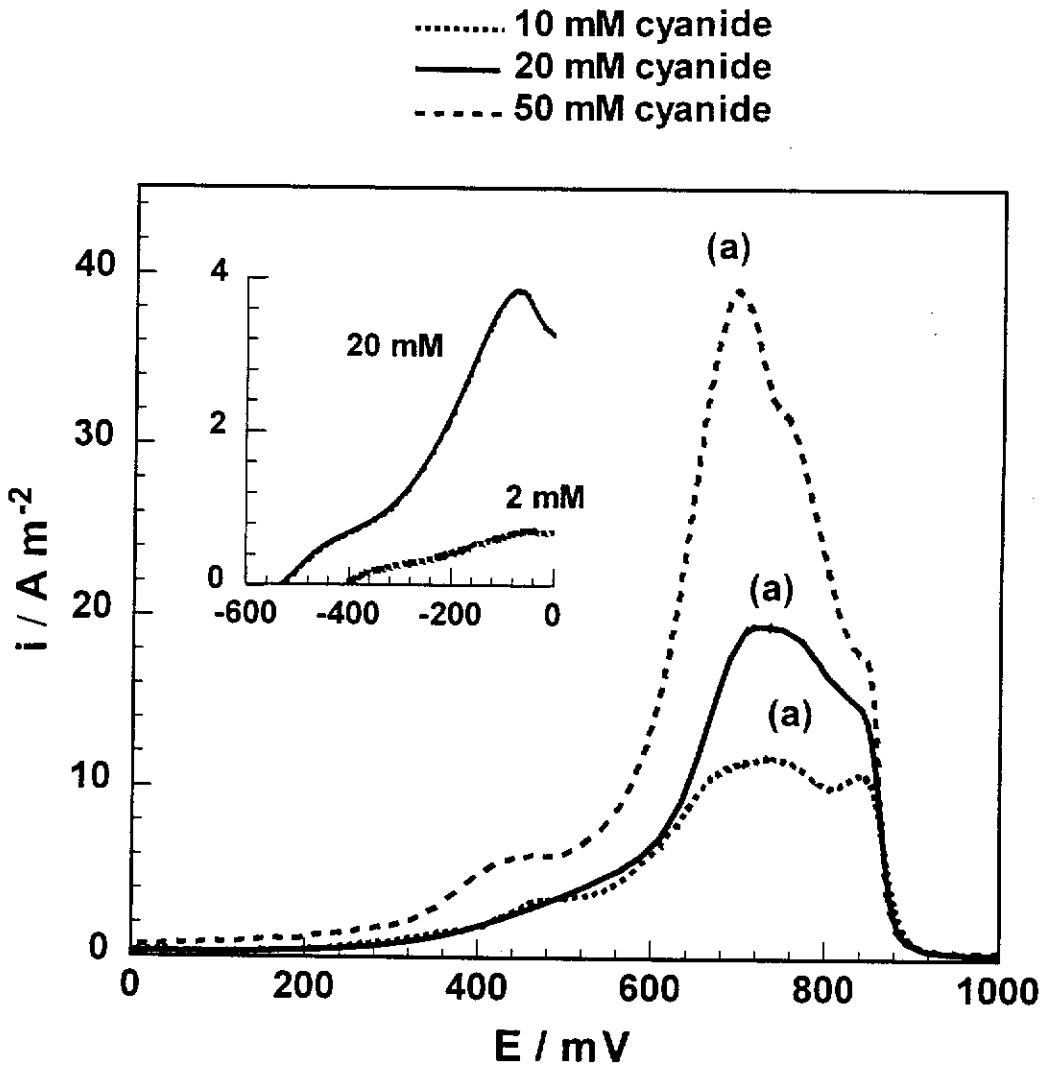

Figure 4.11 – Effect of cyanide concentration on the oxidation of gold at both high and low (inset) overpotentials. The polarisation curves at high overpotentials were measured using solid gold, while those at low overpotentials were measured using plated gold. Experimental conditions: pH 10.0, 1 mV s^{-1}, 25 °C, 300 rpm.

1) The small peak at 420 mV which becomes more pronounced at higher cyanide concentrations;
2) The main gold oxidation peak at 675 mV;
3) A small shoulder at 750 mV.
4) Final peak at 880 mV

It will be shown in section 4.3.6.2 that the final passivation at 880 mV is due to the formation of gold oxide. It is believed that the other peaks are caused by a dissolution – passivation mechanism, where the passive layer dissolves, and then reforms at a higher potential. Some mechanistic information about passivation at higher potentials has been discussed in other investigations (Kirk, Foulkes & Graydon, 1980, Cathro, 1964). Further discussion is beyond the scope of this work.

4.3.3. Effect of Rotation Rate

In the previous sections, it was shown that the dissolution of gold is not diffusion controlled over a wide range of cyanide concentrations. Consistent with this, at both low and high overpotentials, the gold oxidation half reaction has been shown to lack a diffusion limiting plateau. Each of these results can be verified by measuring the kinetic and electrochemical data as a function of rotation rate, as presented in the following sections.

4.3.3.1. Kinetics

For a rotating disc electrode, the flux of reactants to the surface of the electrode can be calculated using the Levich equation. The cyanide concentration used in this section (20 mM) is above the critical cyanide concentration (8 mM), and so only the flux of oxygen needs to be considered. The Levich equation, can be rearranged to give,

$$\frac{r}{\omega^{1/2}} = 0.62 D_o^{2/3} \nu^{-1/6} [O_2] x \qquad \textbf{Equation 4.10}$$

where x is the molar ratio of gold to oxygen, and the other symbols are the same as defined previously. Therefore, a plot of the rate of dissolution of gold vs. $\omega^{1/2}$ will be linear if the reaction is oxygen diffusion controlled, and from the slope, x can be calculated. The plot of the rate of dissolution vs. $\omega^{1/2}$ is shown in Figure 4.12 for gold in an aerated 20 mM cyanide solution. The oxygen diffusion limiting rate is also shown as lines (a) and (b), which represent the four and two electron reduction of oxygen respectively. It can be seen that the dissolution rate of gold in 20 mM cyanide solutions is independent of rotation rate. This is further proof that the dissolution of gold at 20 mM cyanide is chemically controlled as a result of a resistive surface film, and is in agreement with the published results of Zheng *et al.* (1995) and Guan and Han (1993).

4.3.3.2. Electrochemistry – Oxidation

The effect of rotation rate on the oxidation of gold in 20 mM cyanide solutions was investigated at both low and high overpotentials, and the resultant polarisation curves are shown in Figure 4.13. At low overpotentials, it can be seen from the inset that rotation rate has almost no effect on the oxidation of plated gold. This suggests that the rotation rate has no effect on the passivating film of AuCN, a result which is consistent with the findings in the previous section on the kinetic studies.

From Figure 4.13, it can be seen that at high overpotentials, the gold oxidation polarisation curves are very similar, with the exception that the peak current density increases with rotation rate. In a similar style to the previous section, the oxidation current density can be plotted as a function of $\omega^{1/2}$ to determine whether the oxidation of gold is cyanide diffusion controlled at high potentials. Shown in Figure 4.14 is the peak gold oxidation current density vs. $\omega^{1/2}$. It should be remembered that for the oxidation of gold, the potential is applied by a potentiostat, and hence it is not necessary to consider the diffusion of oxygen in this calculation. The theoretical limiting current density for cyanide diffusion can be calculated by the

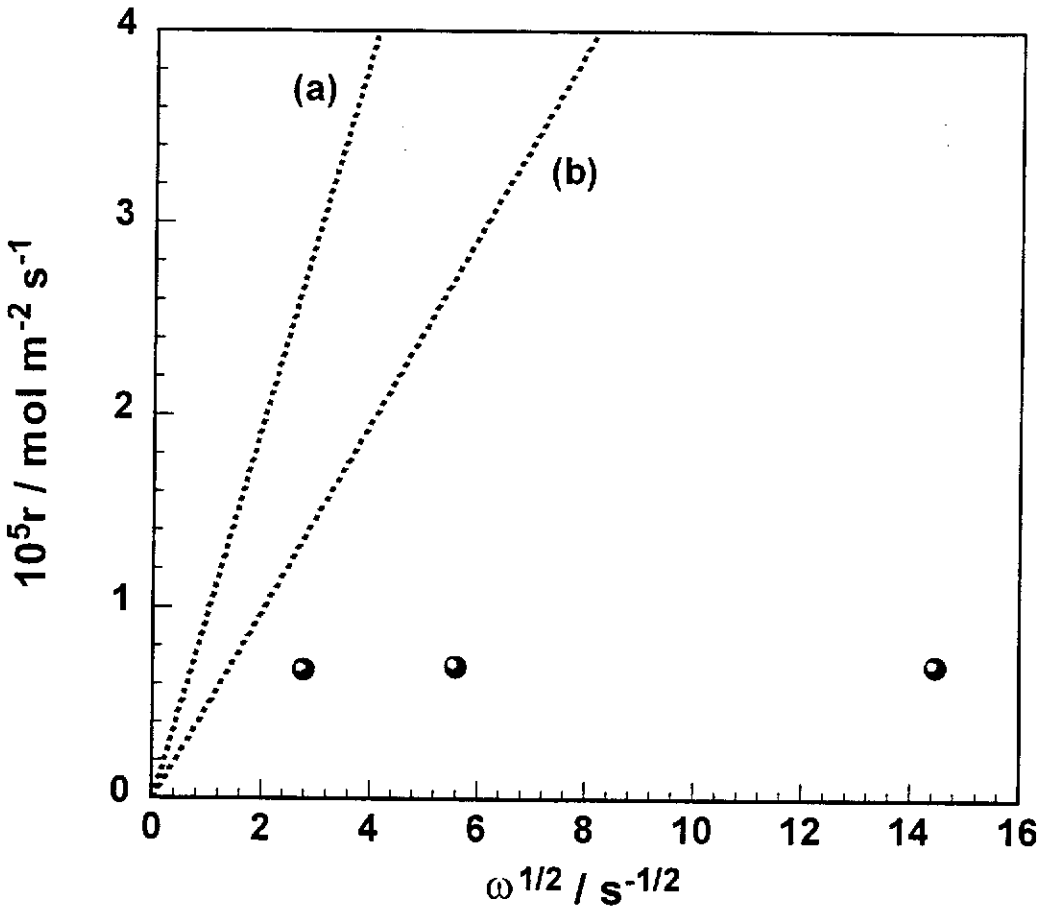

Figure 4.12 – Rate of dissolution of gold versus $\omega^{1/2}$. Lines (a) and (b) are calculated for the diffusion of oxygen with reduction to hydroxide and peroxide respectively. Experimental conditions: air saturated 20 mM cyanide, pH 10.0, 25 °C, 300 rpm.

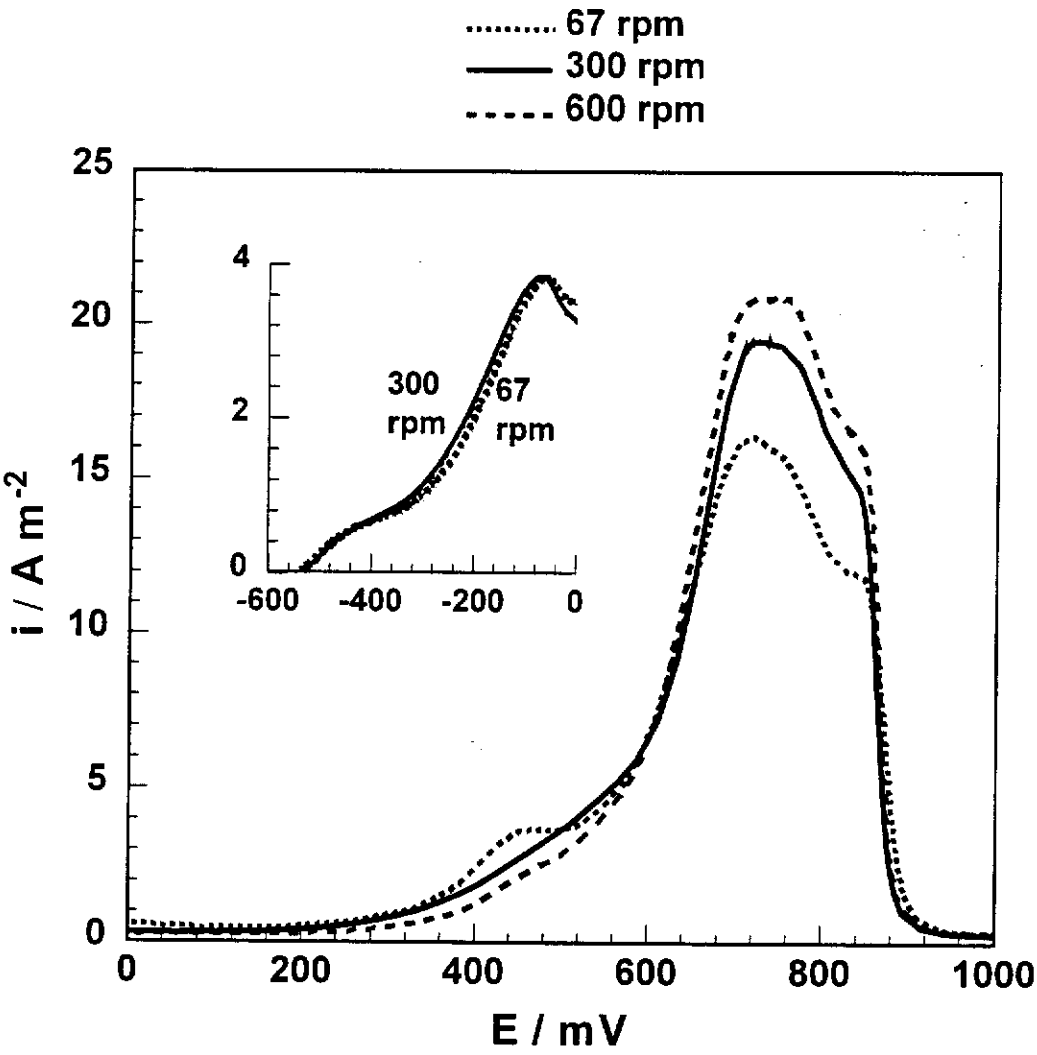

Figure 4.13 – Effect of rotation rate on the oxidation of gold at both high and low (inset) overpotentials. The polarisation curves at high overpotentials were measured using solid gold, while those at low overpotentials were measured using plated gold. Experimental conditions: 20 mM cyanide, pH 10.0, 1 mV s^{-1}, 25 °C, 300 rpm.

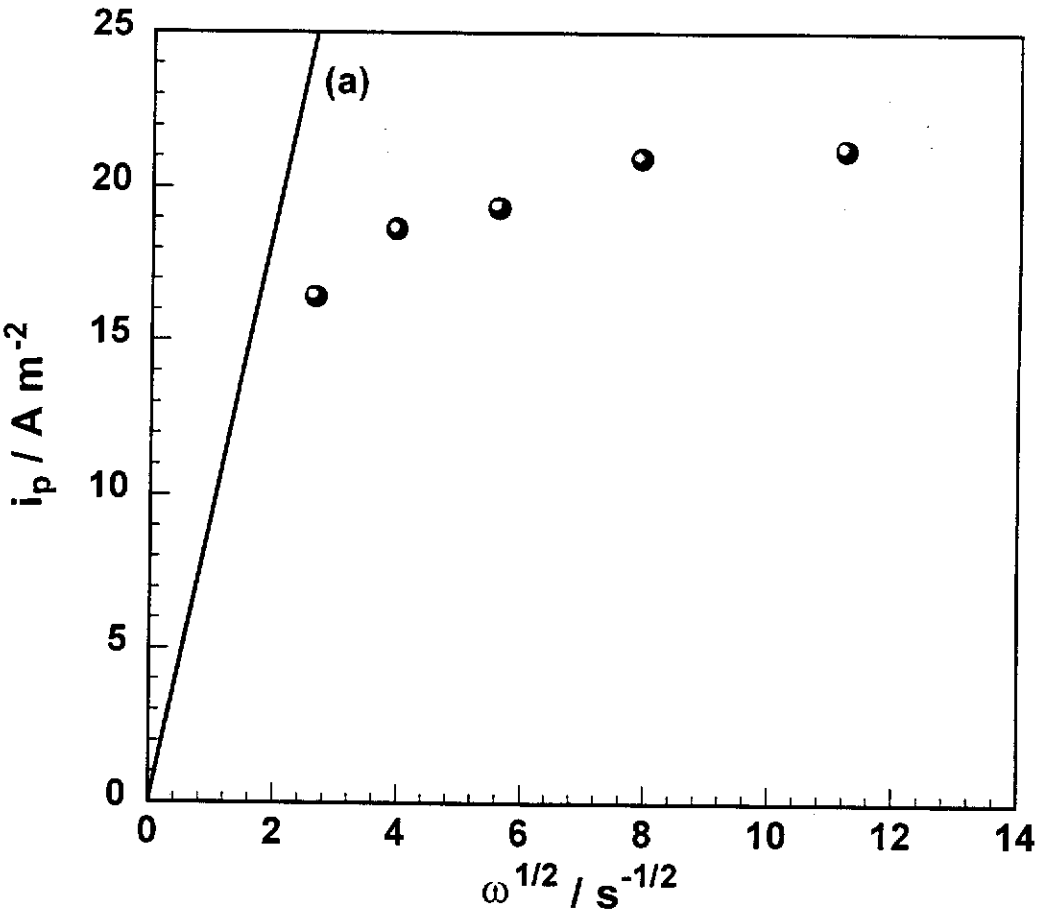

Figure 4.14 – Gold oxidation current density for peak P1 as a function of rotation rate. Line (a) is the theoretical diffusion limiting current density calculated using the Levich equation. Experimental conditions: 20 mM cyanide, pH 10.0, 1 mV s^{-1}, 25 °C, 300 rpm.

electrochemical form of the Levich equation, as shown in Equation 4.11. The factor of 0.5 is introduced because for gold oxidation, two moles of cyanide are consumed for every mole of gold that dissolves.

$$i = 0.5 \times 0.62nF\omega^{1/2}\nu^{-1/6}D_{CN}^{2/3}[CN^-] \qquad \textbf{Equation 4.11}$$

All the symbols are as previously defined. Using a value of D_{CN} already presented in this chapter, the diffusion limiting current density can be calculated as a function of rotation rate, which is shown in Figure 4.14 as line (a). It can be seen that the gold oxidation current density as a function of $\omega^{1/2}$ is not linear, and there is only a slight increase in i as the rotation rate increases. This indicates that the oxidation of gold at high potentials is chemically controlled, which is consistent with the findings of a number of authors, including Bek, Rogozhnikov and Kosolapov (1997), as discussed in Chapter 2. This is best illustrated at a rotation rate of 1200 rpm, where the gold oxidation current density, 21.2 A m^{-2}, is only one fifth of the diffusion limiting current density, 106 A m^{-2}. In contrast to this, at a rotation rate of 67 rpm, the gold oxidation current density is close to the cyanide diffusion limiting current density, suggesting that oxidation of gold is approaching cyanide diffusion control.

4.3.4. Effect of Temperature

It is well known that reaction rates of a system are affected by temperature. According to the Arrhenius equation, the rate constant is an exponential function of the activation energy and the absolute temperature, as shown in Equation 4.12.

$$k = Ae^{-\frac{Ea}{RT}} \qquad \textbf{Equation 4.12}$$

The variables in the Arrhenius equation are defined as follows: k is the rate constant (mol m^{-2} s^{-1}), A is the frequency factor (mol m^{-2} s^{-1}), R is the universal gas constant (8.314 J K^{-1} mol^{-1}), Ea is the activation energy (J mol^{-1}) and T is the temperature (K). It is clear that plotting ln(k) vs. 1/T will yield a straight line with intercept A,

and slope -Ea/R. Provided that the concentration of reactants is constant, either the rate of dissolution, r, or current density, i, can be substituted for k to enable the calculation of the activation energy for the dissolution or oxidation of gold respectively.

4.3.4.1. Kinetics

The dissolution rate as a function of temperature was measured to determine the activation energy for gold cyanidation. For gold leaching, one must be careful using this method, as in the temperature range of 0 to 100 °C, the oxygen solubility decreases with temperature. This decrease in solubility can be compensated for, provided the oxygen solubility and rate of dissolution as a function of temperature are known. If the reaction is first order with respect to oxygen concentration, then the corrected rate of dissolution is simply the ratio of oxygen concentrations at the two temperatures, as shown in Equation 4.13.

$$r_c = \frac{[O_2]_{25}}{[O_2]_T} \times r \qquad \textbf{Equation 4.13}$$

The variables are defined as: r_c and r are the corrected and measured rates of dissolution respectively (mol m^{-2} s^{-1}), and $[O_2]_{25}$ and $[O_2]_T$ are the mole fraction oxygen solubility at 25 °C and T °C respectively. According to Fogg and Gerrard (1991), in the temperature range 0 to 60 °C, the oxygen solubility can be represented as a function of temperature by Equation 4.14.

$$\ln(X_{O_2}) = -171.2542 + \frac{8391.24}{T/K} + 23.2433\ln(T/K) \qquad \textbf{Equation 4.14}$$

where X_{O_2} is the mole fraction solubility of oxygen in water. Therefore, the corrected rates of dissolution can be readily calculated, and are shown in Table 4.4, along with the measured rates of dissolution.

T /°C	$10^5 r$ /mol m^{-2} s^{-1}	r_T/r_{25}	$[O_2]_{25}/[O_2]_T$	$10^5 r_c$ /mol m^{-2} s^{-1}
25	0.69	1	1	0.69
35	1.31	1.89	1.16	1.52
47	2.03	2.94	1.32	2.68
60	3.62	5.25	1.46	5.27

Table 4.4 – Rate of dissolution of gold as a function of temperature. Also shown are the published values $[O_2]_{25}/[O_2]_T$ (Fogg & Gerrard, 1991), and the rate of dissolution, r_c, which is corrected for a constant oxygen concentration. Experimental conditions: air saturated 20 mM cyanide solutions, pH 10.0, 300 rpm.

It can be seen that the measured rate of dissolution of gold increases significantly with temperature, despite the lower oxygen solubility. It is thus clear, that the increase in the measured rates at high temperatures, which is shown as r_T/r_{25}, is far more significant than the correction factor. Therefore, the activation energy will not be significantly affected if the reaction is not first order with respect to oxygen concentration.

The activation energy can now be calculated from an Arrhenius plot of $\ln(r_c)$ versus 1/T, as shown in Figure 4.15. The Arrhenius plot was found to be linear, and the activation energy was calculated to be 47 ± 3 kJ mol^{-1}, which is similar to the value reported by Guan and Han (1993), 60 kJ mol^{-1}, in the temperature range 15 – 35 °C. It is generally recognised that the activation energy is a good guide to whether the process is diffusion or chemically controlled. Power and Ritchie (1975) state that processes which have an activation energy of greater than 25 kJ mol^{-1} are generally chemically controlled. Therefore, the observed activation energy of 47 kJ mol^{-1} is further evidence to show that the dissolution of gold in cyanide solutions is chemically controlled.

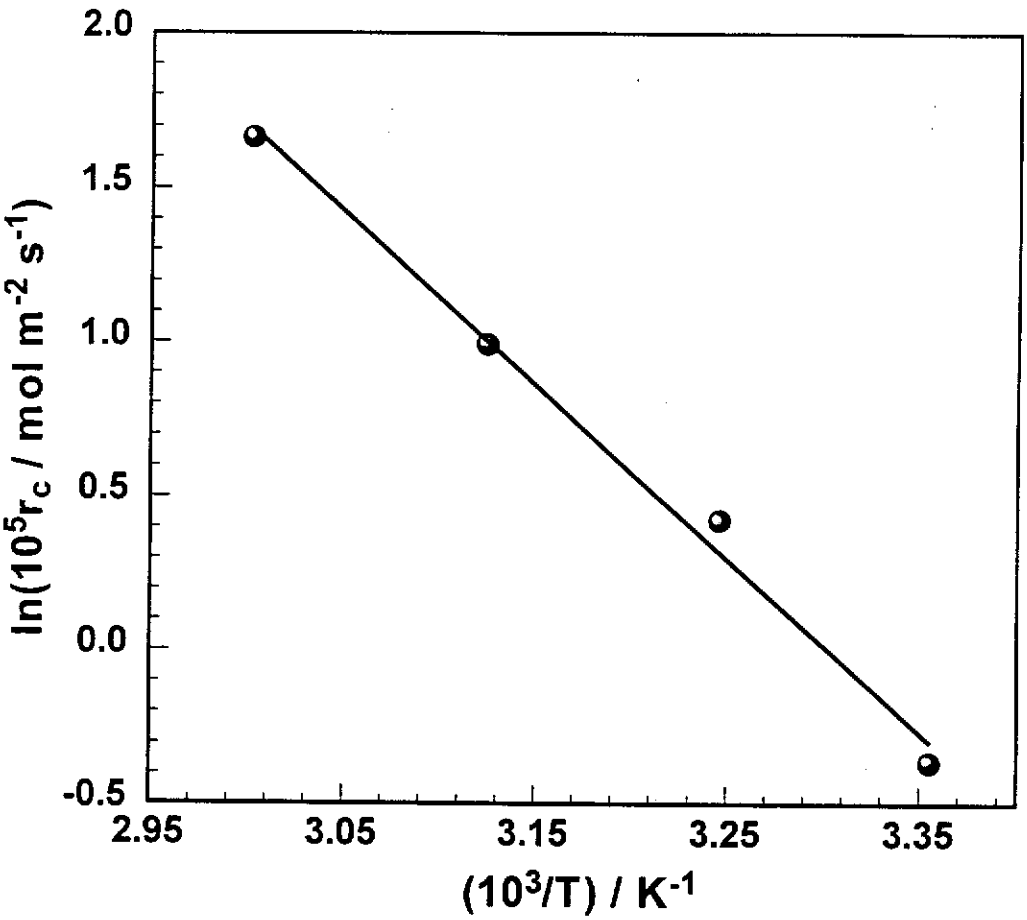

Figure 4.15 – Arrhenius plot for the corrected rate of dissolution of gold as a function of 1/T. Experimental conditions: air saturated 20 mM cyanide, pH 10.0, 300 rpm.

4.3.4.2. Electrochemistry – Oxidation

In a similar manner to the previous section, a study of the effect of temperature on the oxidation of gold in cyanide solutions can also provide useful information, such as the activation energy of the gold oxidation half reaction. It should be noted that the activation energy for gold oxidation is calculated for each of the gold oxidation peaks, and thus is not the same as the activation energy in the previous section.

To determine the activation energy, the oxidation of gold was measured as a function of temperature, and the resultant polarisation curves are shown in Figure 4.16. It is clear that the shape of the peak P1 is unchanged with temperature, although the peak current density is significantly higher at increased temperatures. Another feature of the gold oxidation polarisation curve at high temperatures is the oxidation behaviour at potentials below 0 mV, where there is a large gold oxidation peak, labelled P2. At 60 °C, gold oxidation begins at -550 mV, and as the potential is scanned in the positive direction, the oxidation current density increases rapidly until the current density reaches 19 A m^{-2} at a potential of -215 mV. The activity of gold at potentials below -215 mV suggests that the film of AuCN is unstable at high temperatures, and the ideal situation where the oxidation of gold is not complicated by a surface film is approached at 60 °C. Therefore, at high temperatures, the dissolution of gold should be well represented by Evans' diagrams, which are presented in the following section.

From Figure 4.16, it can be seen that at potentials more positive than -215 mV, the oxidation current density flattens out, and then decreases rapidly, dropping to 5 A m^{-2} at -100 mV. It is uncertain why the gold would passivate at -215 mV, although one possibility arises from the following chapter, which discusses the effect of lead on the dissolution of gold. It will be shown that in solutions containing 1 ppm lead and 20 ppm cyanide, there is a gold oxidation peak that is very similar to peak P2 at 60 °C in Figure 4.16. The similarity in these peaks suggests that the activity of gold in the low potential region at 60 °C could be due to

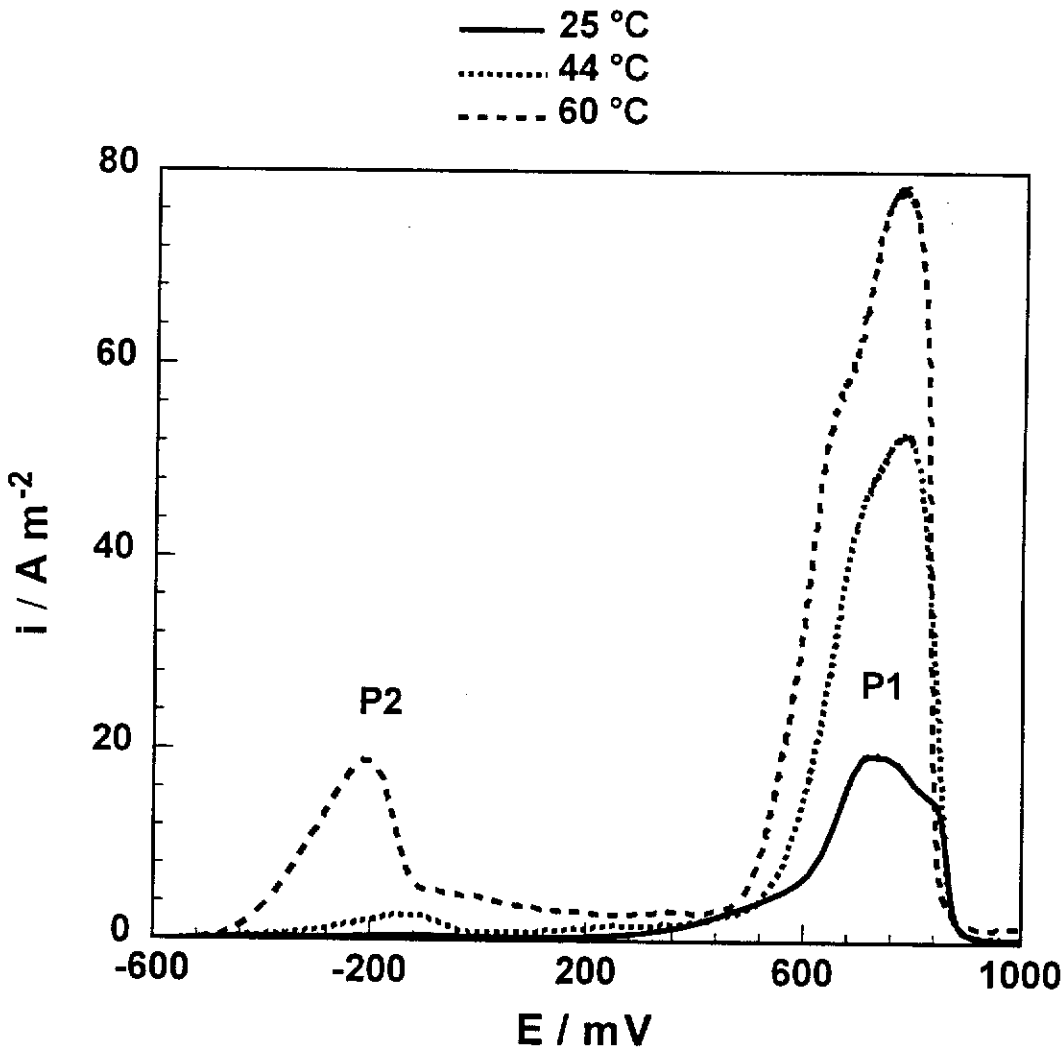

Figure 4.16 – Gold oxidation as a function of temperature. Experimental conditions: 20 mM cyanide, pH 10.0, 1 mV s^{-1}, 300 rpm.

trace levels of lead in the cyanide solution. AR grade cyanide is guaranteed to contain not more than 5 ppm lead w/w, which would result in a 20 mM cyanide solution having at most 0.005 ppm lead w/v. This could be enough lead to activate the surface of the gold at high temperatures.

The activation energy of both the gold oxidation peak P1 and the new gold oxidation peak P2 can be calculated by plotting ln(i) vs. 1/T. The Arrhenius plot of the peak current density at P1 is shown in Figure 4.17. The shape of the graph suggests that the mechanism of the oxidation of gold at P1 depends on temperature. At low temperatures, the activation energy is calculated from the tangent (a) to be 50 kJ mol^{-1}. This is indicative of a reaction that is under chemical control. At higher temperatures, the activation energy is calculated from the tangent (b) to be 21 kJ mol^{-1}. This is indicative of a reaction that is under diffusion control (Power & Ritchie, 1975). The Arrhenius plot for the peak P2, although not shown here, was found to be linear and the activation energy is calculated to be 88 ± 10 kJ mol^{-1}. This indicates that the oxidation of gold at P2 is chemically controlled. The peak at P2 is in the potential region where gold dissolution in aerated cyanide solutions occurs, thus explaining why the dissolution of gold in the previous section was found to be chemically controlled.

4.3.4.3. Electrochemistry – Evans' diagrams

The Evans' diagram representing the dissolution of gold in 20 mM air saturated solutions at 60 °C is shown in Figure 4.18. The Evans' diagram predicts that the rate of dissolution of gold at 60 °C is limited by oxygen reduction, and from the intersection point of the anodic and cathodic curves, the mixed potential and rate of dissolution of gold at 60 °C can be calculated. These values are shown in Table 4.5, where they are compared with the measured mixed potential and rate of dissolution from the kinetic section.

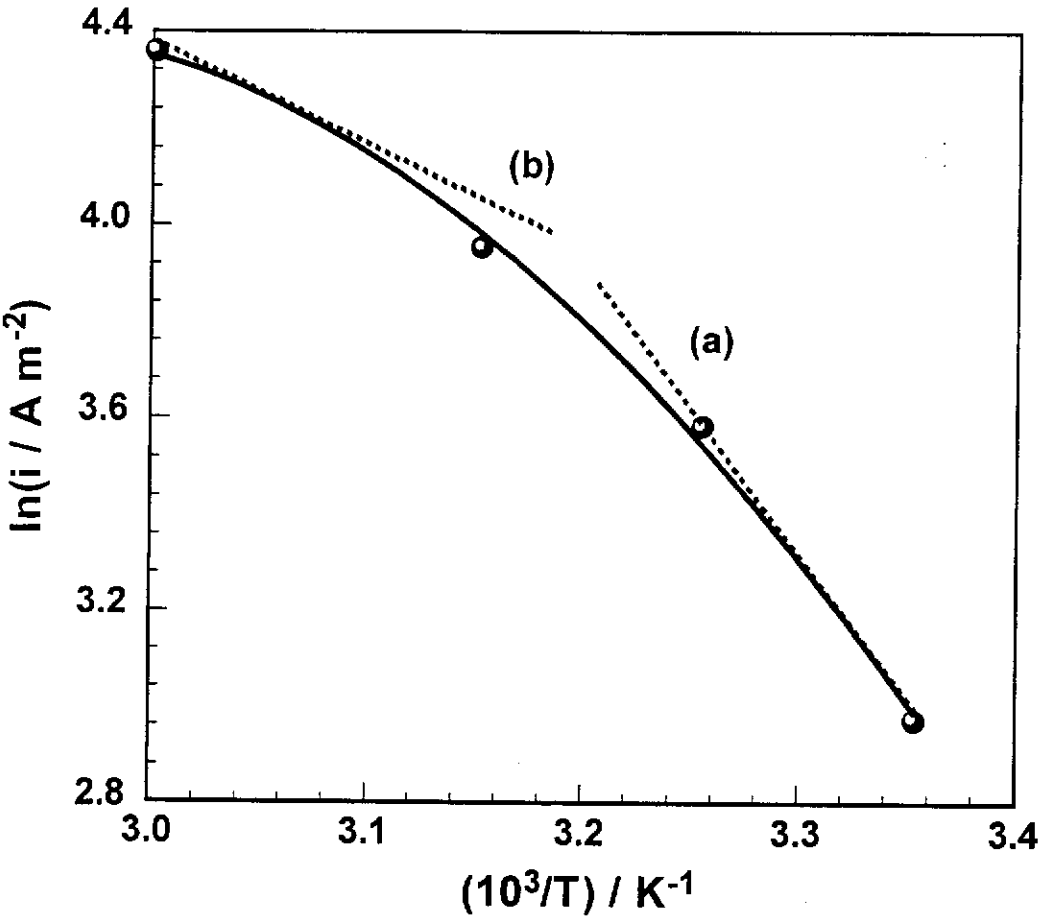

Figure 4.17 – Arrhenius plot of gold oxidation current density for peak P1 as a function of 1/T. Experimental conditions: 20 mM cyanide, pH 10.0, 300 rpm.

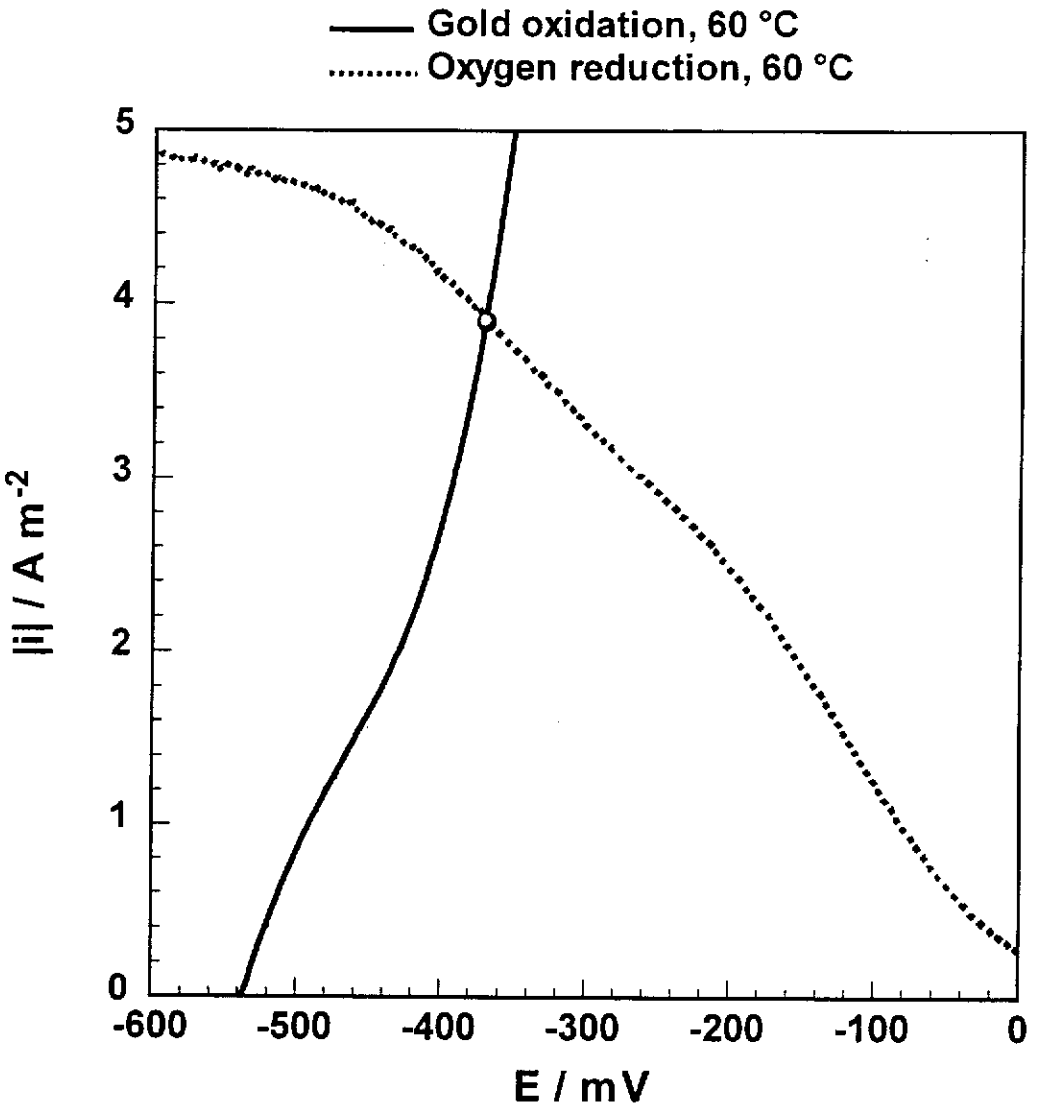

Figure 4.18 – Evans' Diagram representing the leaching of gold at 60 °C in air saturated 20 mM cyanide solutions. Experimental conditions: pH 10.0, 300 rpm.

System		$10^5 r$ /mol m^{-2} s^{-1}	E_m /mV
60 °C	Measured	3.7	-400
	Calculated	4.1	-370

Table 4.5 – Measured and calculated mixed potential and rate of dissolution of gold in an aerated cyanide solution containing 20 mM cyanide at 60 °C. Experimental conditions: pH 10.0, 300 rpm.

It can be seen that the Evans' diagram is very effective at estimating the mixed potential and rate of dissolution of gold at 60 °C, and hence the Evans' diagram is substantially more accurate in situations where the electrochemical reactions are not complicated by surface films.

In summary, both the kinetic and electrochemical data have shown that:

1) The dissolution of gold in 20 mM cyanide solutions is blocked by a surface film, presumably AuCN. The presence of such a film results in the reaction being chemically controlled with and activation energy of 47 ± 3 kJ mol^{-1}.

2) The oxidation of gold results in two main peaks, labelled P1 and P2. Peak P2 is only evident at high temperatures, and the oxidation of gold in this potential region is chemically controlled with an activation energy of 88 ± 10 kJ mol^{-1}. The oxidation of gold at high overpotentials (in the region of peak P1) was found to be under mixed chemical/diffusion control, with an activation energy of 50 kJ mol^{-1} at low temperatures, and 21 kJ mol^{-1} at high temperatures.

3) Evans' diagrams are more accurate under conditions where the process is not complicated by a surface film. This situation is approached at 60 °C, and under these conditions, the Evans' diagram correlated well with the kinetic data.

4.3.5. Effect of Oxygen Concentration

4.3.5.1. Kinetics

The measurement of the effect of oxygen concentration on the dissolution of gold is very important, as in industrial operations, the addition of pure oxygen in place of air is becoming more common. In this section, the dissolution rates at two oxygen concentrations, air and oxygen saturated solutions, are measured. These results are shown in Table 4.6. It can be seen that an increase in oxygen concentration results in an increase in the rate of dissolution. Care must be taken in quantitatively comparing the dissolution rates under conditions of enhanced oxygen concentration, as the dissolution mechanism can change from chemical to *quasi* cyanide diffusion control. It should be recalled from section 4.3.2.1 that the critical cyanide concentration for gold in air saturated cyanide solutions was approximately 8 mM, and as discussed in Chapter 2, the critical cyanide concentration at an oxygen concentration of $[O_2]$ is

$$[CN^-]_{crit,O} = [CN^-]_{crit,air} \times \frac{[O_2]}{[O_2]_{air}} \qquad \textbf{Equation 4.15}$$

where $[CN^-]_{crit,O}$ is the critical cyanide concentration at an oxygen concentration $[O_2]$, and $[CN^-]_{crit,air}$ is the critical cyanide concentration for air saturated solutions (oxygen concentration $[O_2]_{air}$). Thus, the critical cyanide concentration for gold in oxygen saturated cyanide solutions should be 40 mM. This suggests that for oxygen saturated 20 mM cyanide solutions, the gold dissolution rate will be dependent on cyanide film diffusion (as discussed for low cyanide concentrations in section 4.3.2.1). It is therefore difficult to quantitatively determine if the data presented in Table 4.6 fits first order kinetics with respect to oxygen concentration.

Oxygen Concentration	10^5r /mol m^{-2} s^{-1}
Air Saturated (0.25 mM)	0.69
Oxygen Saturated (1.28 mM)	1.49

Table 4.6 – Rate of dissolution of gold in air and oxygen saturated 20 mM cyanide solutions. Experimental conditions: pH 10.0, 25 °C, 300 rpm.

4.3.6. Effect of pH

4.3.6.1. Kinetics

The rate of dissolution of gold in aerated 20 mM cyanide solutions was investigated at two pH values, 10.0 and 12.5. The dissolution rate at pH 12.5 was found to be 0.55×10^{-5} mol m^{-2} s^{-1}. This is 20 % lower than the rate of dissolution at pH 10.0, 0.69×10^{-5} mol m^{-2} s^{-1}. The effect of pH can be explained by the shift in the oxygen reduction polarisation curves with pH, as discussed in detail in Chapter 3. Another factor which needs to be considered is the effect of pH on the gold oxidation reaction, and in particular, the effect of pH on the surface film of AuCN. In section 4.3.6.2, it is shown that the surface film is more stable at pH 12.5 than it is at pH 10.0, which would also result in a decrease in the rate of dissolution with an increase in pH.

4.3.6.2. Electrochemistry – Oxidation

The effect of pH on the oxidation of gold at low and high overpotentials was investigated, and the resultant polarisation curves are shown in Figure 4.19. At low overpotentials, it can be seen from the inset that the oxidation current density is higher at pH 10.0 than it is at pH 12.5. Thus, gold oxidation is faster at lower pH values, suggesting that the nature of the passivating film is dependent upon the pH of

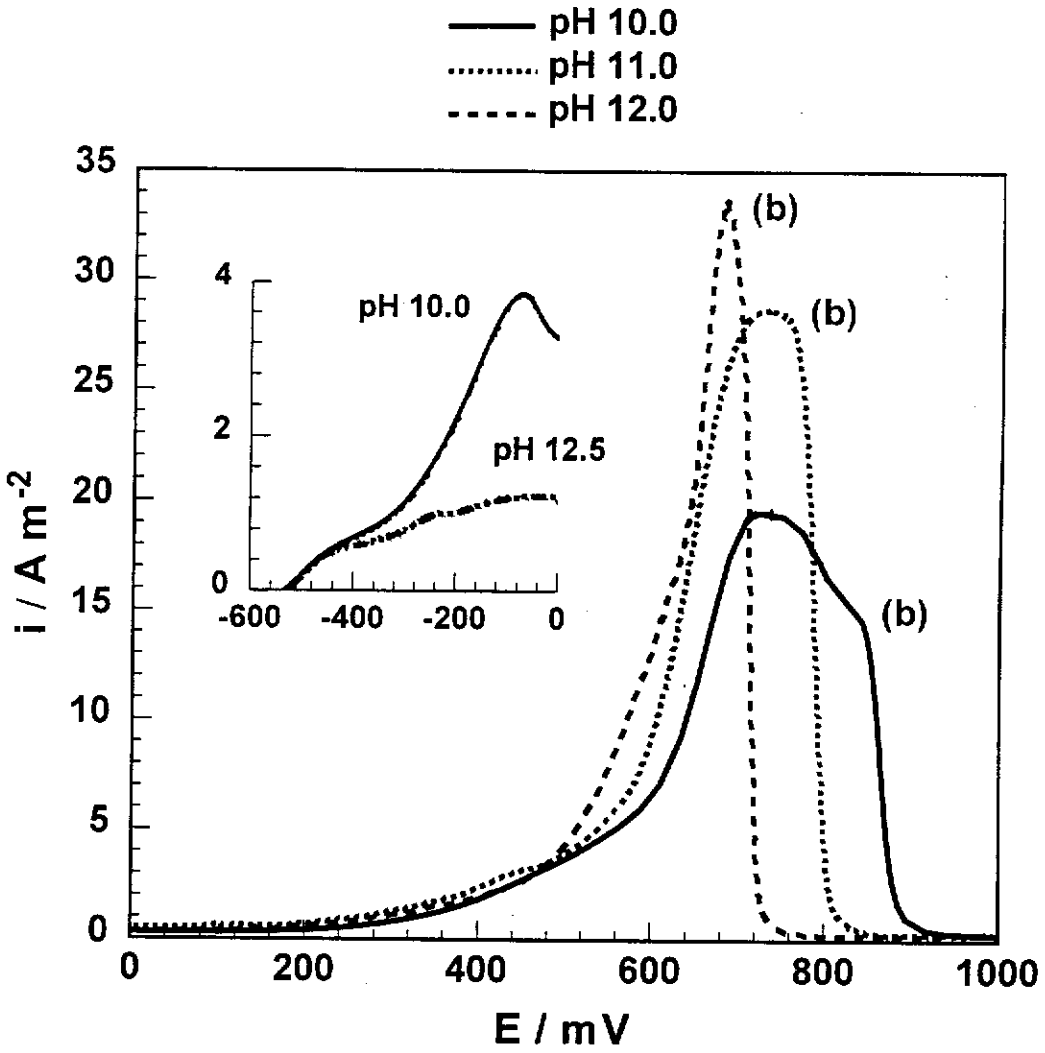

Figure 4.19 – Effect of pH on the oxidation of gold at both high and low (inset) overpotentials. The polarisation curves at high overpotentials were measured using solid gold, while those at low overpotentials were measured using plated gold. Experimental conditions: 20 mM cyanide, pH 10.0, 1 mV s^{-1}, 25 °C, 300 rpm.

the system. The reason for this is uncertain, but one possibility is that the passive film is a basic form of gold cyanide, although such compounds are not thought to exist in aqueous solution (Nicol, 1980a). In any event, the oxidation polarisation curves predict that the dissolution rate will decrease with increasing pH, which is consistent with the measured change in dissolution rate with pH.

At high overpotentials, it is clear from Figure 4.19, that at higher pH values, the peak current density is generally higher, and the oxidation of gold begins at lower potentials. This indicates that at high overpotentials, the passive film that is present on the surface of the gold is more unstable at higher pH values, which is the opposite of the oxidation behaviour at low overpotentials. These results are further evidence that the passivation of gold at high and low overpotentials is caused by different mechanisms. Similar results have also been reported by Cathro and Koch (1964). The potential at which complete passivation occurs, labelled (b), is shown to shift to lower potentials with increasing pH. This indicates that the passivation is due to the formation of a film that involves hydroxide, a result which has been reported by a number of authors (Nicol, 1980a). The passivating film that forms at potential (b) is most likely to be gold hydroxide, which is electrochemically equivalent to gold oxide. Further mechanistic information can be obtained by plotting the passivation potential against pH. As shown in Figure 4.20, this plot was found to be linear, and the slope of the line of best fit was found to be 74 ± 1 mV pH^{-1}, which is similar to the value published by Mughogho and Crundwell (1996), 69 mV pH^{-1}. The oxidation of one mole of gold to gold (III) oxide involves three moles of electons and three moles of hydroxide ions. Hence, a slope of -59 mV pH^{-1}, would be expected for this reaction. It is also possible that the gold oxide is formed from a gold (I) species which already exists at the surface, such as AuCN. For this reaction, a slope of -89 mV pH^{-1} would be expected. From the experimental data, if is difficult to determine which of these mechanisms is dominant, and such work is beyond the scope of this thesis.

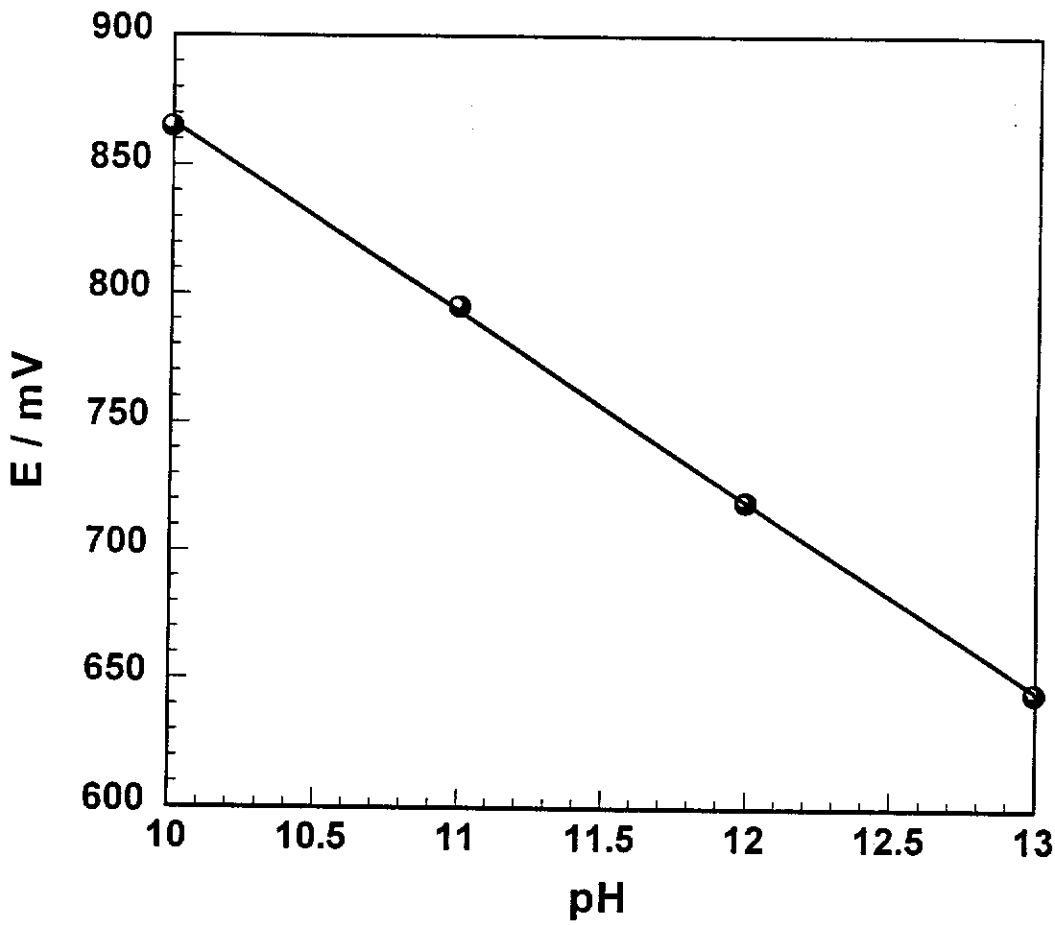

Figure 4.20 – Passivation potential (b), of gold as a function of pH. Experimental conditions: 20 mM cyanide, pH 10.0, 25 °C, 300 rpm.

4.3.7. Effect of Solution Purity

In Chapters 5 and 6, it will be shown that the rate of dissolution of gold in aerated cyanide solutions is dependent on solution impurities which are capable of modifying the structure of the passive surface film. It follows that the oxidation of gold at potentials more negative than 0 mV is also dependent on impurities. It is easy to quantify this effect because the oxidation rate of gold at low potentials in standard AR grade solutions is very low. Only in the presence of certain impurities, does gold oxidation occur to a significant extent in this potential range. At potentials more positive than 0 mV though, bulk oxidation of the gold occurs in AR grade solutions, and hence it is more difficult to establish the effect of impurities on the oxidation of gold in this potential range. For example, Nicol (1980a) showed that the addition of lead had little effect on the oxidation of gold at high overpotentials. The oxidation of gold in ultrapure cyanide solutions was measured to determine the effect of impurities on the anodic behaviour of gold at high overpotentials. Shown in Figure 4.21 is the oxidation of polycrystalline gold in ultrapure and AR grade cyanide solutions containing 0.29 M sodium hydroxide and 0.1 M sodium cyanide. The concentration of sodium hydroxide was set at 0.29 M to negate the need for a background electrolyte. Although there may be some migration effects, the experiment is useful in showing the effect of solution purity. It is clear that in ultrapure cyanide solutions, the gold oxidation current density is very low over the whole potential window. This suggests that in AR grade solutions, the removal of the passive film prior to bulk oxidation is due to the interaction of trace levels of unknown impurities with the surface of the gold. In view of this, it is not surprising that many investigations in the past, as discussed in the review, have resulted in vastly different polarisation curves for the oxidation of gold.

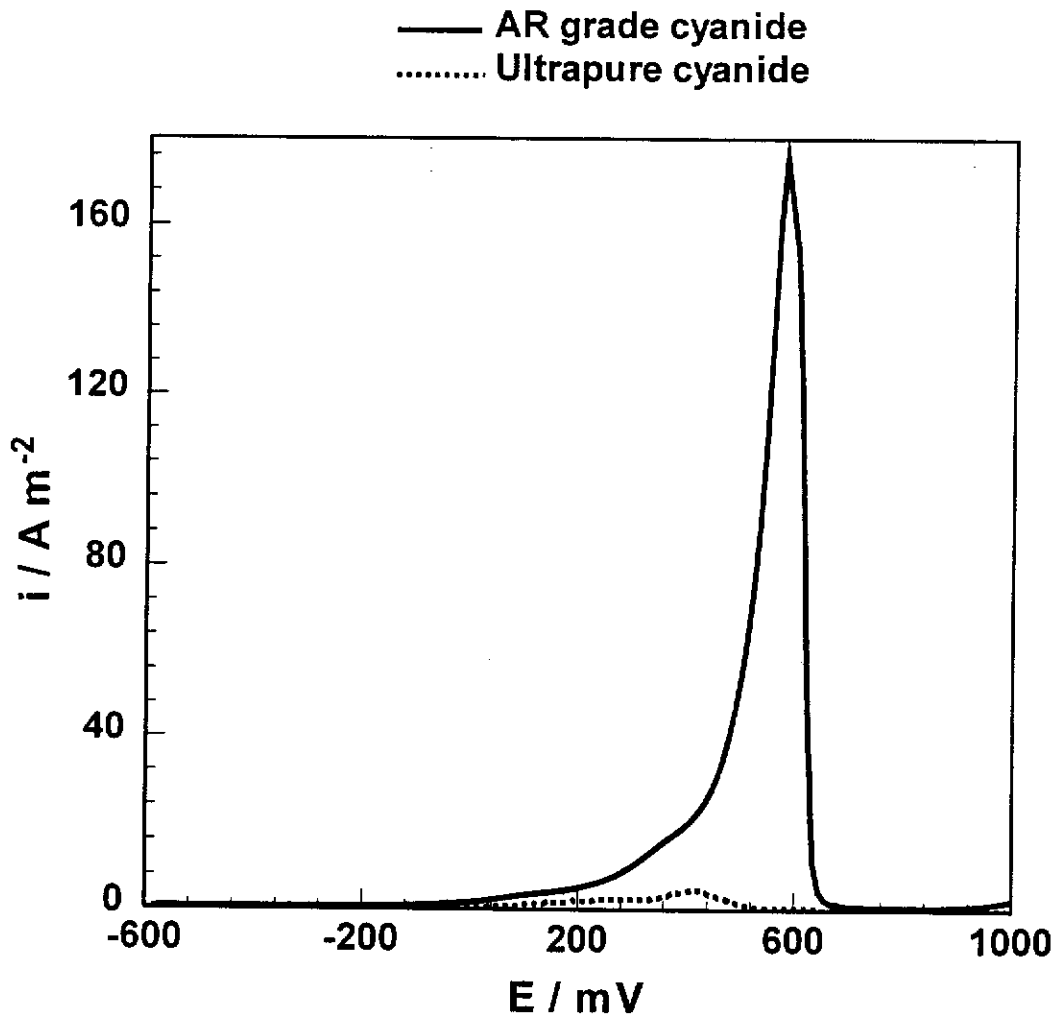

Figure 4.21 – Gold oxidation in ultrapure and AR grade 0.1 M sodium cyanide solutions. Experimental conditions: 0.29 M sodium hydroxide, 1 mV s^{-1}, 25 °C, 300 rpm.

4.4. Summary

1) The leaching of gold in aerated cyanide solutions is not diffusion controlled, and the variation in the measured dissolution rate with changes in experimental conditions is consistent with the surface being passivated by a film of AuCN.

2) The critical cyanide concentration was found to be 8 mM, and at cyanide concentrations below $[CN^-]_{crit}$, the reaction is *quasi* cyanide diffusion controlled, while at cyanide concentrations above $[CN^-]_{crit}$, the reaction is chemically controlled.

3) At 20 mM cyanide, the dissolution rate is independent of cyanide concentration and rotation rate, and the activation energy was calculated to be 47 ± 3 kJ mol^{-1}. These results confirm that the dissolution of gold in 20 mM cyanide solutions is chemically controlled.

4) In ultrapure cyanide solutions, the gold is passive over the entire potential window, suggesting that trace levels of impurities determine the oxidation behaviour of gold. Therefore, it is not surprising that the published polarisation curves show significant variation.

Chapter 5 – The Effect of Solution Phase Additives

5.1. Introduction

In the review, it was shown that the kinetic and electrochemical results for the dissolution of gold in cyanide solutions from many publications were conflicting. These variations are believed to result from variations in either solid or solution phase purity in the reported experiments. In the previous chapter, it was shown that the dissolution of gold in cyanide solutions is chemically controlled. It is speculated that under high purity conditions, the surface of the gold is blocked by a film of AuCN. The objective of the work described in this chapter is to investigate the effect of solution phase purity on the kinetic and electrochemical behaviour of gold. Particular attention is given to the effect of lead on the leaching of gold in cyanide solutions, and its action in reducing the passive effects of the AuCN film are discussed.

5.2. Experimental

The experimental conditions for this chapter are identical to those described in Chapter 4, with the exception of some of the solution compositions. In most experiments, 1 ppm lead is added as lead nitrate. For the measurement of Evans' diagrams, oxygen reduction is carried out on gold surfaces that contain controlled amounts of lead. This is accomplished by electroplating gold from a solution containing 0.02 M potassium dicyanoaurate, 0.23 M potassium cyanide, 0.086 M potassium carbonate and 0.1 mM lead nitrate.

5.3. Results and Discussion

Initially, the dissolution of gold in cyanide solutions in the presence and absence of lead is discussed. The action of lead is then investigated, and the experimental conditions varied independently to obtain further information about the system.

5.3.1. The Action of Lead

5.3.1.1. Kinetics Studies

(a) Dissolution Rates

The rotating electrochemical quartz crystal microbalance was used to measure the leaching rate of gold in a solution containing 20 mM cyanide and 1 ppm lead, which was compared to the leaching of gold in the absence of lead, as shown in Figure 5.1. The dissolution of gold in the absence of lead was discussed in detail in the previous chapter, and the rate of dissolution was found to be relatively low. For the solution containing 1 ppm lead, the initial rate of dissolution is also slow, although the rate increases with time, reaching a maximum after approximately 300 seconds. This maximum rate, 5.5×10^{-5} mol m^{-2} s^{-1} is around 8 times higher than that in the absence of lead, 0.69×10^{-5} mol m^{-2} s^{-1}. It is also worth noting that the mixed potential in the presence of lead, -490 mV, is considerably more negative than that in the absence of lead, -220 mV.

Further information about the effect of lead can be obtained by adding lead during the dissolution process. Gold was immersed into a lead free solution and was allowed to leach for approximately 30 minutes, after which the dissolution rate had reached a constant value of 0.69×10^{-5} mol m^{-2} s^{-1}. Lead was then added to the leach solution to give a final composition of 1 ppm, and it was found that the dissolution

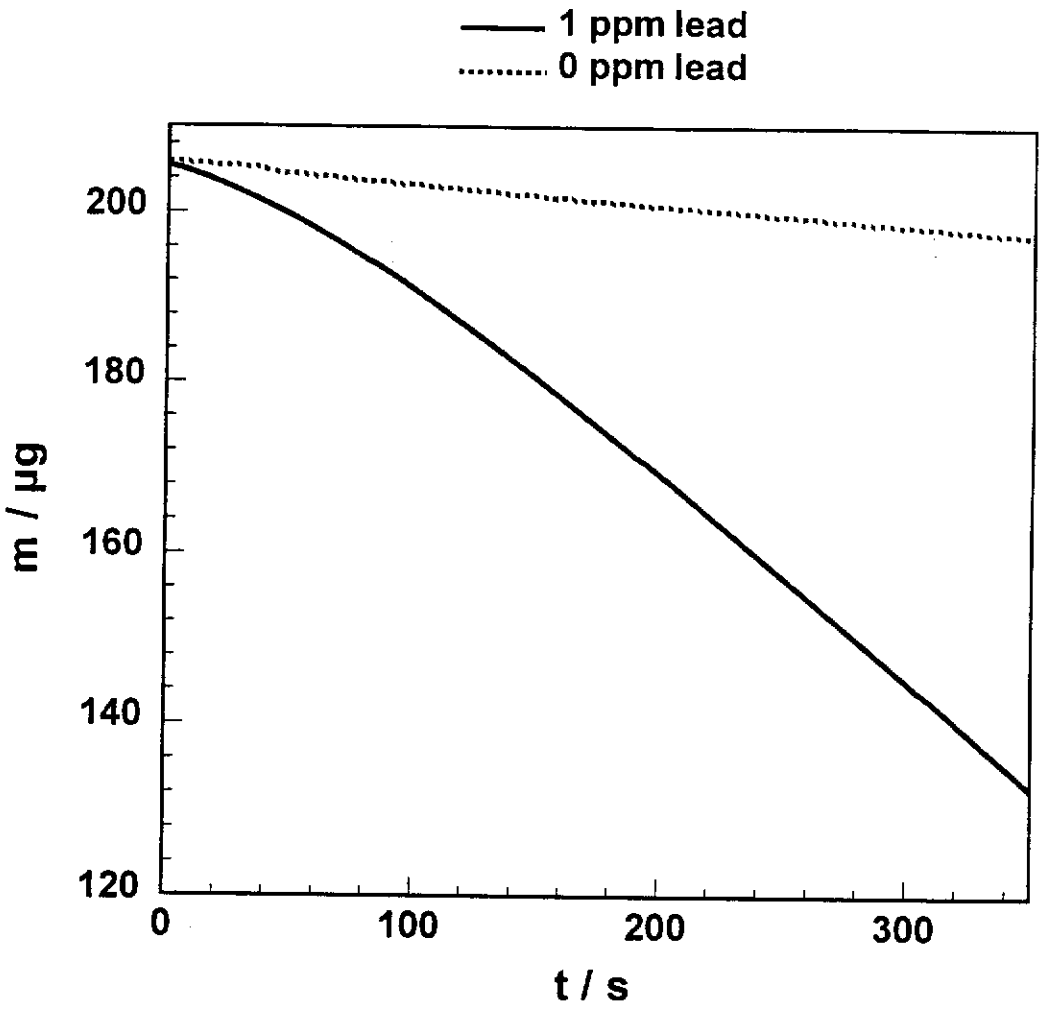

Figure 5.1 – Mass versus time response for the leaching of gold in the presence and absence of 1 ppm lead. Experimental conditions: air saturated 20 mM cyanide solution, pH 10.0, 25 °C, 300 rpm.

rate slowly increased reaching 5.5×10^{-5} mol m^{-2} s^{-1} after 600 seconds. It is worth noting that the time required for the dissolution rate to reach its maximum value was considerably longer than that for gold which is immersed into a solution containing lead. This is not surprising, as in this case, the surface was almost completely passive prior to the addition of lead.

(b) Action of Lead

It is believed that gold is passive in cyanide solutions, probably due to the formation of a surface film of AuCN, as discussed in the previous chapter. The lead therefore must be altering the surface of the gold in order for high rates of dissolution to occur. The most likely explanation for this increase in the rate of dissolution is that the lead is cementing onto the surface of the gold. It is proposed that on initial immersion into the cyanide solution, a film of AuCN forms simultaneously with the cementation of lead onto the surface of the gold. As the cementation of lead continues, the passive film is slowly removed and the rate of dissolution increases. After a certain period, in this case 300 seconds, the passivating film is completely removed, and the rate of dissolution reaches a constant value.

Equation 5.1 shows the reaction for cementation of lead onto gold. It can be seen that for every mole of lead which is reduced, two moles of gold are oxidised. Due to this reaction stoichiometry, and the fact that lead and gold have similar molecular weights (207 g mol^{-1} and 197 g mol^{-1} respectively), it is obvious that as the cementation reaction progresses, there should be a net decrease in the mass of the electrode. This decrease in mass was measured with the REQCM.

$$Pb(II) + 2Au + 4CN^- \rightarrow Pb + 2Au(CN)_2^- \qquad \textbf{Equation 5.1}$$

To measure the cementation of lead on gold, a 20 mM cyanide solution was prepared and thoroughly degassed with argon to ensure that there was no oxygen present. The gold was immersed into the lead free solution, and once the mass and mixed potential had stabilised, lead was added to the solution. The mass changes of

the gold electrode during the experiment are shown in Figure 5.2. Initially, the gold is dissolving at a constant and very low rate, which is due to trace amounts of oxygen which cannot be removed from the system. When the lead is added, the mass of the electrode decreases, which is consistent with cementation occurring. After subtracting the baseline mass losses, the quantity of lead deposited on the gold surface during the experiment is calculated to be approximately 790 ng. Unfortunately, this value cannot be accurately compared to mass of a monlayer of lead, as 1) the surface roughness is not known; and 2) the rate of gold dissolution due to trace levels of oxygen is accelerated in the presence of lead.

(c) Effect of Surface Lead

The theory that lead is affecting the surface of the gold can be further validated by investigating the dissolution of a gold surface which has been modified by lead. The gold sample was immersed into an air saturated solution containing 1 ppm lead. After a specified time, ranging from 60 to 200 seconds, the gold was removed from the cyanide solution and thoroughly rinsed. The gold was then immersed in an air saturated cyanide solution free of lead, and the rate of dissolution was measured. The results are shown in Figure 5.3. For comparison, the rate of gold dissolution recorded in the total absence of lead is shown as a star symbol. It is clear that the rate of dissolution of gold in the lead free solution increases with pretreatment time. This indicates that the lead is retained on the surface of the gold during dissolution and rinsing, and is active when placed in a lead free cyanide solution. A longer pretreatment in the lead solution results in more lead cementation, and hence a higher rate of dissolution. This is analogous to the increase in dissolution rate observed during the first 300 seconds of leaching in a solution containing lead.

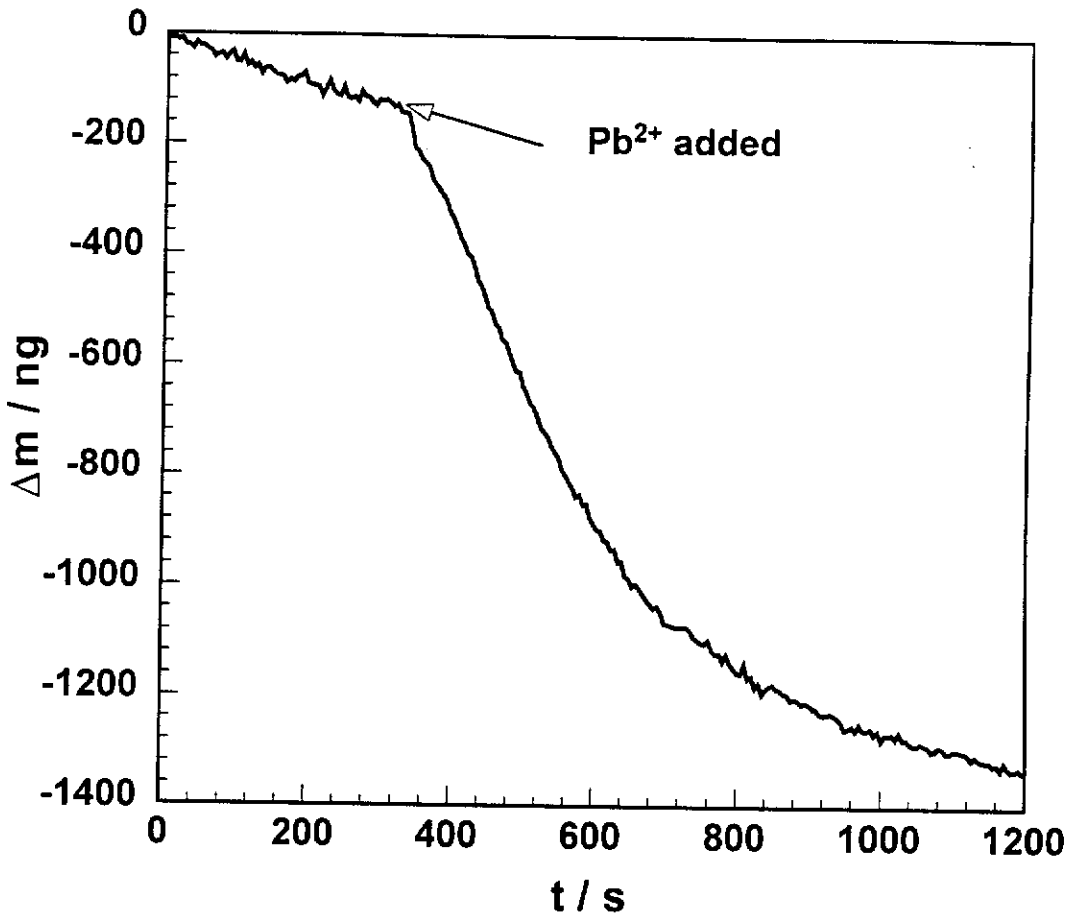

Figure 5.2 – Mass versus time response for the cementation of lead on gold. Cementation commences when the sample of lead nitrate is added to solution (as marked). Experimental conditions: argon saturated 20 mM cyanide solution, 1 ppm lead, pH 10.0, 25 °C, 300 rpm.

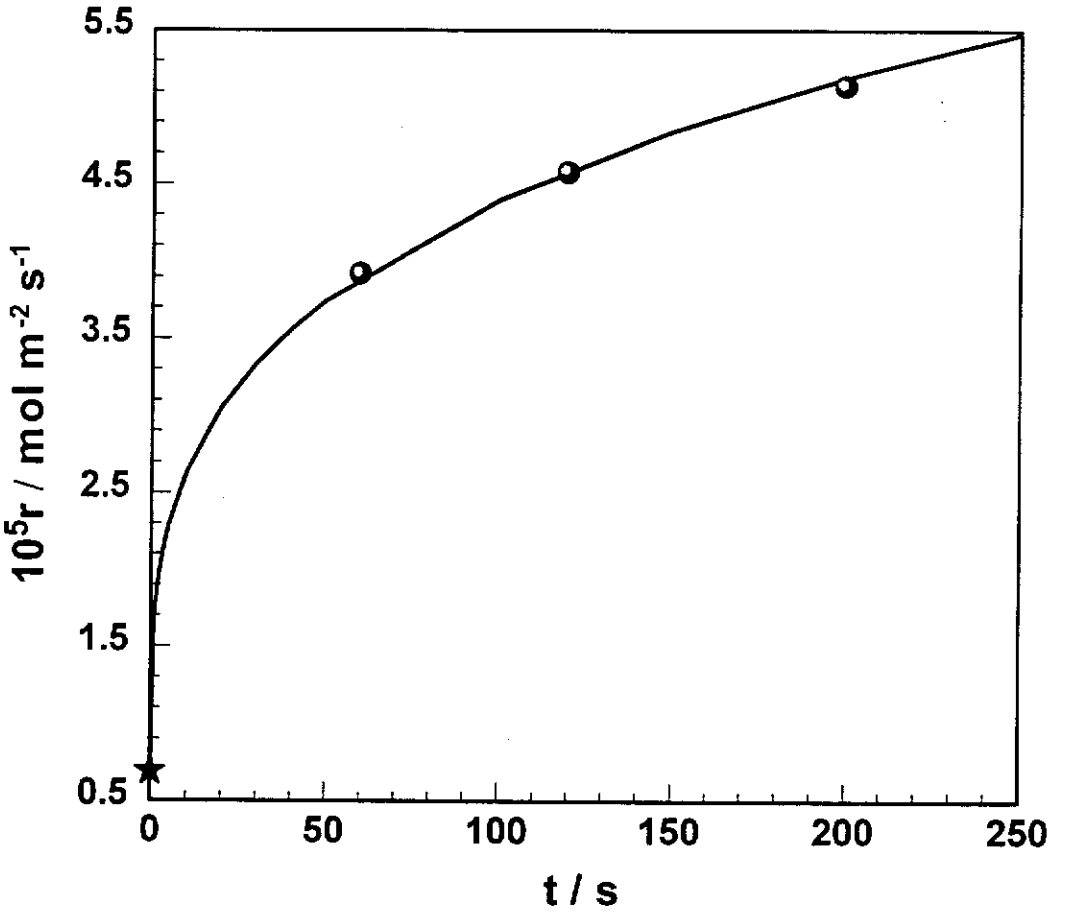

Figure 5.3 – Rate of dissolution of gold in a lead free cyanide solution as a function of lead pretreatment. The x axis represents the period of pretreatment by immersion in an air saturated 20 mM cyanide solution containing 1 ppm lead. Experimental conditions: air saturated 20 mM cyanide, pH 10.0, 25 °C, 300 rpm.

5.3.1.2. Surface Studies

The effect of lead on the leaching of gold in cyanide solutions can be further characterised using scanning electron microscopy. Shown in Figure 5.4 is an SEM image of a polycrystalline gold electrode which had been leached for 24 hours in an air saturated 20 mM cyanide solution containing 1 ppm lead. For comparison, an SEM image of polycrystalline gold leached in the absence of lead is shown in Figure 5.5. Both of the images were obtained at 200x magnification, and it is clear that in the presence of lead, the gold surface has undergone significant leaching, while in the absence of lead, the surface is essentially pristine. The SEM micrographs are thus consistent with the kinetic results in showing that lead significantly enhances the leaching of gold in air saturated 20 mM cyanide solutions.

On further analysis of Figure 5.4, it can be seen that the leaching of the gold surface is uneven, with certain areas of the gold having been preferentially leached. This is even more apparent in Figure 5.6, an optical micrograph at lower magnification (50x). It is also clear that after leaching, a number of the crystal faces are evident. These findings suggest that the leaching of the various gold crystal faces proceed at different rates. Such a finding is not surprising, as it is well known that oxygen reduction is dependent on the crystal orientation (Markovic, Adzic & Vesovic, 1984). Consequently, it is likely that during leaching, oxygen reduction occurs on certain crystal faces, while gold oxidation occurs on other faces.

Some of the other features of the leached surface, shown in Figure 5.4, are labelled with coloured squares, and these are discussed in detail below.

1) Grain boundaries (red squares). It can be seen from Figure 5.4 that the grain boundaries between the different crystals are quite apparent. These boundaries are particularly obvious in Figure 5.7, an SEM micrograph at higher magnification (500x). It is thus clear that initial leaching occurs preferentially around the grain boundaries, a result which is hardly surprising.

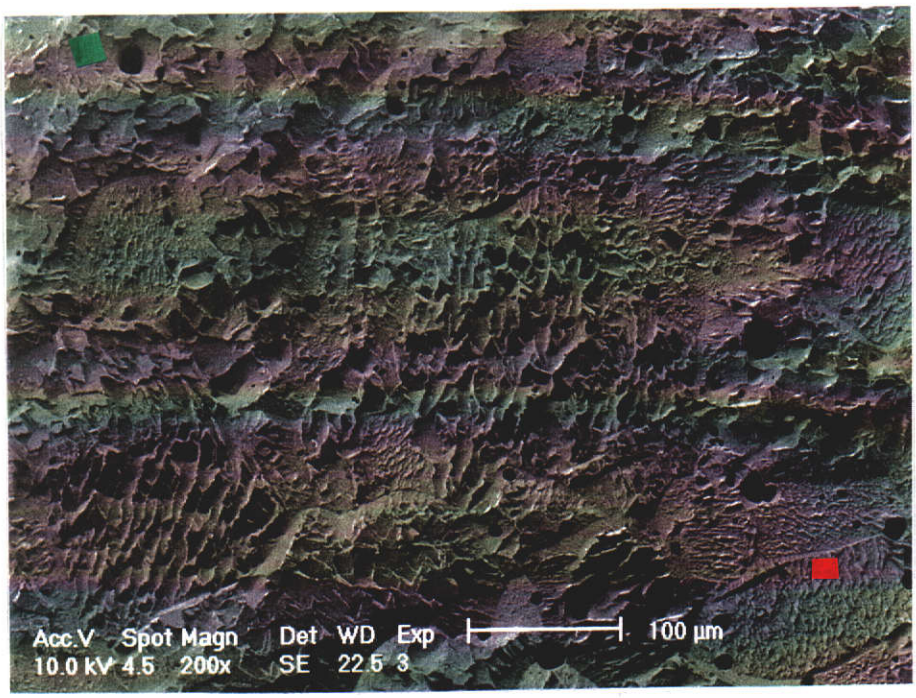

Figure 5.4 – SEM image of polycrystalline gold after 24 hours of leaching in the presence of 1 ppm lead. Experimental conditions: 200x, air saturated 20 mM cyanide, pH 10.0, 25 °C, 300 rpm.

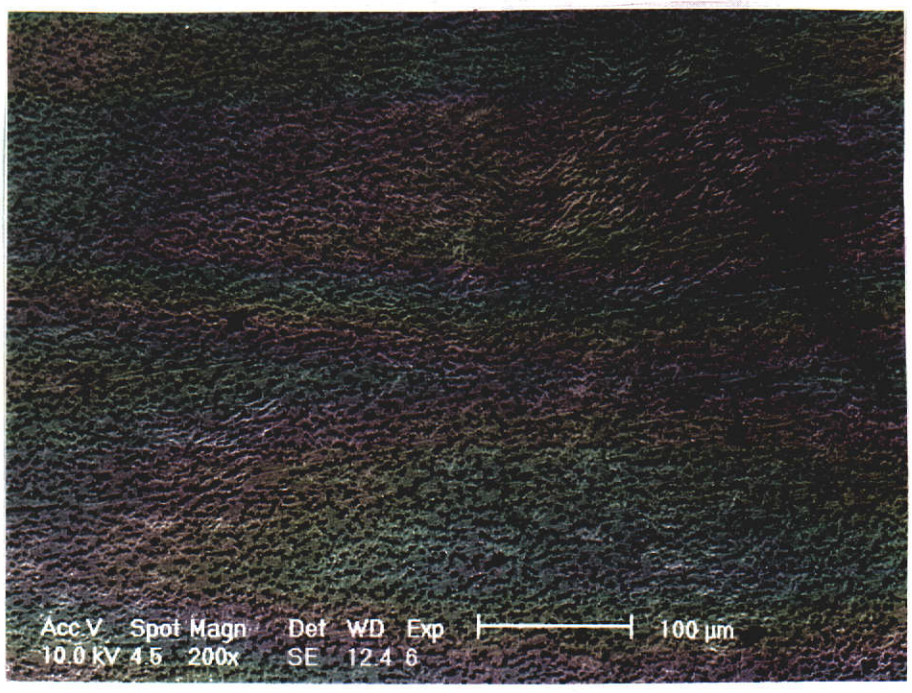

Figure 5.5 – SEM image of polycrystalline gold after 24 hours of leaching in the absence of 1 ppm lead. Experimental conditions: 200x, air saturated 20 mM cyanide, pH 10.0, 25 °C, 300 rpm.

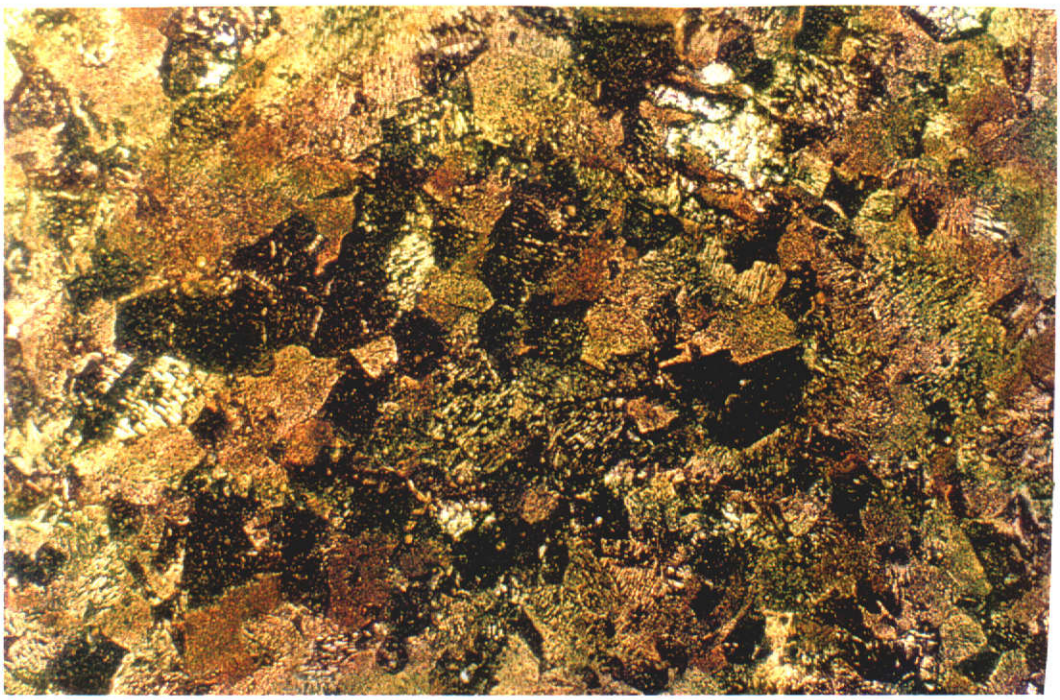

Figure 5.6 – Optical image of polycrystalline gold after 24 hours of leaching in the presence of 1 ppm lead. The image size is 2.6 x 1.8 mm. Experimental conditions: 50x, air saturated 20 mM cyanide, pH 10.0, 25 °C, 300 rpm.

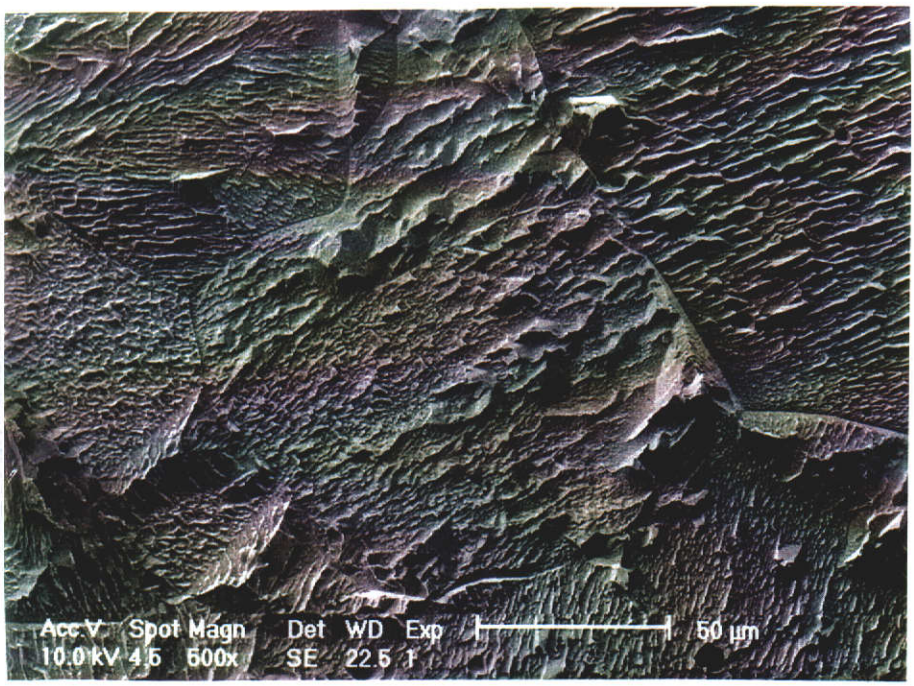

Figure 5.7 – SEM image of polycrystalline gold after 24 hours of leaching in the presence of 1 ppm lead. Experimental conditions: 500x, air saturated 20 mM cyanide, pH 10.0, 25 °C, 300 rpm.

2) Pits (green squares). It is clear from Figure 5.4 that a number of pits have formed on the gold surface during the leaching process. These pits appear to be very symmetrical, a feature which is evident in Figure 5.8, an enlarged view of one of the pits. It is likely that the pits are a result of surface defects, and represent areas which are preferentially leached.

5.3.1.3. Electrochemistry – Oxidation of Gold.

(a) Polarisation Curves

The oxidation of gold in 20 mM cyanide solutions in the presence and absence of 1 ppm lead was investigated using linear sweep voltammetry, and the resultant polarisation curves are shown in Figure 5.9. It is clear that at low overpotentials, the polarisation curves for gold in the presence and absence of lead are markedly different. In the presence of lead, the current density increases rapidly at potentials more positive -550 mV, which suggests that that there is little or no blocking of the surface of the gold at low overpotentials. When the potential reaches -250 mV, the current density flattens out, and then drops rapidly to almost zero at -50 mV. Throughout this chapter, this oxidation peak will be referred to as P2 for simplicity, and is discussed in detail in the following sections. As the potential is increased above -50 mV, it is clear that the oxidation behaviour of the gold is very similar to that in the absence of lead. At potentials above 400 mV, the gold oxidation current density increases exponentially with potential. At 750 mV, the current density flattens out and decreases to zero at 950 mV. This oxidation peak is almost identical to the oxidation peak P1, in the absence of lead, so for simplicity, will also be labelled P1. This chapter will largely deal with the properties of peak P2, as this peak is in the potential region where gold dissolution in cyanide occurs.

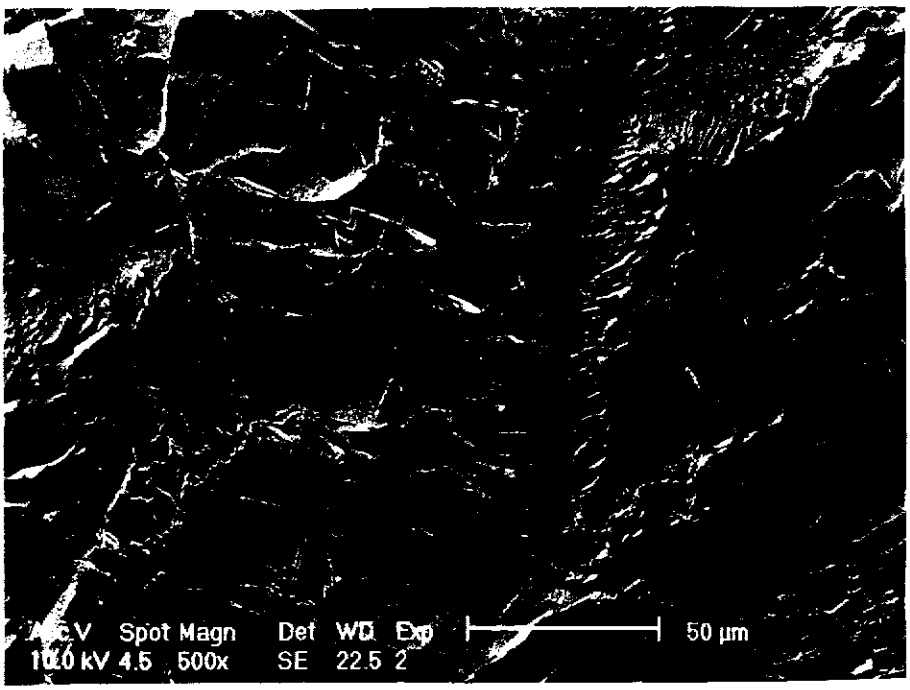

Figure 5.8 – SEM image of polycrystalline gold after 24 hours of leaching in the presence of 1 ppm lead. Experimental conditions: 500x, air saturated 20 mM cyanide, pH 10.0, 25 °C, 300 rpm.

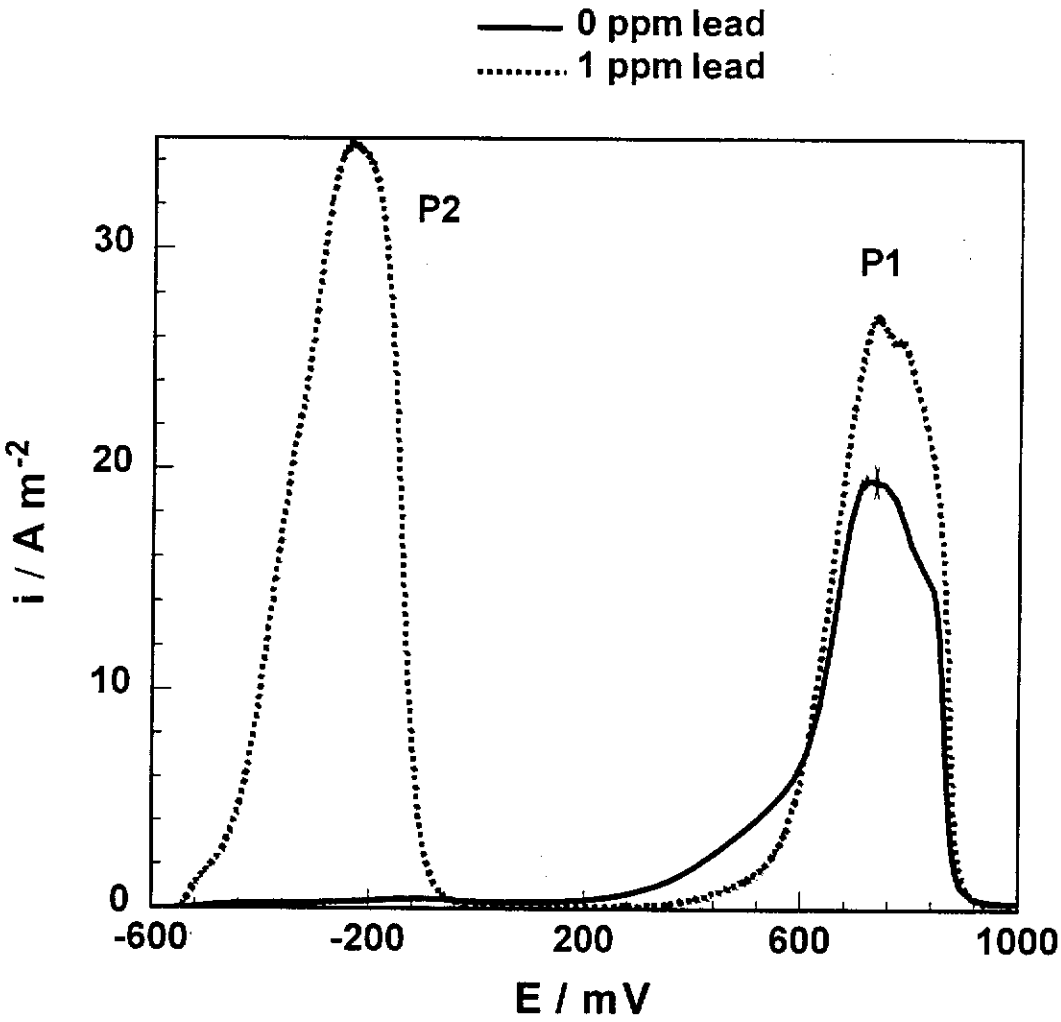

Figure 5.9 – Oxidation of gold in the presence and absence of 1 ppm lead. Experimental conditions: 20 mM cyanide, pH 10.0, 1 mV s^{-1}, 25 °C, 300 rpm.

(b) Identification of Peak P2

The source of the oxidation peak P2 can be resolved by simultaneously measuring the mass and current density during oxidation with the REQCM. If the oxidation peak is due to the oxidation of gold to the gold cyanide complex, then a large mass loss will occur during the course of the experiment. The mass loss, Δm, over a short time interval, Δt, can be equated to the instantaneous current density by Faraday's law, as shown in Equation 5.2

$$i_c = \frac{nF}{MW}\frac{\Delta m}{\Delta t} \qquad \textbf{Equation 5.2}$$

where i_c is the calculated current density (A m^{-2}), n is the number of electrons, F is the Faraday constant (96484 C mol^{-1}) and MW is the molecular weight of gold (197 g mol^{-1}). If the calculated current density matches the measured current density, then it can be assumed that the gold oxidation is the dominant reaction over the measured potential range.

Shown in Figure 5.10 are the recorded and calculated gold oxidation current densities for the oxidation peak P2. It can be seen that the measured and calculated polarisation curves are very similar over the potential range investigated. These similarities confirm that peak P2, which appears in the presence of lead, is actually a gold oxidation peak. Thus, lead enables the gold to oxidise at a much lower potential. It is believed that the lead, by means of cementation, is able to change the structure of the film that normally prevents the gold from oxidising. This enables oxidation to continue until the potential reaches around −250 mV. At this point, there is probably another change to the structure of the surface, causing the gold to become passive again.

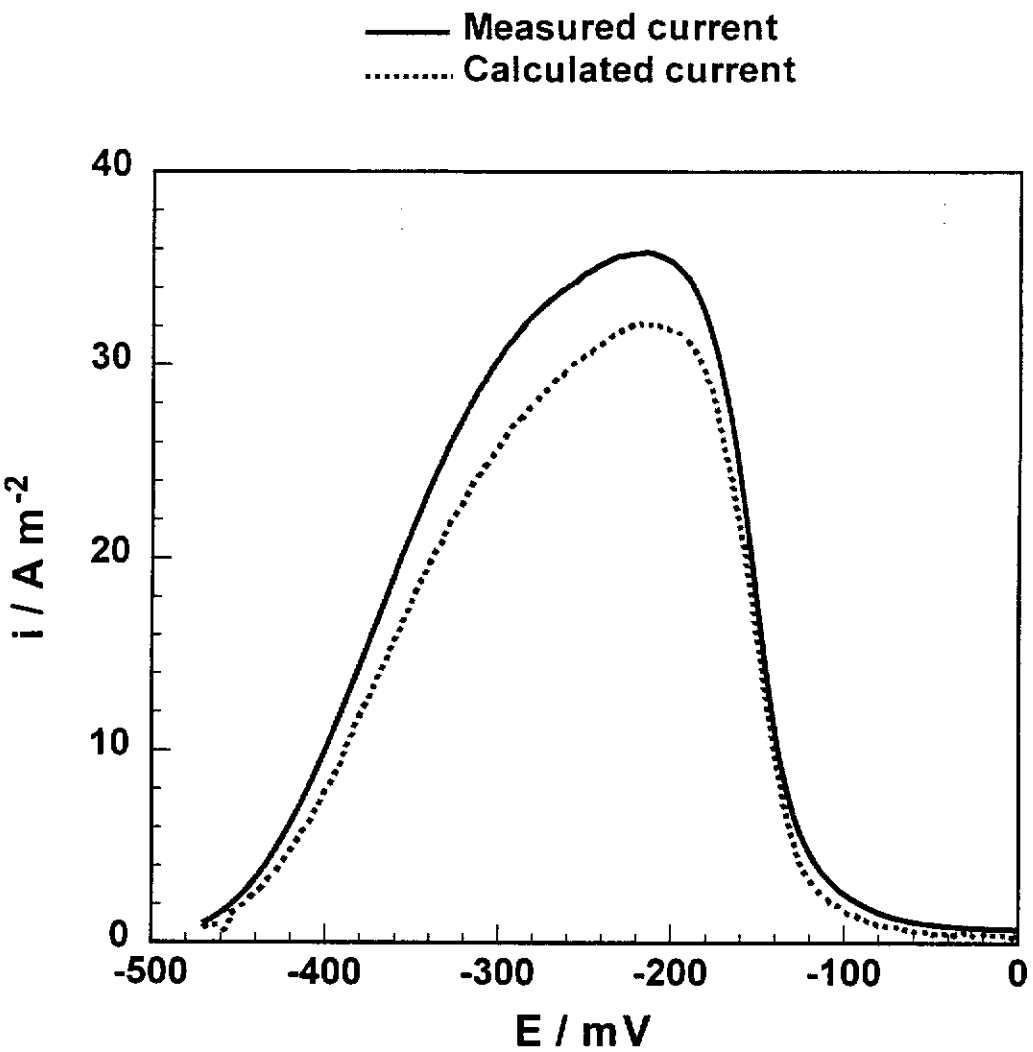

Figure 5.10 – Recorded and calculated current densities for the oxidation of gold in a solution containing 1 ppm lead. Experimental conditions: 20 mM cyanide, pH 10.0, 1 mV s^{-1}, 25 °C, 300 rpm.

(c) Passivation of Peak P2

To investigate the cause of the passivation of gold peak P2, a study of the oxidation of a lead electrode was conducted. Shown in Figure 5.11 is the polarisation curve for the oxidation of lead in a solution containing 20 mM cyanide and 1 ppm lead at pH 10.0. The polarisation curve for gold in the same solution has also been overlaid. It can be seen that the potential at which lead oxidation occurs coincides with the passivation potential of peak P2. This suggests that the passivation of gold at peak P2 is initiated by the oxidation of the lead which is present on the surface of the gold. To obtain further information about the oxidation of lead in cyanide solutions, the process was studied using the REQCM. It was found that the mass of a plated lead electrode increased as the oxidation reaction proceeded, which indicates that the lead is being oxidised to form a solid state product. In section 5.3.6.2, it will be shown that the potential at which gold in a solution containing 1 ppm lead and 20 mM cyanide passivates shifts with pH. It is thus believed that passivation of the gold oxidation peak P2 is due to the oxidation of lead to form lead oxide, as shown in Equation 5.3.

$$Pb + 2OH^- \rightarrow PbO + H_2O + 2e^- \qquad \textbf{Equation 5.3}$$

A Pourbaix diagram can be used to represent the oxidation of lead under a wide range of experimental conditions. The first reaction considered is the chemical reaction of lead ions with hydroxide ions to form the complex $HPbO_2^-$. The relative amounts of Pb^{2+} and $HPbO_2^-$ can be estimated by Equation 5.4 (Pourbaix, 1963), and it is calculated that at pH 10, only 1 % of the lead is present in the form Pb^{2+}. Therefore, in the pH range of cyanidation, the calculations can be simplified by assuming that all of the lead is present in the complexed form, $HPbO_2^-$.

$$\log\left(\frac{HPbO_2^-}{Pb^{2+}}\right) = -28.02 + 3pH \qquad \textbf{Equation 5.4}$$

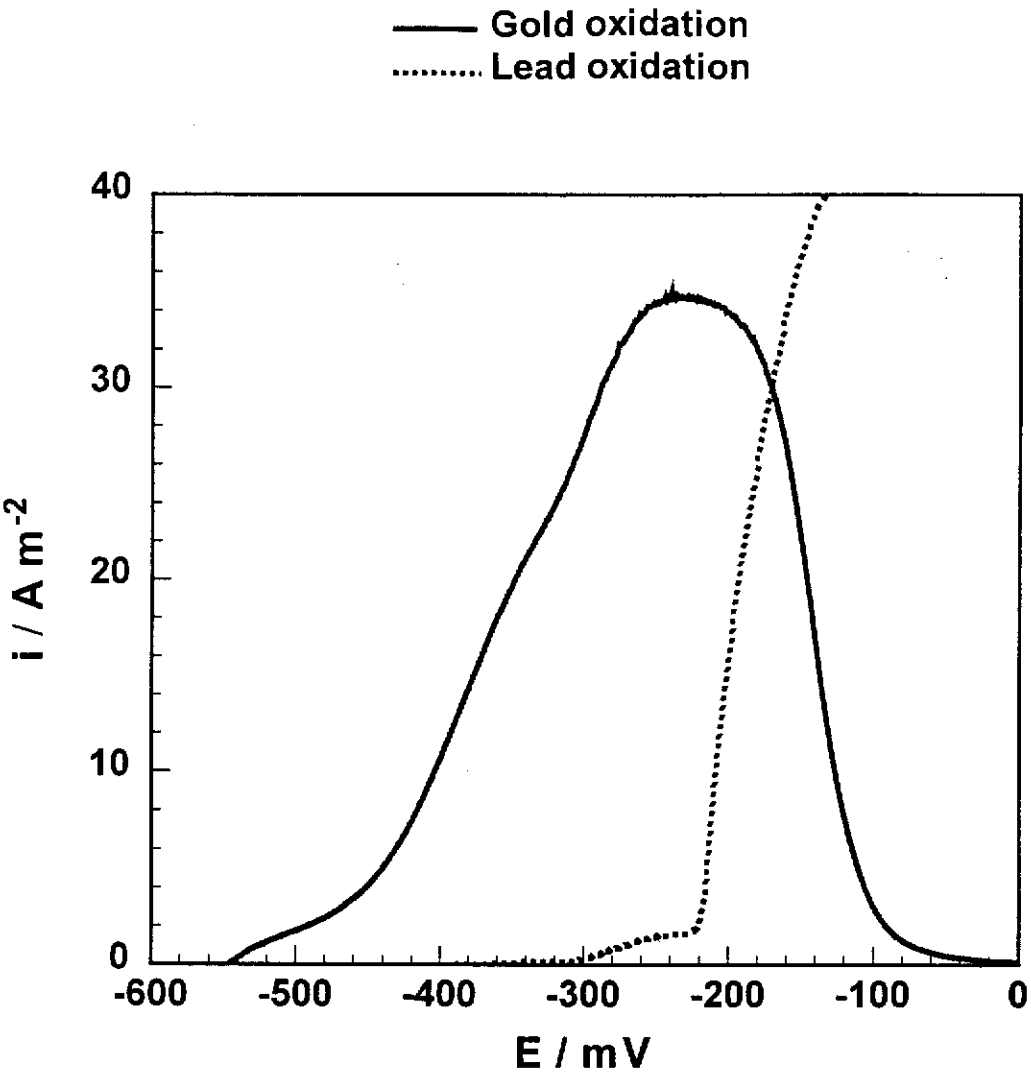

Figure 5.11 – Oxidation of lead and gold in the presence of 1 ppm lead in solution. Experimental conditions: 20 mM cyanide, pH 10.0, 1 mV s^{-1}, 25 °C, 300 rpm.

The two dominant electrochemical reactions in the pH range 9 to 11 and potential range -400 to 0 mV are shown in Equations 5.5 and 5.6. which represent the oxidation of Pb to PbO and $HPbO_2^-$ respectively (Pourbaix, 1963). It is worth noting that Equation 5.5 is thermodynamically equivalent to the reaction by which passivation of gold at peak P2 in the presence of lead is believed to occur, as shown in Equation 5.3.

$$Pb + H_2O \rightarrow PbO + 2H^+ + 2e^-$$
$$E = 0.248 - 0.0592pH \qquad \textbf{Equation 5.5}$$

$$Pb + 2H_2O \rightarrow HPbO_2^- + 3H^+ + 2e^-$$
$$E = 0.702 - 0.0886pH + 0.0295\log[HPbO_2^-] \qquad \textbf{Equation 5.6}$$

The Pourbaix diagram for this system is shown in Figure 5.12, based on a concentration of 1 ppm lead in solution. At pH 10.0, it can be seen that lead should be oxidised to lead oxide at -343 mV. This is more negative than the potential which lead was found to oxidise in Figure 5.11, but it should be remembered that Pourbaix diagrams are based on thermodynamic calculations only, and kinetic factors are not represented. The remainder of the Pourbaix diagram is discussed in detail in section 5.3.6.2, in which the shift in peak P2 is measured as a function of pH.

5.3.1.4. Electrochemistry – Evans' Diagrams

Evans' diagrams representing the dissolution of gold in aerated cyanide solutions in the presence and absence of lead are shown in Figure 5.13. The system containing 1 ppm lead is considerably more difficult to simulate using Evans' diagrams, as oxygen is reduced on a dissolving gold surface which is covered by a layer of lead. It will be recalled from Chapter 3 that oxygen reduction is more rapid on lead than on gold. Thus, to obtain a more reliable representation of oxygen reduction during gold dissolution in a solution containing lead, the oxygen reduction polarisation curves would ideally be performed in the presence of lead. However, it is not possible to add lead to the solution when measuring the oxygen reduction

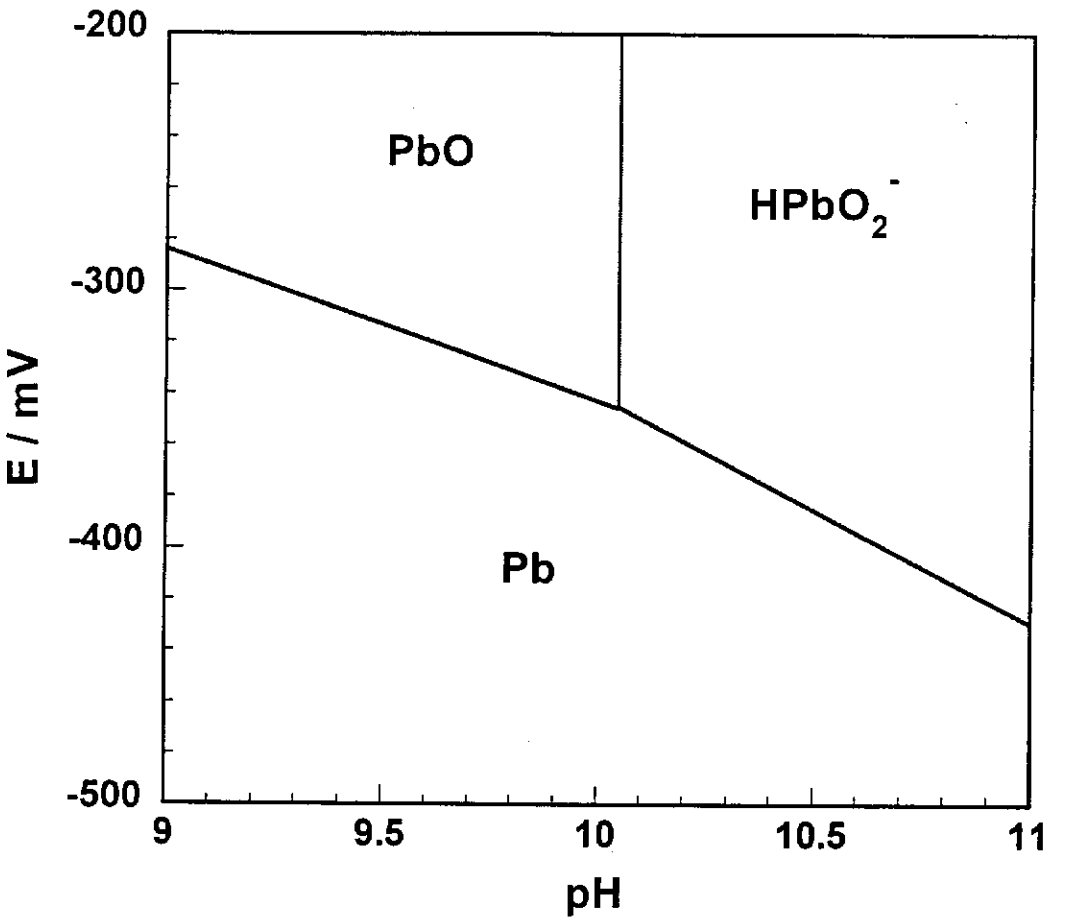

Figure 5.12 – Pourbaix diagram for the lead / water system. System conditions: 1 ppm lead(II), 25 °C.

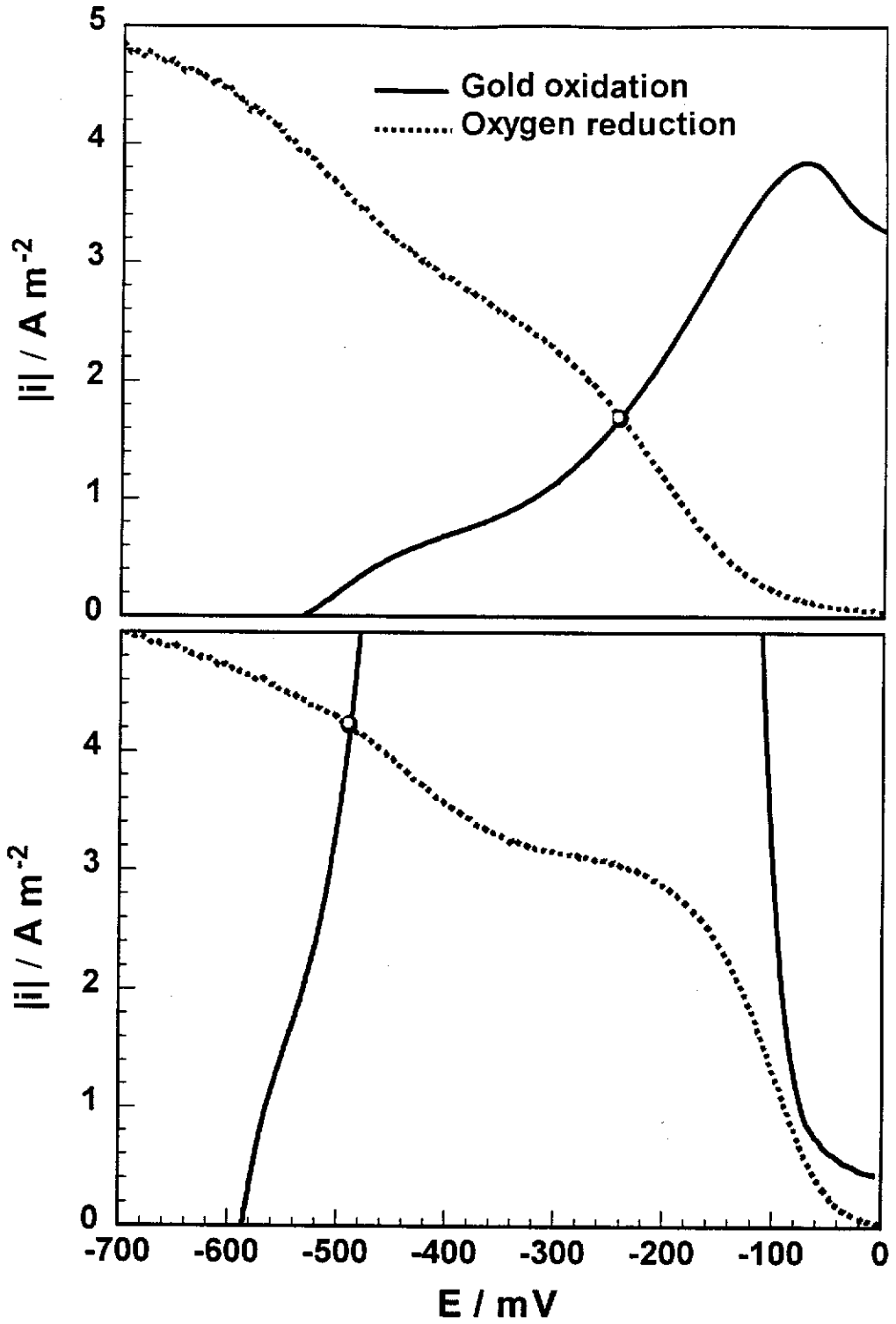

Figure 5.13 – Evans' diagrams representing the dissolution of gold in an air saturated 20 mM cyanide solution in the absence (top) and presence (bottom) of 1 ppm lead. Experimental conditions: pH 10.0, 25 °C, 300 rpm.

polarisation curves, as there would be two reduction reactions, the reduction of oxygen and the reduction of lead. As a compromise, the oxygen reduction polarisation curve was measured on a plated gold surface containing lead. This was prepared by electroplating gold from a plating solution containing 0.1 mM lead.

Shown in Figure 5.13 are two Evans' diagrams representing the effect of lead on the dissolution of gold in air saturated 20 mM cyanide solutions. For each of the Evans' diagrams, the oxidation of gold is indicated by the solid lines, while the reduction of oxygen is indicated by the dotted lines. The intersection points between the anodic and cathodic curves is represented by an open dot. In the previous section, it was shown that there is an additional gold oxidation peak in cyanide solutions containing lead, and only the base of this peak is shown in Figure 5.13. From Figure 5.13, it is immediately obvious that the oxidation peak P2 is in the potential region where oxygen reduction occurs. Therefore, the Evans' diagrams predict that the gold dissolution rate in the presence of 1 ppm lead will be high, while for gold in the absence of lead, the dissolution rate will be significantly lower. It is also clear that oxygen reduction is the limiting step for gold dissolution in aerated solutions containing 20 mM cyanide and 1 ppm lead. Conversely, gold oxidation is the limiting step for gold dissolution in the absence of lead.

The calculated mixed potentials and rates of dissolution for gold in the presence and absence of lead are shown in Table 5.1. These have been compared with the measured gold dissolution rates, presented earlier in the kinetic section.

System		$10^5 r$ /mol m^{-2} s^{-1}	E_m /mV
0 ppm lead	Measured	0.69	-220
	Calculated	1.74	-242
1 ppm lead	Measured	5.5	-490
	Calculated	4.4	-489

Table 5.1 – Calculated and measured mixed potentials and rates of dissolution for gold in an aerated solution containing 20 mM cyanide in the presence and absence of lead. Experimental conditions: pH 10.0, 25 °C, 300 rpm.

The Evans' diagrams predict that for gold in a cyanide solution containing lead, the dissolution rate will be considerably higher and the mixed potential lower than in the absence of lead. These results are consistent with the measured mixed potentials and rates of dissolution, as discussed in section 5.3.1.1. This shows that the Evans' diagrams are effective at qualitatively estimating the effect of lead on the dissolution of gold. Quantitatively though, the Evans' diagrams in the presence of 1 ppm lead were found to be lacking accuracy. Such a discrepancy is not surprising, given the way in which the Evans' diagrams are constructed. The reduction reaction is studied on a clean gold surface that contains a small amount of lead as a co-deposit. The oxygen reduction reaction is also studied in the absence of cyanide. The surface of the gold during the reduction polarisation experiments is thus likely to be different to that of a dissolving gold surface. Hence, for the remainder of this chapter, the Evans' diagrams are only used qualitatively. The main emphasis will be on the kinetic data, as it provides a true measurement of the reaction rate, and the Evans' diagrams are used to explain and rationalise the changes in the measured dissolution rate with experimental conditions.

5.3.2. Effect of Cyanide Concentration

5.3.2.1. Kinetic Studies

The effect of cyanide concentration on the dissolution of gold in a solution containing 1 ppm lead is shown in Figure 5.14. The experimental data is represented by the data points and the dashed line, and these values can be compared to the calculated dissolution rates based on the Levich equation, which represent the maximum dissolution rates that can be obtained. The calculated limiting dissolution rates are shown in Figure 5.14 as lines (a) and (b). Line (a) is the limiting rate of dissolution of gold based on the diffusion of cyanide. Line (b) is the limiting rate of dissolution based on oxygen diffusion when oxygen reduction proceeds by a 4 electron process.

It can be seen from Figure 5.14 that the graph of rate versus cyanide concentration is of a different shape to that expected (as discussed in the review). Instead, at cyanide concentrations below 10 mM, the rate of dissolution increases linearly with cyanide concentration, and at a certain cyanide concentration, between 7.5 and 10 mM, there appears to be a discontinuity in the leach rate with cyanide concentration. The rate of dissolution of gold at cyanide concentrations below 10 mM is considerably lower than those calculated for cyanide or oxygen diffusion control. This suggests that gold surface is partially blocked at low cyanide concentrations, and hence it appears that lead is ineffective at removing the passive film on the gold under these conditions. In contrast, at concentrations above 10 mM cyanide, the rate of dissolution is independent of cyanide concentration, and the measured rates of dissolution are in good agreement with those predicted for oxygen diffusion control. The cause of the discontinuity is discussed in detail in section 5.3.2.3, in which the Evans' diagrams show that at low cyanide concentrations, the anodic and cathodic polarisation curves intersect in the passive gold oxidation region ($E > -100$ mV).

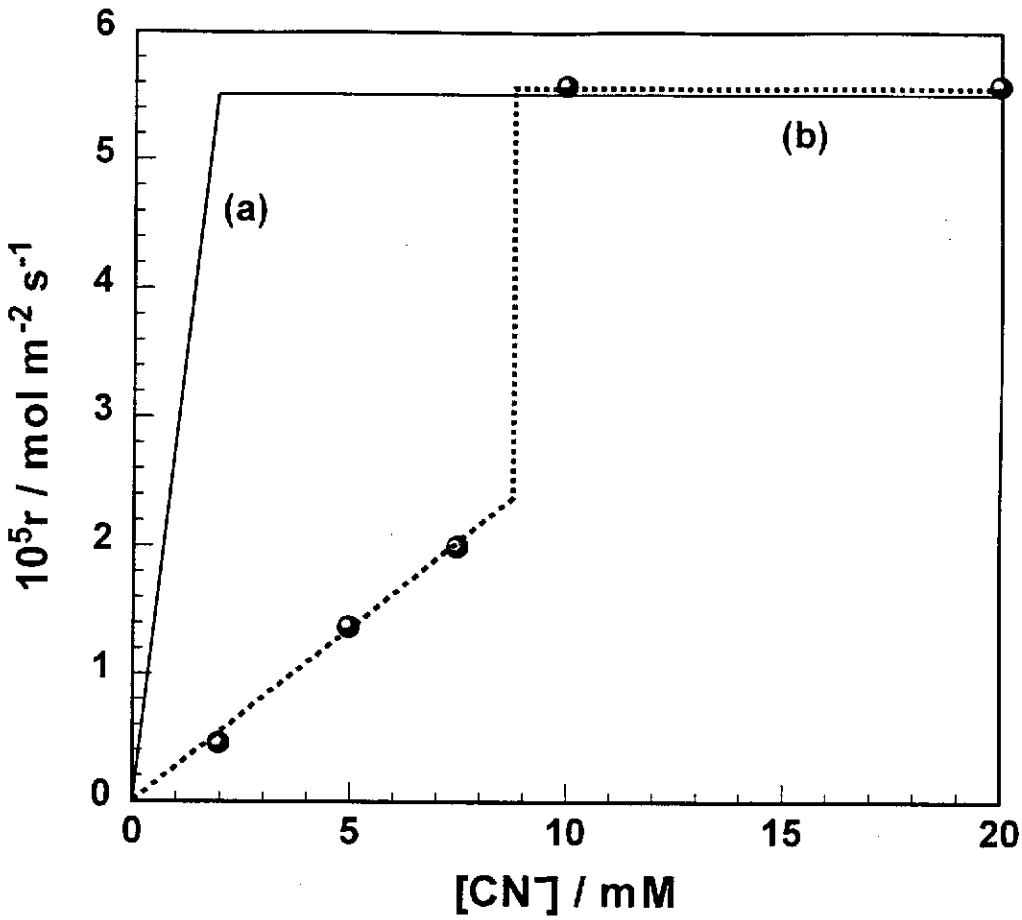

Figure 5.14 – Rate of dissolution of gold as a function of cyanide concentration. Line (a) represents the cyanide diffusion limiting rate, and line (b) represents the oxygen diffusion limiting rate based on the Elsner equation. Experimental conditions: air saturated, 1 ppm lead, pH 10.0, 25 °C, 300 rpm.

It is worth noting that at low cyanide concentrations, the dissolution rates of gold in the presence of lead are still higher than those in the absence of lead. Shown in Table 5.2 are the dissolution rates of gold in 7.5 and 20 mM cyanide solutions in the presence and absence of lead. Also shown is the ratio of the rate of dissolution of gold in 1 ppm lead to the rate at 0 ppm lead. This will be termed the enhancement ratio for lead, as it indicates the degree by which lead enhances gold dissolution. It is clear from Table 5.2 that at 7.5 mM cyanide, the addition of lead enhances gold dissolution, although the effect is not as significant as it is at 20 mM cyanide.

	$10^5 r$ /mol m^{-2} s^{-1}		
$[CN^-]$	**Gold, 0 ppm lead**	**Gold, 1 ppm lead**	**$r_{(1\ ppm)} / r_{(0\ ppm)}$**
7.5 mM	0.54	1.98	3.7
20 mM	0.69	5.57	8.1

Table 5.2 – Comparison of the dissolution rates in 7.5 and 20 mM cyanide solutions in the presence and absence of lead. Also shown is the enhancement ratio, $r_{(1\ ppm)} / r_{(0\ ppm)}$. Experimental conditions: pH 10.0, 25 °C, 300 rpm.

5.3.2.2. Electrochemistry – Oxidation

In section 5.3.1.3, it was shown that for the oxidation of gold in cyanide solutions containing 1 ppm lead, an additional oxidation peak, P2, was observed. The properties of this oxidation peak can be further investigated by measuring the peak oxidation current density as a function of cyanide concentration. As expected, the peak oxidation current density, i_p, was found to increase with cyanide concentration, and shown in Figure 5.15 is a plot of the i_p versus $[CN^-]$. As the oxidation of gold involves only one solution phase reactant, cyanide, the current density for this reaction is limited by bulk cyanide diffusion. The limiting current density can be calculated by the Levich equation for cyanide diffusion, and is shown in Figure 5.15 as line (a).

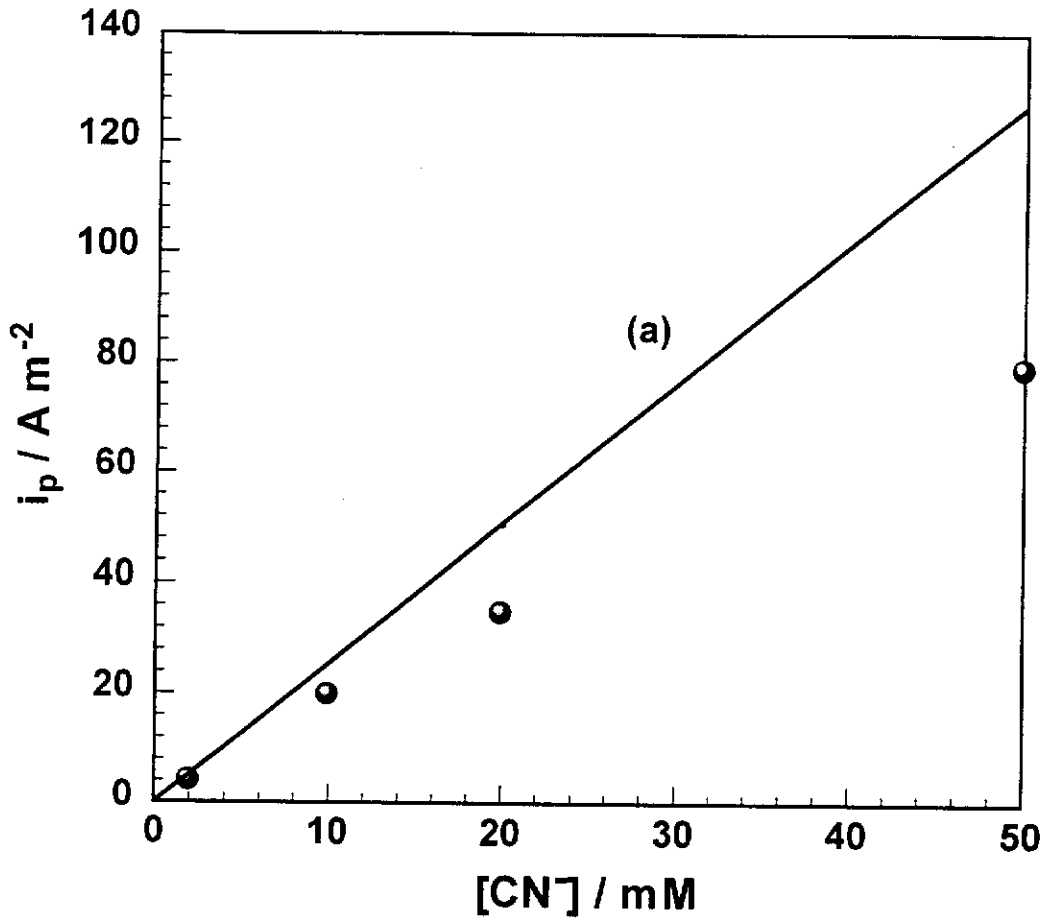

Figure 5.15 – Effect of cyanide concentration on the peak current density for the oxidation peak P2. Line (a) represents the theoretical diffusion limiting current density calculated using the Levich equation. Experimental conditions: 1 ppm lead, pH 10.0, 1 mV s^{-1}, 25 °C, 300 rpm.

At 2 mM cyanide, the measured peak current density for the gold oxidation peak P2 lies on line (a). This indicates that the rate of oxidation is limited by cyanide diffusion at 2 mM cyanide. As the cyanide concentration is increased, the data shifts further away from line (a), indicating that the oxidation is not limited by cyanide diffusion. These results are consistent with the oxidation of gold in cyanide solutions containing 1 ppm lead being under mixed diffusion/chemical control, a finding which is discussed in detail in section 5.3.3.2, where the effect of rotation rate on the peak current density is discussed.

5.3.2.3. Electrochemistry – Evans' Diagrams

Shown in Figure 5.16 is the Evans' diagram representing the dissolution of gold in 2 mM cyanide solutions containing 1 ppm lead. It is clear that the gold oxidation and oxygen reduction polarisation curves intersect at three different potentials. These potentials are shown in Table 5.3, along with the calculated dissolution rates for each of the intersection points.

Estimated Mixed Potential /mV	10^5(Estimated Rate) /mol m^{-2} s^{-1}
-307	3.3
-125	2.0
-62	0.5

Table 5.3 – Calculated mixed potential and corrosion rate at the three intersection points between the gold oxidation and oxygen reduction polarisation curves representing the dissolution of gold in air saturated 2 mM cyanide solutions containing 1 ppm lead. Experimental conditions: pH 10.0, 25 °C, 300 rpm.

The occurrence of three intersection points in Evans' diagrams representing gold cyanidation has also been reported by Guan and Han (1994), although these

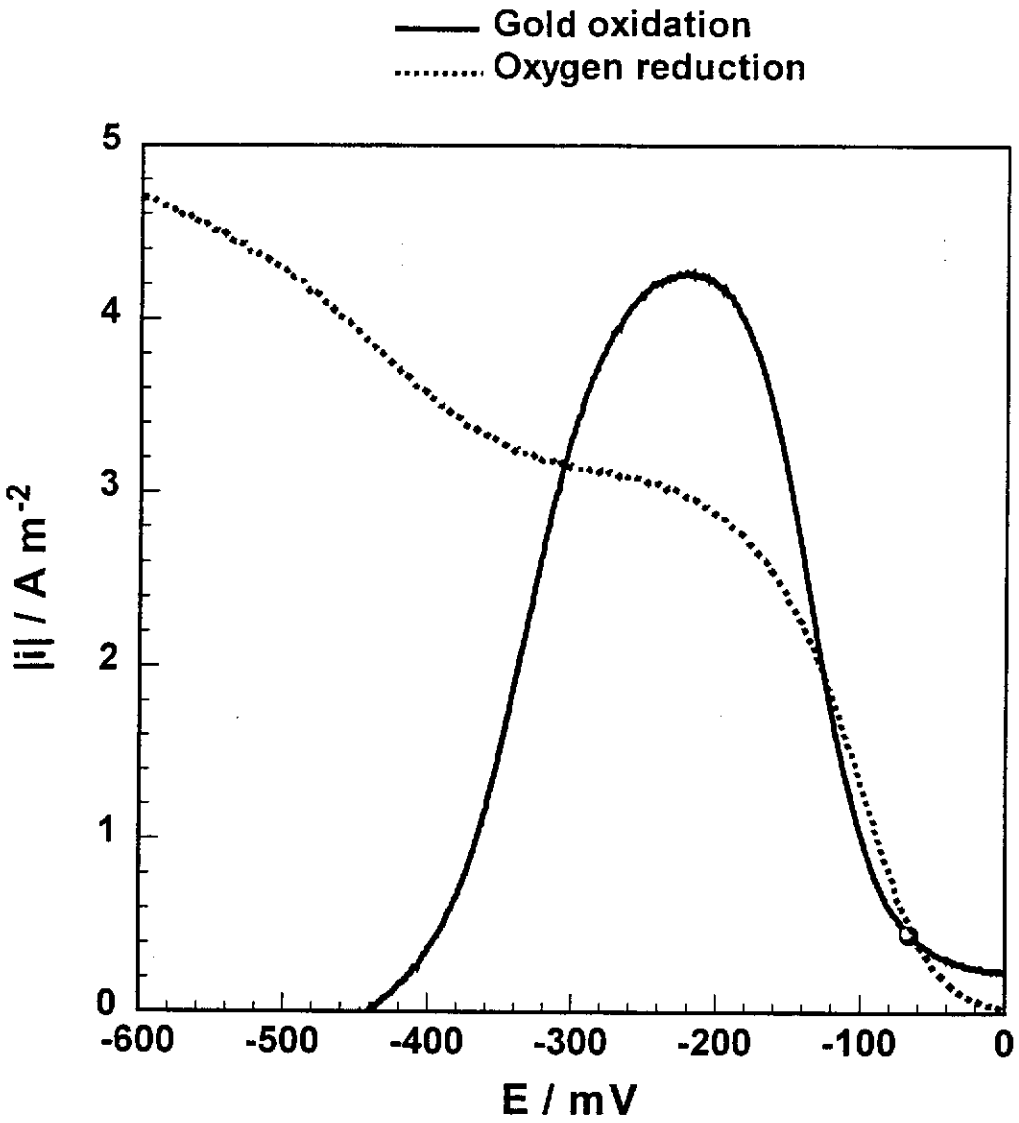

Figure 5.16 – Evans' diagram representing the dissolution of gold in air saturated 2 mM cyanide solutions. Experimental conditions: 1 ppm lead, pH 10.0, 25 °C, 300 rpm.

authors did not specify which of the intersection points determined the mixed potential of the system. In this work, the measured mixed potential was found to be closest to the less negative of the intersection points, so the dissolution rate of gold in 2 mM cyanide solutions is estimated from the Evans' diagram to be 0.5×10^{-5} mol m^{-2} s^{-1}. This is close to the measured rate, 0.45×10^{-5} mol m^{-2} s^{-1}, and shows that the Evans' diagrams are a reliable representation of the effect of cyanide concentration on the dissolution rate of gold in solutions containing 1 ppm lead.

In summary, both the kinetic experiments and the Evans' diagrams show that:

1) For gold in 20 mM cyanide solutions, the addition of 1 ppm lead substantially increases the leaching rate, while for gold in 2 mM cyanide solutions, lead is not as effective at increasing the dissolution rate;
2) The effectiveness of lead can be demonstrated by the use of Evans' diagrams. In the case of 20 mM cyanide solutions, the anodic and cathodic polarisation curves only intersect in the active gold oxidation region;
3) In the case of 2 mM cyanide, the anodic and cathodic polarisation curves intersect in the passive gold oxidation region, which explains the lower observed dissolution rate.

In the following sections, the effect of experimental variables, such as rotation rate and temperature, on the dissolution of gold in cyanide solutions is presented. The main focus of these sections is to demonstrate whether lead enhances the dissolution rate under that set of experimental conditions. Therefore, the remaining Evans' diagrams are mainly concerned with identifying under what conditions the anodic and cathodic polarisation curves intersect in the passive gold oxidation region.

5.3.3. Effect of Rotation Rate

5.3.3.1. Kinetic Studies

The dissolution of gold in a solution containing 20 mM cyanide and 1 ppm lead was measured as a function of rotation rate to determine whether the reaction is diffusion or chemically controlled. A Levich type plot of the rate of dissolution versus $\omega^{1/2}$ is shown in Figure 5.17. Included are the dissolution rates calculated by the Levich equation for the diffusion of oxygen, with line (a) representing the reduction of oxygen to hydroxide, and line (b) representing the reduction of oxygen to peroxide. It should be recalled from the review that a linear relationship between the rate of dissolution and $\omega^{1/2}$ is indicative of a reaction which is diffusion controlled. Also, by rearranging the Levich equation, as shown in Equation 5.7, it is clear that the value of x, the molar ratio of gold to oxygen, can be estimated from the slope of Figure 5.17

$$\text{slope} = \frac{r}{\omega^{1/2}} = 0.62 D_{O_2}^{2/3} \nu^{-1/6} [O_2].x \qquad \textbf{Equation 5.7}$$

where the variables are as defined previously. It can be seen from Figure 5.17, that the experimental data fits a linear relationship, with a slope of 0.85 and an intercept of 0.61. This linearity indicates that the reaction is largely diffusion controlled, and in this case, the dissolution is limited by the diffusion of oxygen to the surface of the electrode. The slope of 0.85 gives a value of 3.5 for x. Therefore, 3.5 moles of oxygen are reacted for every mole of gold that is dissolved. Another way of expressing the stoichiometry is that 87% of the oxygen is reduced to hydroxide, and only 13% of the oxygen forms peroxide as a product.

It is uncertain what causes the non-zero intercept of 0.61 that is evident in Figure 5.17. Similar graphs have been published by Zheng *et al.* (1996), for the system zinc in tri-iodide solutions. These authors attributed the non-zero intercept to

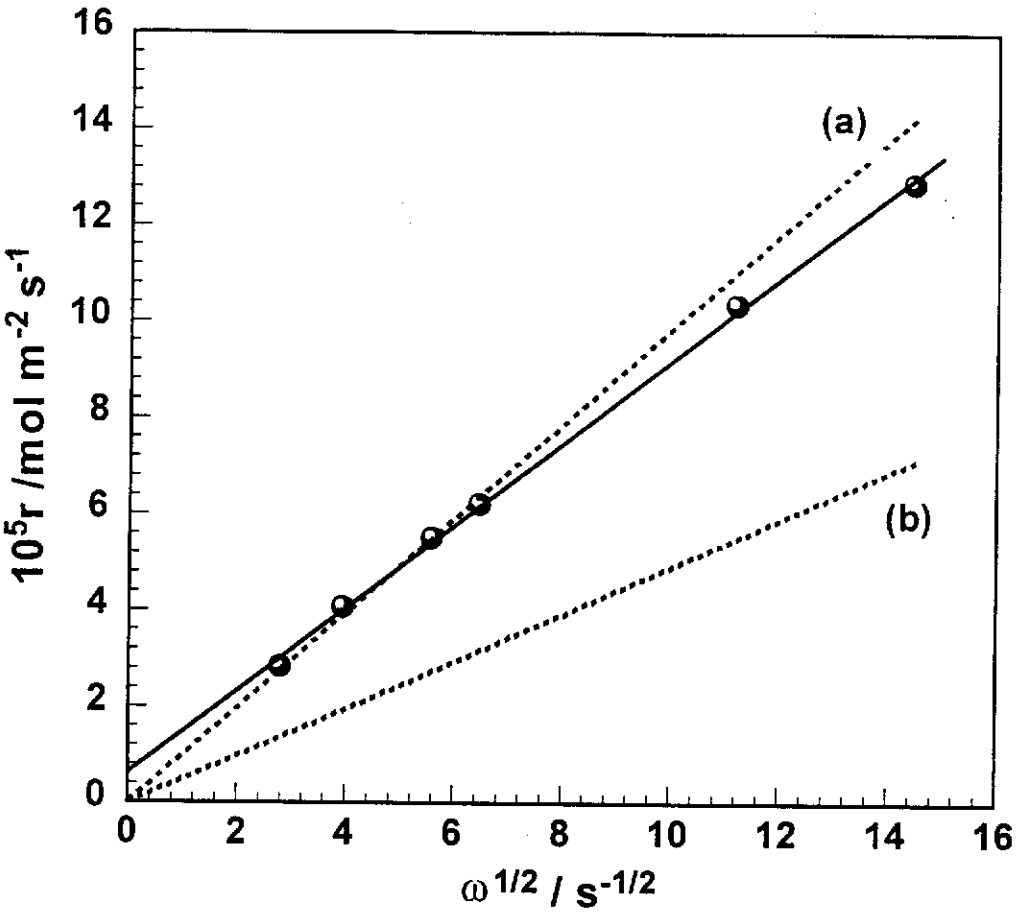

Figure 5.17 – Rate of dissolution of gold versus $\omega^{1/2}$. Lines (a) and (b) are calculated for diffusion of oxygen with reduction to hydroxide and peroxide respectively. Experimental conditions: air saturated 20 mM cyanide solution, 1 ppm lead, pH 10.0, 25 °C.

an additional chemically controlled process, which in their case was the reduction of trace levels of oxygen. It is possible that there is a chemically controlled process that is affecting the dissolution of gold. Kirk, Foulkes and Graydon (1979) discovered a similar phenomenon for the oxidation of gold in cyanide solutions at low overpotentials. They showed that the measured amount of gold cyanide formed during oxidation was higher than the electric charge passed. They attributed this to the reaction of HCN with gold to form hydrogen and the gold cyanide complex, and results shown in Figure 5.17 are consistent with such an explanation.

5.3.3.2. Electrochemistry – Oxidation

The effect of rotation rate on the oxidation of gold in the vicinity of peak P2 was investigated, and shown in Figure 5.18 is the Levich style plot of the peak current density against $\omega^{1/2}$. Also shown is the line representing the maximum theoretical rate of oxidation, which is calculated using the Levich equation for the diffusion of cyanide to the surface of the gold. It must be remembered that in this instance, the potential is applied by a potentiostat, and so the diffusion of oxygen is not considered. Also, the results obtained here are not directly applicable to the kinetic studies (section 5.3.3.1), as the rate of gold dissolution is limited by oxygen diffusion. However, these results are useful in showing how the oxidation of gold in cyanide solutions containing 1 ppm lead varies with experimental conditions.

From Figure 5.18, it can be seen that at the lowest rotation rate, the oxidation current density is close to that for diffusion control, suggesting that the current density had almost reached a limiting plateau prior to passivation. At higher rotation rates, the shift away from the diffusion limiting case becomes more pronounced. This implies that the oxidation rate at higher rotation rates is under mixed diffusion/chemical controlled, and hence, the lead is less effective at removing passivation at higher rotating rates. Similar results have been published by Mussatti, Mager and Martins (1997), and at this stage, it is uncertain what causes this effect.

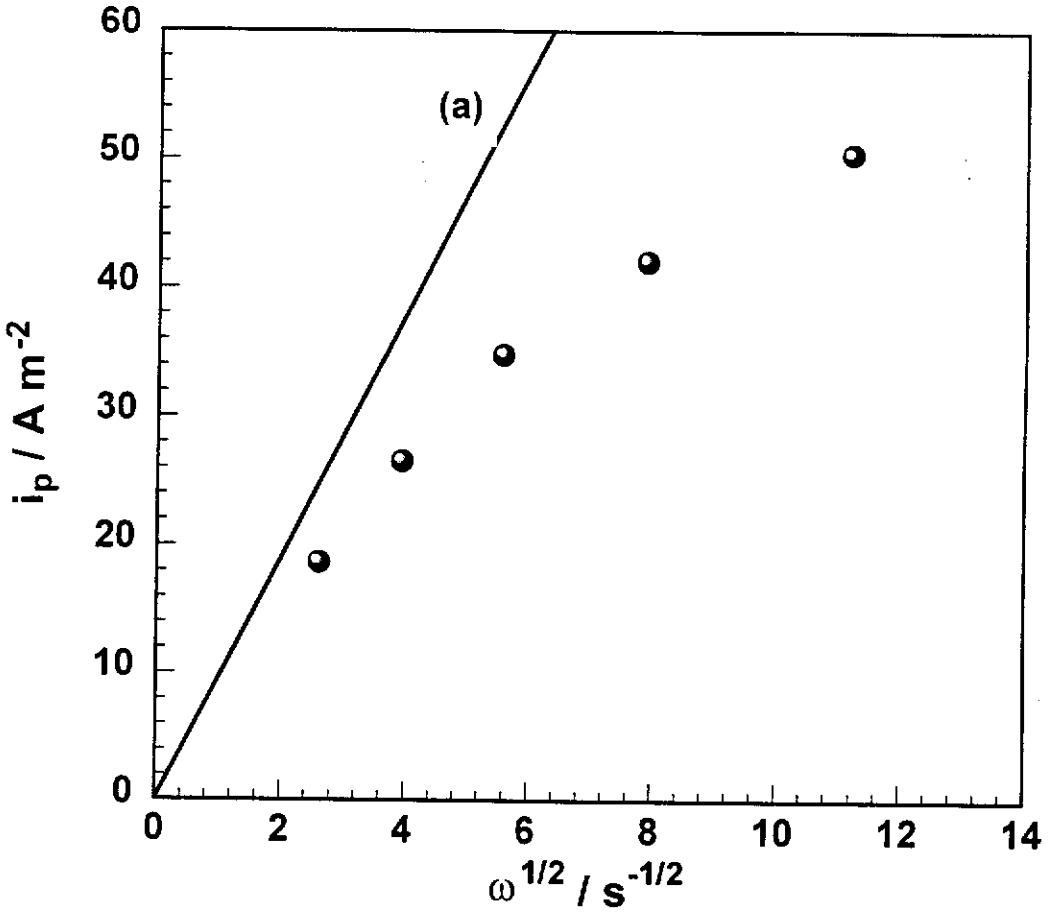

Figure 5.18 – Oxidation current density for peak P2 as a function of rotation rate. Also shown is line (a), calculated for the diffusion of cyanide. Experimental conditions: 20 mM cyanide solution, 1 ppm lead, pH 10.0, 1 mV s^{-1}, 25 °C.

5.3.3.3. Electrochemistry – Evans' Diagrams

Shown in Figure 5.19 is the Evans' diagram representing the dissolution of gold at 75 rpm in a solution containing 20 mM cyanide and 1 ppm lead. It is clear that at 75 rpm, there is only one intersection point between the gold oxidation and oxygen reduction polarisation curves. Therefore, the Evans' diagrams, Figures 5.13 and 5.19, predict that: 1) the dissolution of gold will occur in the active region at both 75 and 300 rpm; and 2) the dissolution rate will increase with rotation rate. These findings are consistent with the kinetic studies, where it was shown in section 5.3.3.1 that the dissolution of gold was diffusion controlled over a wide range of rotation rates.

5.3.4. Effect of Temperature

5.3.4.1. Kinetic Studies

The dissolution rate of gold in a solution containing 20 mM cyanide and 1 ppm lead was measured as a function of temperature, and the results are shown in Figure 5.20. Initially, as the temperature is increased, the rate of dissolution increases until it reaches a maximum of 6.6×10^{-5} mol m^{-2} s^{-1} at 45 °C. At temperatures above 45 °C, the dissolution rate starts to fall, reaching 6.4×10^{-5} mol m^{-2} s^{-1} at 62 °C. Also shown as the dotted line in Figure 5.20 is the solubility of oxygen in water (Fogg & Gerrard, 1991), which decreases as the temperature increases. The reduced solubility of oxygen accounts for the decrease in the rate of dissolution of gold in 1 ppm lead at higher temperatures. Because of this complication, the activation energy for this system cannot be calculated directly, although the reaction rate at higher temperatures can be corrected for a constant oxygen concentration. The method for correcting for oxygen solubility is described in Chapter 4, and simply consists of multiplying the measured rate by the ratio of the oxygen concentrations $[O_2]_{25}$ / $[O_2]_T$. The measured and corrected rates of dissolution are shown in Table 5.4.

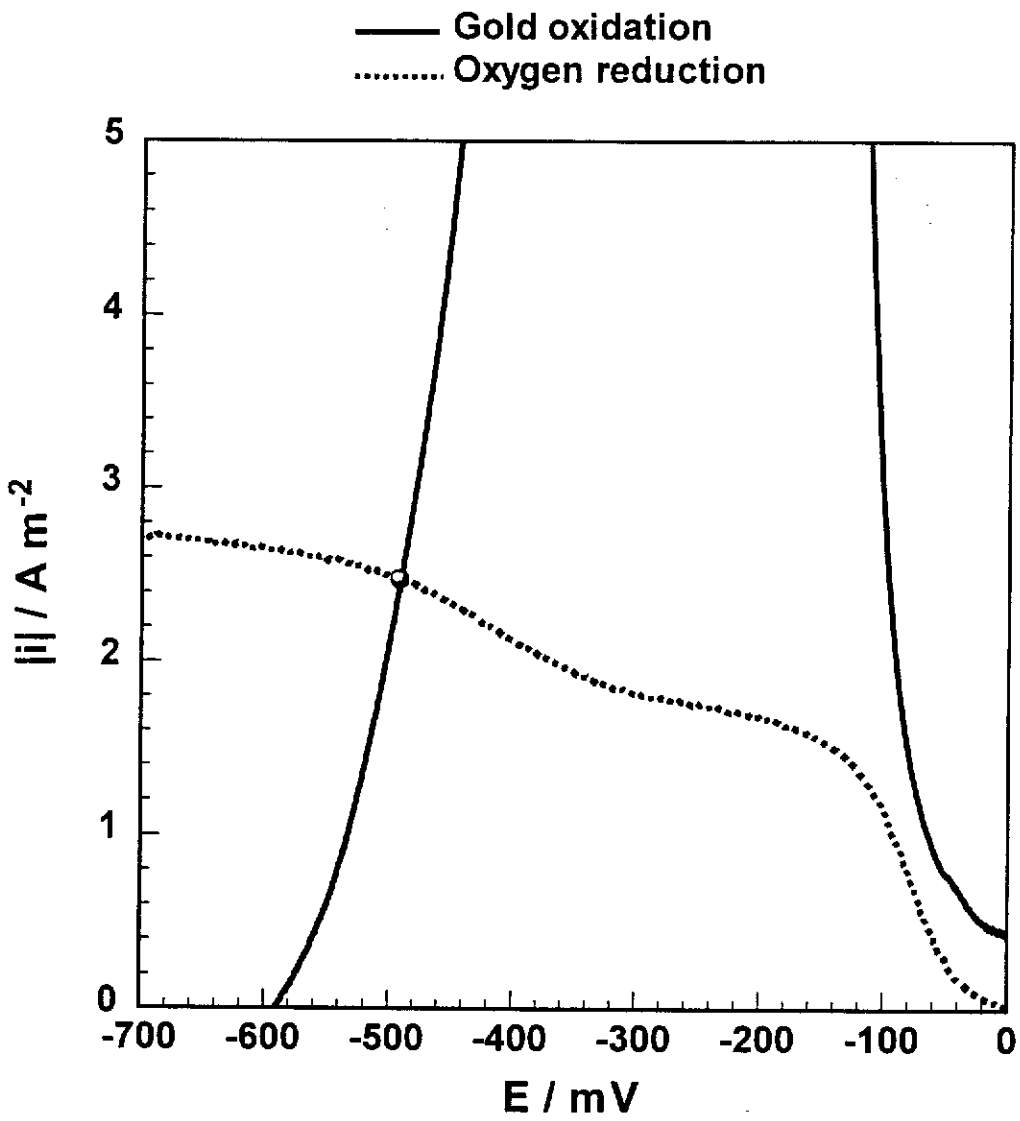

Figure 5.19 – Evans' diagram representing the dissolution of gold in air saturated 20 mM cyanide solutions at 75 rpm. Experimental conditions: 1 ppm lead, pH 10.0, 25 °C.

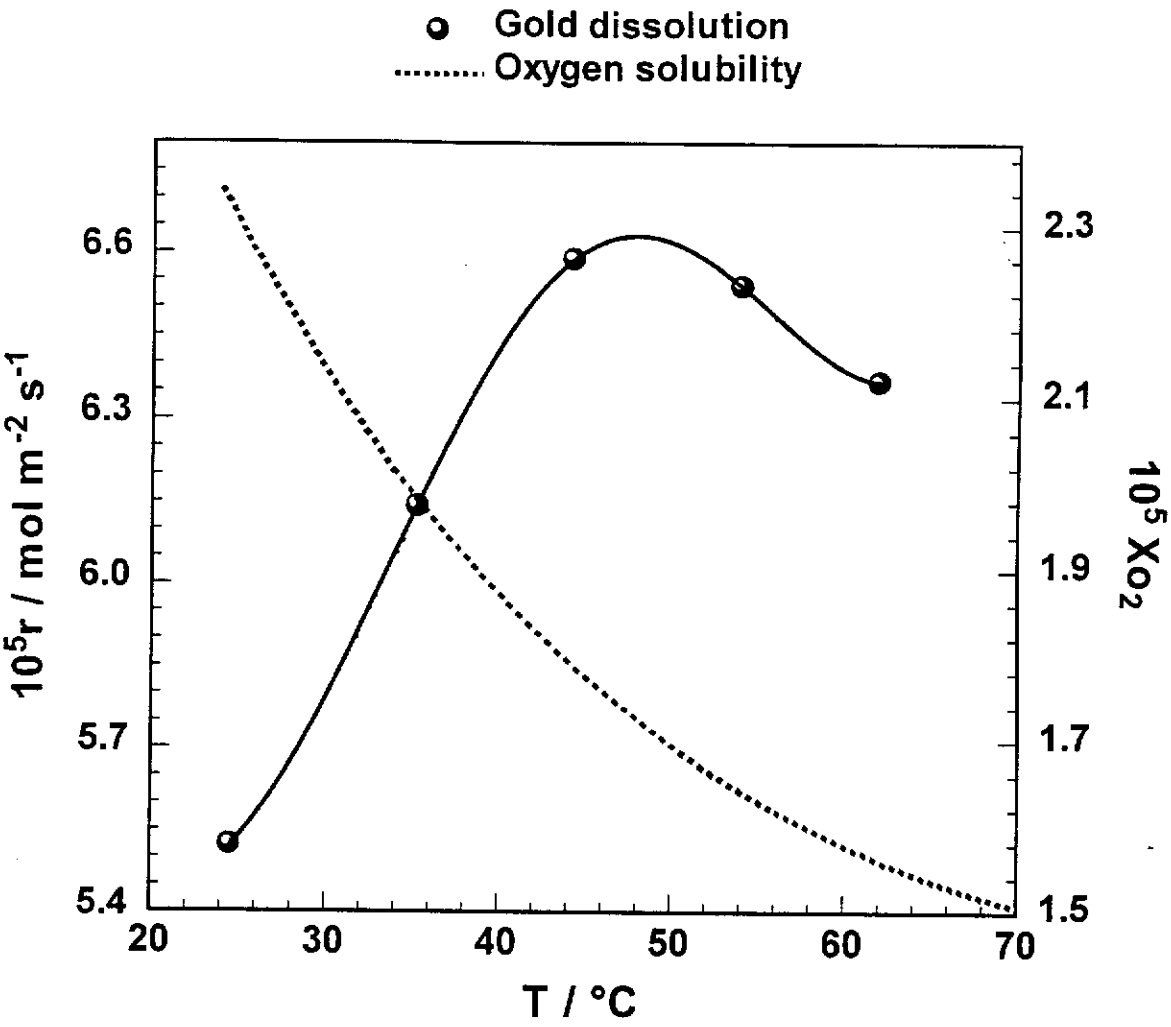

Figure 5.20 – Effect of temperature on the rate of dissolution of gold. Also shown is the mole fraction oxygen solubility in water as a function of temperature. Experimental conditions: air saturated 20 mM cyanide, 1 ppm lead, pH 10.0, 300 rpm.

T /°C	10^5r /mol m^{-2} s^{-1}	10^5Xo$_2$	10^5r$_c$ /mol m^{-2} s^{-1}
25	5.5	2.32	5.6
35	6.1	1.98	8.2
44	6.6	1.79	9.7
54	6.5	1.64	10.5
62	6.4	1.56	10.8

Table 5.4 – Measured, r, and corrected, r_c, rates of dissolution of gold in aerated 20 mM cyanide solutions with 1 ppm lead as a function of temperature. Also shown is the mole fraction solubility of oxygen, Xo_2 at the specified temperatures. Experimental conditions: pH 10.0, 25 °C, 300 rpm.

The activation energy for the dissolution of gold in cyanide solutions containing 1 ppm lead can now be determined using an Arrhenius plot. The Arrhenius plot is based on the corrected rate of dissolution, and is shown in Figure 5.21. It is clear that the data does not display a linear relationship, with the slope decreasing as the temperature increases. This could indicate that at low temperatures, the reaction is chemically controlled, and at high temperatures, the reaction is diffusion controlled. Two tangents have been added to the Arrhenius plot, one at high temperatures, and one at low temperatures. The slope of these tangents can be used to calculate the activation energy for the process. At high temperatures, the activation energy is calculated to be 7 kJ mol^{-1}, while at low temperatures, the activation energy is 21 kJ mol^{-1}. The activation energy for a diffusion controlled process is usually less than 25 kJ mol^{-1} (Power & Ritchie, 1975), so it would appear that the reaction is diffusion controlled at all temperatures. This result is consistent with the findings from section 5.3.3.1, where is was shown that the rate of dissolution rate of dissolution increases linearly with $\omega^{1/2}$ (a criteria for diffusion control).

It is uncertain whether it is possible for a process to have an activation energy as low as 7 kJ mol^{-1}, and thus it is believed that there is a discrepency in the data at

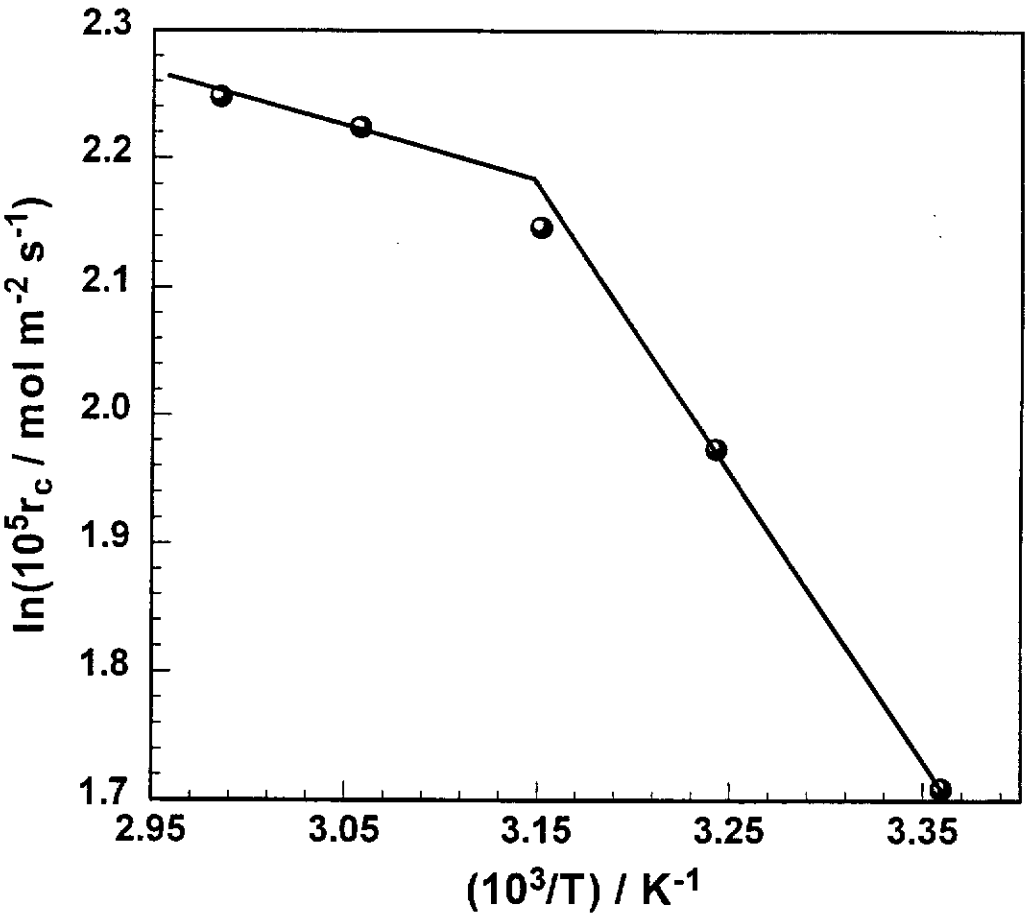

Figure 5.21 – Arrhenius plot for the corrected rate of dissolution of gold as a function of 1/T. Experimental conditions: air saturated 20 mM cyanide, 1 ppm lead, pH 10.0, 300 rpm.

high temperatures. The problem in estimating the activation energy is not restricted to this system though, as a similar result will be shown Chapter 5 when calculating the activation energy for a gold/silver deposit. This could indicate that the method for correcting for changes in oxygen solubility is flawed, or that at higher temperatures, the low activation energy is a feature of oxygen reduction. It is uncertain which of these possibilities is correct, and examining these possibilities further is beyond the scope of this work.

5.3.4.2. Electrochemistry – Oxidation

The oxidation of gold at 25 °C and 60 °C in solutions containing 1 ppm lead and 20 mM cyanide is shown in Figure 5.22 as the dashed and solid lines respectively. The oxidation of gold in the absence of lead at 60 °C, from section 4.3.4.2, has also been added for comparison. The two experiments with 1 ppm lead, show that the current density at peak P2 increases with temperature. It can also be seen that at 60 °C, the gold does not passivate fully at −100 mV. Instead, the current density decreases to 13 A m^{-2} at -65 mV, before increasing to 42 A m^{-2} at 0 mV. For gold in the absence of lead at 60 °C, the oxidation peak is almost identical in shape to the gold oxidation peak P2, in the presence of lead. This suggests that the active oxidation of gold at 60 °C is due the trace levels of lead that exist in the reagents that are used in solution preparation.

Once the gold oxidation polarisation curves have been measured as a function of temperature, the activation energy for the oxidation peak P2 can be estimated. It should be remembered that the value calculated here will be different to that calculated in the previous section as the oxidation of gold is not limited by oxygen diffusion. Shown in Figure 5.23 is an Arrhenius plot of ln(i) versus 1/T. The data were found to fit a linear relationship, and the activation energy can be calculated from the slope of the line of best fit. The calculated activation energy is 14 kJ mol^{-1}. This is indicative of a reaction that is diffusion controlled, as the activation energy is less than 25 kJ mol^{-1}. However, in section 5.3.3.2, it was shown that the Levich plot

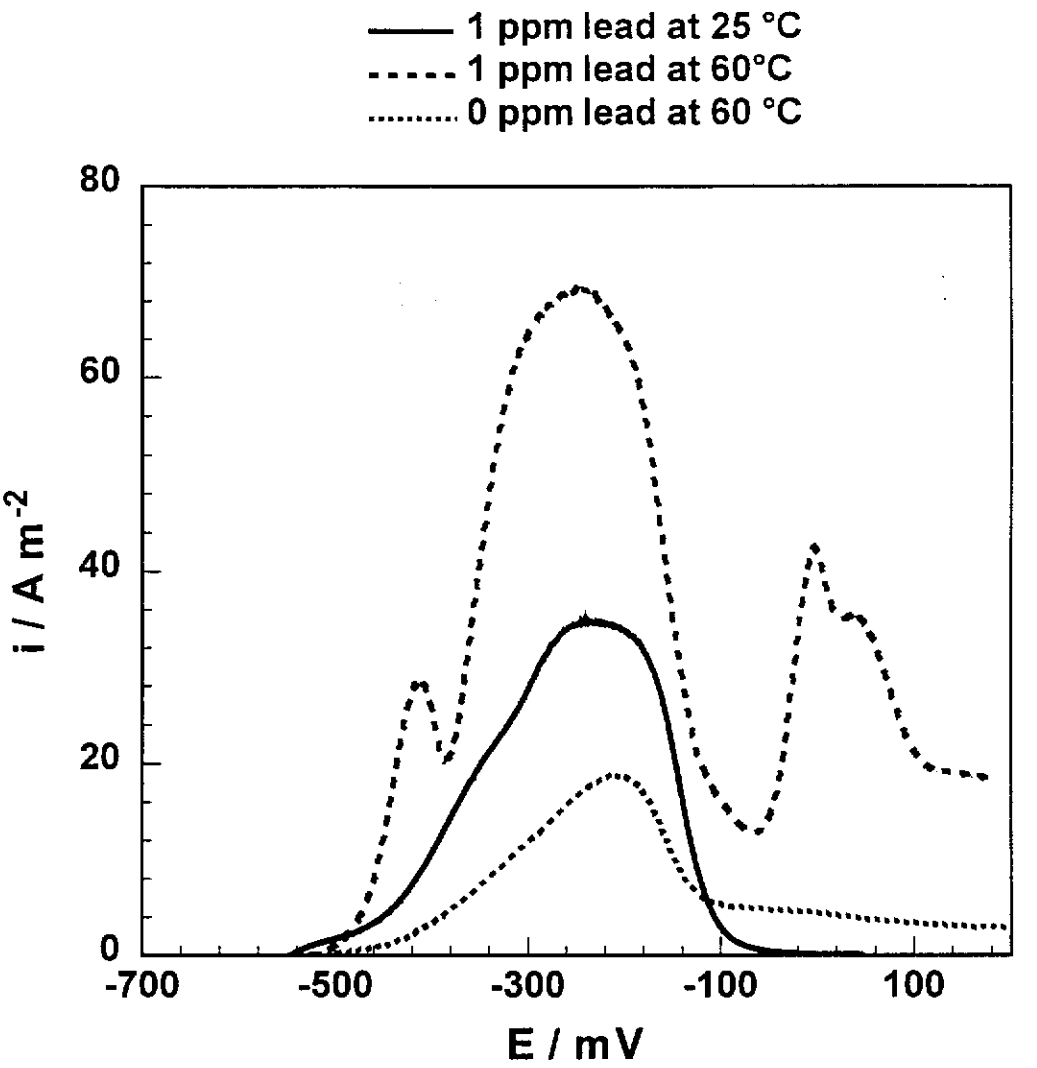

Figure 5.22 – Gold oxidation as a function of temperature. Experimental conditions: 20 mM cyanide, 1 ppm lead, pH 10.0, 1 mV s^{-1}, 300 rpm.

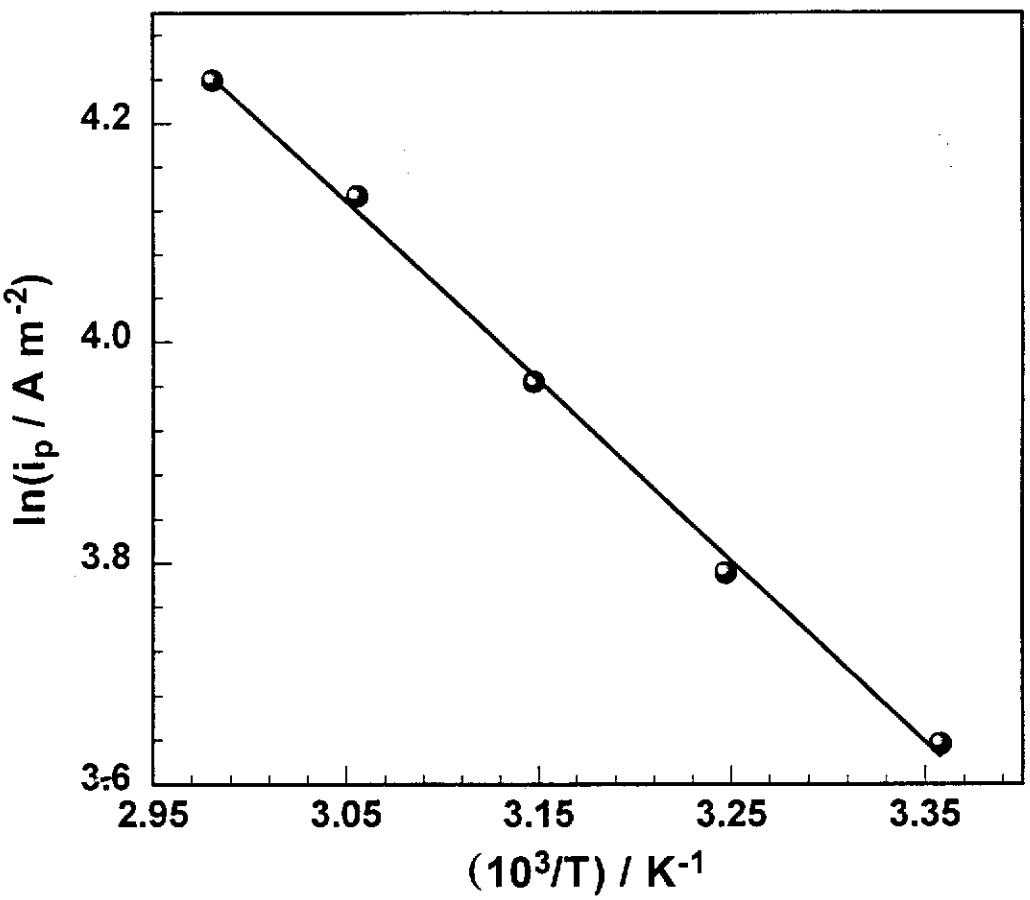

Figure 5.23 – Arrhenius plot of the oxidation current density for peak P2 as a function of 1/T. Experimental conditions: 20 mM cyanide, pH 10.0, 300 rpm.

of current density at peak P2 versus $\omega^{1/2}$ was non linear, suggesting that the oxidation of gold in 1 ppm lead is under mixed diffusion/chemical control. At this stage it is uncertain what causes this discrepancy.

5.3.4.3. Electrochemistry – Evans' Diagrams

Shown in Figure 5.24 is the Evans' diagram representing the dissolution of gold in air saturated cyanide solutions at 60 °C. As discussed in the previous section, at 60 °C, gold in the presence of lead does not fully passivate at -100 mV. Consequently, the gold oxidation polarisation curve in the presence of lead at 60 °C, as shown in Figure 5.24, does not reappear on the Evans' diagram at -100 mV as it does at 25 °C. Hence, there is only one possible intersection point between the oxidation and reduction polarisation curves 60 °C, and so the Evans' diagram predicts that gold dissolution at 60 °C will occur at a high rate.

5.3.5. Effect of Oxygen Concentration

5.3.5.1. Kinetic Studies

The effect of oxygen concentration on the dissolution of gold in a 20 mM cyanide solution containing 1 ppm lead was investigated, and the results are shown in Table 5.5. Also shown are the rates of dissolution, r_L, which were calculated using the Levich equation, assuming that diffusion of oxygen is the limiting step and that oxygen is reduced to hydroxide.

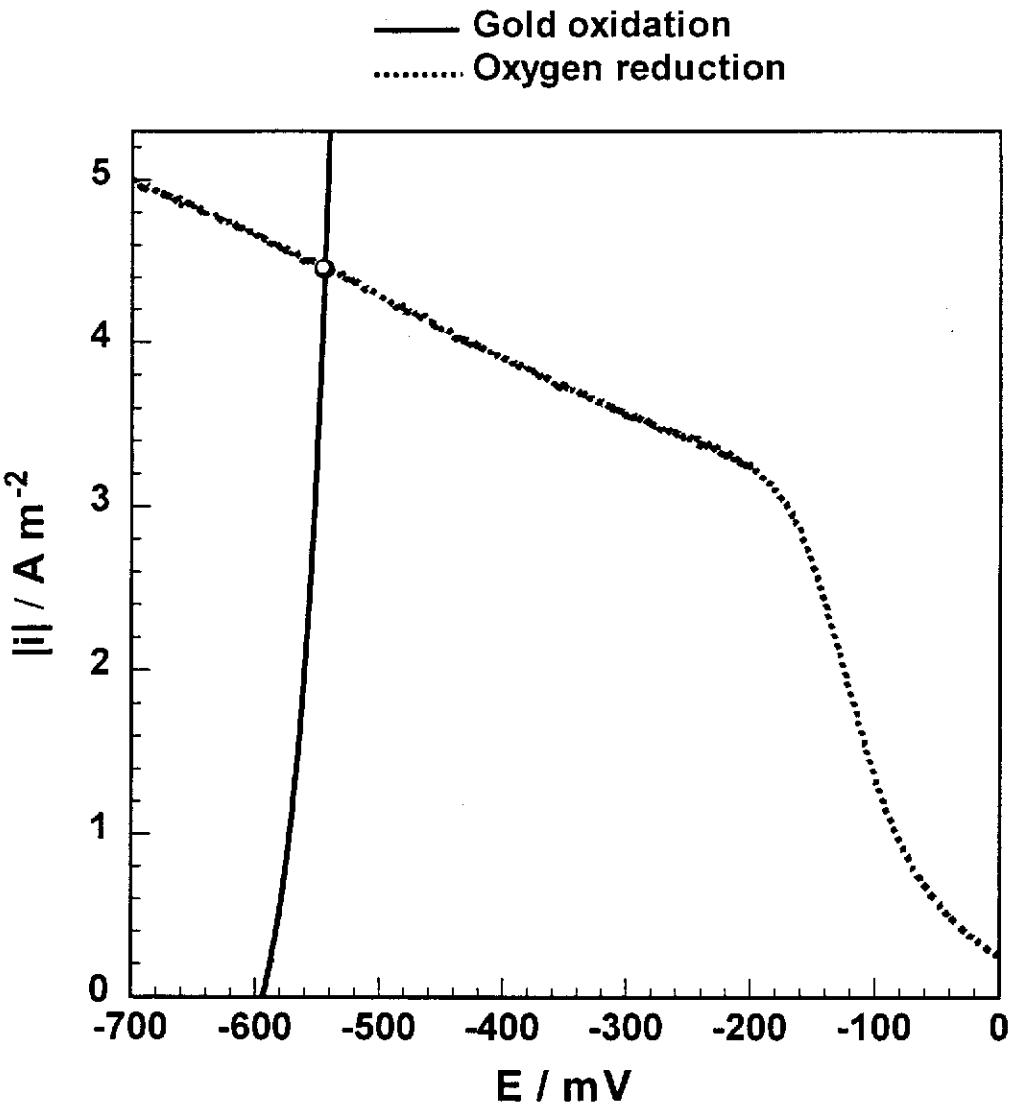

Figure 5.24 – Evans' diagram representing the leaching of gold at 60 °C in air saturated 20 mM cyanide solutions. Experimental conditions: pH 10.0, 1 ppm lead, 300 rpm.

System	$10^5 r_L$ /mol m^{-2} s^{-1}	$10^5 r$ /mol m^{-2} s^{-1}
Air saturated	5.50	5.57
Oxygen Saturated	26.19	1.36

Table 5.5 – Calculated, r_L, and measured, r, dissolution rates of gold in air and oxygen saturated 20 mM cyanide solutions in the presence of 1 ppm lead. Experimental conditions: pH 10.0, 25 °C, 300 rpm.

It is clear that the active nature of the lead depends on experimental conditions, which has already been demonstrated by the effect of cyanide concentration, as discussed in section 5.3.2.1. In this case, it can be seen that: 1) for air saturated solutions, the dissolution rate is oxygen diffusion controlled; 2) for oxygen saturated solutions, the dissolution rate is not diffusion controlled; and 3) for oxygen saturated solutions, the dissolution rate is significantly lower than for air saturated solutions. Therefore, it appears that lead is ineffective at reducing passivation at high oxygen concentrations.

The mechanism of gold dissolution in oxygen saturated solutions containing 1 ppm lead was further investigated by repeating the leaching experiment using a lead pretreated gold electrode, as discussed in section 5.3.1. In this instance, the electrode was pretreated by immersion in an oxygen saturated solution containing 1 ppm lead for 300 seconds. The electrode was then rinsed, and immersed in an air saturated lead free solution. The dissolution rate in this solution was low, indicating that the lead pretreatment was ineffective at removing passivation. This suggests that the nature of the lead on the surface of the gold must be different when the solutions are oxygen saturated. If the passivating action was due to the oxygen alone, a higher rate would be observed when the electrode is transferred to the air saturated solution. It is believed that in an oxygen saturated solution, the lead on the surface of the gold is oxidised to form lead oxide. When the gold is transferred to the lead free solution, the lead, which remains as lead oxide, is not active in reducing passivation.

5.3.5.2. Electrochemistry – Evans' Diagrams

The Evans' diagram representing the dissolution of gold in oxygen saturated 20 mM cyanide solutions containing 1 ppm lead is shown in Figure 5.25. It is clear that the gold oxidation and oxygen reduction polarisation curves intersect at three different potentials, -390, -113 and -37 mV. This is similar to the Evans' diagram for low cyanide concentrations, as discussed in section 5.3.2.3, and in a similar manner, the measured mixed potential in this case was closest to the more anodic of the intersection points. Consequently, the Evans' diagrams show that gold is passive in oxygen saturated solutions containing 20 mM cyanide and 1 ppm lead, and explains why low dissolution rates are obtained in the kinetic section. Hence, if lead is added to a leach circuit to improve the recovery of gold, then increasing the oxygen concentration of the leach solution will actually decrease the leaching rate.

5.3.6. Effect of pH

5.3.6.1. Kinetics

The dissolution rate of gold in solutions containing 1 ppm lead and 20 mM cyanide was investigated as a function of pH, and the results are shown in Figure 5.26. It can be seen that there appears to be a critical pH, at which the mechanism for gold dissolution in the presence of lead changes. At pH values above the critical pH, the rate of dissolution of gold is low, and hence chemically controlled. At pH values below the critical pH, the rate of dissolution is diffusion controlled. The change in the mechanism of dissolution at the critical pH can be easily explained using Evans' diagrams. In the following two sections, it will be shown that the potential at which the gold oxidation peak P2 passivates is a function of pH. This results in the anodic and cathodic polarisation curves intersecting in the passive region at higher pH values.

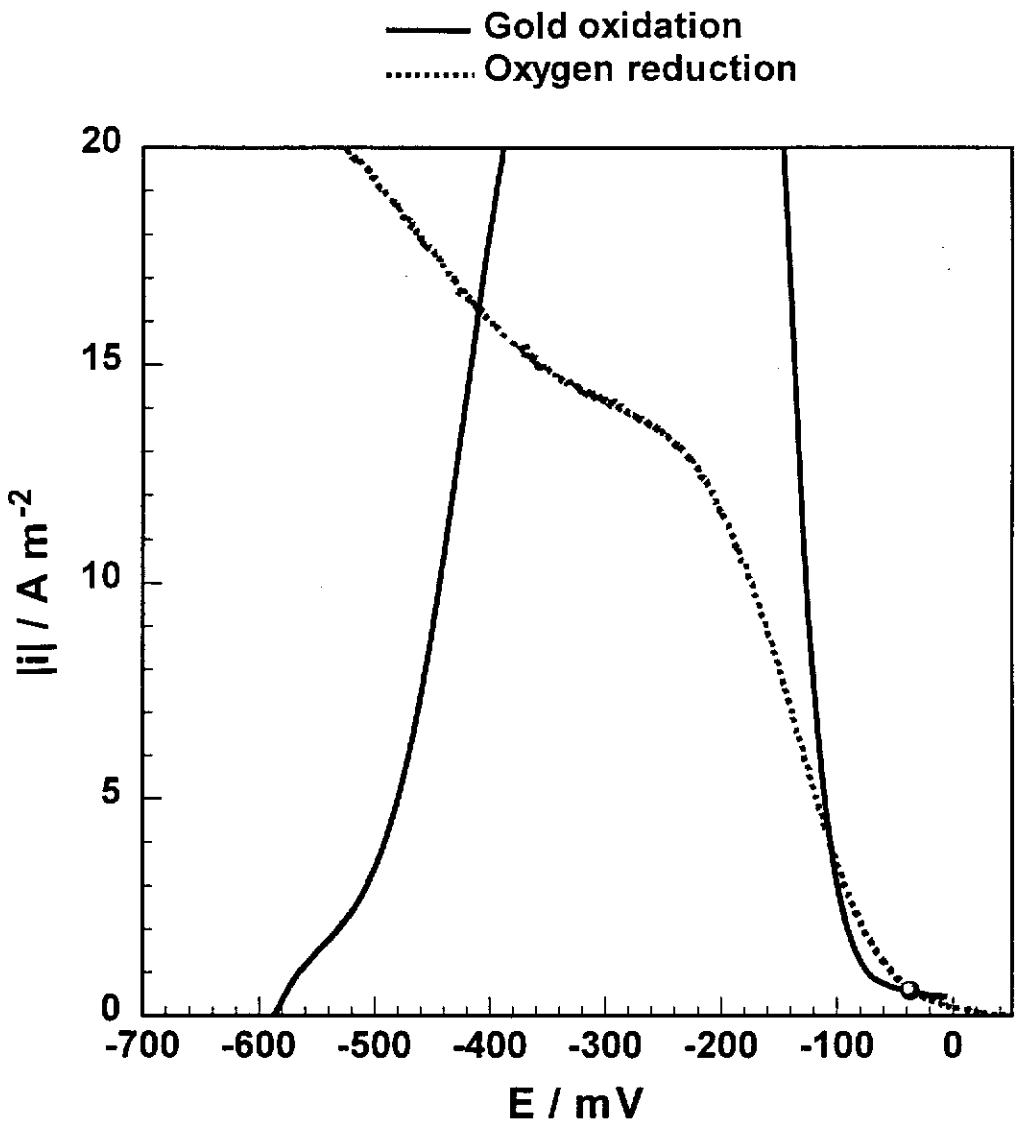

Figure 5.25 – Evans' diagram representing the leaching of gold in oxygen saturated 20 mM cyanide solutions. Experimental conditions: 1 ppm lead, pH 10.0, 25 °C, 300 rpm.

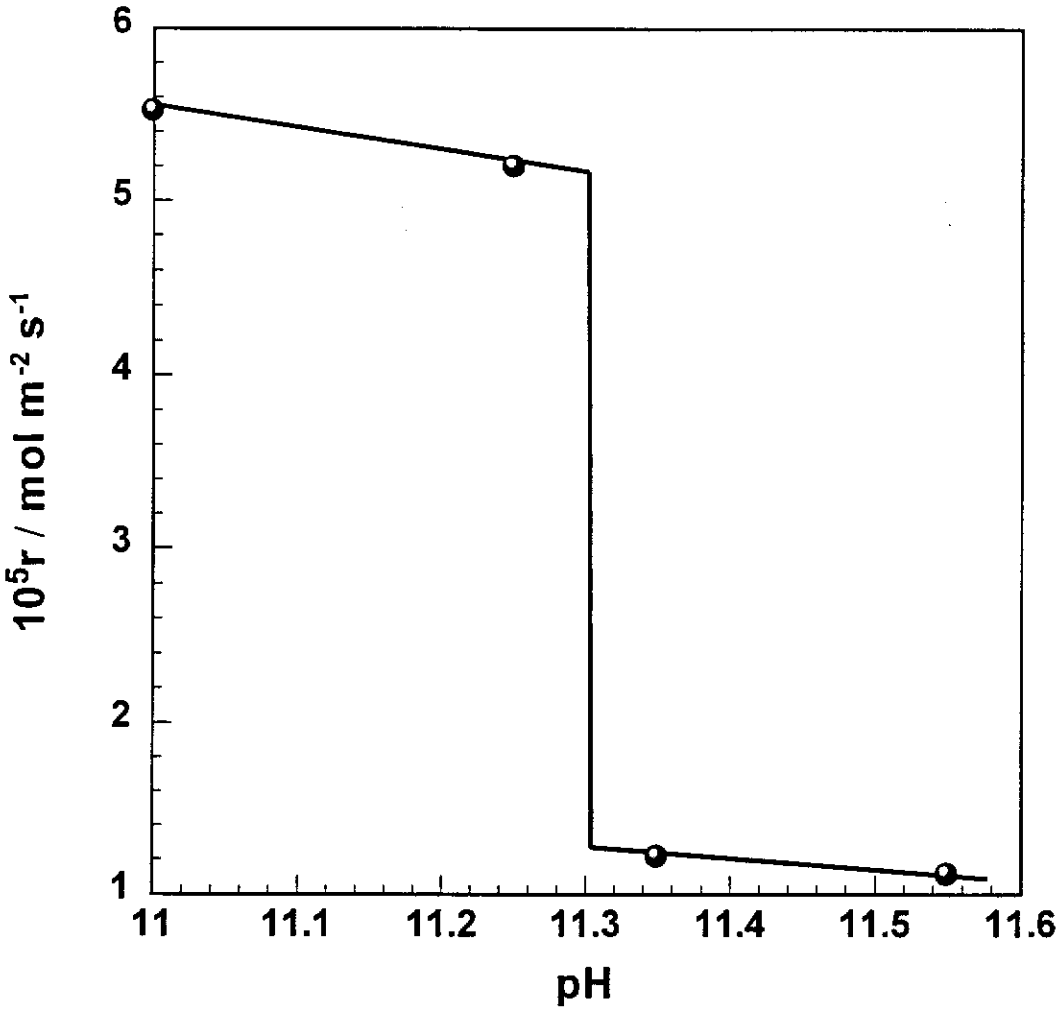

Figure 5.26 – Effect of pH on the dissolution of gold. Experimental conditions: air saturated 20 mM cyanide solution, 1 ppm lead, 25 °C, 300 rpm.

5.3.6.2. Electrochemistry – Oxidation

The effect of pH on the oxidation of gold in solutions containing 1 ppm lead and 20 mM cyanide was investigated, and the resultant polarisation curves are shown in Figure 5.27. It can be seen that the potential at which passivation of the gold oxidation peak P2 occurs shifts with pH. As the pH is lowered, the gold passivates at progressively more positive potentials. This implies that the mechanism by which passivation occurs involves hydroxide. It will be recalled from the Pourbaix diagram, as shown in Figure 5.12, that lead is oxidised to either PbO or $HPbO_2^-$ in the pH range 9 to 11. Either of these reactions can explain why passivation of peak P2 occurs. Lead oxide may not be as effective at reducing the passivation of gold as lead, so once the lead is oxidised to PbO, a passive film reforms on the surface of the gold. On the other hand, if the lead were stripped from the surface as $HPbO_2^-$, there would be nothing to stop the surface from reforming its protective film. The possibility that the gold oxidation peak P2 is passivated by gold oxide or gold hydroxide was not considered a possibility, as gold oxide does not form until very high potentials, as discussed in the previous chapter in section 4.3.1.3.

The results in section 5.3.1.3 are consistent with the passivation of the gold oxidation peak P2 being caused by the formation of lead oxide at pH 10.0. The mechanism of passivation at different pH values can be determined by measuring the passivation potential as a function of pH. These are shown in Figure 5.28 as the circle symbols. The experimental data can be split into two regions, pH 10 to 11.5, and pH 11.5 to 12.5. In the pH range 10 to 11.5, the passivation potential decreases linearly with pH, giving a slope of -55 mV pH^{-1}. The measured slope is close to the value of -59 mV pH^{-1} that is calculated by the Nernst equation for a reaction that involves a stoichiometrically equal number of electrons and hydroxide ions. This suggests that in the pH range 10 to 11.5, passivation of the gold oxidation peak P2 is caused by the oxidation of lead on the surface to form PbO, as shown in Equation 5.5. In the pH range 11.5 to 12.5, the slope of the line of best fit is 96 mV pH^{-1}, which is close to the calculated value of 89 mV pH^{-1} for a process involving two electrons and three hydroxide ions. This suggests that in the pH range 11.5 to 12.5,

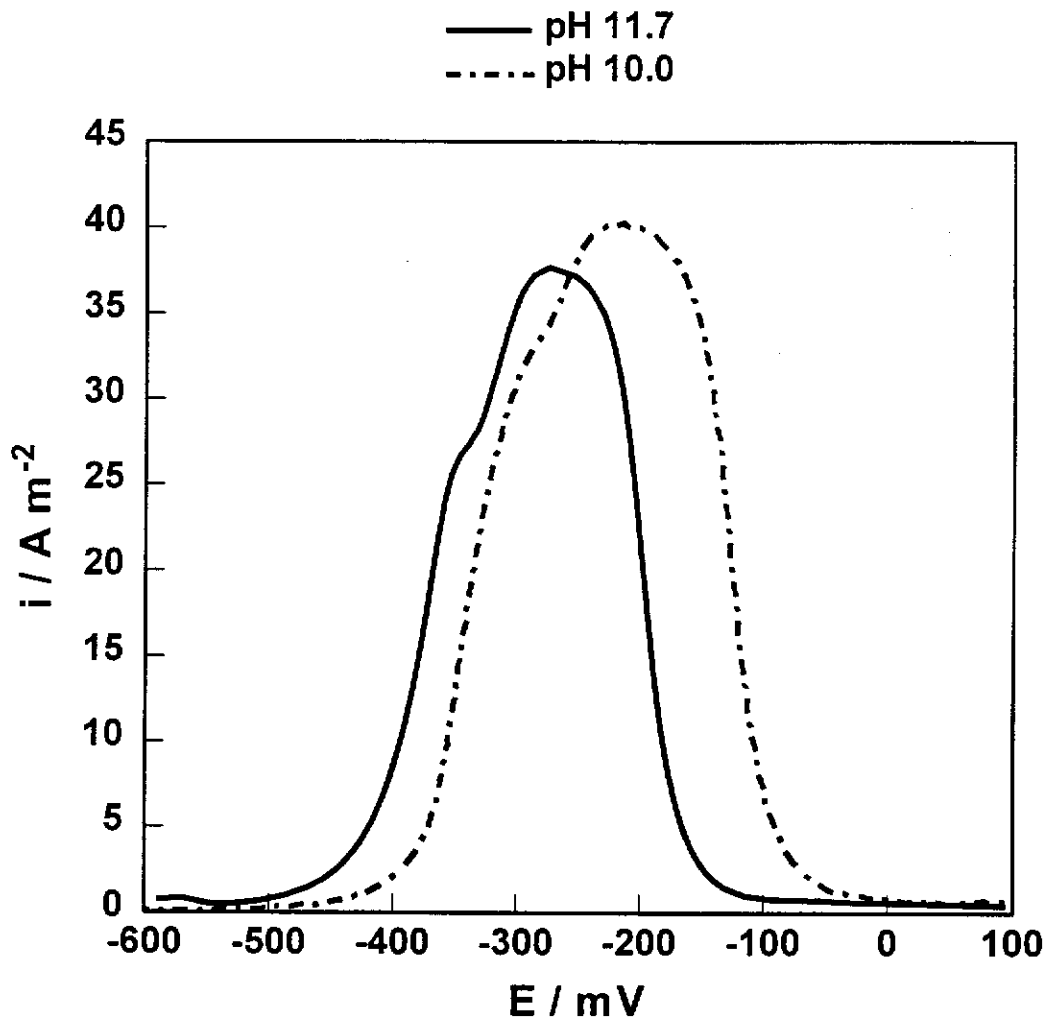

Figure 5.27 – Effect of pH on the gold oxidation peak P2. Experimental conditions: 20 mM cyanide, 1 ppm lead, 1 mV s^{-1}, 25 °C, 300 rpm.

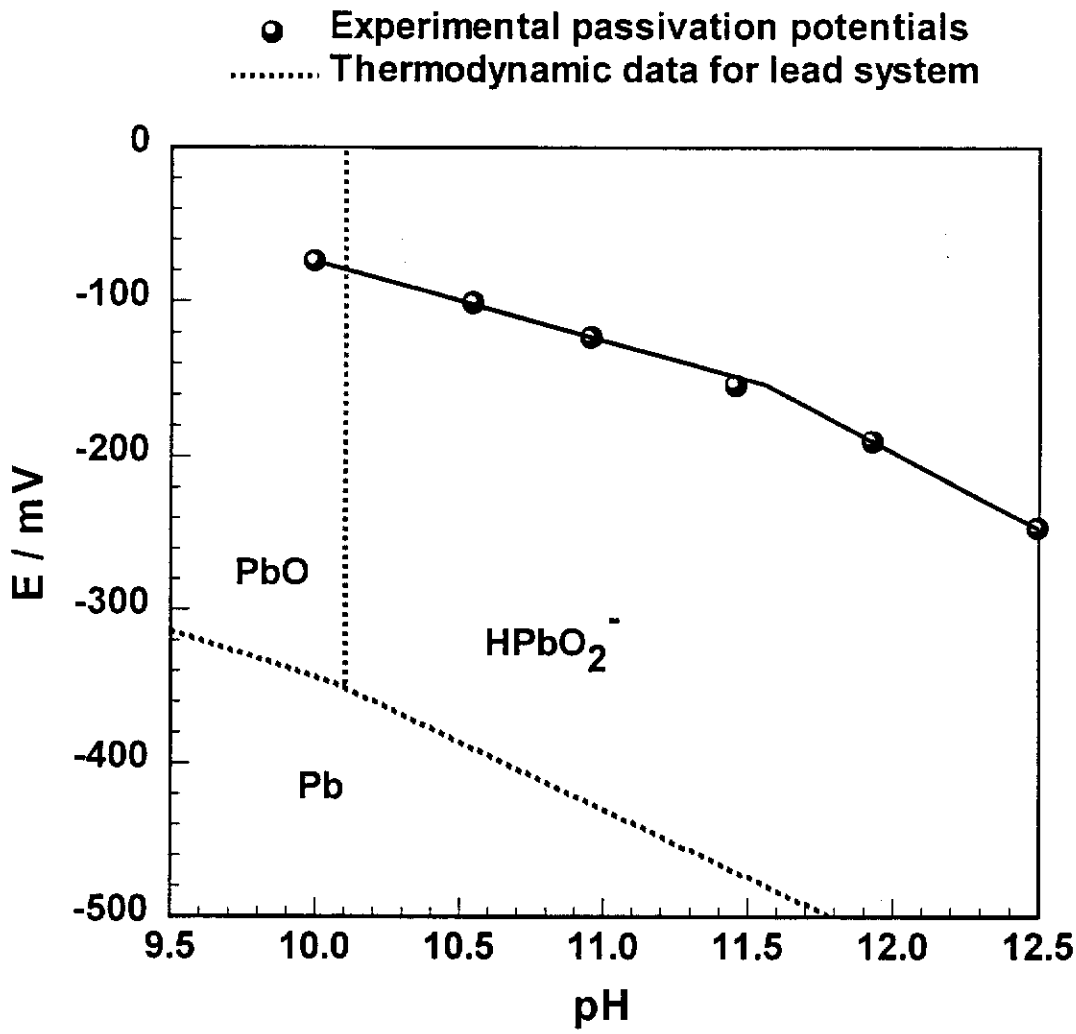

Figure 5.28 – Passivation potential of gold oxidation peak P2 as a function of pH. Also shown is the Pourbaix diagram for the lead/water system as the dotted lines. Experimental conditions: 20 mM cyanide, 1 ppm lead, 25 °C, 300 rpm.

passivation is caused by the oxidation of lead on the surface to form $HPbO_2^-$, as shown in Equation 5.6. The Pourbaix diagram of lead, which was discussed in detail in section 5.3.1.3 has been overlaid in Figure 5.28 for comparison. The experimental data is of the same shape as the Pourbaix diagram, although the experimental data has been offset to high potential and pH values. This is not surprising, as the Pourbaix diagram only represents the thermodynamics of a reaction, and kinetic factors are not considered.

5.3.6.3. Electrochemistry – Evans' Diagrams

The effect of pH on the dissolution of gold in aerated cyanide solutions containing 1 ppm lead can be demonstrated by the use of Evans' diagrams, as shown in Figure 5.29. It is clear that at pH 11.5, the oxygen reduction and gold oxidation polarisation curves intersect at three different potentials, -435, -120 and -100. In a similar manner to section 5.3.2.3, the measured mixed potential is closest to the more anodic of the intersection points, -100 mV. Consequently, the Evans' diagrams are consistent with the kinetic studies (section 5.3.6.1) in showing the dissolution rate will be considerably lower at pH 11.5 than that at pH 10.0.

In summary, from both the kinetic studies and Evans' diagrams, it has been shown that:

1) The dissolution of gold in cyanide solutions containing 1 ppm lead is dependent on experimental conditions;
2) Lead is less active at reducing passivation when the leach solutions contains a low concentration of cyanide, high concentration of oxygen or is at a high pH;
3) The lower rates of dissolution under these conditions is attributed to the anodic and cathodic polarisation curves intersecting in the passive region of gold oxidation.

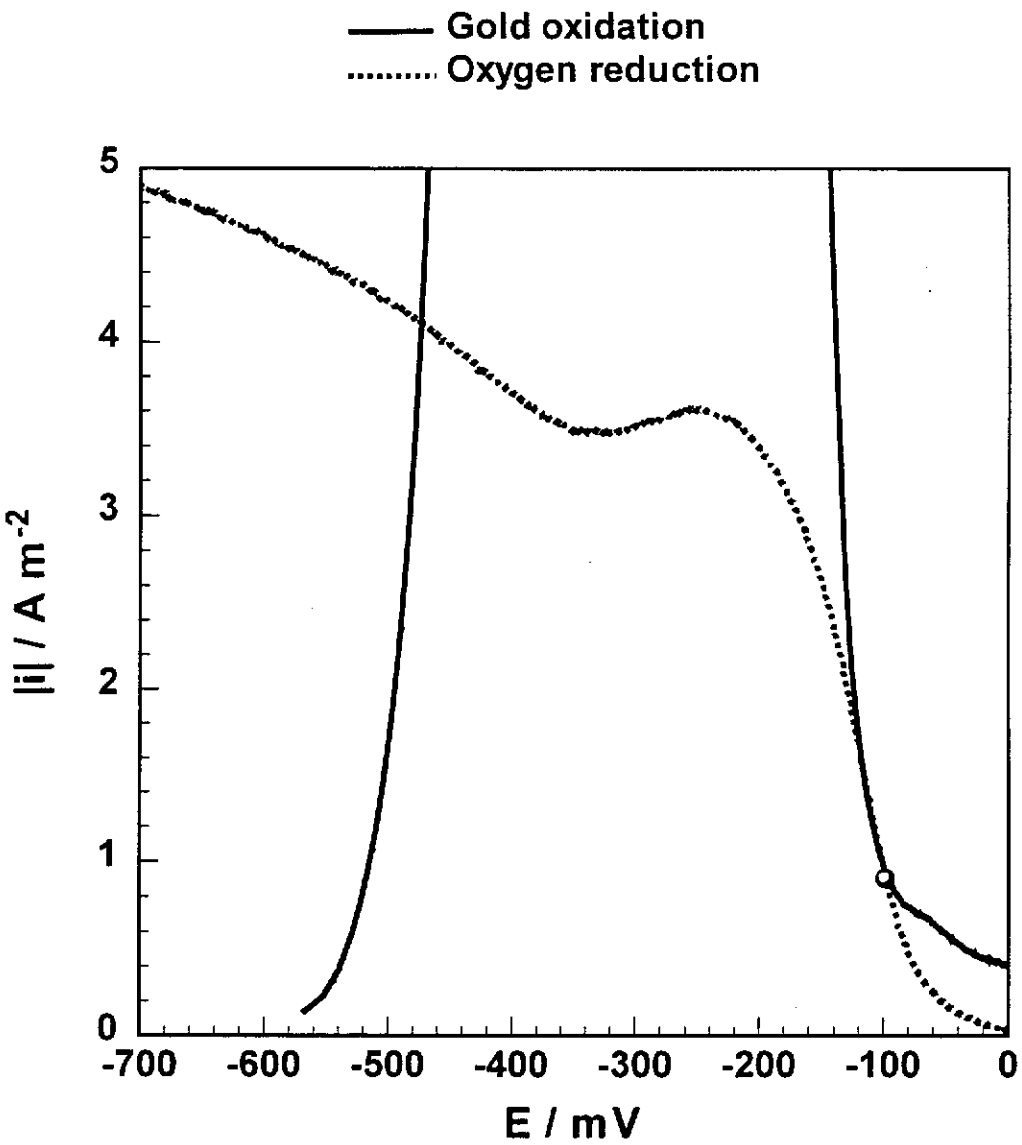

Figure 5.29 – Evans' diagram representing the leaching of gold in air saturated 20 mM cyanide solutions at pH 11.5. Experimental conditions: 1 ppm lead, 25 °C, 300 rpm.

5.3.7. Effect of Lead Concentration

5.3.7.1. Kinetics

Ideally, the rate of dissolution of gold in aerated cyanide solutions should be investigated as a function of lead concentration. Unfortunately, at pH 10.0 and at lead concentrations higher than 10 ppm, a precipitate forms, which is most likely lead hydroxide (Mussatti, Mager & Martins, 1997). Therefore, the dissolution rate can be only measured in solutions containing up to 10 ppm lead. For solutions containing 10 ppm lead and 20 mM cyanide, the gold dissolution rate, 6.1×10^{-5} mol m^{-2} s^{-1}, is higher than that measured for solutions containing 1 ppm lead, 5.5×10^{-5} mol m^{-2} s^{-1}. This result is not surprising, given that lead enhances the reduction of oxygen, and hence in the presence of lead, a higher percentage of oxygen is reduced to hydroxide.

The maximum rate of dissolution calculated from the Levich equation for oxygen diffusion control is 5.5×10^{-5} mol m^{-2} s^{-1} (for Elsners equation). It thus appears that the measured dissolution rate in solutions containing 10 ppm lead is higher than the maximum obtainable rate. This discrepancy can also be explained by taking the results from section 5.3.3.1 into account. It will be recalled that the graph of dissolution rate vs. $\omega^{1/2}$ graph, Figure 5.17, shows a non-zero intercept. The occurrence of such a non-zero intercept could explain why the dissolution rate in solutions containing 10 ppm lead is higher than the calculated value.

Better information can be obtained on the behaviour of gold in cyanide solutions containing high concentrations of lead by monitoring the cementation of lead onto the surface of the gold to form lead metal and the gold cyanide complex. This reaction can be effectively studied by measuring the mixed potential of the system as a function of time (Robertson, 1995). Such experiments were carried out at pH 12.0 to prevent the lead from precipitating. The solutions were thoroughly degassed with argon to remove oxygen and to ensure that the measured mixed potential represents the cementation reaction.

Shown in Figure 5.30 is a mixed potential versus time plot for the cementation of lead on gold. Also included are the equilibrium (rest) potential lines for gold and lead in cyanide solutions. These are shown as the solid lines. In analysing the potential – time response of gold in 1 ppm lead, it can be seen that:

1) For the first 50 seconds, the mixed potential is very similar to the rest potential line for gold in the absence of lead. This indicates that there is very little lead on the surface of the gold.
2) After 50 seconds, the mixed potential rises as the lead starts plating onto the surface, and equilibrium is reached after 200 seconds. The final mixed potential is between the equilibrium potentials of lead and gold, and hence the gold is only partially covered by lead.

When 10 ppm lead is added to solution, the shape of the potential response is similar, although cementation occurs at a faster rate. At steady-state, the surface is still only partially covered by lead. In the case of 50 ppm lead, the potential behavior is nearly identical to that for a lead electrode. This indicates that cementation is very fast, and the gold is completely covered by lead.

5.3.7.2. Electrochemistry – Oxidation.

The oxidation of gold in cyanide solutions was measured as a function of lead concentration at pH 12.0, and the resultant gold oxidation polarisation curves are shown in Figure 5.31. These polarisation curves are slightly different to the ones presented so far in this chapter, as a high pH is required to ensure that the lead does not precipitate. There is no problem in comparing these results with the other polarisation curves, provided that it is remembered that both oxidation peaks, P1 and P2 shift with pH. From the experimental data, it can be seen that at 50 ppm lead, gold oxidation is impeded, with the oxidation peak at -250 mV being narrower, and the oxidation peak at 700 mV having almost been eliminated. At 100 ppm lead, there is very little gold oxidation over the entire potential window. That is, the gold

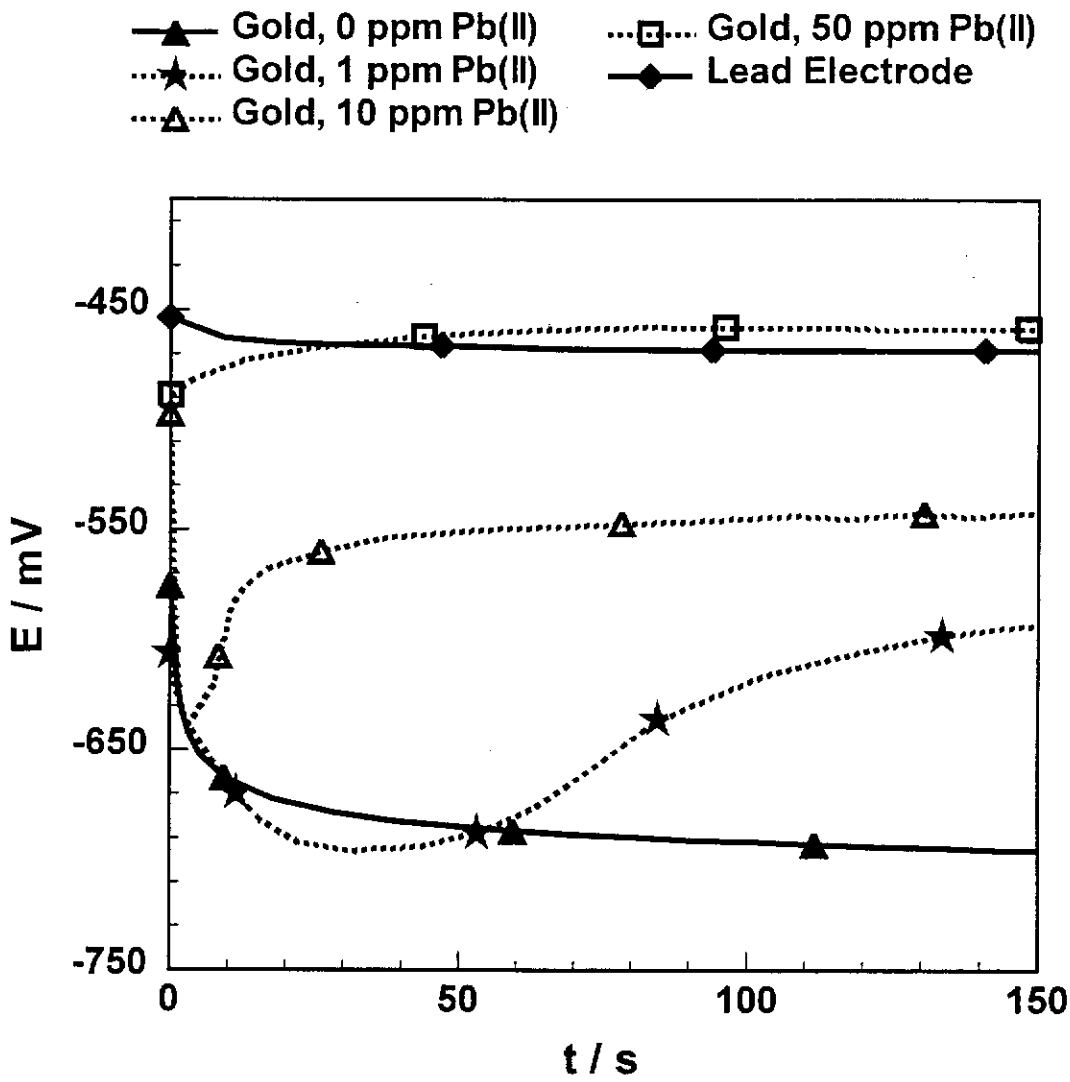

Figure 5.30 – Mixed potential versus time for the cementation of lead on gold. Also shown are the rest potential lines (solid) for gold and lead. Experimental conditions: argon saturated 20 mM cyanide, pH 12.0, 25 °C, 300 rpm.

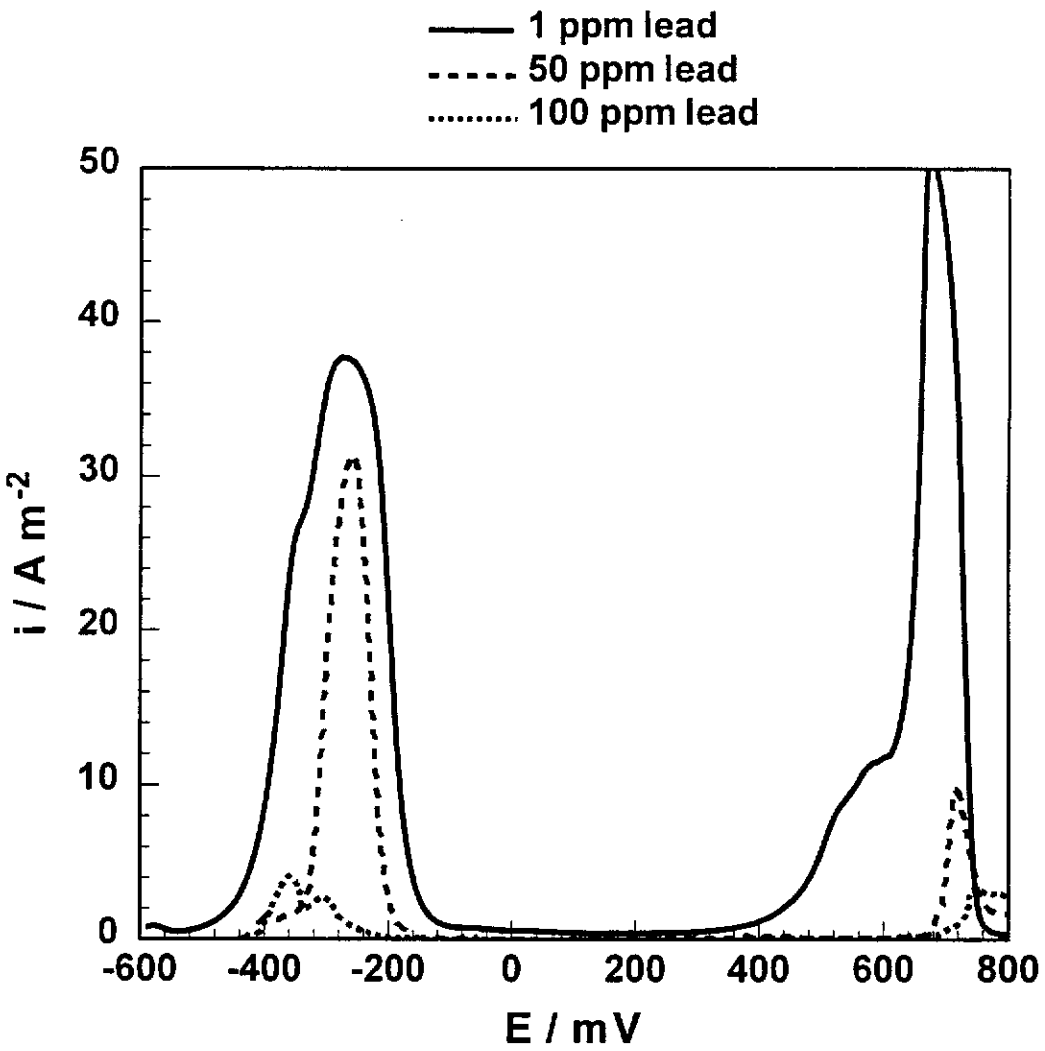

Figure 5.31 – Effect of lead concentration on the oxidation of gold. Experimental conditions: 20 mM cyanide, pH 12.0, 1 mV s^{-1}, 25 °C, 300 rpm.

surface is almost completely blocked in the presence of 100 ppm lead. In the previous section, it was shown that at lead concentrations above 50 ppm, the gold surface was completely covered by a layer of lead. It is therefore believed that at high lead concentrations, the surface is blocked by a layer of lead. This is an unusual result, as at high lead concentrations, you would expect a lead covered gold surface to behave as a lead electrode. Therefore, according to the Pourbaix diagram (Figure 5.12) for lead, you would expect the lead on the surface to be oxidised to form $HPbO_2^-$ in the potential range studied. At this stage, it is uncertain what causes this result.

5.3.7.3. Electrochemistry – Evans' Diagrams

The effect of lead on the dissolution of gold in aerated cyanide solutions was simulated using Evans' diagrams, and shown in Figure 5.32 is the Evans' diagram representing gold dissolution in the presence of 10 ppm lead. It is clear that there is only one intersection point between the anodic and cathodic polarisation curves. Thus, the Evans' diagram is consistent with the kinetic studies in showing that the dissolution rate of gold in 20 mM cyanide solutions containing 1 ppm lead is oxygen diffusion controlled.

5.3.8. Effect of Other Solution Additives

5.3.8.1. Kinetics

Although the action of lead on the dissolution of gold in cyanide solutions has been discussed in detail in this chapter, there are other additives that are known to alter the dissolution rate of gold in aerated cyanide solutions. Fink and Putnam (1950) have reported that thallium, bismuth, mercury and sulfide ions all have an

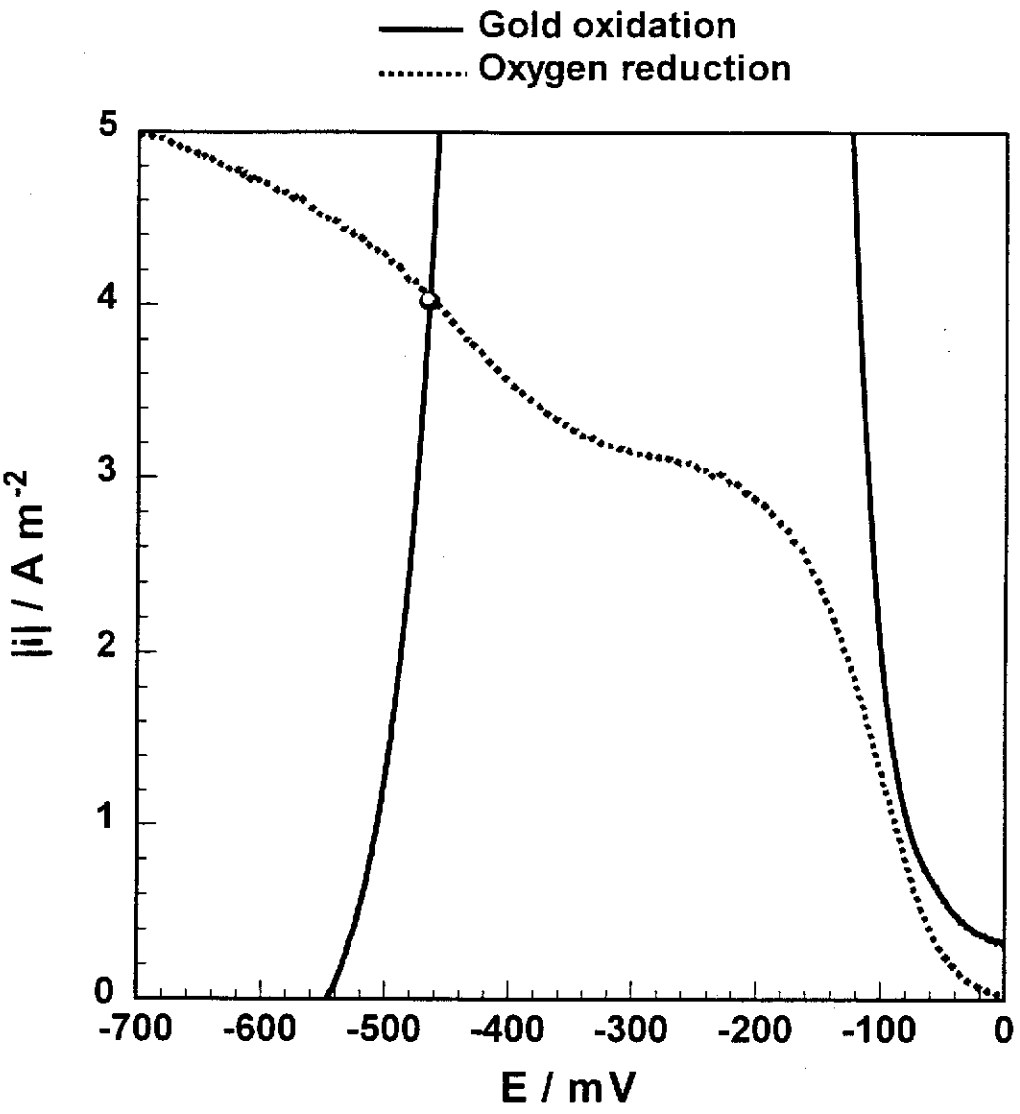

Figure 5.32 – Evans' diagram representing the dissolution of gold in air saturated 20 mM cyanide solutions containing 10 ppm lead. Experimental conditions: pH 10.0, 25 °C, 300 rpm.

effect on the dissolution of gold. Accordingly, the effect of a range of different ions on the dissolution of gold in cyanide solutions was investigated, and the results are shown in Table 5.6.

Of these results, the most interesting aspect from an industrial point of view is the effect of silver ions, as silver is usually present in leach circuits. The effect that silver has on dissolution is not reported in the literature, and therefore is discussed in detail below. The action of most of the other ions has been demonstrated in previous studies (Fink, 1950), and will not be discussed in further detail in this Thesis.

	Concentation	
Additive	**10^{-5} M**	**5×10^{-4} M**
Thallium	Enhancing	Enhancing
Bismuth	Enhancing	Unable to test[1]
Silver	Enhancing	Enhancing
Sulfide	Minor Enhancing	Retarding
Copper	None	None
Nickel	None	None
Cadmium	None	None
Tin	None	Retarding
Antinomy	None	Retarding

[1] Bismuth hydroxide is highly insoluble

Table 5.6 – Effect of some additives on the dissolution of gold in air saturated 20 mM cyanide. Experimental conditions: pH 10.0, 25 °C, 300 rpm.

The leaching of gold in air and oxygen saturated cyanide solutions containing 1 ppm silver was investigated, and the mass versus time responses are shown in Figure 5.33. For both air and oxygen saturated cyanide solutions with 1 ppm silver,

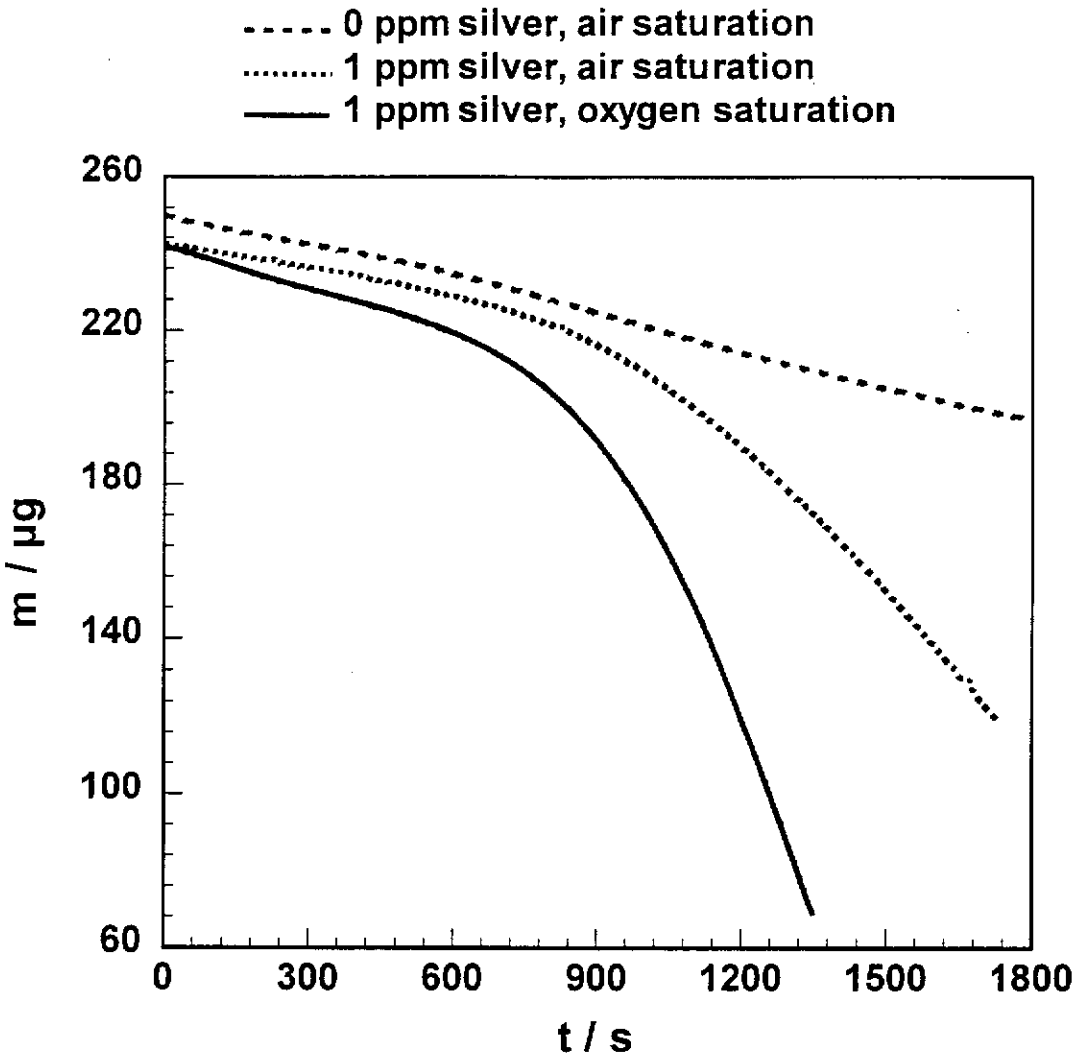

Figure 5.33 – Mass versus time response for the leaching of gold in the presence of 1 ppm silver. Experimental conditions: air saturated 20 mM cyanide, pH 10.0, 25 °C, 300 rpm.

the rate of dissolution is low for at least 800 seconds. After this initial period, the rate of dissolution increases and reaches a constant rate. This constant rate is significantly higher than that for gold in the absence of silver, which is also shown in Figure 5.33. It is believed that the action of silver is similar to lead in that passivation is eliminated by cementation. The cementation of silver on gold is likely, as the standard reduction potential for silver cyanide, -0.31 V (Bard, 1973), is substantially higher than that for gold cyanide, -0.57 V. The initial period of the leaching curve where the rate of dissolution of gold in the presence of 1 ppm silver is similar to that for gold in the absence of silver and is probably due to the time required for significant cementation to occur. To reduce passivation, enough silver would have to deposit on the gold surface to disrupt the formation of the surface film.

The dissolution rate of gold in the presence of silver has been compared with the results for gold in the presence and absence of 1 ppm lead. Shown in Table 5.7 are the leaching rates of these systems in air and oxygen saturated solutions.

	$10^5 r$ /mol m^{-2} s^{-1}	
System	**Air Saturated**	**Oxygen Saturated**
Gold	0.69	1.49
Gold with 1 ppm lead	5.50	1.36
Gold with 1 ppm silver	3.59	8.42

Table 5.7 – The effect of lead and silver on the rate of dissolution of gold in air and oxygen saturated solutions containing 20 mM cyanide. Experimental conditions: pH 10.0, 25 °C, 300 rpm.

The most notable aspect of these results is that the rate of dissolution of gold in a solution containing 1 ppm silver is enhanced under oxygen saturation. This is in contrast to the case of gold in a solution containing 1 ppm lead, where the rate is lower at higher oxygen concentration. Table 5.7 also shows that the rate of dissolution of gold in air saturated solutions containing silver is lower than that for

air saturated solutions containing lead. In the following sections, it will be shown that although silver helps to reduce the passivation of gold in cyanide solutions, it is not as effective as lead. Interestingly, in the following chapter, it will also be shown that silver present on the surface of the gold as a co-deposit is more effective at eliminating passivation than silver in solution, which appears on the gold surface as a cementation deposit. Presented in Table 5.8 is a comparison between the rate of dissolution of gold in a solution containing 1 ppm silver and a gold deposit that contains 1 % silver. It is uncertain why silver in the solid phase is considerable more active than silver in solution, but it could be that in solutions containing 1 ppm silver, not enough silver cements onto the gold surface to completely eliminate passivation.

	10^5r /mol m^{-2} s^{-1}	
System	**Air Saturated**	**Oxygen Saturated**
Gold deposit containing 1 % silver[1]	4.3	17.0
Gold with 1 ppm silver in solution	3.6	8.42

[1] From section 6.3.1.1.

Table 5.8 – Dissolution of gold in air or oxygen saturated cyanide solutions with silver as either a solution or solid phase impurity. Experimental conditions: 20 mM cyanide, 25 °C, 300 rpm.

5.3.8.2. Electrochemistry – Oxidation

In the kinetic studies, it was found that silver in solution was able to increase the rate of dissolution of gold. The role of silver is thought to be similar to that of lead, where the surface is modified by cementation. The effect of silver on the oxidation of gold is shown in Figure 5.34, and it can be seen that the presence of silver increases the electrochemical activity of gold in the potential range of -400 to 300 mV. It is also clear that 1 ppm silver in solution is not as effective at removing the passivation on the gold surface as 2.5 ppm silver. Presumably, for 1 ppm silver

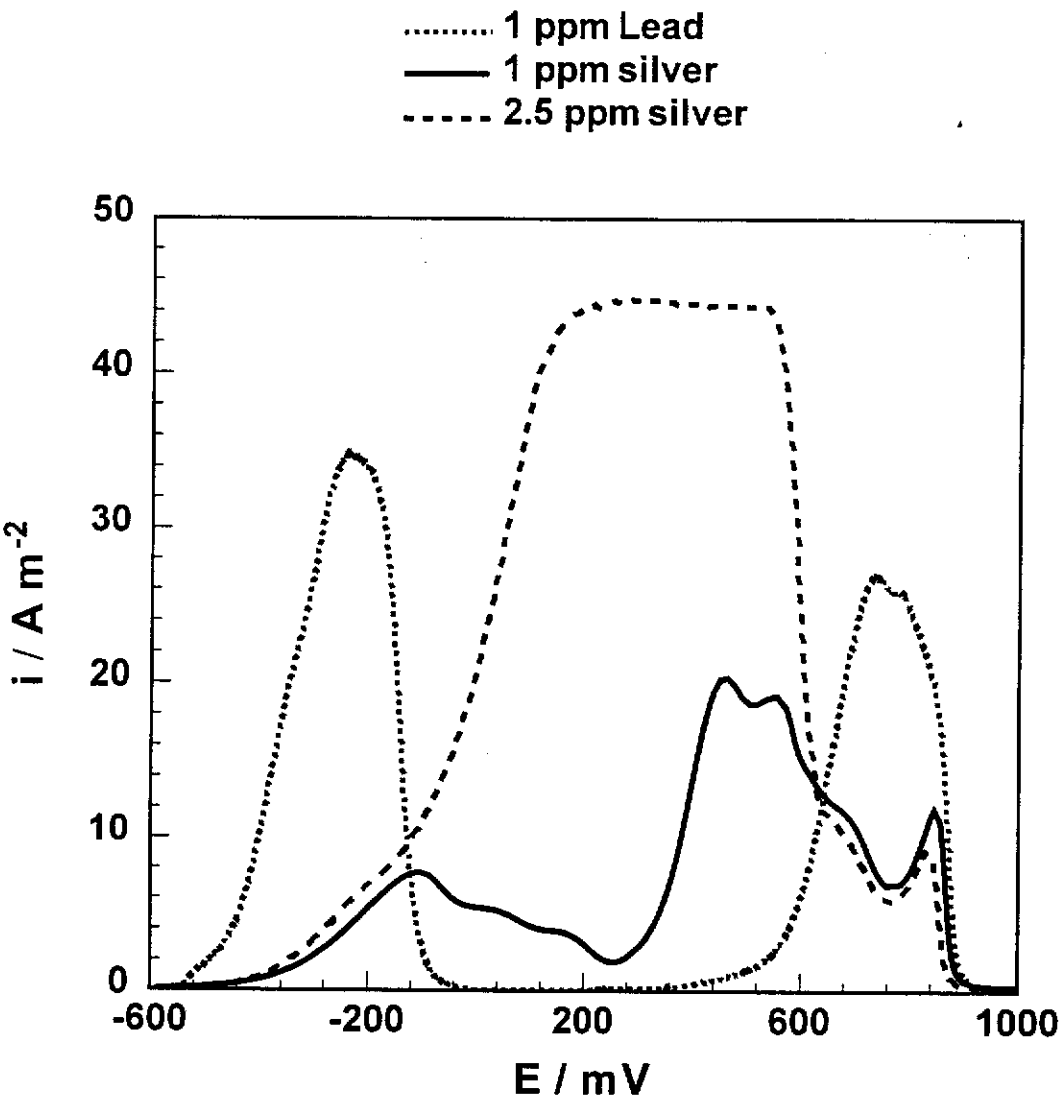

Figure 5.34 – Effect of silver on the oxidation of gold. Experimental conditions: 20 mM cyanide, pH 10.0, 1 mV s^{-1}, 25 °C, 300 rpm.

in solution, not enough silver cements onto the surface to completely eliminate passivation.

The oxidation of gold in the presence of 1 ppm lead is also presented in Figure 5.34, and it is shown that there are a couple of differences between the anodic behavior of gold in the presence of silver and lead. The first feature to note is the potential at which rapid oxidation occurs. For gold in a solution containing 1 ppm silver, rapid oxidation begins at around 300 mV more positive than that for gold in a solution containing 1 ppm lead. Therefore, at low overpotentials, silver is not as effective as lead in removing the passivating film that exists on gold. It is also interesting to note that in the presence of 2.5 ppm silver, the gold does not passivate at -150 mV as it does in the case of lead. This is further proof that the passivation is a feature of the lead on the surface rather than the gold itself.

5.3.8.3. Electrochemistry – Evans' diagrams

It will be recalled from Chapter 3 that oxygen reduction is sensitive to the electrode substrate. Thus, to ensure that the Evans' diagrams in the presence of silver are as accurate as possible, oxygen reduction is represented by the oxygen polarisation curve on a silver modified gold deposit. The silver modified gold deposit was prepared by electroplating from a solution with identical composition to that described in section 5.2, with the exception that 0.1 mM silver nitrate was substituted for the lead nitrate. This deposit will be termed gold/silver, and the reduction of oxygen on this substrate is discussed in detail in the following chapter. The Evans' diagrams representing the dissolution of gold in air and oxygen saturated 20 mM cyanide solutions in the presence of 1 ppm silver are shown in Figure 5.35. It is clear that there is only one intersection point between the anodic and cathodic polarisation curves at both oxygen concentrations. Therefore, the Evans' diagrams show that higher oxygen concentrations will increase the dissolution rate of the gold, and indicate that Evans' diagrams are also effective at qualitatively representing the dissolution of gold in the presence of silver in solution.

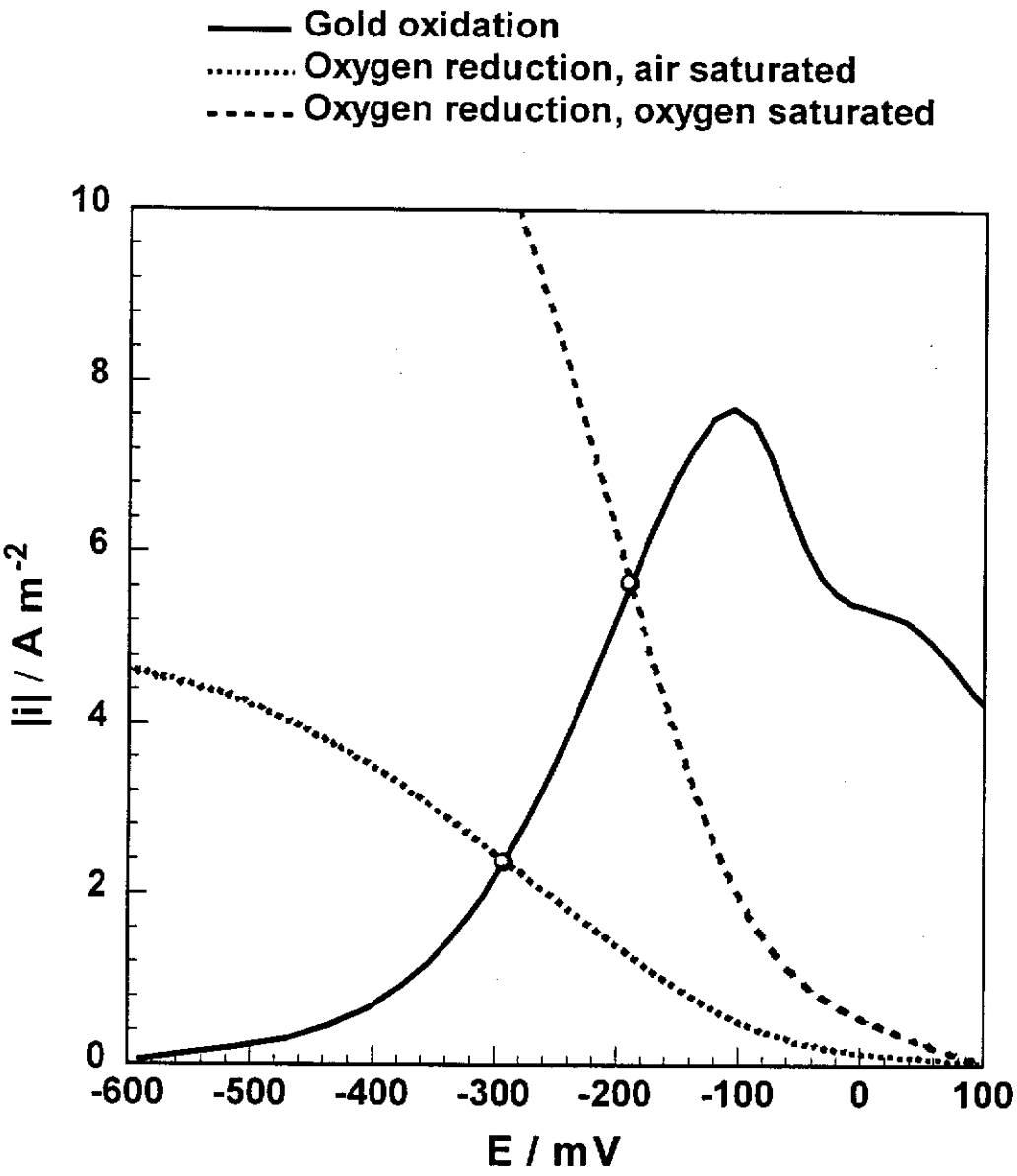

Figure 5.35 –Evans' diagrams representing the dissolution of gold in air and oxygen saturated 20 mM cyanide solutions containing 1 ppm silver. Experimental conditions: pH 10.0, 25 °C, 300 rpm.

5.4. Summary

1) The leaching of gold in aerated cyanide solutions is significantly enhanced by the presence of 1 ppm lead in solution.

2) The role of lead is to cement onto the surface of the gold and disrupt the formation of a passive layer of AuCN.

3) In air saturated 20 mM cyanide solutions containing 1 ppm lead at pH 10.0, the dissolution of gold is oxygen diffusion controlled.

4) The enhancing action of lead is limited to a small range of dissolution conditions. High pH values, low cyanide concentrations and high oxygen concentrations result in lower dissolution rates.

5) The addition of 1 ppm lead results in an additional gold oxidation peak, P2, at -400 mV. The oxidation of gold in the region of this peak was found to be under mixed diffusion/chemical control.

6) High concentrations of lead (above 50 ppm) were found to impede the oxidation of lead over the entire potential window investigated. This is attributed to the blocking of the gold surface by a layer of lead.

7) The presence of silver in solution also enhances the leaching of gold, although the effect is not as significant as the addition of lead. In contrast to lead though, the addition of silver to oxygen saturated cyanide solutions substantially increases the dissolution rate.

Chapter 6 – The Effect of Solid Phase Additives

6.1. Introduction

In the review, it was shown that the kinetic and electrochemical results for the dissolution of gold in cyanide solutions from many publications were conflicting. These variations are believed to be a result of differences in solution and solid phase purity between the reported experiments. The effect of solution phase purity was investigated in Chapter 4, where various additives, in particular lead, were found to significantly enhance the leaching of gold in cyanide solutions. The objective of the work described in this chapter was to investigate the effect of solid phase purity on the kinetic and electrochemical behaviour of gold. To study the leaching of gold as a function of solid phase purity, it is required that a controlled and reproducible level of an additive be introduced into the gold. This was accomplished by modifying the gold composition during the electroplating process by adding the metal ions of interest to the plating solution. In the majority of experiments, the metal additive was silver, because this is the most common impurity present in native gold.

6.2. Experimental

The experimental conditions for the experiments described in this chapter are identical to those described in Chapter 4, with the exception of the plating solution composition. In this work, the plating solution contained either 0.1 mM silver nitrate or 0.1 mM lead nitrate in addition to 0.02 M potassium dicyanoaurate, 0.23 M potassium cyanide and 0.086 M potassium carbonate. This produced a controlled and reproducible amount of silver or lead within the plated gold.

6.3. Results and Discussion

The dissolution rate of gold containing controlled amounts of lead or silver was measured and compared to that of gold, which was reported in Chapter 4. Lead was investigated primarily to show that the action of lead in the solid phase is identical to lead in solution (described in Chapter 5), and silver in the solid phase was investigated because nearly all naturally occurring gold contains some silver (Hurlbut & Klein, 1977). In the remainder of this chapter, the lead modified gold will be referred to as gold/lead, while the silver modified gold will be referred to as gold/silver. Initially, the effect of the solid phase impurities was investigated, and then the experimental conditions were varied independently to obtain further information about the reaction.

6.3.1. Effect of Solid Phase Impurities

6.3.1.1. Kinetic Studies

The leaching response of the gold/lead and gold/silver samples is shown in Figure 6.1. The data from Chapter 4 (the leaching of gold) has also been added for comparison. It is clear that solid phase purity does affect the leaching of gold in cyanide solutions, and the dissolution of gold/lead and gold/silver is discussed in detail below.

(a) Gold/lead

From Figure 6.1, it can be seen that the leaching rate of gold/lead, 0.7×10^{-5} mol m^{-2} s^{-1}, is the same as that for gold. This finding is surprising, given that lead is known to enhance the leaching of gold in cyanide solutions (as discussed in Chapter 5). During the electroplating process, the lead in solution will co-deposit with the gold, and hence form a lead modified gold surface. The leaching rate would

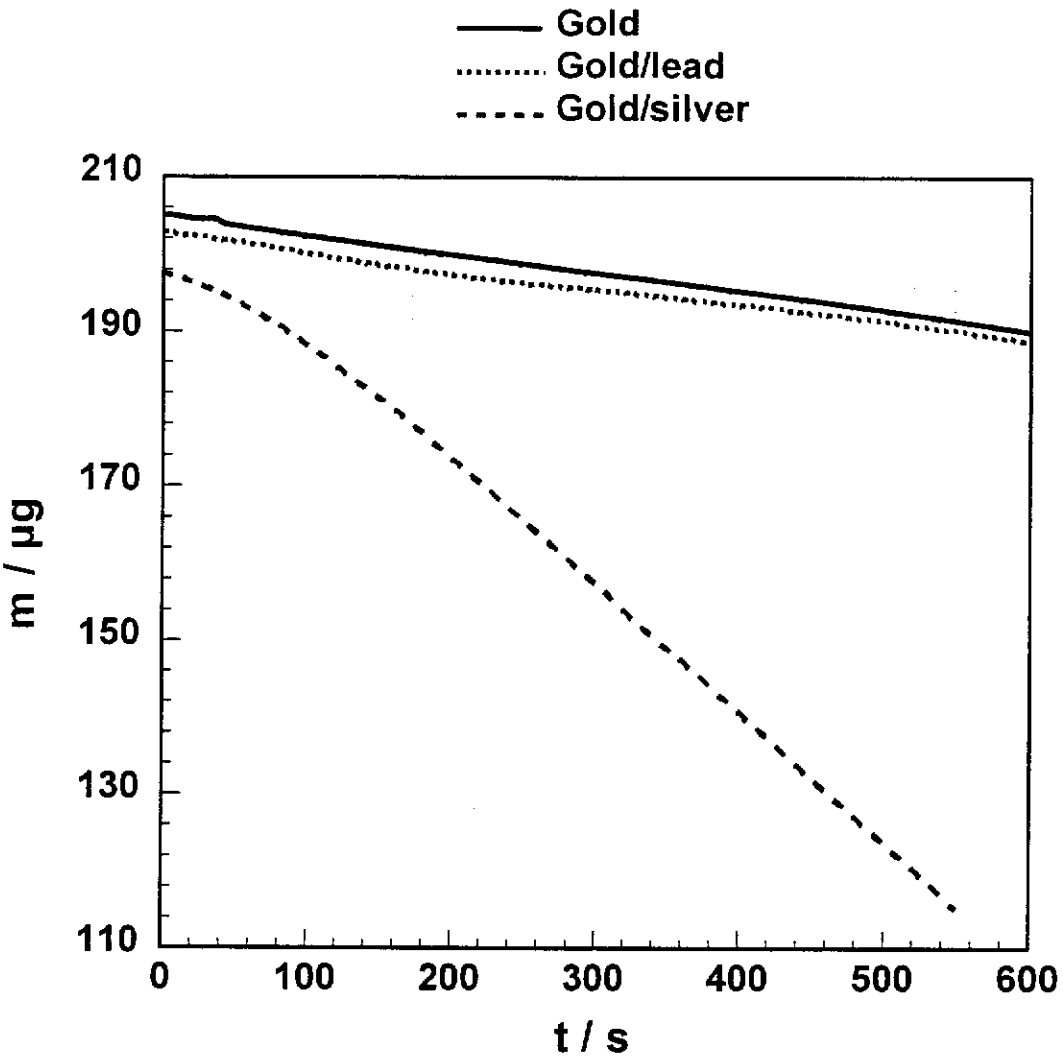

Figure 6.1 – Mass versus time response for the leaching of gold/lead and gold/silver. Experimental conditions: air saturated 20 mM cyanide solutions, pH 10.0, 25 °C, 300 rpm.

be expected to be similar to that for gold with lead in solution, which modifies the gold surface by cementation. One reason for this discrepancy could be that the lead concentration on the surface of the plated gold/lead is too high, although no attempt has been made to quantify this. In the following section, the voltammograms for gold/lead are shown to be very similar to those of gold in a solution containing lead. This implies that the action of lead in the plated gold/lead is identical to that in solution. Consequently, it was decided that no more kinetic experiments would be conducted with gold/lead as the effect of lead in solution was examined in detail in Chapter 5.

(b) Gold/silver

From Figure 6.1, it can be seen that gold/silver leaches significantly faster than gold, with the rate of dissolution (after 200 seconds) reaching 4.3×10^{-5} mol m^{-2} s^{-1}, as compared to 0.7×10^{-5} mol m^{-2} s^{-1}. It is known that silver does not passivate in cyanide solutions (Hiskey & Sanchez, 1990), making it likely that passivation will not occur at the silver sites on the gold/silver surface. It is thus believed that the silver prevents the passivation of gold/silver by stopping the formation of a continuous passive film. In this way, the mechanism by which silver prevents passivation is similar to that of lead in solution, as outlined in Chapter 5.

It is interesting to note that the gold/silver dissolution rate is not constant during the first 200 seconds of leaching, with the rate of dissolution increasing with time. Such a finding is consistent with a transient passive film being formed on the gold surface, which initially hinders the rate of dissolution. As this film is removed from the surface, the dissolution approaches a constant rate. The most likely explanation for the initial passivation is that cyanide is adsorbed on the surface of the gold and then reacts to form AuCN, as discussed in Chapter 4, and in the ensuing sections of this chapter.

The remainder of the kinetic studies were performed using gold/silver, and the concentration of silver in these samples was estimated in two ways. In the first instance, the concentration was determined by analysis of the deposit. A measured

mass of gold/silver was plated, and then dissolved in warm aqua regia. The aqua regia was then diluted and hydrochloric acid was added to form 25 mls of a solution containing a 20 % chloride matrix. This ensures that the silver remains in solution as $AgCl_2^-$ and does not precipitate. The concentration of silver in the solution was measured by inductively coupled plasma (ICP) / atomic emission spectroscopy (AES). The concentration of silver in the gold/silver sample was calculated to be 0.98 % by mass.

The second method of estimating the concentration of silver in the plated gold was by using the rotating EQCM to measure the plating rate of silver from a solution identical in composition to the gold/silver plating solution in all aspects except that potassium gold cyanide was excluded. A value of 0.44×10^{-5} mol m^{-2} s^{-1} was obtained for the silver plating rate. The mass fraction of silver in the gold/silver is simply the plating rate of silver divided by the plating rate of gold/silver. A composition of 1.0 mass percent silver was obtained in this way, which is similar to that obtained by chemical analysis.

6.3.1.2. Electrochemistry – Oxidation.

In a similar manner to that already presented in Chapters 4 and 5, the electrochemical oxidation of gold/silver is now described. This is then followed by the Evans' diagrams for these systems. The oxidation curves are presented over a wide potential and current density range, while the Evans' diagrams focus on the intersection of the oxidation and reduction polarisation curves of the constituent half reactions.

Shown in Figure 6.2 is the oxidation polarisation curves for gold/lead and gold/silver. It is clear that each of these samples exhibit different electrochemical characteristics. The oxidation polarisation curve for gold/lead shows two large oxidation peaks, while the polarisation curve for gold/silver exhibits a diffusion limiting current density. The oxidation behaviour of each of these samples is discussed in detail below.

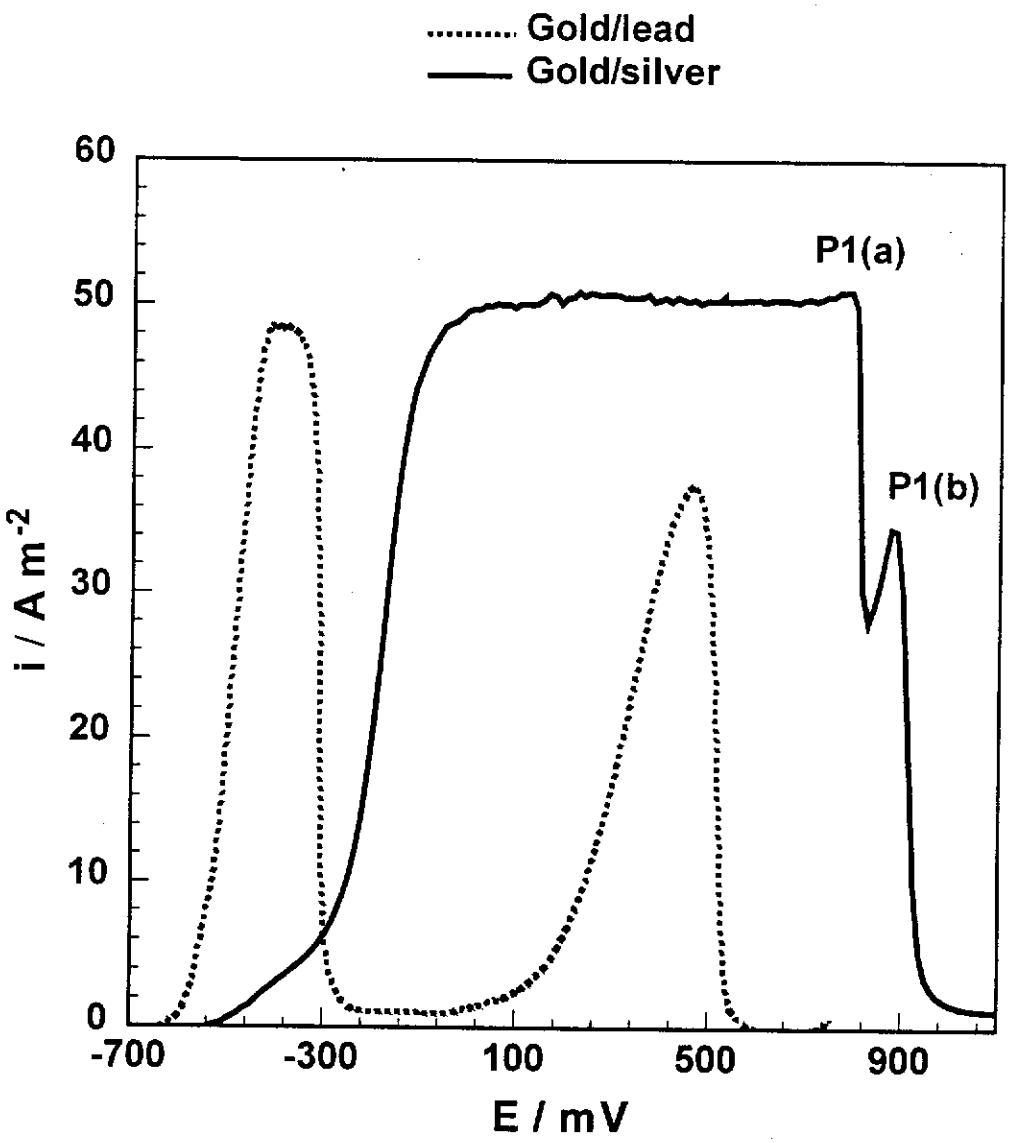

Figure 6.2 – Oxidation polarisation curves for gold/lead and gold/silver. Experimental conditions: 20 mM cyanide solutions, pH 10.0, 1 mV s^{-1}, 25 °C, 300 rpm.

(a) Gold/lead

It is interesting to note that the oxidation behaviour of gold/lead is virtually identical to that of gold in a solution containing lead (see Figure 5.9). The gold oxidation peak at -400 mV is due to the presence of lead on the surface. In the case of lead in solution, the lead is deposited on the surface by cementation, whilst for gold/lead, the lead is incorporated within the deposit during the plating process. The similarity in the voltammograms indicates that the effect of lead on the surface in each case is identical.

(b) Gold/silver

It can be seen from Figure 6.2 that gold/silver oxidises to give a polarisation curve which exhibits a diffusion limiting current density. This result is very similar to the early work of Kudryk and Kellogg (1954), suggesting that their work was conducted using gold that contained impurities. The impurity in their gold sample would probably be silver, as this is the most common impurity found in gold. Further discussion of the gold/silver polarisation curve is split into three potential regions, as presented below.

1) -500 to -300 mV

It can be seen from Figure 6.2 that gold/silver begins to oxidise at approximately -550 mV, and in the potential range -550 to -300 mV, there is only a small increase in current density with increases in potential. This result is unusual, and is consistent with the gold surface being partially blocked in the potential region -550 to -300 mV. It was shown in the previous section that gold/silver in 20 mM cyanide solutions appeared to be blocked by a transient film for the first 200 seconds of dissolution. To determine if transient passivation affects the oxidation of gold/silver, the reaction was investigated as a function of potential scan rate, and the oxidation of gold/silver at 1 mV s^{-1} and 0.1 mV s^{-1} is shown in Figure 6.3. At 0.1 mV s^{-1}, it is clear that once the gold begins to oxidise at -550 mV, the current

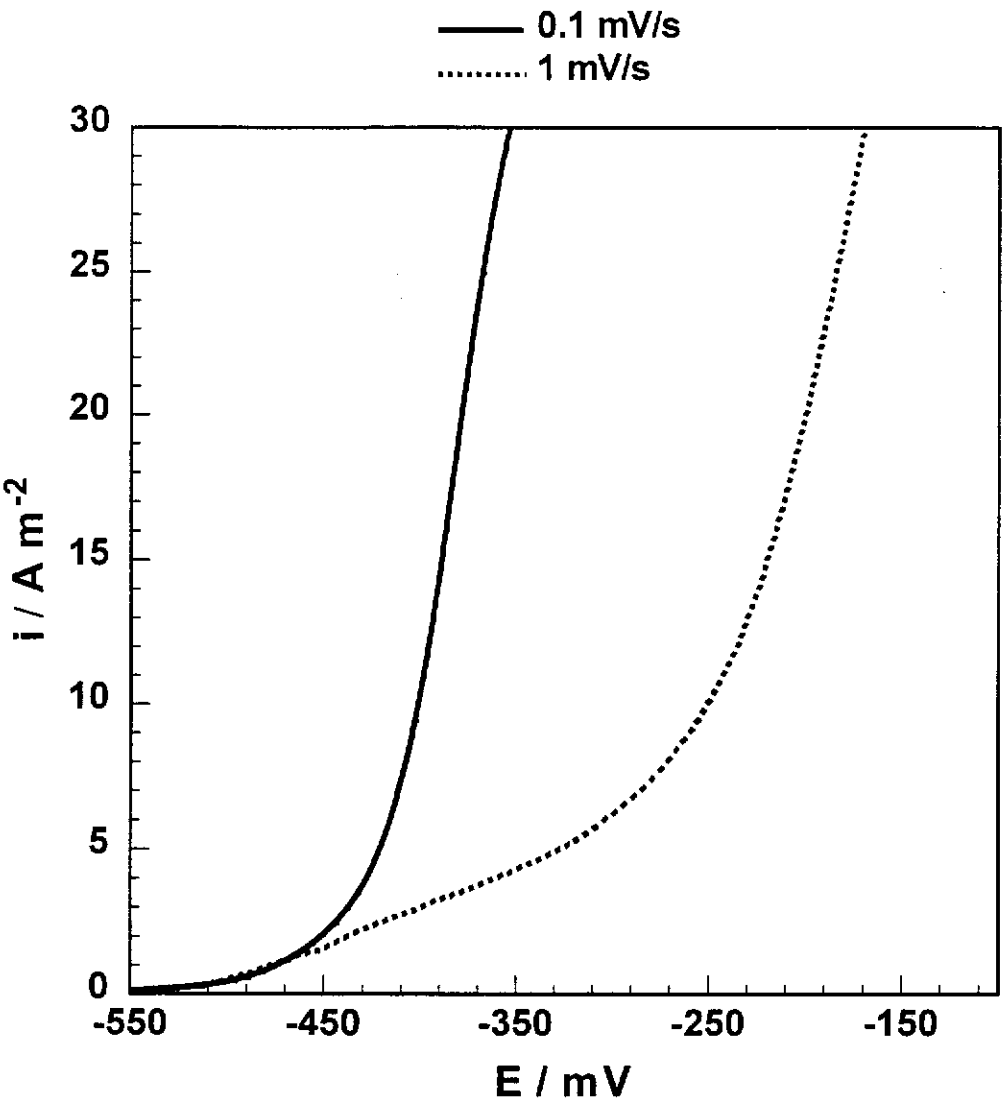

Figure 6.3 – Effect of potential scan rate on the oxidation of gold/silver. Experimental conditions: 20 mM cyanide solutions, pH 10.0, 25 °C, 300 rpm.

density increases exponentially with potential. This suggests that when scan rates of 1 mV s^{-1} are adopted, the non-ideal behaviour of gold at low overpotentials is due to the blocking of the gold surface by a transient passive film. In the remaining sections of this chapter, however, due to plating and time constraints, scan rates of 1 mV s^{-1} have been used when presenting the oxidation data over a wide potential range. For the Evans' diagrams, the oxidation and reduction curves intersect in the potential region where the transient passivation occurs, and so scan rates of 0.1 mV s^{-1} are used in these sections.

2) -300 to 700 mV

It can be seen from Figure 6.2 that at potentials more positive than -300 mV, the current density increases exponentially with potential until it reaches a diffusion limiting plateau at 0 mV. It should be remembered that the oxidation polarisation curves are measured in the absence of oxygen, and so in this case, the current density is limited by cyanide diffusion. The measured limiting current density, 50 A m^{-2}, can be readily compared to the cyanide diffusion flux, as calculated by the Levich equation. The literature values of D_{CN} range from 1.77×10^{-9} to 2.18×10^{-9} m^2 s^{-1} literature (Hiskey & Sanchez, 1990, Guan & Han, 1994, Lide, 1995), for which the calculated limiting current density is 49 and 56 A m^{-2} respectively (under the experimental conditions represented in Figure 6.2).

3) Potentials above 700 mV

It can be seen from Figure 6.2 that at 800 mV, the gold oxidation current density decreases due to the formation of a passive film on the surface of the gold/silver. To remain consistent with the previous chapters, the passivation at 800 mV is denoted P1(a). In section 6.3.2.2, the passivation potential P1(a) is shown to shift with cyanide concentration, indicating that the passivation is due to the formation of a cyanide surface film. As the potential is increased above 800 mV, the current density increases again, suggesting that the cyanide film has been dissolved. When the potential reaches 890 mV, denoted P1(b), the gold is completely passivated by the formation of another surface film. In section 6.3.6.2, it will be

shown that the passivation potential P1(b). is dependent on pH. This suggests that the surface film which is formed at this potential is either gold oxide or gold hydroxide. The behaviour of gold/silver at high overpotentials is thus similar to that of gold, as discussed in section 4.3.1.3.

6.3.1.3. Electrochemistry – Evans' Diagrams

The Evans' diagrams representing the dissolution of gold/silver in 20 mM cyanide solutions were constructed from the oxidation polarisation plot of gold/silver and the reduction polarisation curves of oxygen on gold/silver. In section 6.3.1.2, it was shown that transient passivation of gold is not important at a scan rate of 0.1 mV s^{-1}, so the gold/silver oxidation polarisation curves which are used in the construction of the Evans' diagrams were measured using this scan rate. Shown in Figure 6.4 are the Evans' diagrams representing the dissolution of gold and gold/silver in aerated cyanide solutions. As in the other chapters, the Evans' diagrams are defined as a plot of i versus E, and the oxygen reduction curves are inverted for clarity. It is worth noting that for gold/silver, the anodic and cathodic polarisation curves can only intersect once, and hence the Evans' diagrams in this chapter are simpler than those presented in the previous chapter. Consequently, two Evans' diagrams are presented in single graph, and in Figure 6.4, the Evans' diagram for gold is represented by solid lines, and the Evans' diagram for gold/silver is represented by broken lines.

In this work, the major use of Evans' diagrams is to predict changes in the reaction when the experimental conditions are changed. An excellent example of the value of Evans' diagrams is shown in Figure 6.4 for the dissolution of gold and gold/silver in aerated cyanide solutions. The dissolution rate of gold is predicted to be low, whereas the dissolution rate for gold/silver is predicted to be significantly higher. It is also clear that for gold/silver, oxygen reduction is the limiting step for gold/silver dissolution. These predictions closely match the experimental results from the kinetic studies in section 6.3.1.1.

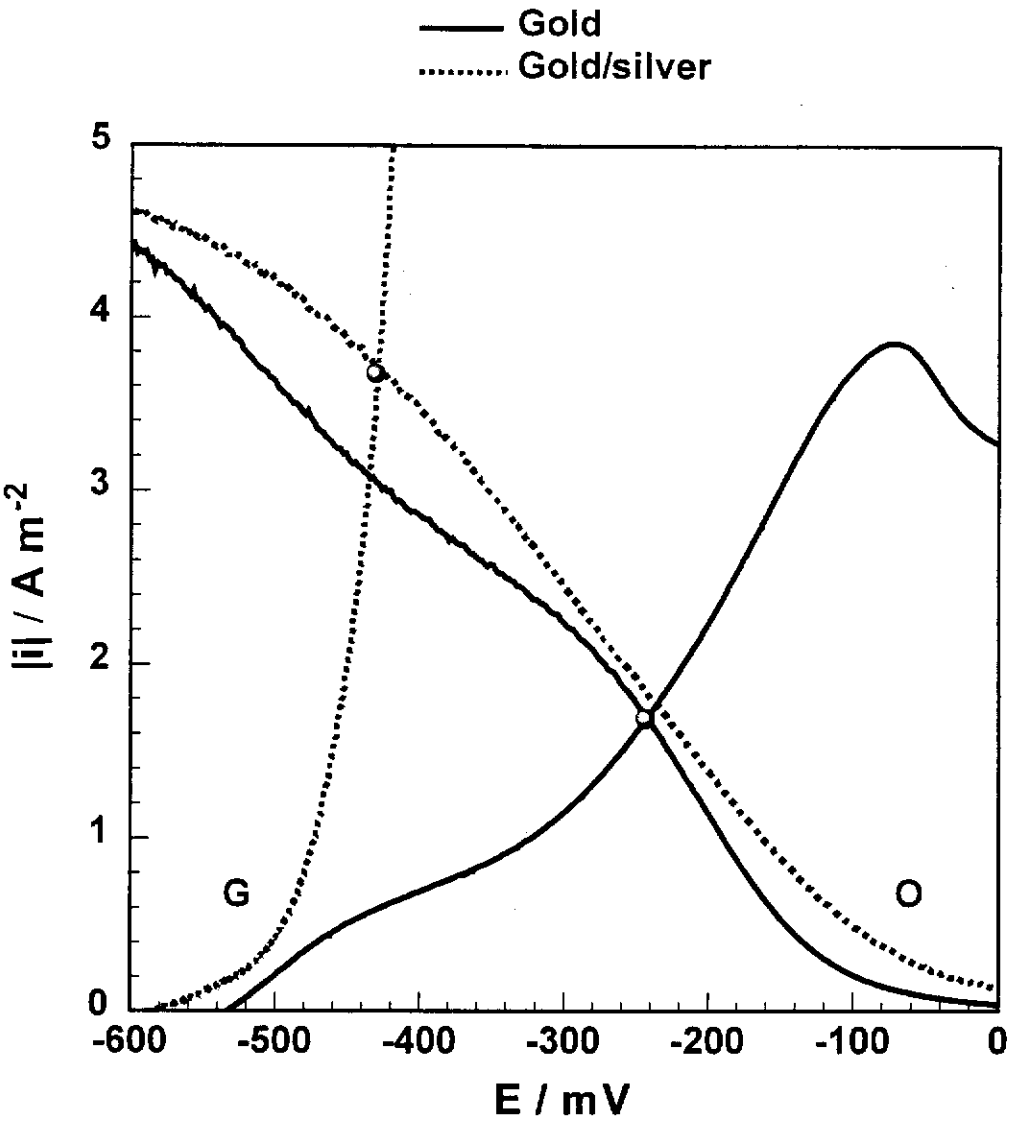

Figure 6.4 – Evans' diagrams representing the leaching of gold (solid lines) and gold/silver (broken lines) in air saturated 20 mM cyanide solutions. The anodic and cathodic polarisation curves are labelled (G) and (O) respectively. Experimental conditions: pH 10.0, 25 °C, 300 rpm.

From the Evans' diagrams shown in Figure 6.4, the dissolution rate and mixed potential of gold/silver in aerated cyanide solutions can be estimated. Table 6.1 shows a comparison of the predicted values with the results obtained in the kinetic studies (section 6.3.1.1).

	$10^5 r$ /mol m^{-2} s^{-1}	E_m /mV
Measured	4.3	-410
Calculated	3.9	-430

Table 6.1 – Measured rates and mixed potentials compared with those calculated from the Evans' diagrams for dissolution gold/silver in air saturated 20 mM cyanide solutions. Experimental conditions pH 10.0, 300 rpm, 25 °C.

It is clear that the measured and calculated values compare reasonably well, although the calculated mixed potential and rate are slightly lower than those measured in the kinetics section. This discrepancy is not surprising, given the way in which the Evans' diagrams are constructed. The reduction reaction is studied on a clean gold/silver surface in the absence of cyanide. Such a surface is likely to be different to that of a dissolving gold surface. Consequently, in a similar manner to the previous chapter, the Evans' diagrams in the following sections will be only analysed qualitatively. The main emphasis will be on the kinetic data, as it provides an actual measurement of the reaction rate, and the Evans' diagrams are used to explain the changes in the measured dissolution rate with experimental conditions.

6.3.2. Effect of Cyanide Concentration

6.3.2.1. Kinetics

The dissolution rate of gold/silver was measured as a function of cyanide concentration, and shown in Figure 6.5 are the mass versus time responses for the leaching of gold/silver in air saturated solutions containing 2 and 20 mM cyanide. The distinguishing feature of the two leaching reactions is the time required for the rate of dissolution to reach a constant value. For 2 mM cyanide solutions, the dissolution rate remains at approximately 0.12×10^{-5} mol m^{-2} s^{-1} for around 500 seconds. After this, the reaction rate increases rapidly, reaching a value of 3.4×10^{-5} mol m^{-2} s^{-1}, which is approaching the dissolution rate of 4.3×10^{-5} mol m^{-2} s^{-1} for gold/silver in 20 mM cyanide. As discussed in section 6.3.1.1, the induction period indicates that gold/silver is initially blocked by a transient surface film, which hinders leaching until the film begins to dissolve. The longer induction period at low cynaide concentrations is consistent with the passivation being caused by the formation of an intermediate gold cyanide film, as shown in Equation 6.1. At higher cyanide concentrations, it can be expected that such a film will be more easily dissolved to form $Au(CN)_2^-$, as discussed in the review.

$$Au + CN^- \xrightarrow{-e^-} AuCN \xrightarrow{+CN^-} Au(CN)_2^- \qquad \textbf{Equation 6.1}$$

The dissolution rates of gold/silver in air saturated solutions were plotted as a function of cyanide concentration, as shown in Figure 6.6. Also shown are the lines indicating the maximum theoretical rates of dissolution predicted by the Levich equation for diffusion control. Line (a) in Figure 6.6 refers to the rate of dissolution of gold based on the diffusion of cyanide. Lines (b) and (c) both refer to the rate of dissolution being limited by oxygen diffusion, but varying in the assumed reaction stoichiometry. Line (b) refers to oxygen diffusion control if the reaction product is hydroxide, as shown in Equation 6.2. Line (c) refers to diffusion control given that peroxide is formed, as shown in Equation 6.3.

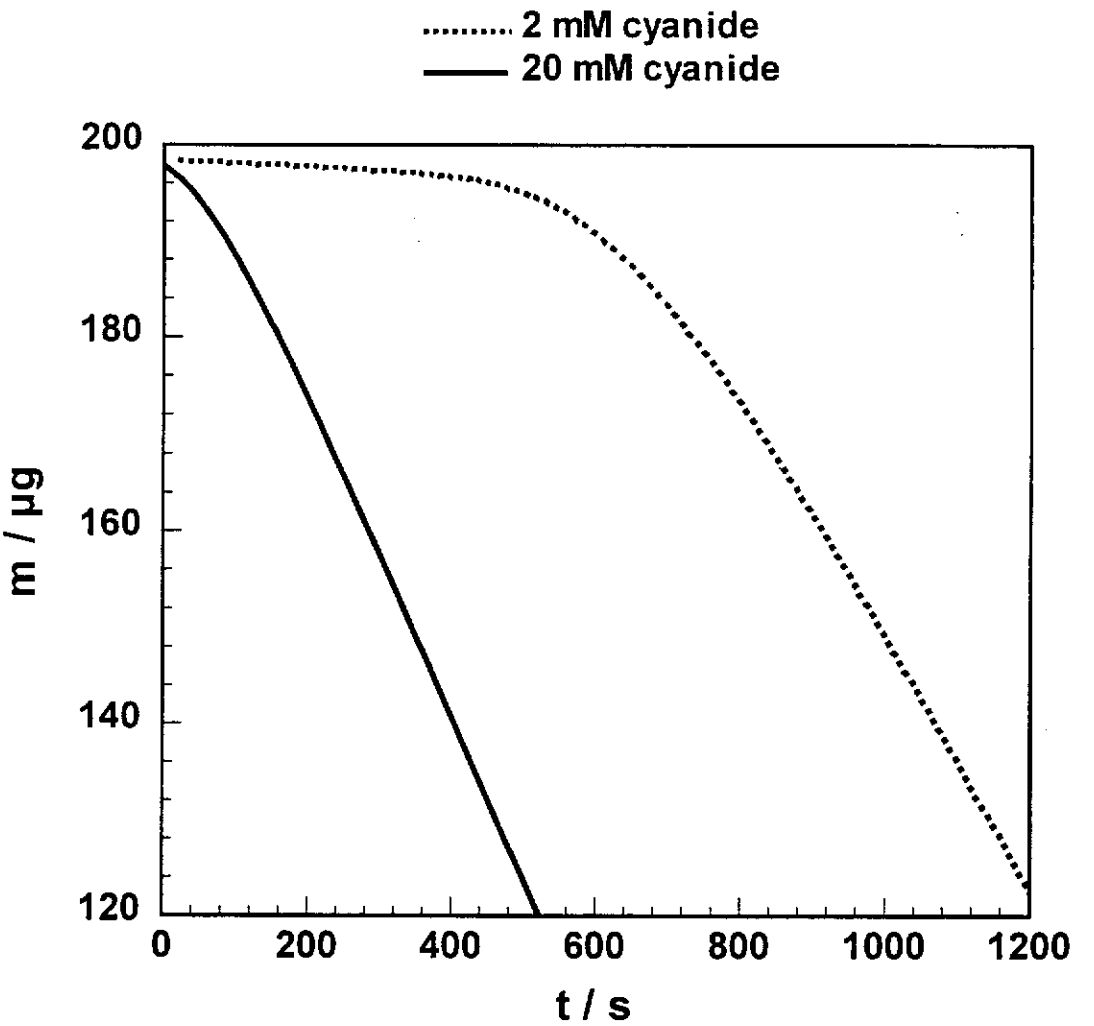

Figure 6.5 – Mass versus time response for the leaching of gold/silver in 2 and 20 mM cyanide solutions. Experimental conditions: air saturated, pH 10.0, 25 °C, 300 rpm.

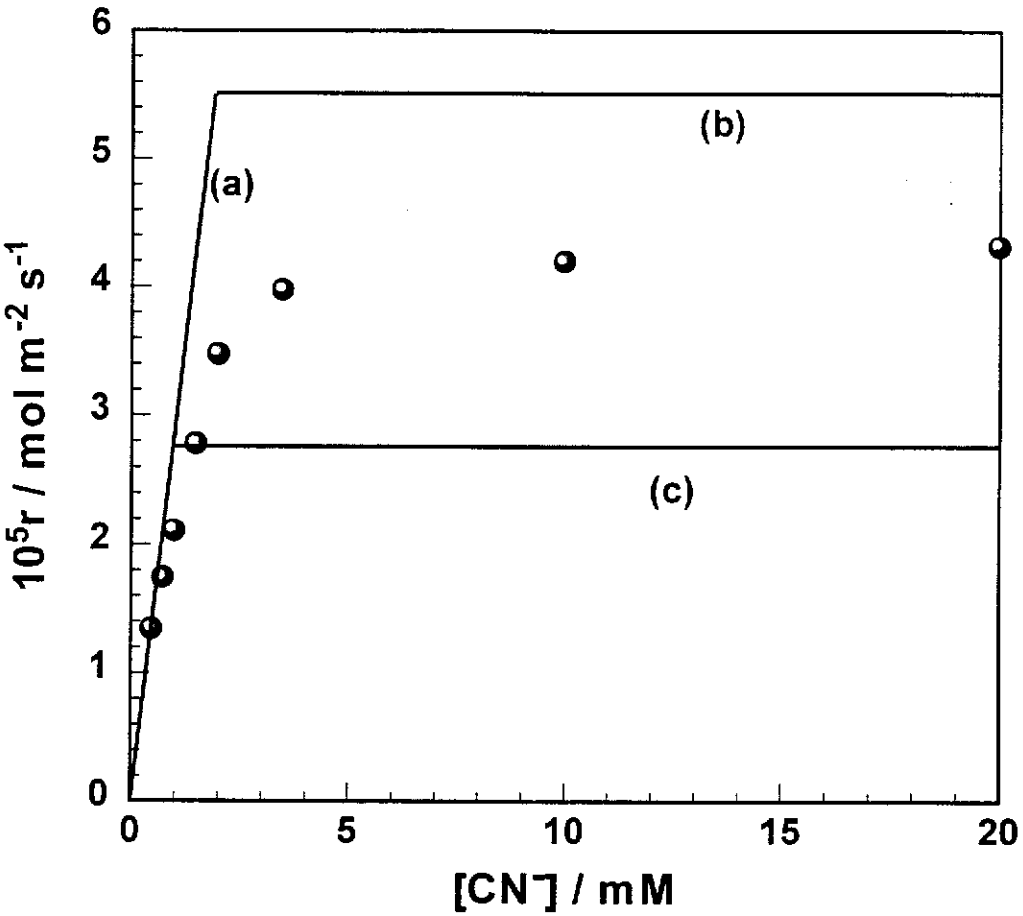

Figure 6.6 – Effect of cyanide concentration on the rate of dissolution of gold/silver. Line (a) represents the cyanide diffusion limiting rate, and lines (b) and (c) represent the oxygen diffusion limiting rate when dissolution occurs according to the Elsner and Bodländer equations respectively. Experimental conditions: air saturated, pH 10.0, 25 °C, 300 rpm.

$$4Au + 8CN^- + O_2 + 2H_2O \rightarrow 4Au(CN)_2^- + 4OH^- \quad \textbf{Equation 6.2}$$

$$2Au + 4CN^- + O_2 + 2H_2O \rightarrow 2Au(CN)_2^- + 2OH^- + H_2O_2 \quad \textbf{Equation 6.3}$$

As shown in Figure 6.6, at low cyanide concentrations, the rate of dissolution of gold/silver rate closely matches line (a), indicating that the dissolution of gold/silver is limited by cyanide diffusion. As the cyanide concentration is increased progressively to 2.1 mM, the rate of dissolution begins to deviate from the cyanide diffusion model. The deviation of the measured rate of dissolution from line (a) indicates that the dissolution of gold/silver is no longer solely limited by cyanide diffusion.

At the critical cyanide concentration, 2.1 mM, the rate of dissolution of gold/silver becomes essentially independent of cyanide concentration, and is limited by oxygen diffusion. The maximum measured rate of dissolution, 4.3×10^{-5} mol m^{-2} s^{-1}, for gold/silver in 20 mM cyanide solutions, lies approximately half way between lines (a) and (b). There are hence two possible mechanisms for oxygen reduction during the dissolution of gold/silver in air saturated solutions containing 20 mM cyanide. The first possibility is that peroxide is not produced during the dissolution process. If this were the case, then 78 % of the oxygen would be reduced to hydroxide, and the remaining oxygen would leave the electrode unreacted. The second possibility is that oxygen reduction involves the formation of both peroxide and hydroxide during the reduction process. By referring to Equation 6.4, it is a simple task to calculate the proportion of oxygen which is reduced to hydroxide. The flux of oxygen to the gold/silver surface, as calculated by the Levich equation, is 1.38 mol m^{-2} s^{-1}, which is the sum of paths (a) and (b) (x + y). Using the molar ratios of oxygen to gold, which are 2 and 4 for paths (a) and (b) respectively, it is a simple matter to show that $2x + 4y = r$, where r is the measured dissolution rate. Solving for x and y, the proportion of oxygen which is reduced to hydroxide ($y / (x + y)$), is calculated to be 56 %.

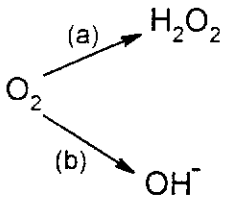

Equation 6.4

The critical cyanide concentration for gold/silver which was calculated from Figure 6.6 can be compared with that found in previous investigations, as discussed in the review and shown in Figure 2.8. The critical cyanide concentration for gold (from section 4.3.2.1), and gold/silver from this section have been added to this graph, and is presented in Figure 6.7. It is obvious that the previous work shows significant variation in the measured critical cyanide concentration. This variation has been discussed in the review and in Chapter 3, and it was concluded that a low critical cyanide concentration corresponds gold that is of lower purity. The measured critical cyanide concentration of 2.1 mM for gold/silver, which is of lower purity, is thus consistent with this explanation.

6.3.2.2. Electrochemistry – Oxidation.

The oxidation of gold/silver was investigated as a function of cyanide concentration, and the resulting polarisation curves are shown in Figure 6.8. It is clear that the limiting current density for gold/silver oxidation increases with increasing cyanide concentration. The limiting current density at 10 mM cyanide is one fifth of that for 50 mM cyanide and one half that for 20 mM cyanide. This is consistent with the current density being limited by cyanide diffusion in the potential range 0 to 700 mV.

The oxidation behaviour of gold/silver at potentials greater than 700 mV was found to vary with cyanide concentration. The potential at which the initial passivation occurs, P1(a), shifts with cyanide concentration, which indicates the passivation is due to the formation of a cyanide surface film. Conversely, the passivation potential P1(b) was found to be independent of cyanide concentration. These findings are consistent with those for gold in Chapter 3.

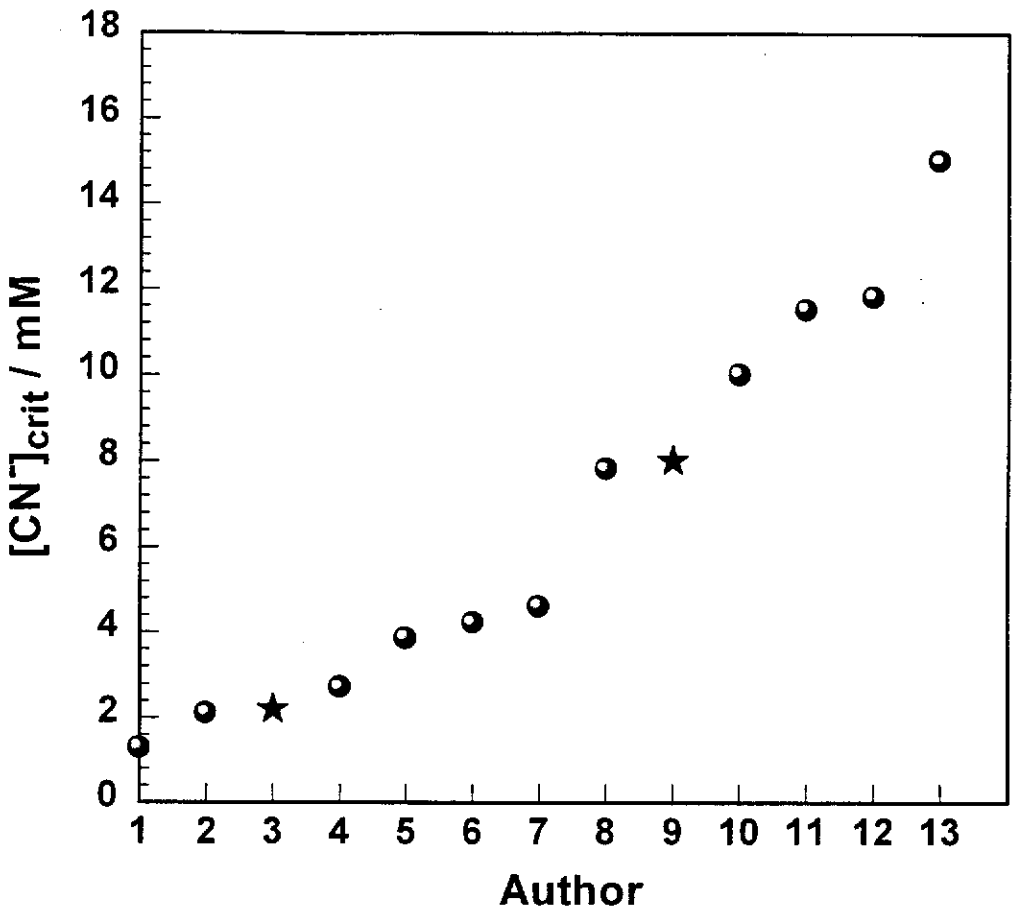

	Author		Author
1	Kakovskii and Kholmanskikh (1960)	8	Churchill and Laxen (1966)
2	Guan and Han (1993)	9	**Gold (This Work)**
3	**Gold/silver (This Work)**	10	Trindade and Monhemius (1993)
4	Kudryk and Kellogg (1954)	11	Beyer (1936)
5	Barksy, Swainson, and Hedley (1934)	12	La Brooy, Komosa and Muir (1991)
6	White (1919)	13	Zheng *et al.*, (1995)
7	Kameda (1949a)		

Figure 6.7 – Critical cyanide concentration for gold/silver and gold compared with the published critical cyanide concentrations of previous authors.

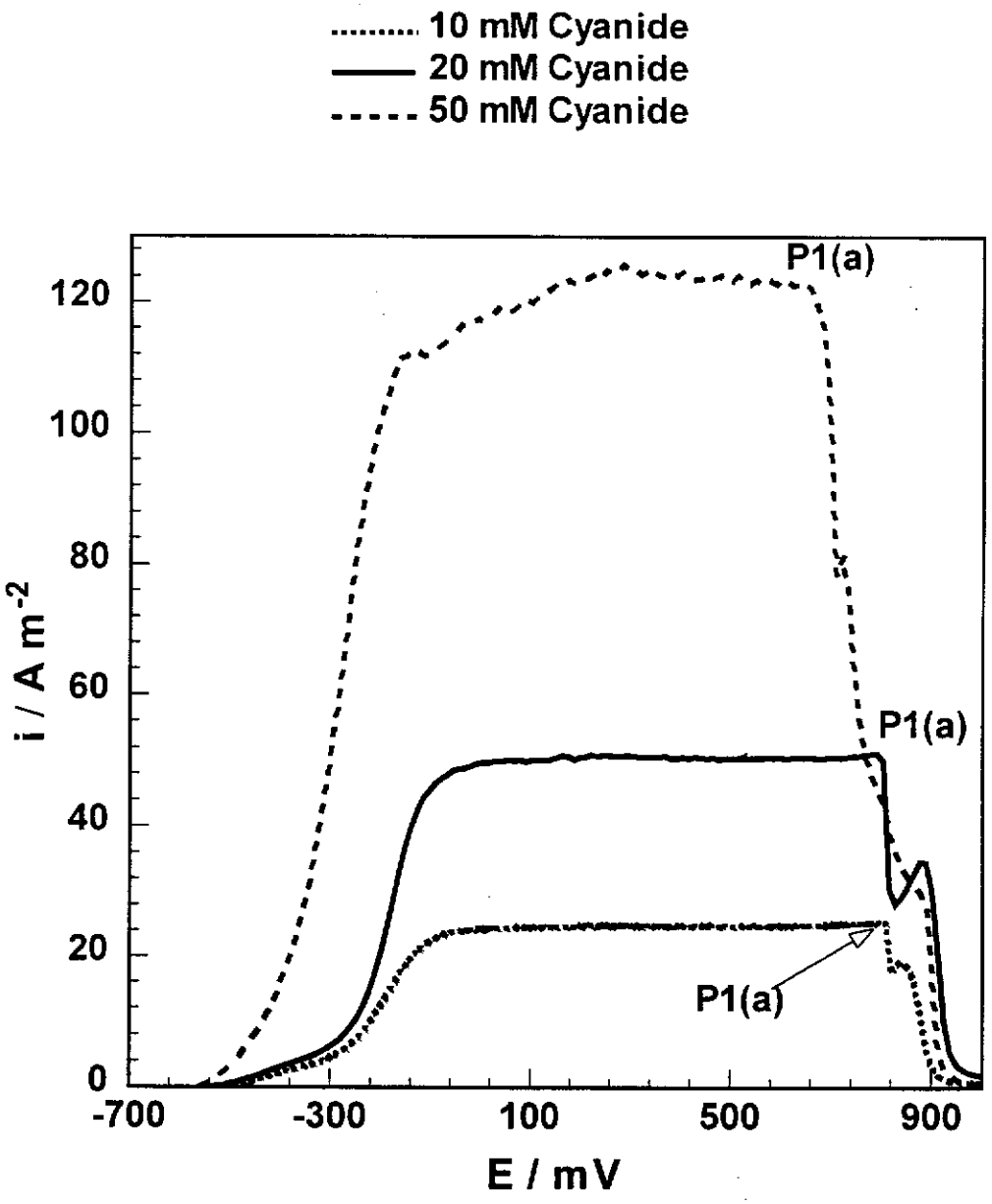

Figure 6.8 – Effect of cyanide concentration on the oxidation polarisation curves for gold/silver. Experimental conditions: pH 10.0, 1 mV s^{-1}, 25 °C, 300 rpm.

It is interesting to note the gold/silver oxidation current density in the low overpotential region. At potentials more positive than the rest potential, the current density for the oxidation of gold/silver in 50 mM cyanide solutions increases exponentially with potential until a limiting current density is reached. At 10 and 20 mM cyanide, the oxidation polarisation curves are slightly different. The current density remains low, below 5 A m^{-2}, until the potential reaches -300 mV. At potentials more positive than -300 mV, an exponential increase in gold/silver oxidation current density occurs. The gold/silver oxidation behavior in the potential region of -500 to -300 mV was found to be quite difficult to reproduce. This type of behavior suggests that at lower cyanide concentrations, there is a surface film present on the gold/silver in this potential region. Surface preparation and other small changes in the system would be likely to affect such a film, thus explaining the reproducibility difficulties.

It will be recalled from the previous section that the dissolution rate of gold/silver appeared to be inhibited in the initial stages of reaction, particularly at low cyanide concentrations. It is believed that the gold is passivated by a transient surface film, which is removed more rapidly at higher cyanide concentrations. It is possible that a similar mechanism is in place for the oxidation curves. As outlined in Chapter 4 for gold, it is believed that initially the gold is oxidised to form AuCN, which then passivates the surface. The surface passivation is removed by the reaction of AuCN with CN^- to form $Au(CN)_2^-$, which is swept away from the surface. The passive film would thus be expected to dissolve at a faster rate in higher cyanide concentration solutions.

6.3.2.3. Electrochemistry – Evans' Diagrams.

The Evans' diagrams representing the dissolution of gold/silver in air saturated 2 and 20 mM cyanide solutions are shown in Figure 6.9. It should be remembered that oxygen reduction on gold/silver cannot be measured as a function of cyanide concentration, and is thus represented by a single curve at both cyanide

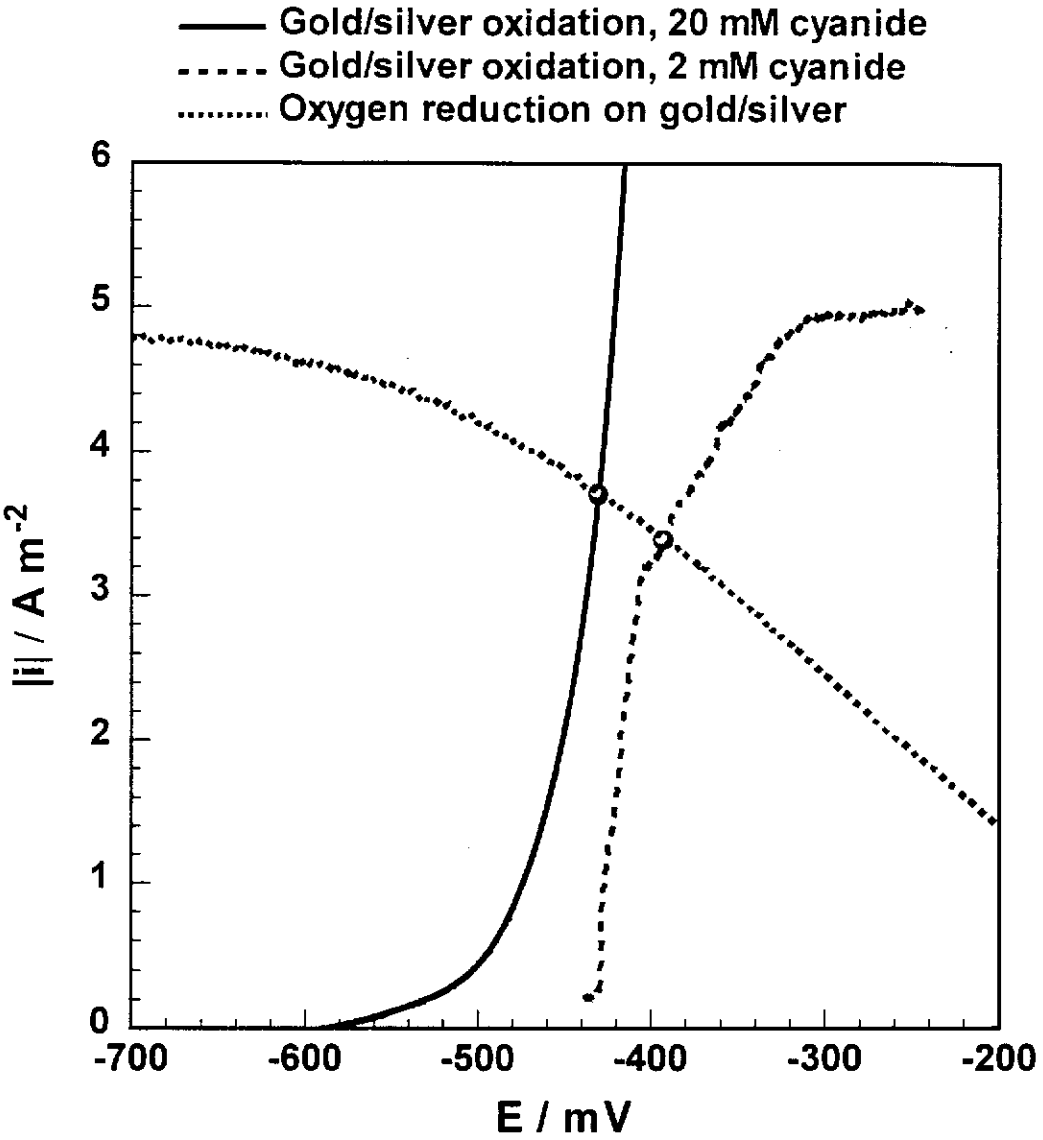

Figure 6.9 – Evans' diagrams representing the leaching of gold/silver in air saturated 2 and 20 mM cyanide solutions. Experimental conditions: pH 10.0, 25 °C, 300 rpm.

concentrations. It can be seen from Figure 6.9 that the polarisation curve for the oxidation of gold in 2 mM cyanide has a peculiar shape. Initially there is a rapid increase in current density until the potential reaches -400 mV. The oxidation curve then flattens out before reaching a limiting current density at -300 mV. There seems to be a different mechanism of oxidation in the potential region of -400 to -300 mV. What causes this effect is unknown.

The Evans' diagrams shown in Figure 6.9, predict that: 1) the dissolution rate is slightly lower for 2 mM cyanide solution than it is for 20 mM cyanide solutions; and 2) for 2 mM cyanide solutions, the dissolution rate is neither cyanide nor oxygen diffusion controlled. Each of these findings is consistent with the results from the kinetic studies, as discussed in section 6.3.2.1.

In summary, from the kinetic and electrochemical data, it has been shown that:

1) At cyanide concentrations below 2.1 mM, the rate of dissolution of gold/silver is close to cyanide diffusion controlled, while at concentrations above 2.1 mM, the reaction is oxygen diffusion controlled.

2) The oxidation of gold/silver is cyanide diffusion controlled in the potential region 0 to 800 mV.

3) Both the dissolution and oxidation of gold/silver appear to be hindered by a transient passive film, which is dissolved more rapidly at high cyanide concentrations. The experimental results are consistent with the passive film being AuCN, which is the same as the proposed passivation mechanism for gold (as discussed in Chapter 4).

6.3.3. Effect of Rotation Rate

6.3.3.1. Kinetics

In a similar manner to the previous chapters, the leaching of gold/silver in aerated cyanide solutions was investigated as a function of rotation rate to verify that the reaction is diffusion controlled. The data is presented as a Levich plot of the dissolution rate versus $\omega^{1/2}$, as shown in Figure 6.10. Included are the theoretical dissolution rates based on the diffusion of oxygen, with line (a) representing the reduction of oxygen to hydroxide, and line (b) representing the reduction of oxygen to peroxide. It is clear that the experimental data has a linear relationship with a non-zero intercept, and the implications of this are discussed below.

(a) Linear relationship

Systems that display a linear relationship between the rate of dissolution and $\omega^{1/2}$ are usually diffusion controlled processes. Therefore, the data shown in Figure 6.10 implies that the dissolution of gold/silver in 20 mM cyanide solutions is limited by the diffusion of oxygen to the gold surface, a finding which is consistent with the results presented in the previous sections. The slope of the data in Figure 6.10 can be used to estimate the molar ratio of gold to oxygen, x_O, as shown in Equation 6.5, a rearranged form of the Levich equation. From x_O, the proportion of oxygen which is reduced to hydroxide can be readily calculated.

$$\text{Slope} = 0.62 x_O D_O^{2/3} \nu^{-1/6} [O_2] \qquad \textbf{Equation 6.5}$$

Using the values of D_O, ν and $[O_2]$ already specified in this thesis, the slopes obtained from Figure 6.10 can be used to calculate x_O, and hence the proportion of oxygen which is reduced to hydroxide. In the case of gold/silver containing 1 % silver, it is calculated that 34 % of the oxygen is reduced to hydroxide, which is

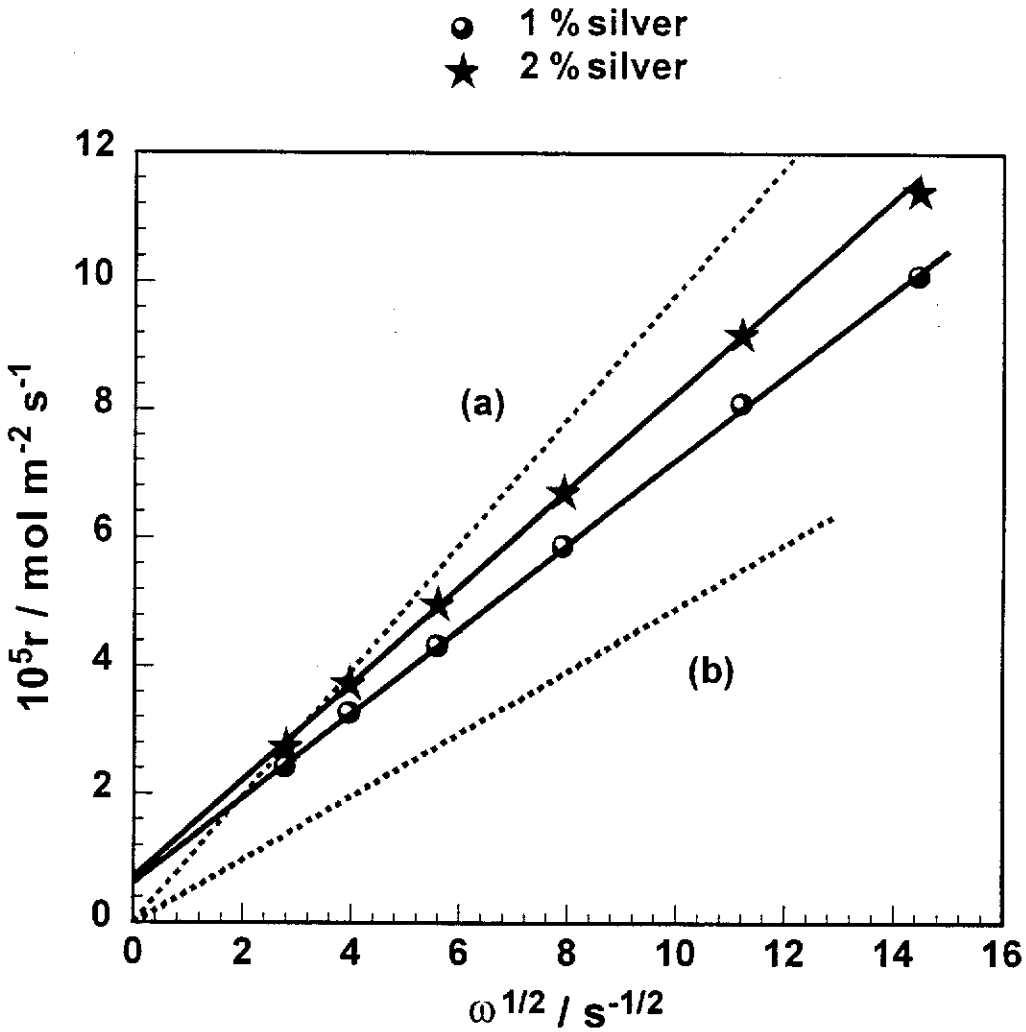

Figure 6.10 – Rate of dissolution of gold/silver versus $\omega^{1/2}$. Lines (a) and (b) are calculated for diffusion of oxygen with reduction to hydroxide and peroxide respectively. Experimental conditions: air saturated 20 mM cyanide solutions, pH 10.0, 25 °C.

lower than that calculated in section 6.3.2.1, 56 % (due to the non-zero intercept observed in Figure 6.10). The same data was also measured for a gold/silver which contains 2 % silver. and it is calculated that in this instance, 54 % of the oxygen is reduced to hydroxide. The higher value obtained for the 2 % silver deposit suggests that the silver sites on the gold surface enhance the reduction of oxygen. This result is not surprising, as it was shown in Chapter 3 that oxygen reduction occurs at a higher rate on silver than it does on gold. Thus, the dissolution of gold/silver occurs by bimetallic corrosion, with oxygen preferentially reducing at silver sites.

(b) Non-zero intercept

It is clear from Figure 6.10 that the data for both the 1 and 2 % silver deposits exhibit a common non-zero intercept. This implies that the offset from the origin is due to a process which is common to both systems. Similar graphs have been published by Zheng *et al.* (1996), for the system zinc in tri-iodide solutions. They attributed the non-zero intercept to an additional chemically controlled process, which in their case was the reduction of trace levels of oxygen. It is possible that there is a chemical process that is affecting the dissolution of gold. In Chapter 5, the rate of dissolution gold in the presence of 1 ppm lead was measured as a function of rotation rate. It was shown that this data had a y intercept of 0.61, which is identical to that measured here. This indicates that the non-zero intercept is due to a process which is common to each of the systems. In Chapter 5, it was postulated that the evolution of hydrogen could account for the observed non-zero intercept, a process which could also account for the data presented in this section.

6.3.3.2. Electrochemistry – Oxidation

The oxidation of gold/silver in solutions containing 20 mM cyanide was investigated as a function of rotation rate in the range 75 to 2000 rpm. The oxidation curves measured over a wide range of rotation rates were found to be identical in nature (see Figure 6.8), with the limiting current density increasing with rotation rate. The potential region of interest to cyanidation is discussed in the following section,

and the remainder of this section focuses on the limiting plateau. To verify that the oxidation of gold/silver is diffusion controlled over a range of rotation rates, the oxidation current density at 200 mV was plotted against $\omega^{1/2}$, as shown in Figure 6.11. It should be remembered that in this case, the potential is applied by a potentiostat, and so the system is not limited by the process of oxygen diffusion. The line of best fit is linear and passes through the origin. This is indicative of a diffusion controlled process which, in this case, is the diffusion of cyanide. Using the slope of this data, the diffusion coefficient for cyanide can be calculated, as shown in Equation 6.6 (a modified version of the Levich equation). It must be remembered that due to the reaction stoichiometry, the oxidation current density is equivalent to one half of the cyanide flux.

$$D_{CN} = \left[\frac{\text{Slope} \times 2}{0.62nF\nu^{-1/6}[CN^-]} \right]^{3/2} \qquad \textbf{Equation 6.6}$$

Using a value for ν of 0.8904×10^{-6} $m^2 s^{-1}$ for water at 25 °C, the diffusion coefficient for cyanide was calculated to be 1.88×10^{-9} $m^2 s^{-1}$. This is within the range of 1.77 to 2.18×10^{-9} $m^2 s^{-1}$ that has appeared in the literature (Hiskey & Sanchez, 1990, Guan & Han, 1994, Lide, 1995).

6.3.3.3. Electrochemistry – Evans' Diagrams.

Evans' diagrams were constructed to demonstrate the effect of rotation rate on the dissolution of gold/silver. Two rotation rates are represented, 300 and 75 rpm, as shown in Figure 6.12. Not surprisingly, the Evans' diagrams predict that the dissolution rate will increase with rotation rate, and the limiting step for dissolution over a range of rotation rates will be reduction of oxygen. These findings are consistent with the results from the kinetic studies, section 6.3.3.1. It is also worth noting that the Evans' diagrams also show that the mixed potential will become more negative with increasing rotation rate. In contrast with this, over the wide range of rotation rates in the kinetic studies, the mixed potential was found to become more

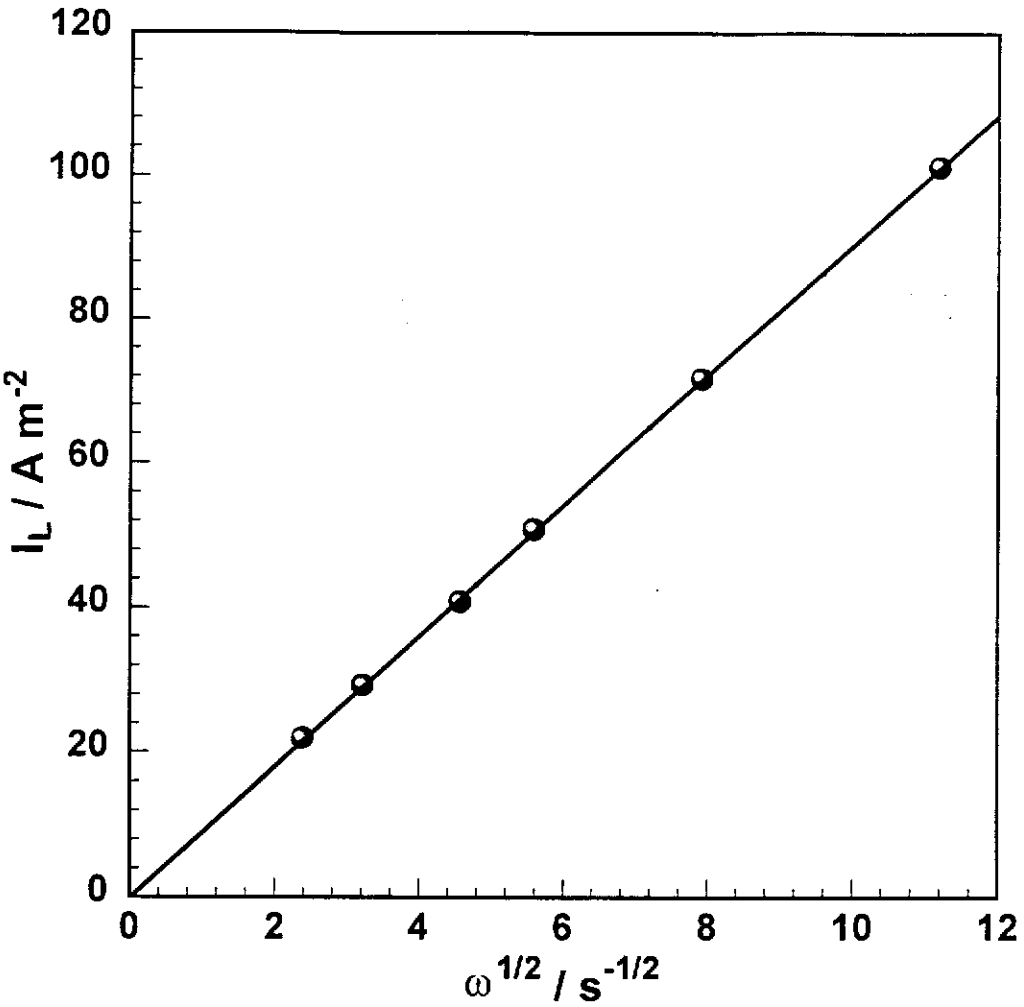

Figure 6.11 – Effect of rotation rate on the gold/silver oxidation limiting current density. Experimental conditions: 20 mM cyanide solutions, pH 10.0, 25 °C, 300 rpm.

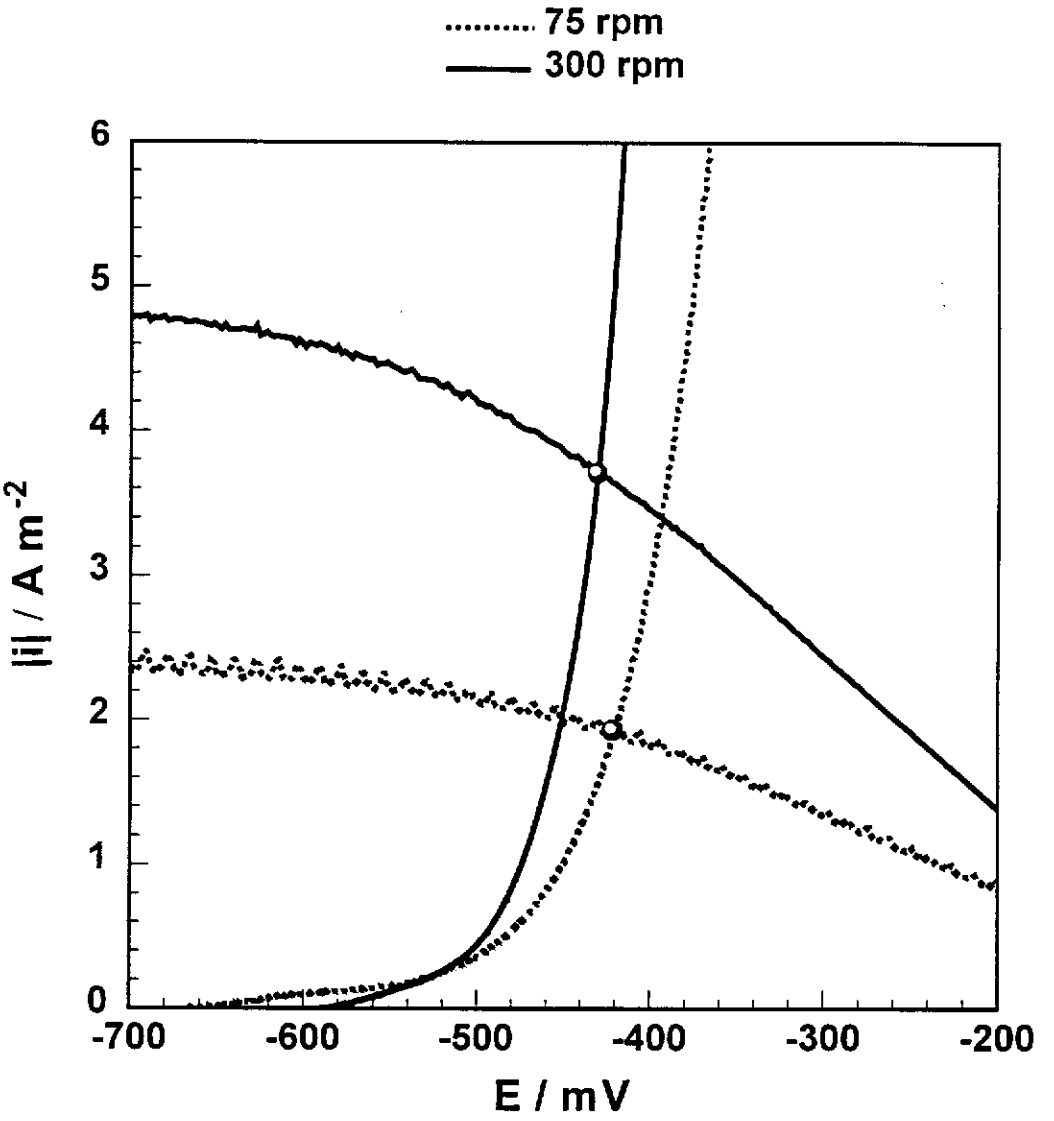

Figure 6.12 – Evans' diagrams representing the leaching of gold/silver at 75 (broken lines) and 300 rpm (solid lines) in air saturated solutions containing 20 mM cyanide. Experimental conditions: pH 10.0, 25 °C.

positive with increasing rotation rate. It is thus believed that the Evans' diagrams do not accurately represent the change in gold oxidation with rotation rate. It is not clear why this discrepancy occurs.

6.3.4. Effect of Temperature.

6.3.4.1. Kinetics

The dissolution rate of gold/silver in cyanide solutions was measured as a function of temperature, and the results are shown in Figure 6.13. Initially, as the temperature is increased, the rate of dissolution increases until it reaches a maximum of 5.5×10^{-5} mol m^{-2} s^{-1} at 45 °C. At temperatures above 45 °C, the dissolution rate falls, reaching 5.4×10^{-5} mol m^{-2} s^{-1} at 60 °C. Also shown in Figure 6.13 is the solubility of oxygen in water (Fogg & Gerrard, 1991), which decreases as temperature increases. This reduced solubility accounts for the decrease in the rate of dissolution of gold/silver at higher temperatures. Under these conditions, the activation energy for the process cannot be calculated directly, although the reaction rate at higher temperatures can be corrected for the lower oxygen solubility, by using the ratio of the oxygen concentration at 25 °C to that at the elevated temperature. This method is only valid if there is a linear relationship between the rate of dissolution and the oxygen concentration. If the reaction is controlled by the diffusion of oxygen, as suggested in section 6.3.3.1, the reaction will be first order with respect to oxygen concentration, and the assumed linear relationship between the rate of dissolution and oxygen concentration should be valid. The calculated rates of dissolution, based on this assumption, are shown in Table 6.2

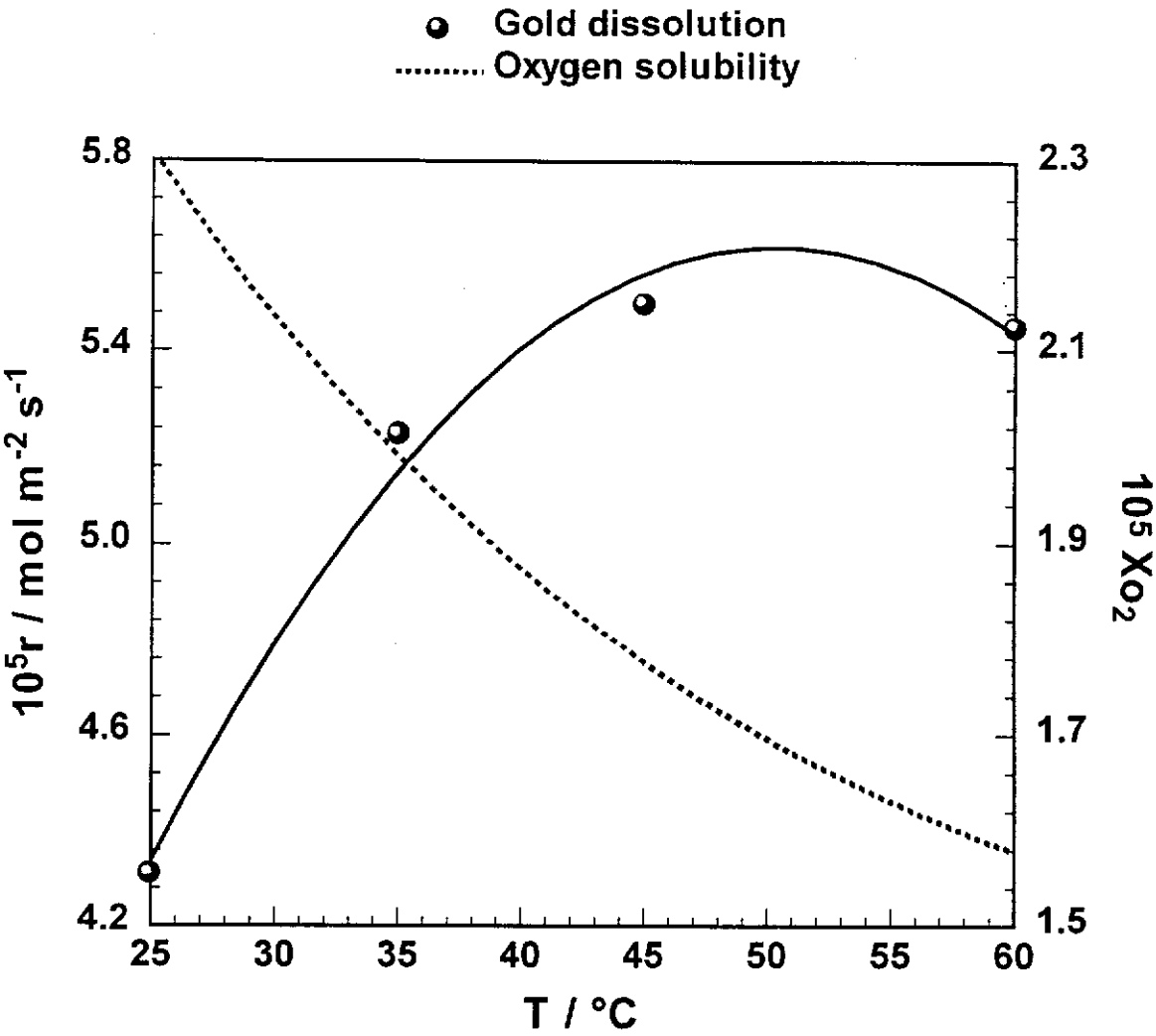

Figure 6.13 – Effect of temperature on the rate of dissolution of gold/silver. Also shown is the mole fraction solubility of oxygen in water as a function of temperature. Experimental conditions: air saturated 20 mM cyanide solutions, pH 10.0, 300 rpm.

T /°C	$10^5 r$ /mol m^{-2} s^{-1}	$10^5 Xo_2$	$10^5 r_c$ /mol m^{-2} s^{-1}
25	4.3	2.30	4.3
35	5.2	1.99	6.0
45	5.5	1.78	7.1
60	5.4	1.59	7.9

Table 6.2 – Rate of dissolution of gold/silver as a function of temperature. Also shown are the published values of the mole fraction oxygen solubility in water, Xo_2, at elevated temperatures; and the rate of dissolution, r_c, which is corrected for a constant oxygen concentration. Experimental conditions: air saturated 20 mM cyanide solutions, pH 10.0, 300 rpm.

The activation energy for the dissolution of gold/silver in cyanide solutions can now be determined using an Arrhenius plot. The Arrhenius plot is based on the corrected rate of dissolution, and is shown in Figure 6.14. Two tangents to the curve have been added to the Arrhenius plot, one at high temperatures, and one at low temperatures. The slope of these tangents can be used to calculate the activation energy for the process. At high temperatures, the activation energy is calculated to be 6 kJ mol^{-1}, while at low temperatures, the activation energy is 25 kJ mol^{-1}. The activation energy for a diffusion controlled process is usually less than 25 kJ mol^{-1} (Power & Ritchie, 1975), so it would appear that the reaction is diffusion controlled at all temperatures investigated.

It is uncertain whether it is possible for a process to have an activation energy as low as 6 kJ mol^{-1}, and thus it is believed that there is a problem with the data at high temperatures. This problem is not restricted to this system though, as a similar result were found in Chapter 5 when calculating the activation energy for gold in a solution containing lead. This could indicate that the method for correcting for changes in oxygen solubility is flawed, or that at higher temperatures, the low activation energy is a feature of oxygen reduction. It is uncertain which of these possibilities is correct.

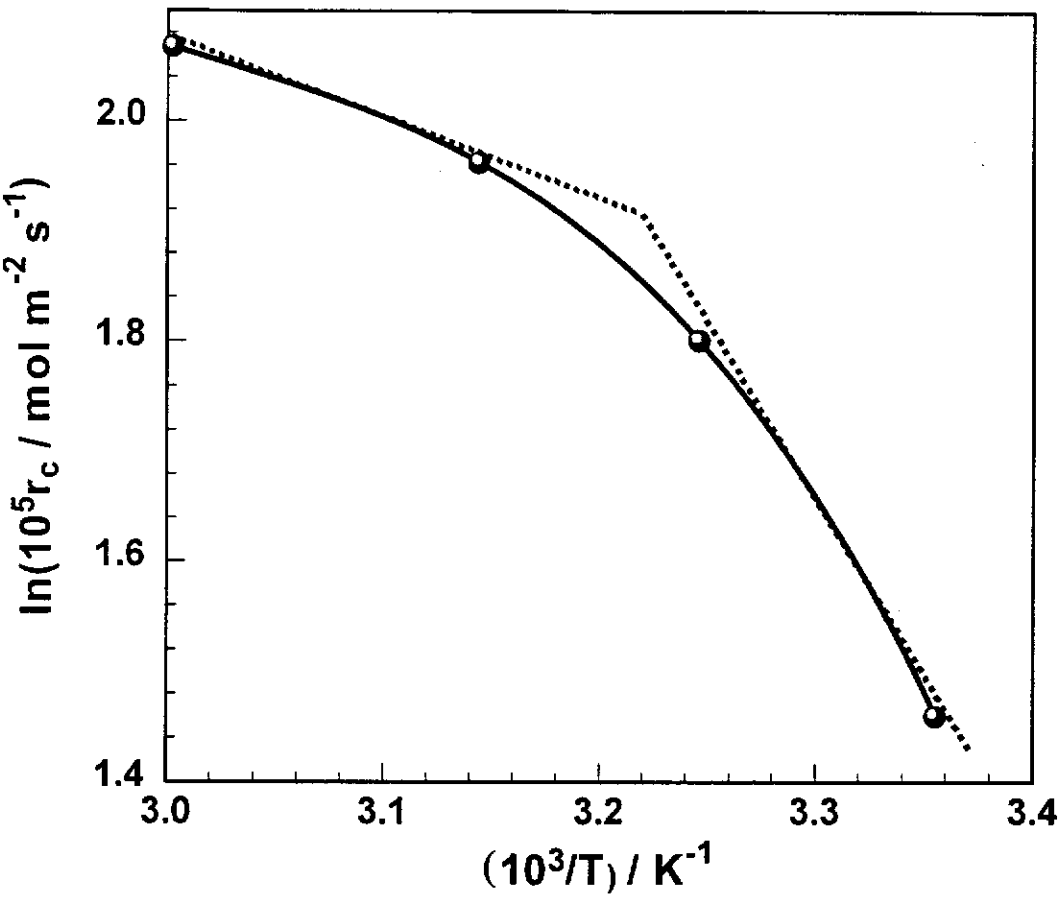

Figure 6.14 – Arrhenius plot of the corrected rate of dissolution of gold/silver as a function of 1/T. Experimental conditions: air saturated 20 mM cyanide solutions, pH 10.0, 300 rpm.

6.3.4.2. Electrochemistry – Oxidation.

The temperature response of the gold/silver oxidation limiting current density can provide further evidence that the oxidation of gold/silver is controlled by cyanide diffusion at higher potentials. An Arrhenius plot of the log(i) vs 1/T for gold/silver oxidation in 20 mM cyanide solutions is shown in Figure 6.15. The data was found to display a linear relationship between log(i) and 1/T, and hence the activation energy can be estimated from the slope of the graph. The activation energy was calculated to be 12.5 ± 1 kJ mol^{-1}, which is indicative of a reaction that is diffusion controlled (Power & Ritchie, 1975). This result is not surprising, and corresponds well with the findings from the effect of rotation rate in section 6.3.3.2, which showed that the current density was limited by cyanide diffusion at potentials above 0 mV.

6.3.4.3. Electrochemistry – Evans' Diagrams.

The effect of temperature on the rate of dissolution of gold/silver in aerated 20 mM cyanide solutions can be demonstrated using Evans' diagrams. In this case, the Evans' diagrams represent the dissolution of gold/silver at two temperatures, 25 °C and 60 °C, as shown in Figure 6.16. It is clear that at higher temperatures, both oxidation of gold and reduction of oxygen are enhanced to some extent. Consequently, the Evans diagrams predict that the rate of dissolution will be higher at 60 °C than it is at 25 °C. It is also clear that oxygen reduction remains the limiting step for dissolution as the temperature is increased. These results are consistent with the results from the kinetic studies, as discussed in section 6.3.4.1.

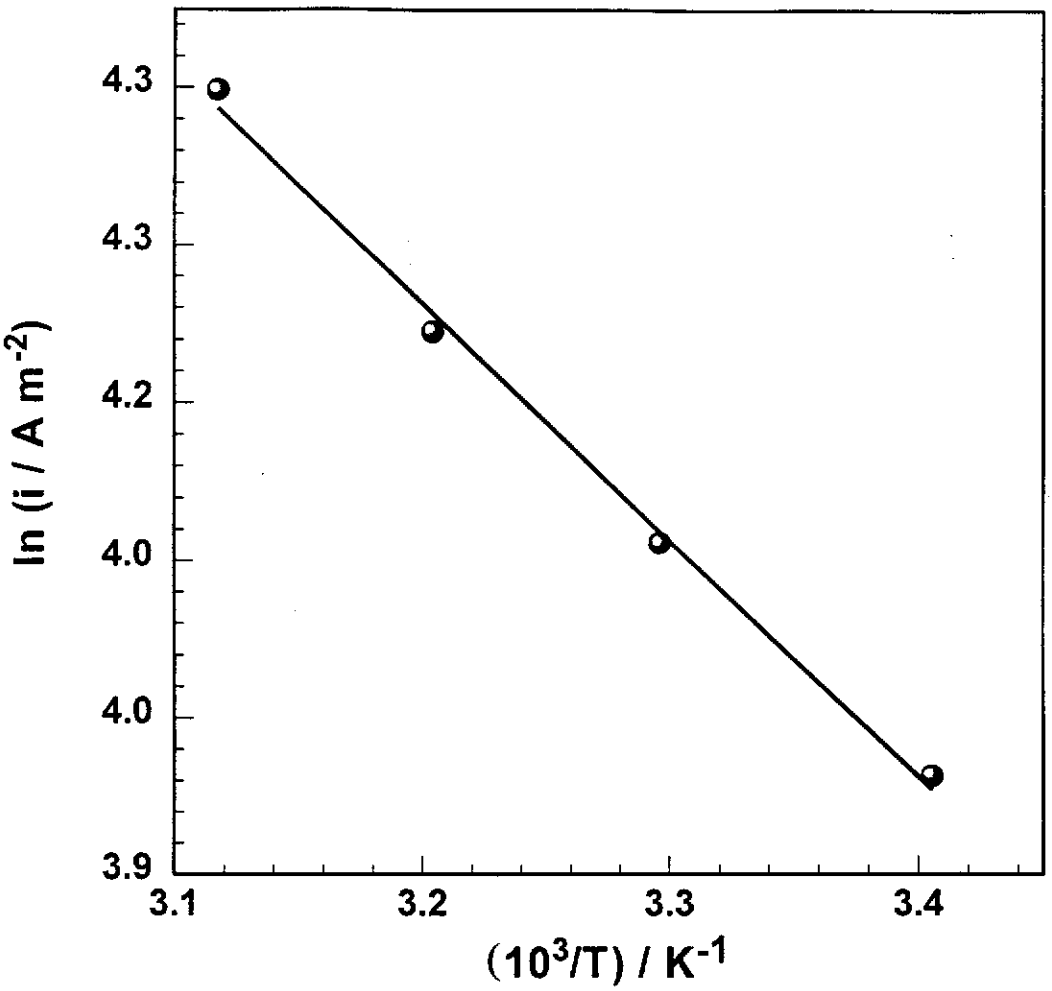

Figure 6.15 – Arrhenius plot of the gold/silver limiting current density as a function of 1/T. Experimental conditions: 20 mM cyanide solutions, pH 10.0, 300 rpm.

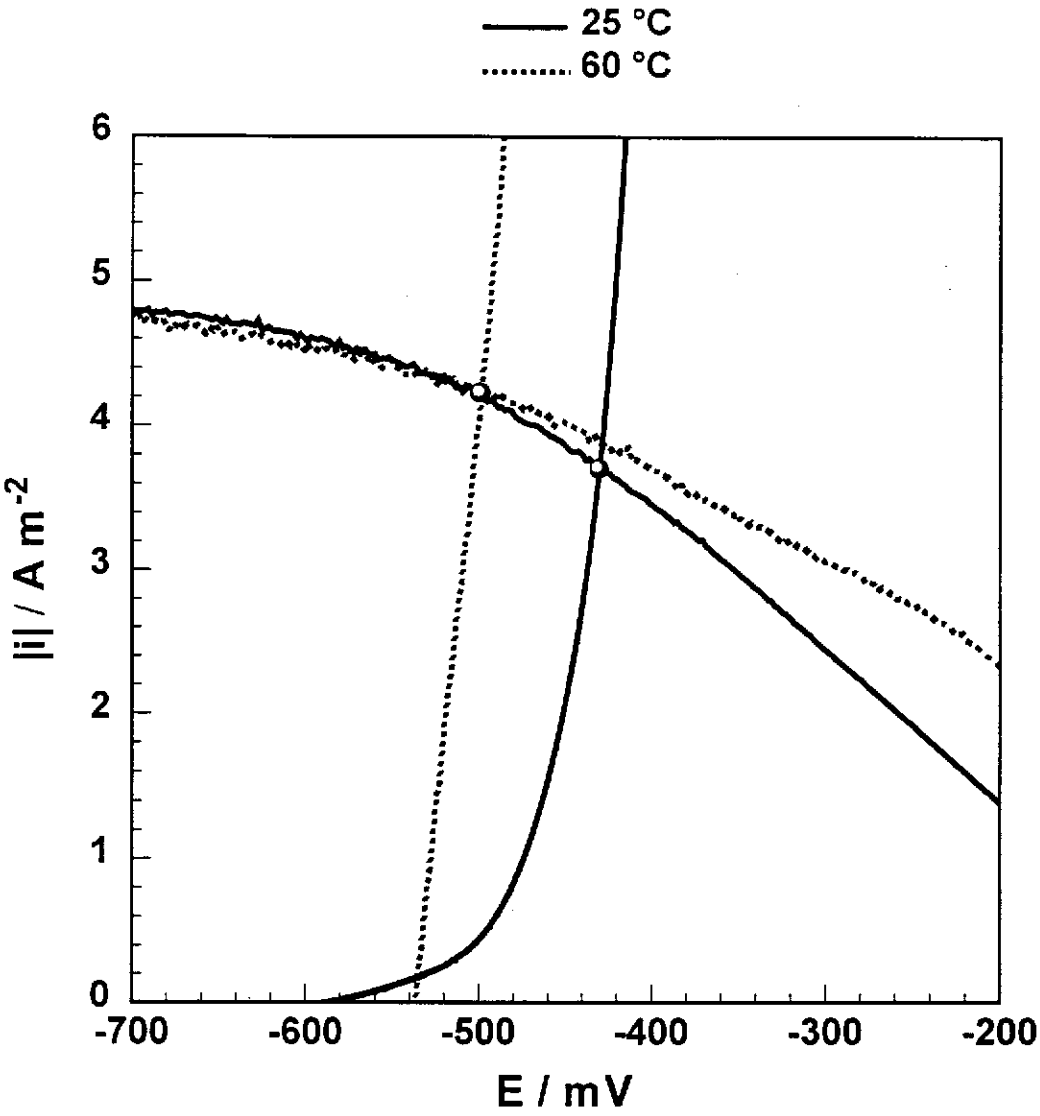

Figure 6.16 – Evans' diagrams representing the leaching of gold/silver at 25 °C (solid lines) and 60 °C (broken lines) in air saturated 20 mM cyanide solutions. Experimental conditions: pH 10.0, 300 rpm.

6.3.5. Effect of Oxygen Concentration

6.3.5.1. Kinetics

The rate of dissolution of gold/silver in 20 mM cyanide has been found to be controlled by the diffusion of oxygen to the electrode surface, and thus any increases in oxygen concentration should result in an increase in the rate of dissolution. It should be recalled from the review, that in oxygen saturated solutions, the theoretical critical cyanide concentration is 9.7 mM, as compared to 1.9 mM for air saturated solutions. In this case, the cyanide concentration chosen (20 mM) is above the theoretical critical cyanide concentration for both air and oxygen saturated solutions. Thus, the dissolution rate of gold/silver should be controlled by oxygen diffusion in both instances. The dissolution rate as a function of oxygen concentration is shown in Table 6.3. Also shown is the calculated proportion of the oxygen which is reduced to hydroxide, assuming that both peroxide and hydroxide are produced as stable products. This calculation does not allow for the non-zero intercept that was observed in the rate versus $\omega^{1/2}$ diagram, as these measurements were not made for oxygen saturated solutions.

Oxygen Concentration	**10^5r /mol m^{-2} s^{-1}**	**Proportion of oxygen reduced to hydroxide[1]**
Air saturated	4.3	55 %
Oxygen saturated	17	30 %

[1] Proportion of oxygen reduced to hydroxide is calculated without allowing for the non-zero intercept in the rate versus $\omega^{1/2}$ diagram.

Table 6.3 – Effect of oxygen concentration on the rate of dissolution of gold/silver. Also shown is the calculated proportion of the oxygen which is reduced to hydroxide. Experimental conditions: 20 mM cyanide, pH 10.5, 300 rpm, 25 °C.

The rate of dissolution of gold/silver was found to be considerably higher in oxygen saturated solutions than in air saturated solutions. This indicates that gold/silver does not passivate in the presence of higher oxygen concentrations, which is the result that has been obtained for cyanidation in the past. It is therefore not surprising that plant operation follows the trends for gold/silver, as nearly all naturally occuring gold contains some silver (Hurlbut & Klein, 1977, p. 221).

It is worth noting that the mixed potential for gold dissolution in oxygen saturated solutions, -270 mV, is considerably more positive than the mixed potential for air saturated solutions, -410 mV. A more positive mixed potential corresponds to more positive reduction potential, and hence, a lower proportion of oxygen which reduced to hydroxide. This explains why the calculated proportion of oxygen that is reduced to hydroxide, as shown in Table 6.3, is less in oxygen saturated solutions than in air saturated solutions.

6.3.5.2. Electrochemistry – Evans' Diagrams

The Evans' diagrams representing the dissolution of gold/silver in air and oxygen saturated 20 mM cyanide solutions are shown in Figure 6.17. The Evans' diagrams show that increases in oxygen concentration significantly enhances the dissolution rate, and that for oxygen saturated solutions, oxygen reduction remains the limiting step for dissolution. This result was expected, given the theoretical critical cyanide concentration for oxygen saturated solutions of 9.5 mM, is below the solution cyanide concentration, of 20 mM. Each of these results are consistent with the results from the kinetic studies, as discussed in section 6.3.5.1

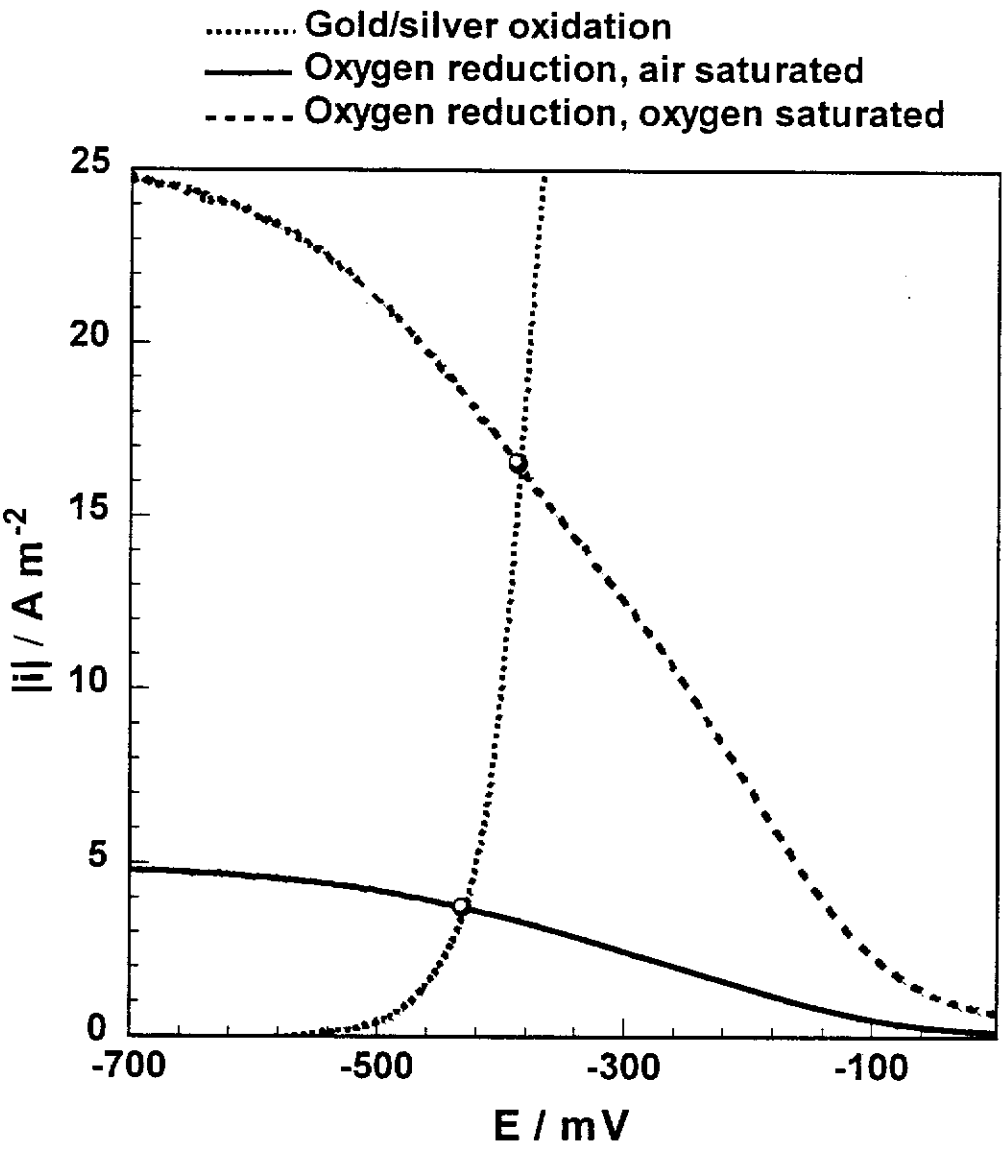

Figure 6.17 – Evans' diagrams representing the leaching of gold/silver in air and oxygen saturated 20 mM cyanide solutions. Experimental conditions: pH 10.0, 25 °C, 300 rpm.

6.3.6. Effect of pH

6.3.6.1. Kinetics

The dissolution of gold/silver in aerated 20 mM cyanide solutions was measured at pH 12.5 and compared to the measured rate at pH 10.0. As was the case for oxygen saturated cyanide solutions, the proportion of oxygen reduced to hydroxide was calculated without allowing for the non-zero intercept which was observed in Figure 6.10. The dissolution rates at pH 10.0 and 12.5 are shown in Table 6.4. It is clear that the rate of dissolution, and hence the oxygen reduction mechanism changes with pH. This is due to a shift in the reduction potential of oxygen with pH, an effect which was examined in Chapter 3. Thus, at higher pH values, oxygen becomes more difficult to reduce.

pH	$10^5 r$ / mol m^{-2} s^{-1}	Proportion of peroxide reduced to hydroxide /%
10.0	4.3	55
12.5	3.3	20

Table 6.4 – Effect of pH on the rate of dissolution of gold/silver. Also shown is the calculated proportion of the oxygen which is reduced to hydroxide. Experimental conditions: air saturated 20 mM cyanide solutions, 300 rpm, 25 °C.

6.3.6.2. Electrochemistry – Oxidation

The increase in pH from 10 to 12.5 was found to have no effect on the oxidation of gold/silver in cyanide solutions at potentials lower than 0 mV. At higher potentials, the gold/silver is passivated at two potentials, P1(a) and P1(b). The passivation at P1(b) was found to shift with pH, indicating that the surface film

that is causing the passivation is either gold oxide or gold hydroxide. This is similar to the results for gold, as discussed in section 4.3.1.3.

6.3.6.3. Electrochemistry – Evans' Diagrams

The Evans' diagrams demonstrating the effect of pH on the rate of dissolution of gold/silver in aerated cyanide solutions are shown in Figure 6.18. The oxidation of gold was found to be unaffected by pH at low overpotentials, and thus is represented by the same polarisation curve at both pH values. Conversely, pH was found to have a significant effect on the reduction of oxygen, an aspect which was discussed in detail in Chapter 3. Thus, the Evans' diagrams show that the dissolution rate decreases with increasing pH, a finding which is consistent with the kinetic results (section 6.3.6.1).

6.3.7. Effect of Lead

6.3.7.1. Kinetics

It has already been demonstrated in Chapter 4, that trace levels of lead can substantially increase the dissolution rate of gold. Consequently, the effect of lead on the dissolution of gold/silver was investigated. It can be seen from Table 6.5 that the rate of dissolution of gold/silver in both air and oxygen saturated solutions increases with the addition of 1 ppm lead. The most likely reason for this is that the reduction of oxygen is enhanced in the presence of lead, a finding which was discussed in Chapter 4 for the case of gold in cyanide solutions containing lead. Thus, bimetallic corrosion is occurring, with the reduction of oxygen preferentially occurring at lead sites. It is interesting that in the presence of lead, the proportion of oxygen which is reduced to hydroxide does not change significantly with oxygen concentration. This indicates that during dissolution of gold/silver in solutions

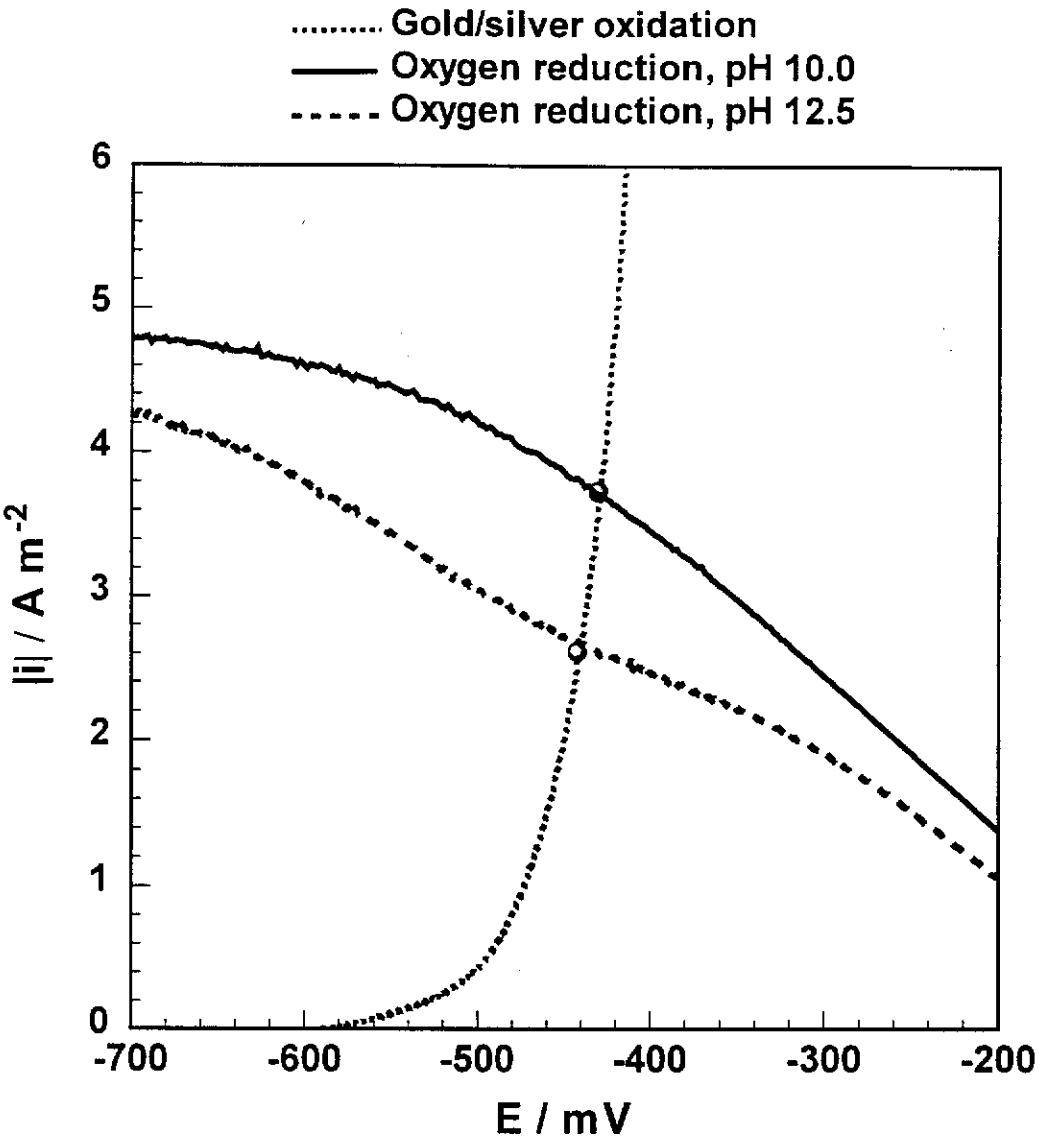

Figure 6.18 – Evans' diagrams representing the leaching of gold/silver in air saturated 20 mM cyanide solutions at pH 10.0 and 12.5. Experimental conditions: 25 °C, 300 rpm.

containing lead, there are a large number of lead sites on which oxygen reduction can occur. This is not surprising given that lead will cement on the surface of the gold/silver, resulting in a large number of active sites.

Solution	$10^5 r$ /mol m^{-2} s^{-1}	Proportion of peroxide reduced to hydroxide /%
Air saturated	4.3	55
Air saturated with lead	5.5	100
Oxygen saturated	17	30
Oxygen saturated with lead	25	90

Table 6.5 – Effect of oxygen concentration on the rate of dissolution of gold/silver in the presence and absence of 1 ppm lead. Also shown is the calculated proportion of the oxygen which is reduced to hydroxide. Experimental conditions: 20 mM cyanide solutions, 300 rpm, 25 °C.

The action of lead can be further quantified by examining the rate of dissolution of gold/silver as a function of cyanide concentration in the presence of lead. This data is presented in Figure 6.19. It is clear that the dissolution rates follow the behaviour expected for a system which exhibits diffusion control. That is, the data points lie very close to the lines (a) and (b), which are calculated from the Levich equation, and represent the diffusion of cyanide and diffusion of oxygen (when dissolution occurs by the Elsner equation) respectively. From Figure 6.19, the critical cyanide concentration for gold/silver in the presence of lead was estimated to be 2.1 mM. This is also very close to the value calculated using the Levich equation of 1.9 mM for when dissolution occurs according to the Elsner equation.

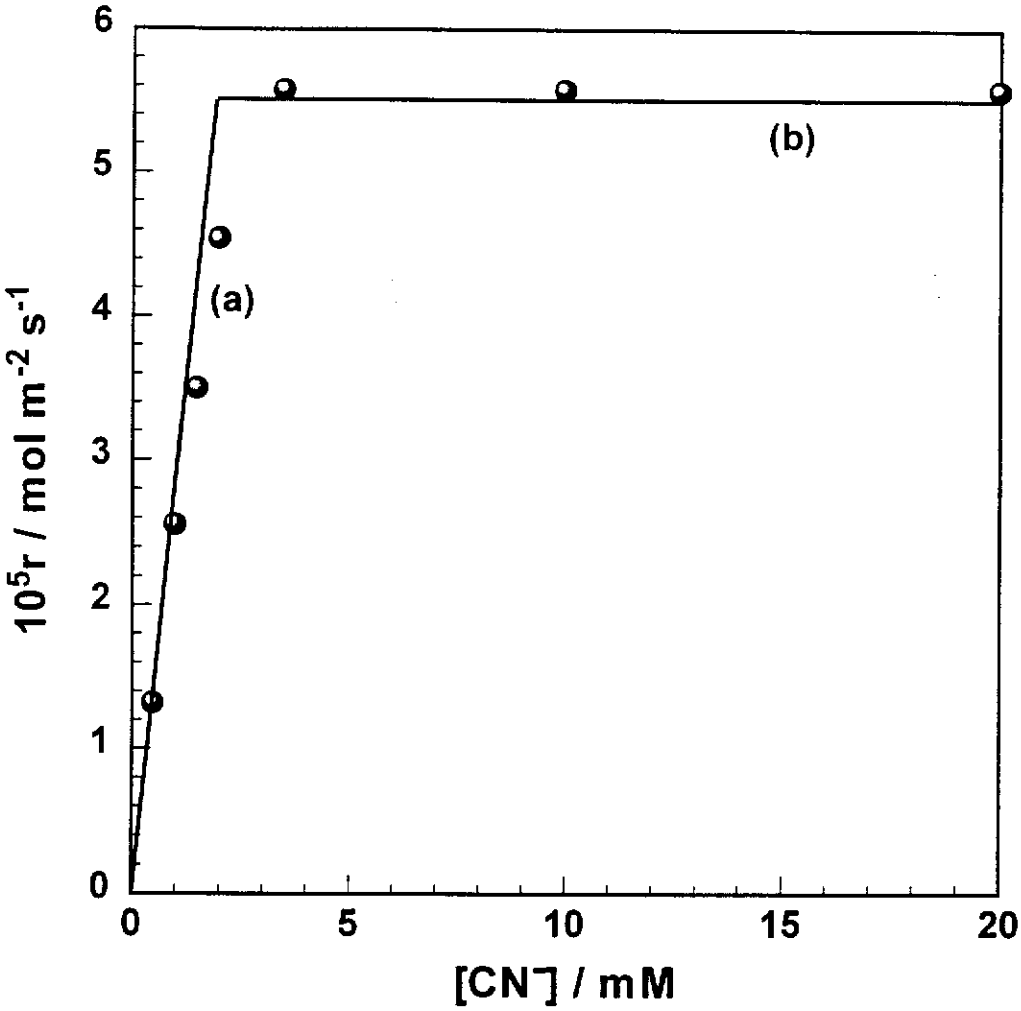

Figure 6.19 – Effect of cyanide concentration on the rate of dissolution of gold/silver in the presence of 1 ppm lead. Line (a) represents the cyanide diffusion limiting rate, and line (b) represents the oxygen diffusion limiting rate when dissolution occurs according to the Elsner equation. Experimental conditions: air saturated solutions, pH 10.0, 25 °C, 300 rpm.

6.3.7.2. Electrochemistry – Oxidation

The effect of lead on the oxidation of gold/silver was investigated, and the resultant polarisation curves are shown in Figure 6.20. It is clear that in the presence of lead, oxidation of gold/silver occurs at more negative potentials, and thus lead acts as a catalysis for the oxidation reaction. This suggests that lead is more effective than silver at removing the passivating film of AuCN. The oxidation of gold in a solution containing 20 mM cyanide and 1 ppm lead has been overlaid in Figure 6.20, from which it can be seen that the anodic polarisation curve for gold/silver with lead shows certain features from the other two curves in Figure 6.20. At -200 mV, gold/silver begins to passivate, as it does in the case of gold in the presence of lead in solution. However, unlike that for gold, the current density begins to increase again at -150 mV, following the shape of gold/silver in the absence of lead. This indicates that the passivation at -200 mV is not caused by lead completely blocking the surface, but is more likely due to a change in the nature of the lead on the surface. In Chapter 4, it was concluded that the passivation of gold in solutions containing 1 ppm lead was due to the formation of lead oxide. These results on the effect of lead on the oxidation of gold/lead are consistent with this finding.

6.3.7.3. Electrochemistry – Evans' Diagrams

The Evans' diagrams demonstrating the effect of lead on the dissolution of gold/silver in aerated cyanide solutions are shown in Figure 6.21. The system containing 1 ppm lead is considerably more difficult to simulate using Evans' diagrams, as during dissolution, oxygen is reduced on a surface containing lead. Therefore, oxygen reduction in this instance is represented by the polarisation curve of oxygen on gold/lead. It is clear from Figure 6.21 that the presence of lead enhances both the oxidation of gold and the reduction of oxygen. Therefore, the Evans' diagrams predict lead will increase the rate of dissolution of gold in 20 mM cyanide solutions, a result which is consistent with the kinetic studies (section 6.3.7.1).

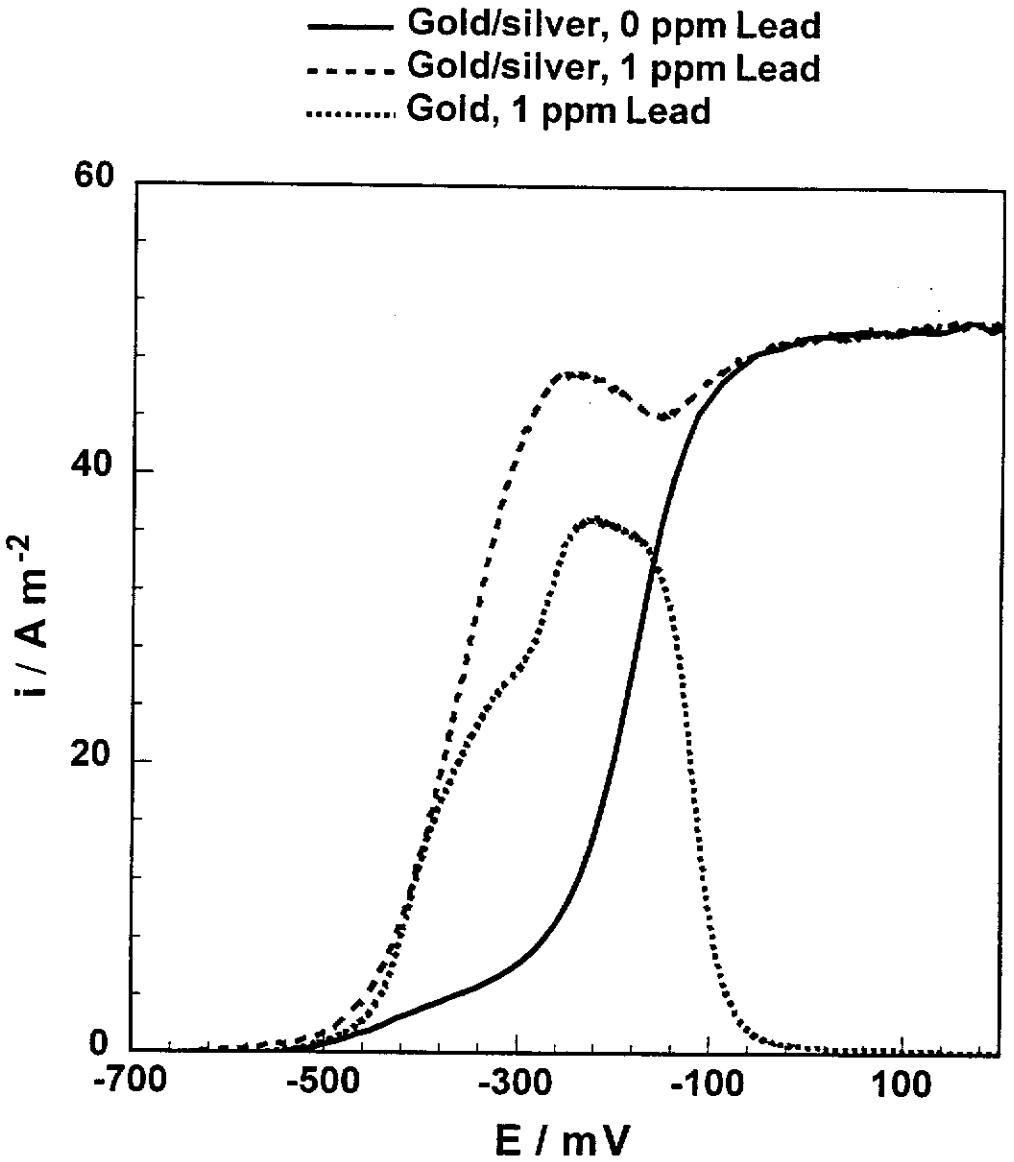

Figure 6.20 – Oxidation polarisation curves for gold/silver in the presence and absence of 1 ppm lead. Also shown is the polarisation curve for the oxidation of gold in the presence of 1 ppm lead (from Chapter 5). Experimental conditions: 20 mM cyanide solutions, pH 10.0, 1 mV s^{-1}, 25 °C, 300 rpm.

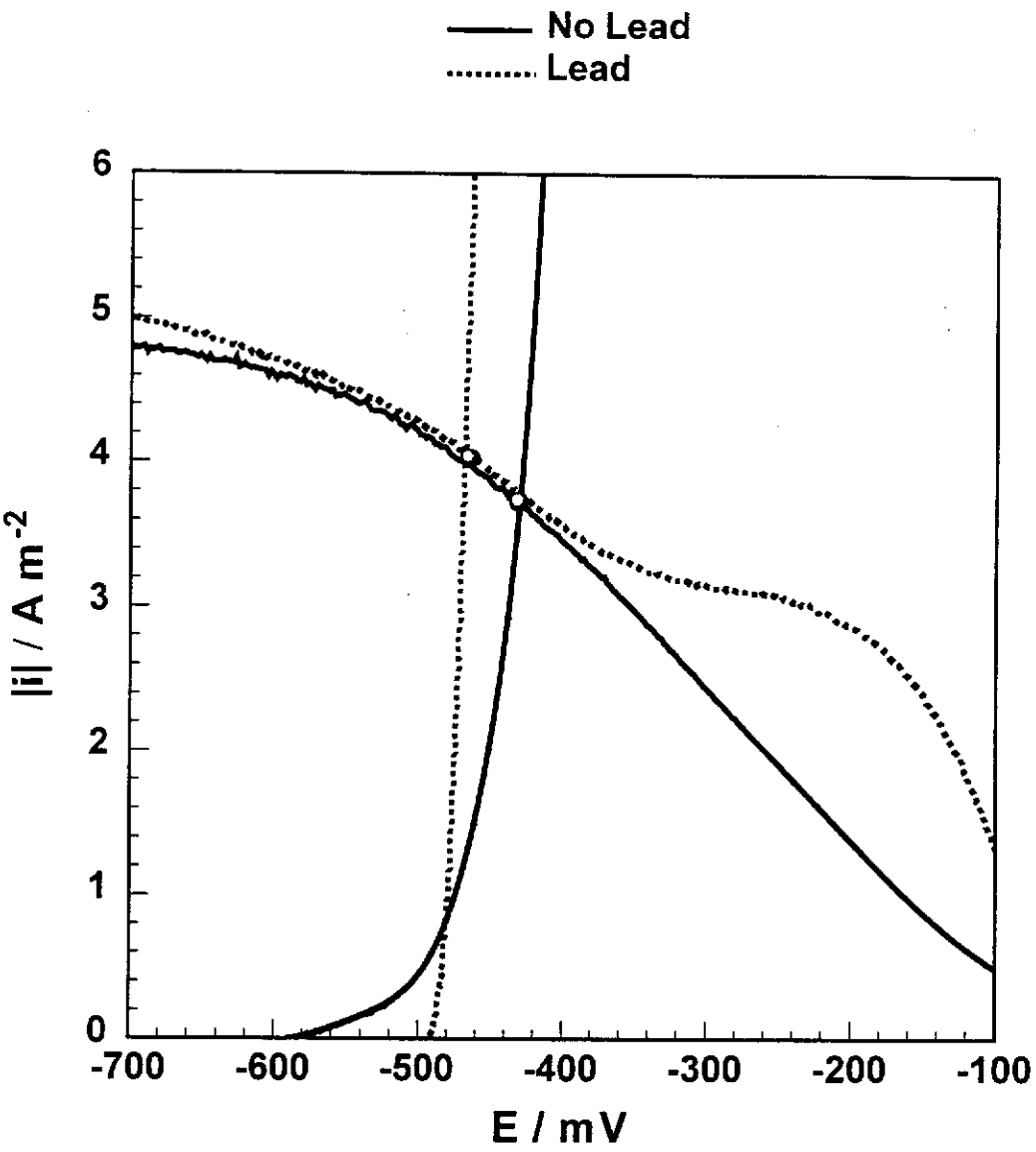

Figure 6.21 – Evans' diagrams representing the leaching of gold/silver in air saturated 20 mM cyanide solutions in the presence (broken lines) and absence (solid lines) of 1 ppm lead. Experimental conditions: pH 10.0, 25 °C, 300 rpm.

6.4. Summary

1) The leaching rate of gold/silver in aerated cyanide solutions is significantly higher that for gold.

2) The silver, which is co-deposited with gold during the plating process, is believed to stop the formation of a blocking film of AuCN.

3) At cyanide concentrations below 2.1 mM, the rate of dissolution of gold/silver is cyanide diffusion controlled, while at concentrations above 2.1 mM, the dissolution is oxygen diffusion controlled.

4) During the dissolution of gold/silver in cyanide solutions, a proportion of the oxygen is reduced to peroxide, while the remainder is reduced to hydroxide. The distribution between these reactions is dependent on experimental conditions, with the proportion of oxygen reduced to hydroxide increasing with temperature and decreasing with oxygen concentration and pH.

5) The addition of 1 ppm lead enhances the dissolution of gold/silver in cyanide solutions, particularly at high oxygen concentrations. In the presence of lead, very little peroxide is formed as a reaction product.

6) Gold/silver oxidises to give a polarisation curve which is almost identical to the pioneering work of Kudryk and Kellogg (1954). Therefore, it is believed that these authors conducted their experiments with lower purity gold.

Chapter 7 – Conclusions and Recommendations

This thesis has presented a detailed investigation into the gold cyanidation process. The study was conducted using a rotating electrochemical quartz crystal microbalance, an instrument which allows the mass changes at the solid-solution interface to be measured in real time. A proportion of this project was devoted to the on-going development of the REQCM. As will be apparent from the results presented in the preceding chapters, this instrument proved to be a powerful technique for investigating leaching reactions, such as the dissolution of gold in cyanide solutions.

The leaching of gold in aerated 20 mM cyanide solutions was found to blocked by a surface film, thought to be AuCN. The presence of such a film results in the reaction being chemically controlled, with an activation energy of 47 ± 3 kJ mol^{-1}. At cyanide concentrations below 8 mM, the dissolution rate was shown to increase with cyanide concentration, and under typical plant conditions (100 ppm CN^-), the dissolution rate of pure gold was shown to be very low. Complimentary electrochemical techniques were also used to investigate the dissolution process, and consistent with the kinetic data, it was shown that gold oxidation at potentials more negative than 300 mV proceeded at a low rate.

The leaching of gold in cyanide solutions was shown to be critically dependent on the purity of the system. To quantify this effect, studies were performed using leach solutions and gold samples which had been modified by various additives. Lead was investigated as a solution additive, and it was shown that the presence of 1 ppm lead significantly enhanced the leaching rate of gold. It is believed that lead modifies the surface of the gold during dissolution, thereby reducing the effect of the passive film. For gold in an air saturated solution containing 20 mM cyanide and 1 ppm lead, the dissolution reaction was found to be oxygen diffusion controlled. These findings were supported by electrochemical studies, which showed that in the presence of lead, gold readily oxidises in the potential region where oxygen reduction occurs. The effectiveness of lead was investigated over a range of experimental conditions, and it was shown that lead is

only beneficial under specific circumstances. For example, at high pH values, low cyanide concentrations or high oxygen concentrations, lead addition is not beneficial. The results from this work have rationalised a number of the conflicting studies on the effect of lead, which have been published in the past. Silver was also investigated as a leach solution additive, and it was shown that silver acts in a similar manner to lead in reducing the passivation of gold.

To investigate the effect of solid phase purity on the dissolution of gold in cyanide solutions, a small amount of silver was added to the gold electroplating solution. This produced a gold/silver deposit, which contained 1 % silver in the solid phase. It was shown that the dissolution of gold/silver in air saturated 20 mM cyanide solutions was oxygen diffusion controlled, and during the dissolution process, both peroxide and hydroxide are produced as reaction products (of oxygen reduction). The critical cyanide concentration for gold/silver in air saturated solutions was measured to be 2.1 mM, and at cyanide concentrations below this value, the dissolution reaction is cyanide diffusion controlled. The majority of native gold contains some silver, and therefore it is believed that the studies of gold/silver dissolution are an accurate representation of industrial cyanidation. Consequently, studies were performed to optimise the leaching of gold/silver. It was shown that high oxygen concentrations result in high gold/silver dissolution rates, and it is a simple matter to show that the optimum cyanide concentration, $[CN^-]$, under conditions of enhanced oxygen concentration, $[O_2]$, can be represented by

$$[CN^-] = [O_2] \times \frac{[CN^-]_{crit}}{[O_2]_{air}} \qquad \textbf{Equation 7.1}$$

where $[CN-]_{crit}$ is the critical cyanide concentration (2.1 mM) for air saturated solutions, and $[O_2]_{air}$ is the concentration of oxygen in air saturated solutions. It has also been shown that the addition of low concentrations of lead to the solution results in an increase in the dissolution rate of gold/silver. In this instance, it is believed that the role of lead is to enhance the reduction of oxygen.

It is believed that the results from studying the effect of both solution and solid phase purity can be used to rationalise the majority of the published kinetic and electrochemical results from gold cyanidation. For example, the classic gold oxidation polarisation curve published by Kudryk and Kellogg (1954) is almost identical to the polarisation curves presented in Chapter 6 for the oxidation of gold/silver. It is therefore believed that these authors utilised gold of lower purity during their studies. Not surprisingly, these authors also showed that the dissolution of gold was diffusion controlled.

As a result of this study, a better understanding of the gold cyanidation process has been developed, and in particular, by choosing the appropriate experimental conditions, the results from a laboratory investigation can be correlated with the performance of a cyanidation plant. This is a critical point to consider when developing or investigating modifications to the cyanidation process. For example, the leaching of gold in ammonia-cyanide solutions has received some attention as a process that can selectively recover gold from copper-gold ores. A number of kinetic studies of gold in ammonia-cyanide solutions have been performed (e.g. Zheng *et al.*, 1995, La Brooy, Komosa & Muir, 1991). Unfortunately, the rotating disc investigations in these studies used gold of high purity, and therefore there were problems using the results to explain the behaviour of ores. Recently, the ammonia-cyanide process has been studied using the gold/silver samples described in this thesis (Drok & Ritchie, 1997). This has the potential to lead to a better understanding of such an industrial process. Provided that the gold in ores can be characterised, the techniques described in this thesis can also be used to determine the kinetics of gold leaching in industrial cyanidation liquors. If these studies show that the leaching reaction is hindered, then a number of additives can be effectively evaluated in a short period of time. Another recommendation arising from this work is that cyanidation plants analyse the gold that exists in leach tailings. It is possible that this gold could be of higher purity, and consequently is not leached in the available residence time. If this is the case, then measures can be taken to minimise the loss of gold during the leaching process.

Although this work has contributed to the understanding of the cyanidation process, there are still a number of aspects of the dissolution reaction which are unclear. One suggestion for future studies would be to properly characterise the passive film which exists on gold under conditions of high purity. Such a study should be performed using modern surface analysis techniques, such as X-ray photoelectron spectroscopy (XPS), low energy electron diffraction (LEEDS), Auger spectroscopy, Raman spectroscopy and scanning tunnelling microscopy (STM). It would also be interesting to investigate the interaction between the gold surface and lead. In particular, characterising the surface under active and passive conditions would provide a further insight into the action of lead on the dissolution of gold in cyanide solutions.

Finally, it will be apparent from the results presented in this thesis that by using the rotating electrochemical quartz crystal microbalance to study the leaching of gold, a large number of rapid experiments can be conducted in order to achieve a greater understanding of the cyanidation process. The REQCM can be used to study a range of heterogeneous reactions, including leaching, deposition, and adsorption. For such systems where problems are encountered or where aspects of the process are poorly understood, it is recommended that they be investigated using a similar approach to that described in this thesis.

References

Adanuvor, P.K. and White. R.E. 1988, 'Oxygen reduction on silver in 6.5M caustic soda solution', *Journal of the Electrochemical Society*, vol. 135, no. 10, pp. 2509-2517.

Adzic, R.R., Tripkovic, A.V. and Markovic, N.M. 1980, 'Oxygen reduction on electrode surfaces modified by foreign metal ad-atoms: lead ad-atoms on gold', *Journal of Electroanalytical Chemistry*, vol. 114, pp. 37-51.

Albery, W.J., Hitchman, M.L. and Ulstrup, J. 1968, 'Ring - Disc Electrodes Part 9 - Applications to First Order Kinetics', *Faraday Transactions*, vol. 64, pp. 2831 - 2840.

Albery, W.L. and Hitchman, M.L. 1971, *Ring-Disc Electrodes*, Oxford University Press, London.

AMIRA Project P420 1995, *Plant survey questionaire*, AMIRA, Melbourne.

Anastasijevic, N.A., Strbac, S. and Adzic, R.R. 1988, 'Oxygen reduction on the Au (311) electrode surface in alkaline electrolyte', *Journal of Electroanalytical Chemistry*, vol. 240, pp. 239-252.

Baltruschat, H. and Heitbaum, J. 1983, 'On the potential dependence of the CN stretch frequency on Au electrodes studied by SERS', *Journal of Electroanalytical Chemistry*, vol. 157, pp. 319-326.

Bard, A.J. 1973, *Encyclopedia of Electrochemistry of the Elements*, Marcel Dekker, New York.

Bard, A.J. and Faulkner, L.R. 1980, *Electrochemical Methods - Fundamentals and Applications*, John Wiley and Sons, New York.

Barksy, G., Swainson, S.J. and Hedley, N. 1934, 'Dissolution of gold and silver in cyanide solutions', *American Institute of Mining, Metallurgical and Petroluem Engineers Transactions*, vol. 112, pp. 660 - 677.

Bek, R.Y., Rogozhnikov, N.A. and Kosolapov, G.V. 1997, 'The kinetics of anodic dissolution of gold in cyanide electrolytes and the interface layer composition', *Russian Journal of Electrochemistry*, vol. 33, no. 2, pp. 119-125.

Beyers, E. 1936, 'Some of the factors which influence the rates of dissolution of gold and silver in cyanide solutions', *Journal of the Chemical and Metallurgical Society of South Africa*, vol. 37, pp. 37-89.

Bianci, G., Mazza, F. and Mussini, T. 1962, 'Catalytic decomposition of acid hydrogen peroxide solutions on platinum, iridium, palladium and gold surfaces', *Electrochimica Acta*, vol. 7, pp. 457-473.

Bodländer, G. 1896, 'Die chemie des cyanidverfahrens', *Zeitschrift fuer Angewandte Chemie*, vol. 9, pp. 583-587.

Bruckenstein, S., Michalski, M., Fensore, A., Li, Z. and Hillman, A.R. 1994, 'Dual quartz crystal microbalance oscillator circuit. Minimising effects due to liquid viscosity, density and temperature', *Analytical Chemistry*, vol. 66, pp. 1847-1852.

Cathro, K.J. 1963, 'The effect of oxygen in the cyanide process for gold recovery', *Proceedings of the Australasian Institute of Mining and Metallurgy*, vol. 207, pp. 181-205.

Cathro, K.J., Koch, D.F.A. 1964, 'The anodic dissolution of gold in cyanide solutions', *Journal of the Electrochemical Society*, vol. 111, no. 12, pp. 1416-1420.

Chen, C.K., Lung, T.N. and Wan, C.C. 1980, 'A study of the leaching of gold and silver by acidothioureation', *Hydrometallurgy*, vol. 5, no. 2/3, pp. 207-212.

Clarke, D. 1996, *Personal Communication.*

Conway, B.E., Bockris, J.O.M., Yeager, E., Khan, S.U.M. and White, R.E. 1993. *Comprehensive Treatise of Electrochemistry. Volume 7 Kinetics and Mechanisms of Electrode Processes*, Plenum Press, New York.

Davies, M., Clark, M., Yeager, E. and Hovorka, F. 1959, 'The oxygen electrode 1. Isotopic investigations of electrode mechanisms', *Journal of the Electrochemical Society*, vol. 106, pp. 56-61.

Delahay, P. 1950, 'A polarographic method for the indirect determination of polarization curves for oxygen reduction on various metals. II. Application to nine common metals.', *Journal of the Electrochemical Society*, vol. 97, pp. 205-212.

Department of Minerals and Energy 1997, *Personal Communication.*

Dorin, R. and Woods, R. 1991, 'Determination of leaching rates of precious metals by electrochemical techniques', *Journal of Applied Electrochemistry*, vol. 21, no. 5, pp. 419-424.

Drok, K.J. and Ritchie, I.M. 1997, 'An investigation of the selective leaching of gold over copper using ammoniacal cyanide', in *World Gold '97*, Aus.I.M.M., Melbourne, pp. 87-93.

Eagleson, M. 1994, *Concise Encylopedia of Chemistry*, Walter de Gruyter & CO, Berlin.

Eisenberg, M., Tobias, C.W. and Wilke, C.R. 1954, 'Ionic mass transfer and concentration polarisation at rotating electrodes', *Journal of the Electrochemical Society*, vol. 101, pp. 306-319.

Eisenmann, E.T. 1978, 'Kinetics of the Electrochemical reduction of dicyanoaurate', *Journal of the Electrochemical Society*, vol. 125, no. 5, pp. 717-723.

Elsner, L. 1846, 'Uber das verhalten verschiedener metalle in einer wassrigen losung von cyankalium', *Journal fuer Praktische Chemie*, vol. 37, pp. 441-446.

Evans, D.H., Lingane, J.J. 1963, 'The chronopotentiometric reduction of oxygen at gold electrodes', *Journal of Electroanalytical Chemistry*, vol. 6, pp. 283-299.

Fink, C.G., Putnam, G.L. 1950, 'The action of sulphide ion and of metal salts on the dissolution of gold in cyanide solutions', *Mining Engineering*, vol. 187, pp. 952-955.

Fischer, P. and Heitbaum, J. 1980, 'Mechanistic aspects of cathodic oxygen reduction', *Electroanalytical Chemistry*, vol. 112, pp. 231-238.

Fleming, C. 1992, 'Hydrometallurgy of precious metals recovery', *Hydrometallurgy*, vol. 30, pp. 127-162.

Floyd, T. 1996, *Electronic Devices*, Prentice-Hall, Englewood Cliffs.

Fogg, P.G.T. and Gerrard, W. 1991, *Solubility of Gases in Liquids. A Critical Evaluation of Gas/Liquid Systems in Theory and Practice*, John Wiley & Sons, Chichester, West Sussex.

Gold Fields Mineral Services 1996, 'Gold', *Metals and Minerals Annual Review*, pp. 17-23.

Gregory, D.P. and Riddiford, A.C. 1956, 'Transport to the surface of a rotating disk', *Journal of the Chemical Society*, pp. 3756-3764.

Guan, Y. and Han, K.N. 1993, 'The dissolution behaviour of gold and copper from gold and copper alloys', *Minerals and Metallurgical Processing*, vol. 10, pp. 66-74.

Guan, Y.C. and Han, K.N. 1994, 'An electrochemical study on the dissolution of gold and copper from gold copper alloys', *Metallurgical & Materials Transactions B. Process Metallurgy & Materials Processing Science*, vol. 25, no. 6, pp. 817-827.

Habashi, F. 1967, 'Kinetics and mechanism of gold and silver dissolution in cyanide solution', *Montana Bureau of Mines and Geology Bulletin*, vol. 59.

Hiskey, J.B. and Sanchez, V.M. 1990, 'Mechanistic and kinetic aspects of silver dissolution in cyanide solutions', *Journal of Applied Electrochemistry*, vol. 20, pp. 479-487.

Hoare, J.P. 1968, *The Electrochemistry of Oxygen*, Interscience Publishers, New York.

Hosking, J.W. 1982, 'Review of analytical methods for determining trace amounts of gold in ores and process streams', in *Carbon-in-Pulp Technology for the Extraction of Gold*, Aus.I.M.M., Melbourne.

Hurlbut, C.S. and Klein, C. 1977, *Manual of Mineralogy, 19th Edition*, John Wiley & Sons, New York.

Jeffrey, M.I., Drok, K.J., La Brooy, S.R. and Ritchie, I.M. In Press, 'Oxygen reduction during the dissolution of gold and copper in alkaline cyanide solutions', *Hydrometallurgy*.

Johnson, W.D. 1894, 'Abstraction of gold and silver from their solutions in potassium cyanide', US Pat. 522260.

Jüttner, K. 1984, 'Oxygen reduction electrocatalysis by underpotential deposited metal atoms at different single crystal faces of gold and silver', *Electrochimica Acta*, vol. 29, no. 11, pp. 1597-1604.

Jüttner, K. 1986, 'Surface Structural Effects in Electrocatalysis', *Electrochimica Acta*, vol. 31, no. 8, pp. 917-927.

Kakovskii, I.A. and Kholmanskikh, Y.B. 1960, 'Investigation of the kinetics of cyaniding copper and gold', *Izvestiya Akademii Nauk SSSR. Otdelenie Tekhnicheskikh Nauk, Metallurgiya i Toplivo*, vol. 5, pp. 207-218.

Kameda, M. 1949a, 'Fundamental studies on dissolution of gold in cyanide solutions. II on equations and effects of cyanide strength and other variables on dissolution rate', *Science Reports of Reseach Institutes, Tomoku University*, vol. VI, no. 4, pp. 223-230.

Kameda, M. 1949b, 'Fundamental studies on dissolution of gold in cyanide solutions. III effects of alkalis, lead acetate, and some impurities contained in foul cyanide solutions', *Science Reports of Reseach Institutes, Tomoku University*, vol. VI, no. 4, pp. 435-444.

Kirk, D.W., Foulkes, F.R., Graydon, W.F. 1978, 'A study of anodic dissolution of gold in aqueous alkaline cyanide', *Journal of the Electrochemical Society*, vol. 125, no. 9, pp. 1436-1443.

Kirk, D.W., Foulkes, F.R. and Graydon, W.F. 1979, 'Electron stoichiometry of anodic dissolution of gold in aqueous alkaline cyanide', *Journal of the Electrochemical Society*, vol. 126, no. 12, pp. 2287-2288.

Kirk, D.W., Foulkes, F.R. and Graydon, W.F. 1980, 'Gold passivation in aqueous alkaline cyanide', *Journal of the Electrochemical Society*, vol. 127, no. 9, pp. 1962-1969.

Kudryk, V., Kellogg, H.H. 1954, 'Mechanism and rate-controlling factors in the dissolution of gold in cyanide solution', *J. Metals*, vol. 6, pp. 541-548.

Kunimatsu, K., Seki, H., Golden, W.G., Gordon II, J.G. and Philpott, M.R. 1988, 'A study of the gold/cyanide solution interface by in situ polarization-modulated fourier transform infrared reflection adsorption spectroscopy', *Langmuir*, vol. 4, no. 2, pp. 337-341.

La Brooy, S.R., Komosa, T. and Muir, D.M. 1991, 'Selective leaching of gold from copper-gold ores using ammonia-cyanide mixtures', in *Fifth Aus.I.M.M. Extractive Metallurgy Conference*, Aus.I.M.M., pp. 127-132.

La Brooy, S.R., Linge, H. and Walker, G. 1994, 'Review of gold extraction from ores', *Minerals Engineering*, vol. 7, no. 10, pp. 1213-1241.

Levich, V.G. 1962, *Physicochemical Hydrodynamics*, Prentice Hall, Englewood Cliffs, New Jersey.

Lide, D.R. 1995, *CRC Handbook of Chemistry and Physics*, CRC Press, Boca Raton, Florida.

Liu, G.Q. and Yen, W.T. 1995, 'Effects of sulphide minerals and dissolved oxygen on the gold and silver dissolution in cyanide solution', *Minerals Engineering*, vol. 8, no. 1-2, pp. 111-123.

Lorenzen, L., van Deventer, J.S.J. 1992, 'Electrochemical interactions between gold and its associated minerals during cyanidation', *Hydrometallurgy*, vol. 30, pp. 177-194.

Mac Arthur, D.M. 1972, 'A study of gold reduction and oxidation in aqueous media', *Journal of the Electrochemical Society*, vol. 119, no. 6, pp. 672-677.

Mahoney, M.R. and Cooney, R.P. 1985, 'Intensely-scattering phase in surface enhanced raman scattering by cyanide on gold electrodes', *Journal of the Chemical Society, Faraday Transactions 1*, vol. 81, pp. 2115-2122.

Markovic, R.R., Adzic, R.R. and Vesovic, V.B. 1984, 'Oxygen reduction on the gold single crystal electrodes with (110) and (111) orientations', *Journal of Electroanalytical Chemistry*, vol. 165, pp. 121-133.

Marsden, J. and House, I. 1992, *The Chemistry of Gold Extraction*, Ellis Horwood Ltd., Chichester, West Sussex, England.

Maxey, A., Gonnella, P., Ball, Y. and Herkenhoff, P. 1997, 'Gold', in *Register of Australian Mining 1996/97*, Ed. Louthean, R., Resource Information Unit Ltd. Bassendean, WA.

McCarley, R.L. and Bard, A.J. 1992, 'Surface reactions of Au(111) with aqueous cyanide studied by scanning tunneling microscopy', *Journal of Physical Chemistry*, vol. 96, pp. 7410-7416.

Morgan, H.M. 1993, 'Overview of the Australasian gold industry', in *Australasian Mining and Metallurgy - The Sir Maurice Mawby Memorial Volume*, vol. 2, Eds. Woodcock, J.T. and Hamilton, J.K., Aus.I.M.M., Melbourne, pp. 801-804.

Mughogho, D.T. and Crundwell, F.K. 1996, 'Gold dissolution in dilute cyanide solutions', in *Electrochemistry in Mineral and Metals Processing IV*, vol. 96-6, Eds. Woods, R., Doyle, F.M. and Richardson, P., The Electrochemical Society, Pennington, New Jersey, pp. 275-283.

Mussatti, D., Mager, J. and Martins, G.P. 1997, 'Electrochemical aspects of the dissolution of gold in cyanide electrolytes containing lead', in *Aqueous Electrotechnologies: Progress in Theory and Practice*, Ed. Dreisinger, D., Minerals, Metals and Materials Society, Warrendale, Pennsylvania, pp. 247-265.

Nadkarni, R.M., Jelden, C.E., Bowles, K.C., Flanders, H.E. and Wadsworth, M.E. 1967, 'A kinetic study of copper precipitation on iron', *Transactions of the Metallurgical Society AIME*, vol. 239, no. 4, pp. 581-585.

Nicol, M., Fleming, C. and Paul, R. 1987, 'The chemistry of the extraction of gold', in *The Extractive Metallurgy of Gold*, vol. 2, Ed. Stanley, G.G., South African Institute of Mining and Metallurgy, Johannesburg, S. Africa, pp. 831-905.

Nicol, M.J. 1980a, 'The anodic behaviour of gold', *Gold Bulletin*, vol. 13, pp. 105-111.

Nicol, M.J. 1980b, *Extended Abstracts: 31st Meeting of the International Society of Electrochemistry*, vol. 1, Venice.

Osseo-Asare, K., Xue, T. and Ciminelli, V.S.T. 1984, 'Solution chemistry of cyanide leaching systems', in *Precious Metals: Mining Extraction and Processing*, The Metallurgical Society/AIME., Warrendale, Pennsylvania, pp. 173-197.

Pan, T.P. and Wan, C.C. 1979, 'Anodic behaviour of gold in cyanide solution', *Journal of Applied Electrochemistry*, vol. 9, no. 5, pp. 653-655.

Pang, J. and Ritchie, I.M. 1981, 'Mass transfer at the surface of a rotating cylinder', *Electrochimica Acta*, vol. 26, no. 9, pp. 1342-1350.

Perdriel, C.I., Arvia, A.J. and Ipohorski, M. 1986, 'Electrochemical faceting of polycrystalline gold in 1 M H_2SO_4.', *Journal of Electroanalytical Chemistry*, vol. 215, pp. 317-329.

Pesic, B. and Sergent, R.H. 1991, 'A rotating disk study of gold dissolution by bromine', *Journal of Metals*, vol. 43, no. 12, pp. 35-37.

Poskus, D. and Agafonovas, G. 1995, 'Adsorption of cyanide-containing species from potassium cyanide solutions on gold electrodeposits', *Journal of Electroanalytical Chemistry*, vol. 393, no. 1-2, pp. 105-112.

Pourbaix, M. 1963, *Atlas d'Equilibres Electrochimiques*, Gauthier-Villars, Paris.

Power, G.P. and Ritchie, I.M. 1975, 'Metal displacement reactions', in *Modern Aspects of Electrochemistry*, vol. II, Plenum Press, London, pp. 199-250.

Power, G.P. and Ritchie, I.M. 1983, 'Mixed potentials. Experimental illustration of an important concept in practical electrochemistry', *Journal of Chemical Education*, vol. 60, no. 12, pp. 1022-1026.

Power, G.P., Ritchie, I.M. and Sjepcevich, G. 1981, 'A versatile design of rotating disk apparatus', *Chemistry in Australia*, vol. 48, pp. 468-471.

Ritchie, I.M., Zheng, J., La Brooy, S.R. and Singh, P. 1994, 'Extension of electrochemical windows by the use of an electrochemical quartz crystal microbalance', in *Extended abstracts: 186th Annual meeting of the Electrochemical Society*, vol. II 94-2, The Electrochemical Society, Pennington, New Jersey, pp. 1044-1045.

Robertson, S.G. 1995, *PhD Thesis: The zincate immersion process for plating aluminium: a kinetic, electrochemical and morphological study*, Murdoch University, Murdoch, WA.

Rogozhnikov, N.A. and Bek, R.Y. 1987, 'Double-layer capacity and the zero-charge potential of a gold electrode in cyanide solutions', *Elektrokhimiya*, vol. 23, no. 10, pp. 1440-1443.

Rogozhnikov, N.A. and Bek, R.Y. 1996, 'Adsorption of cyanide ions on gold', *Russian Journal of Electrochemistry*, vol. 32, no. 12, pp. 1333-1336.

Sawaguchi, T., Yamada, T., Okinaka, Y. and Itaya, K. 1995, 'Electrochemical scanning tunneling microscopy and ultrahigh-vacuum investigation of gold cyanide adlayers on Au(111) formed in aqueous solution', *Journal of Physical Chemistry*, vol. 99, no. 38, pp. 14149-14155.

Sheveleva, L.D., Kokovskii, I.A. 1979, 'Lead compounds and dissolution of gold in cyanide solutions', *Tsvetnye Metally*, vol. 7, pp. 100-102.

Sun, X., Guan, Y.C. and Han, K.N. 1996, 'Electrochemical behavior of the dissolution of gold-silver alloys in cyanide solutions', *Metallurgical and Materials Transactions B*, vol. 3, pp. 355-361.

Thompson, P.F. 1947, 'The dissolution of gold in cyanide solutions', *Transactions of the Electrochemcial Society*, vol. 91, pp. 41-71.

Thurgood, C.P., Kirk, D.W., Foulkes, F.R. and Graydon, W.F. 1981, 'Activation energies of anodic gold reactions in aqueous alkaline cyanide', *J. Electrochem. Soc.*, vol. 128, no. 8, pp. 1680-1685.

Trindade, R.B.E. and Monhemius, A.J. 1993, 'The use of anthraquinone as a catalyst in the cyanide leaching of gold', *Minerals Engineering*, vol. 6, no. 6, pp. 565-574.

Vazquez, M.V., Desanchez, S.R., Calvo, E.J. and Schiffrin, D.J. 1994, 'The electrochemical reduction of oxygen on polycrystalline copper in borax buffer', *Journal of Electroanalytical Chemistry*, vol. 374, no. 1-2, pp. 189-197.

Wang, X. and Forssberg, K.S.E. 1990, 'The chemistry of cyanide-metal complexes in relation to hydrometallurgical processes of precious metals', *Mineral Processing and Extractive Metallurgy Review*, vol. 6, pp. 81-125.

Ward, M.D. 1995, 'Principles and applications of the electrochemical quartz crystal microbalance', in *Physical Electrochemistry: Principles, Methods and Applications*, Ed. Rubinstein, I., Marcel Dekker, New York, pp. 293-338.

Weichselbaum, J., Tumilty, J.A. and Schmidt, C.G. 1989, 'The effects of sulfide and lead on the rate of gold cyanidation', in *The Aus.I.M.M. Annual Conference Perth/Kalgoorlie*, Aus.I.M.M., Melbourne, pp. 221-224.

White, H.A. 1919, 'The solubility of gold in cyanide solutions', *Journal of the Chemical, Metallurgical and Mining Society of South Africa*, vol. 20, pp. 1-8.

Zhang, H.G. 1997, *PhD Thesis: Some aspects of the use of thiourea in gold processing*, Murdoch University, Murdoch, WA.

Zheng, J., Khan, M., La Brooy, S.R., Ritchie, I.M. and Singh, P. 1996, 'The chronopotentiometric method for measuring the kinetics of metal dissolution and cementation reactions', *Journal of Applied Electrochemistry*, vol. 26, pp. 509-514.

Zheng, J., Ritchie, I.M., La Brooy, S.R. and Singh, P. 1995, 'Study of gold leaching in oxygenated solutions containing cyanide-copper-ammonia using a rotating quartz crystal microbalance', *Hydrometallurgy*, vol. 39, no. 1-3, pp. 277-292.

Zurilla, R.W., Sen, R.K. and Yeager, E. 1978, 'The kinetics of the oxygen reduction reaction on gold in alkaline solution', *Journal of the Electrochemical Society*, vol. 125, no. 7, pp. 1103-1109.